VOLUME 77 JULY 5, 1973 NUMBER 14

JPCHAx

THE JOURNAL OF PHYSICAL CHEMISTRY

PUBLISHED BIWEEKLY BY THE AMERICAN CHEMICAL SOCIETY

THE JOURNAL OF

PHYSICAL CHEMISTRY

BRYCE CRAWFORD, Jr., *Editor*
STEPHEN PRAGER, *Associate Editor*
ROBERT W. CARR, Jr , FREDERIC A. VAN-CATLEDGE, *Assistant Editors*

EDITORIAL BOARD: A. O. ALLEN (1970–1974), C. A. ANGELL (1973–1977), J. R. BOLTON (1971–1975), F. S. DAINTON (1972–1976), M. FIXMAN (1970–1974), H. S. FRANK (1970–1974), R. R. HENTZ (1972–1976), J. R. HUIZENGA (1969–1973), W. J. KAUZMANN (1969–1973), R. L. KAY (1972–1976), W. R. KRIGBAUM (1969–1973), W. J. MOORE (1969–1973), R. M. NOYES (1973–1977), J. A. POPLE (1971–1975), B. S. RABINOVITCH (1971–1975), H. REISS (1970–1974), S. A. RICE (1969–1975), F. S. ROWLAND (1973–1977), R. L. SCOTT (1973–1977), W. A. ZISMAN (1972–1976)

AMERICAN CHEMICAL SOCIETY, *1155 Sixteenth St., N W., Washington, D. C. 20036*

Books and Journals Division

JOHN K CRUM *Director*
RUTH REYNARD *Assistant to the Director*

CHARLES R. BERTSCH *Head, Editorial Processing Department*
D. H. MICHAEL BOWEN *Head, Journals Department*
BACIL GUILEY *Head, Graphics and Production Department*
SELDON W. TERRANT *Head, Research and Development Department*

©Copyright, 1973, by the American Chemical Society. Published biweekly by the American Chemical Society at 20th and Northampton Sts., Easton, Pa. 18042. Second-class postage paid at Washington, D. C., and at additional mailing offices.

All manuscripts should be sent to *The Journal of Physical Chemistry*, Department of Chemistry, University of Minnesota, Minneapolis, Minn. 55455.

Additions and Corrections are published once yearly in the final issue. See Volume 76, Number 26 for the proper form.

Extensive or unusual alterations in an article after it has been set in type are made at the author's expense, and it is understood that by requesting such alterations the author agrees to defray the cost thereof.

The American Chemical Society and the Editor of *The Journal of Physical Chemistry* assume no responsibility for the statements and opinions advanced by contributors.

Correspondence regarding accepted copy, proofs, and reprints should be directed to Editorial Processing Department, American Chemical Society, 20th and Northampton Sts., Easton, Pa. 18042. Head: CHARLES R. BERTSCH. Assistant Editor: EDWARD A. BORGER. Editorial Assistant: JOSEPH E. YURVATI.

Advertising Office: Centcom, Ltd., 142 East Avenue, Norwalk, Conn. 06851.

Business and Subscription Information

Send all new and renewal subscriptions *with payment* to: Office of the Controller, 1155 16th Street, N.W., Washington, D. C. 20036. Subscriptions should be renewed promptly to avoid a break in your series. All correspondence and telephone calls regarding changes of address, claims for missing issues, subscription service, the status of records, and accounts should be directed to Manager, Membership and Subscription Services, American Chemical Society, P.O. Box 3337, Columbus, Ohio 43210. Telephone (614) 421-7230.

On changes of address, include both old and new addresses with ZIP code numbers, accompanied by mailing label from a recent issue. Allow four weeks for change to become effective.

Claims for missing numbers will not be allowed (1) if loss was due to failure of notice of change in address to be received before the date specified, (2) if received more than sixty days from date of issue plus time normally required for postal delivery of journal and claim, or (3) if the reason for the claim is "issue missing from files."

Subscription rates (1973): members of the American Chemical Society, $20.00 for 1 year; to nonmembers, $60.00 for 1 year. Those interested in becoming members should write to the Admissions Department, American Chemical Society, 1155 Sixteenth St., N.W., Washington, D. C. 20036. Postage to Canada and countries in the Pan-American Union, $5.00; all other countries, $6.00. Single copies for current year: $3.00. Rates for back issues from Volume 56 to date are available from the Special Issues Sales Department, 1155 Sixteenth St., N.W., Washington, D. C. 20036.

Subscriptions to this and the other ACS periodical publications are available on microfilm. Supplementary material not printed in this journal is now available in microfiche form on a current subscription basis. For information on microfilm or microfiche subscriptions, write Special Issues Sales Department at the address above.

Notice to Authors last printed in the issue of June 21, 1973

THE JOURNAL OF
PHYSICAL CHEMISTRY

Volume 77, Number 14 July 5, 1973

JPCHAx 77(14) 1725–1818 (1973)

ห้องสมุด กรมวิทยาศาสตร์
10 มี.ค. 2516

COMMUNICATIONS TO THE EDITOR

■ Supplementary material for this paper is available separately, in photocopy or microfiche form. Ordering information is given in the paper.

* In papers with more than one author, the asterisk indicates the name of the author to whom inquiries about the paper should be addressed.

AUTHOR INDEX

THE JOURNAL OF
PHYSICAL CHEMISTRY

Registered in U. S. Patent Office © Copyright, 1973, by the American Chemical Society

VOLUME 77, NUMBER 14 JULY 5, 1973

The Cyanogen–Active Nitrogen Reaction[1]

Michael Berger and G. B. Kistiakowsky*

The Gibbs Chemical Laboratory, Harvard University, Cambridge, Massachusetts 02138 *(Received February 12, 1973)*

Publication costs assisted by the National Science Foundation

The reaction of cyanogen and active nitrogen has been studied using a low-pressure flow reactor with on-line mass spectrometric observation of reactants and products. At total pressures in the range of 3 Torr, atomic nitrogen pressures in the range of 15 μ, and $(C_2N_2)_0/(N)_0$ ratios larger than 0.05, a rapid reaction sets in but only after an induction period and results in the recombination of as many as 30 N atoms per molecule of cyanogen consumed. The products from cyanogen are quantitatively only C_4N_2 and a wall polymer of $(C_{1.16}N)_n$ composition. Experiments with $C_2^{15,15}N_2$ and $^{13,13}C_2N_2 + {}^{12,12}C_2N_2$ mixtures show isotopic scrambling of "unreacted" cyanogen, recombined N_2, and dicyanoacetylene. The reaction is accelerated by oxygen atoms and is inhibited to different degrees and in different manner by additions of NH_3, O_2, and H_2. A mechanism is presented which describes the observed scrambling and the other features of the reaction considerably better than previously proposed reaction mechanisms.

Introduction

When certain carbonaceous compounds including cyanogen are added to active nitrogen,[2] CN emission and rapid recombination of nitrogen atoms result. While optical observations of CN emission in active nitrogen have been oriented to the elucidation of CN formation and excitation,[3-8] nonoptical methods have been used to study the mechanism of the overall reaction, especially the catalytic recombination of nitrogen atoms.

Haggart and Winkler[9] proposed that the initial step in the reaction with cyanogen is the direct attack and addition of a nitrogen atom to form an intermediate complex, $C_2N_2{\cdot}N$, which either decomposes into CN and NCN radicals or reacts with nitrogen atoms to form cyanogen and molecular nitrogen. The CN radicals are assumed to have no role in the recombination of nitrogen atoms, but NCN reacts with a nitrogen atom to give CN and N_2. Recent evidence does not support this mechanism.

In particular, Bayes[3b] has shown that the attack by nitrogen atoms is not the initiation step. Modifying Bayes's mechanism, Arrington, Bernadini, and Kistiakowsky[10] (subsequently referred to as ABK) suggested that the initial step is the dissociation of cyanogen into CN radicals upon collision with N_2 ($A^3\Sigma$). The ABK mechanism is then

$$N_2(A^3\Sigma) + C_2N_2 \longrightarrow N_2 + 2CN \quad \text{(i)}$$

$$CN + N + N_2 \longrightarrow NCN + N_2 \quad (1)$$

$$NCN + N \longrightarrow CN + N_2(A^3\Sigma) \quad (2)$$

This is a branching chain mechanism since the N_2 ($A^3\Sigma$) produced in reaction 2 can dissociate more cyanogen. Termination is by CN recombination and by diffusion of radicals to the wall where they polymerize.

Safrany and Jaster[11] (subsequently referred to as SJ) proposed a mechanism in which the initiation is by reaction i. However, the N atom recombination occurs by the chain

$$CN + N \longrightarrow N_2 + C \quad (3)$$

$$C_2N_2 + C \longrightarrow C_2N + CN \quad (4)$$

$$C_2N + N \longrightarrow 2CN \quad (5)$$

Evidence for C_2N radicals is that the polymer formed is slightly carbon rich, $(C_{1.27}N)_n$, and that C_4N_2 is a (minor) product of the reaction. Also, recently atomic carbon has been observed directly in the cyanogen–active nitrogen system.[12]

Because of this disagreement on how nitrogen atom recombination is catalyzed by C_2N_2, we undertook the study of the reaction.

Experimental Section

The reaction was studied by means of flow technique using a cylindrical Pyrex reactor (22 mm i.d.) and observing the composition of the gases with a 60° sector mass spectrometer. This apparatus has been described elsewhere,[10] the improvements being mainly a redesigned ion source providing greater sensitivity of the mass spectrometer to atoms and free radicals entering the source through the pin hole at the end of the reactor. Reaction time, t, defined as the ratio of the distance between the C_2N_2 injector and the ion source pin hole and the gas mass flow velocity, was varied by moving the injector. Flow rates are estimated to be accurate to within 10%.

The total pressure in the reactor, measured with a silicone oil manometer, was varied between 0.5 and 5.0 Torr. Typically, the reactor flow velocity was 3 mm/msec at 3 Torr. Up to 1% dissociation of the N_2 carrier gas was achieved by a microwave discharge maintained by ≤ 125 W, 2450 MHz Raytheon Microtherm microwave generator with an air-cooled Broida type-5 cavity located about 500 msec of flow time upstream from the reaction region. The nitrogen atom concentration was varied by changing the microwave power and by use of a by-pass which shunted some of the carrier gas around the discharge region.

The concentration of nitrogen atoms was determined by nitric oxide titration.[13] The nitric oxide was purified by three vacuum distillations and was introduced through the C_2N_2 injector. The end point was followed visually and mass spectrometrically. In the absence of an added reactant, there was no detectable nitrogen atom decay down the reactor tube at 3 Torr, identical titration end points being obtained at 200 and 20 msec from the mass spectrometer sampling pin hole. During an experiment the initial nitrogen atom concentration was monitored by a calibrated 1P28 phototube observing the yellow Lewis–Rayleigh first positive emission and located 150-msec upstream of the reaction zone.

The nitrogen (Matheson Prepurified; impurities 0.015%; mainly O_2), ammonia (Matheson Anhydrous Grade, 99.99% minimum purity), hydrogen (Matheson Prepurified Grade, 99.95% minimum purity), and oxygen (Baker Air Zero GAs, 2 ppm maximum hydrocarbons) were used without further purification.

Cyanogen (Matheson CP Grade) had 0.5% CO_2 and 0.3% HCN as the major impurities. CO_2 was easily removed at Dry Ice temperatures, but HCN remained. However, the reaction of HCN with active nitrogen is much slower[10,11] than the reaction of cyanogen and hence its presence in such small quantities is not considered to be important.

Isotopically enriched cyanogen was prepared by dropwise addition of 95% $K^{12}C^{15}N$ or 90% $K^{13}C^{14}N$ (Isomet Corp.) onto a warm concentrated solution of $CuSO_4$. Complete removal of CO_2 was effected with a 1-propanol bath (−127°) with no loss of cyanogen. C_2N_2 was separated from the HCN and H_2O by the use of a toluene slush bath (−95°), and contained no more than 2% HCN. As determined by mass spectrometric analysis, $C_2^{15,15}N_2$ was better than 94% isotopically pure, and the other cyanogen had the expected isotopic distribution: 80% $^{13,13}C_2N_2$, 18% $^{13,12}C_2N_2$, and 1.5% $^{12,12}C_2N_2$.

Results

1. Experiments with Isotopically Unlabeled Cyanogen. At very low flows of cyanogen, $(C_2N_2)_0/(N)_0$ being less than 0.05, there was little or no reaction, as shown by small consumption of nitrogen atoms and cyanogen. A diffuse glow pervaded the entire reaction tube for distances corresponding to more than 1 sec of reaction time. This bluish or blue-white glow, in which the Lewis–Rayleigh afterglow is still present, has been termed the "blue flame condition" by Radford and Broida.[6] As the flow of cyanogen was increased, the flame became localized around the injection point, extending downstream for about 30 msec when the flame was brightest, and the consumption of nitrogen atoms was accelerated. The very bright lilac or pink flame is known as the "regular flame condition."[6] With still more cyanogen the intensity of the emission decreased, yet nitrogen atom consumption became even more rapid.

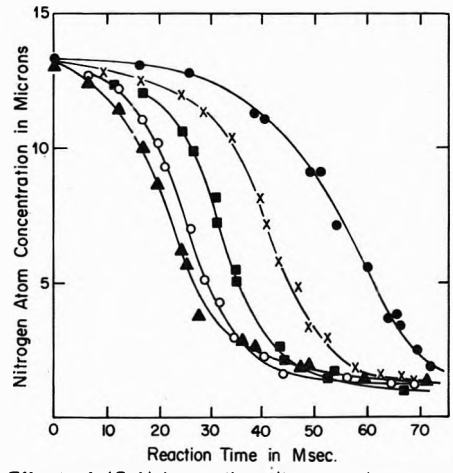

Figure 1. Effect of $(C_2N_2)_0$ on the nitrogen atom concentration decay with time: $(C_2N_2)_0$ in μ: ●, 1.1; ×, 1.5; ■, 2.24; ○, 3.3; ▲, 6.35. Conditions: (N_2) = 2.90 Torr; $(N)_0$ = 13.3 μ.

The concentration *vs.* time profiles show characteristic features of complex reactions involving reactive intermediates. First, the reaction rate reaches a maximum only when about half the nitrogen atoms have already been consumed, well after the completion of reactant interdiffusion. Thus there is a significant induction period. Figure 1 shows nitrogen atom concentration *vs.* time profiles for various initial concentrations of cyanogen, $(C_2N_2)_0$. The time for complete interdiffusion was found to be about 10 msec at 2.90 Torr. As the figure shows, greater additions of cyanogen shorten the induction period, but do not increase the maximum rate of nitrogen atom consumption once the "regular flame condition" has been attained. In Figure 1 this corresponds to $(C_2N_2)_0$ greater than 1.5 μ.

Second, a finite residual nitrogen atom concentration, $(N)_\infty$ (as well as that of C_2N_2) remains after the reaction ceases. This effect has been noted elsewhere.[11,14] This $(N)_\infty$ increases with a decrease in the total pressure and/or initial nitrogen atom concentration and depends on the conditioning of the reactor walls. It will be shown later that a finite $(N)_\infty$ is a consequence of processes which compete with nitrogen atoms for reactive intermediates.

Third, the overall stoichiometry indicates a chain reaction. Typically, the overall chain length

$$\bar{\nu} = [(N)_0 - (N)_\infty]/[(C_2N_2)_0 - (C_2N_2)_\infty]$$

has a large value (~30) in the range of total pressure studied (1.8–4.3 Torr) and is independent of the initial nitrogen atom or cyanogen concentrations. Moreover, the rates of cyanogen and nitrogen atom consumption vary in

TABLE I: Chain Length Defined as $[\Delta(N)/\Delta(C_2N_2)]_t$ vs. Time[a]

t, msec	$(N)_t$, μ	$(C_2N_2)_t$, μ	Chain length $\Delta(N)/\Delta(C_2N_2)$
0.0	21.7 ± 0.2	2.10 ± 0.03	
10.0	19.2	2.05	50 ± 20
15.0	13.5	1.93	48 ± 10
17.5	8.0	1.81	46 ± 8
20.0	3.8	1.72	46 ± 5
25.0	1.3	1.63	28 ± 10
30.0	0.5	1.61	40 ± 20
40.0	0.2	1.60	30 ± 30

[a] This table is based on data in Figure 2.

parallel so that the chain length is nearly constant throughout the course of the reaction; see Table I and Figure 2. SJ[11] experimenting at total pressures of about 0.2 Torr obtained a chain length of about 4. Arrington,[14] however, under conditions very similar to ours reported a chain length of about 30.

Dicyanoacetylene is produced in very small yields, no more than 0.2 μ partial pressure. A typical concentration *vs.* time profile is shown in Figure 2. Note that the maximum rate of C_4N_2 production occurs about 5 msec after the time of maximum rate of nitrogen atom consumption. This "lag" was observed consistently.

In general the total yield of C_4N_2 is proportional to the square of the concentration of nitrogen atoms consumed and is independent of $(C_2N_2)_0$. This is illustrated in Figure 3. All data points refer to "completed" reaction, being obtained after 55 msec. Since the data of Figure 3 were obtained at 4.3 Torr, for $(N)_0 > 14$ μ, $(N)_\infty$ was very small and the approximation that the amount of nitrogen atoms consumed, $\Phi(-(N)) = ((N)_0 - (N)_\infty) \cong (N)_0$, was used in the plot.

SJ[11] reported that the C_4N_2 yield was on the order of $0.0001\ (N)_0$, while our results indicate a value $0.005\ (N)_0$. Since our experiments were conducted at total pressures greater than theirs by more than a factor of 20, we suspected that C_4N_2 formation occurred *via* a three-body radical mechanism. Indeed the total yields of C_4N_2, $\Phi(C_4N_2)$, at a given $(N)_0$ (14.5 μ) and at 4.3 and 1.82 Torr N_2 (a pressure ratio of 2.36) were in the 2.4 ratio. Thus the relation $\Phi(C_4N_2) = k\ (N)_0^2(N_2)$ describes the total yield of C_4N_2 very well.

Since no C_4N_2 was available for calibration of the mass spectrometer, its ionization cross section was estimated using the additivity rule[15] as $\sigma(C_4N_2)/\sigma(C_2N_2) = 1.50$. Using this ratio we find that 20 ± 5% of the consumed cyanogen becomes C_4N_2 at 3.5 ± .5 Torr total pressure.

A brown-black polymer was formed on the walls of the reactor. Microanalysis (Galbraith Laboratories) showed the polymer to be carbon rich, $(C_{1.16\pm0.02}N)_n$ being the composition of two separate samples. If the polymer is formed by the radicals diffusing to the wall, C_2N and CN are implicated rather than NCN and CN as some workers[3b,9,10] have suggested.

An experiment was performed to determine how much polymer is formed by inserting weighed glass rings into the reactor tube to form a close-fitting glass sleeve. The reaction was run for 140 min holding the injector in a fixed position; afterwards the rings were removed and reweighed. If the total increase in weight, 8.77 ± 0.30 mg, is the polymer, the amount of carbon contained in it accounts for 80% of the consumed cyanogen. Since C_4N_2 accounts for the other 20%, a very good mass balance is obtained. No other carbon-containing reaction product could be detected.

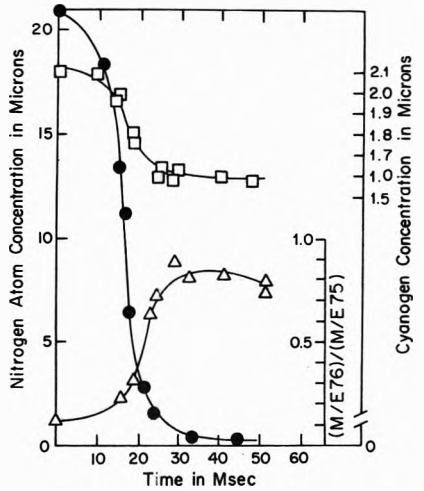

Figure 2. Concentration *vs.* reaction time for nitrogen atoms, C_2N_2, and C_4N_2: ●, (N) in μ; □, (C_2N_2) in μ; △, (C_4N_2) as $(m/e\ 76)/(m/e\ 75)$ where $(m/e\ 75)$ is a background reference peak. Conditions: $(N_2) = 4.1$ Torr; $(C_2N_2)_0 = 2.1$ μ; $(N)_0 = 21.7$ μ.

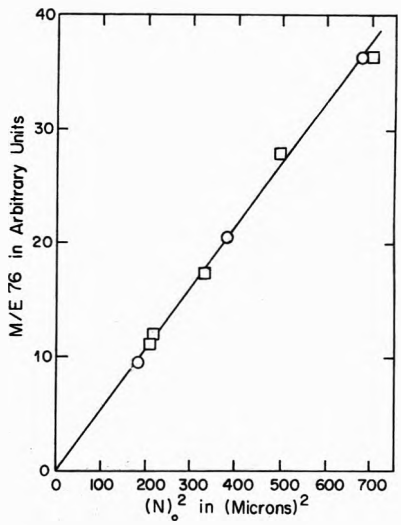

Figure 3. $\Phi(C_4N_2)$ *vs.* $(N)_0^2$. $\Phi(C_4N_2)$ is plotted as the $(m/e\ 76)$ peak height in arbitrary units. $(C_2N_2)_0$ in μ: □, 1.95; ○, 2.85. Conditions: $(N_2) = 4.30$ Torr; $t = 55$ msec; the nitrogen atom consumption is complete.

This experiment was also used to demonstrate that polymer formation is mainly a heterogeneous process. With the use of a double-beam recording microdensitometer (Joyce, Loebl and Co., Ltd., Model E12MK III), the optical density of the polymer-coated rings was measured. Figure 4 shows the optical density of the deposit and nitrogen atom concentration *vs.* the position of the rings relative to the injector. Note that the maximum optical density occurs within 1 cm (corresponding to about 3.5 msec) of the maximum reaction rate.

The optical density can be assumed to be approximately proportional to the amount of polymer deposited on the ring. If the radicals diffuse to the wall and polymerize there while the gas as a whole is flowing down the reactor, the amount of polymer formed at any locus is proportional to the concentration of free radicals at that locus. The near coincidence of maximum reaction rate with maxi-

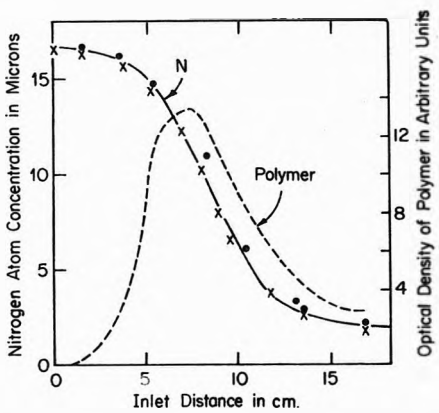

Figure 4. Nitrogen atom concentration and optical density of polymer *vs.* inlet distance: (N) in μ: ●, recorded after 11 min; ×, recorded after 125 min. Conditions: N_2 flow = 250 cc (NTP)/min; (N_2) = 3.6 Torr; $(C_2N_2)_0$ = 4.75 μ; $(N)_0$ = 16.5 μ.

mum polymer formation indicates that this is so and that the wall accommodation coefficient for the free radicals is near unity. The alternate assumption, that polymerization occurs in the gas phase and is followed by condensation on the walls, would require the polymer deposit to maximize further down the reactor tube because of longer diffusion time of the polymer. Polymer formation in this reaction is evidently a heterogeneous process, and since the wall accommodation coefficient is near unity, it must involve free radicals.

Free CN radicals were observed mass spectrometrically about the instant of fastest N atom consumption, but the concentration was too small for quantitative measurement. A semiquantitative estimate indicates a partial pressure of the order of 0.1 μ.

It is possible to make an indirect estimate of the maximum CN concentration. Since the composition of the polymer indicates that it is composed mainly of CN radicals, we assume for simplicity that only these are involved. The total weight of the polymer, 8.8 mg, corresponds to 2×10^{20} CN radicals deposited in 8.45×10^3 sec, or 2.5×10^{16} CN radicals/sec for the total deposit. About two-thirds of the CN is polymerized when (CN) is near its maximum value, *i.e.*, between the 5- and 1-cm loci, see Figure 4. Thus in this region the rate of CN radical deposition is 3.3×10^{15} CN/sec per cm length. Since 1-cm length of reactor tube corresponds to 3.8 cc, the rate of CN radical deposition is 8.7×10^{14} CN sec^{-1} cc^{-1}. Taking the mean diffusion time to be about 3 msec,[9,16] we estimate $(CN)_{max} = 2.6 \times 10^{12}$ radicals/cc, or on the order of 0.1 μ. This value agrees well with other estimates of $(CN)_{max}$ ($\lesssim$ 0.1 μ) from direct observations of the CN radical.[7]

Oxygen and ammonia and to a lesser extent hydrogen inhibit the cyanogen active-nitrogen reaction. The additives were introduced downstream of the discharge, about 150 msec upstream of the cyanogen injection. The fact that O_2 and NH_3 have about the same quenching efficiencies and are 50 times better quenchers than H_2 has been reported before.[17] We have additionally found that when O_2 is the quencher, the reaction can still be brought to the same degree of completion, $(N)_\infty$, as in the absence of quencher, if enough extra cyanogen is added. But even the additions of very large amounts of cyanogen cannot compensate completely for the quenching effect of added H_2 or NH_3.

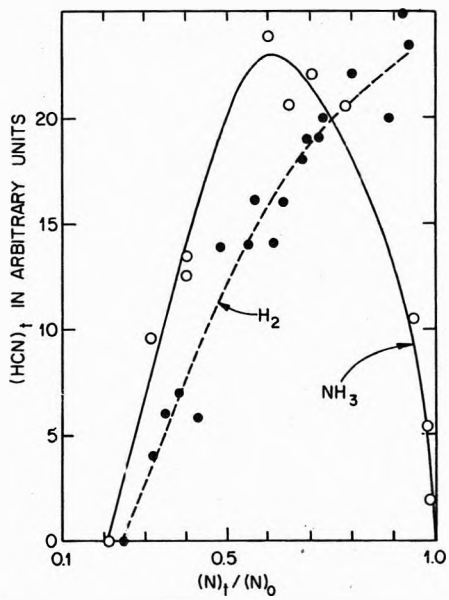

Figure 5. Quenching by H_2 and NH_3. $(HCN)_t$ *vs.* $(N)_t/(N)_0$: ●, H_2 added (up to 250 μ maximum); ○, NH_3 added (up to 4.2 μ maximum). Conditions: (N_2) = 1.96 Torr; $(C_2N_2)_0$ = 4.3 μ; $(N)_0$ = 14.0 μ; t = 37 msec.

Scavenging of CN radicals has been suggested as the main mechanism of H_2 and NH_3 quenching. To test this, HCN (m/e 27) was monitored at 37 msec of reaction time as H_2 and NH_3 were added; Figure 5 shows the results, the x axis, expressed as $(N)_t/(N)_0$, increasing with increased additions of NH_3 or H_2. When $(N)_t/(N)_0 = 1.0$ there is effectively no reaction, hence complete quenching. Note the striking difference between the two plots of HCN production; when NH_3 is added, the amount of HCN first increases, but larger additions, causing extensive quenching, result in decreasing amounts of HCN which tend to zero; on the other hand, increasing quenching by H_2 causes a monotonic increase in HCN.

Evidently NH_3 quenches the cyanogen reaction not only by scavenging CN radicals to form HCN but also by reaction with a precursor of CN. It is well known[18] that NH_3 is an efficient scavenger of N_2 ($A^3\Sigma$) and if that is the initiator of the cyanogen-active nitrogen reaction, its removal would inhibit the production of CN radicals and so decrease the amount of HCN. H_2, on the other hand, is a very inefficient scavenger of N_2 ($A^3\Sigma$),[19] and its inhibitory effect must be entirely due to a reaction with CN.

O_2 quenches by reactions with C atoms ($k = 3.3 \times 10^{-11}$ cc/sec[20,21] and CN radicals ($k = 8 \times 10^{-12}$ cc/sec[17,22]), the competition with C_2N_2 for C atoms explaining why quenching can be suppressed by excess C_2N_2. The reaction goes "to completion" because the O atoms produced in this quenching act themselves (see below) as chain carriers.

It has been shown[23] that addition of O atoms (from the reaction[24] NO + N → N_2 + 0) greatly increases the luminosity of the cyanogen-active nitrogen reaction flame. We find that oxygen atoms have a strong influence on the kinetics of this reaction as well.

The general effect of the introduction of NO about 150 msec upsteam of the cyanogen injector is to decrease the chain length by increasing the consumption of cyanogen. Small additions of NO (a few per cent of $(N)_0$) accelerate the reaction by reducing the induction period and extending the N atom recombination to lower values of $(N)_\infty$

without much effect on the maximal rate. When, however, enough NO has been added to reduce $(N)_0$ to about 6 μ, the reaction ceases, as it does under these conditions also in the absence of oxygen atoms.

Since the reaction of oxygen atoms with cyanogen is slow ($k = 1.2 \times 10^{-16}$ cc/sec at room temperature[17,25]) compared with initiation reaction i[26] and the reaction O + CN → CO + N would quench the overall reaction, we suggest that some other intermediate (see below) is involved in a process that does not break the N atom recombination chain but prevents the re-formation of cyanogen.

2. Experiments with Isotopically Labeled Cyanogen. (a) Heavy Carbon. No isotopic scrambling was observed when ^{13}C labeled cyanogen was introduced into active nitrogen in the reactor which had been coated with polymer prepared from unlabeled cyanogen. The mass spectrum showed a small peak at m/e 80 which corresponds to $^{13,13,13,13}C_4^{14,14}N_2$. Thus the identity of the peak at m/e 76 observed with unlabeled cyanogen is put on a firm basis.

For the study of reaction kinetics ^{13}C cyanogen was mixed with ^{12}C cyanogen to give the following initial isotopic cyanogen mixture

m/e	%
52	48.0 ± 0.5
53	10.8 ± 0.2
54	41.2 ± 0.5

Figure 6 shows the concentration *vs.* time profiles for nitrogen atoms and each isotopic cyanogen. The rate of carbon scrambling in cyanogen, $R^{12,13}$, is defined as

$$R^{12,13} = d(53)/dt = d(53)/dt)_{meas} + (d(53)/dt)_{lost\ by\ reaction}$$

$$= (d(53)/dt)_{meas} + [(53)/(\Sigma)][(d\Sigma)/dt]$$

where Σ is the sum of all cyanogen isotopes. The second term in the above expression is only about 10% of the rate of scrambling when the rate of scrambling is maximal, but accounts for about 50% of the rate of scrambling near the end of the reaction, when (53) is about 50% of the total cyanogen.

From Figure 6 one can conclude that carbon scrambling involves the participation of a reactive intermediate which reaches maximum concentration during the fastest part of the overall reaction.

We shall define per cent scrambling as follows

$$\%\ \text{carbon scrambling} = 100\{[(53/\Sigma)^{expt} - (53/\Sigma)_0]/[(53/\Sigma)^{scr} - (53/\Sigma)_0]\}$$

where $(53/\Sigma)^{expt}$ is the experimentally determined ratio at long reaction times (75 msec), and $(53/\Sigma)^{scr}$ is the ratio calculated assuming that *all* carbon originally in the mixture has been randomized by reaction. Thus with ^{12}C = 53.4% and ^{13}C = 46.6%, complete scrambling should give the following isotopic cyanogen distribution

m/e	%
52	28.5
53	49.7
54	21.8

Table II shows that almost 100% scrambling has occurred when just enough cyanogen is added to bring the nitrogen atom recombination to completion by the observation time. More cyanogen causes the per cent scrambling to decrease while the total amount of cyanogen undergoing scrambling continues to increase.

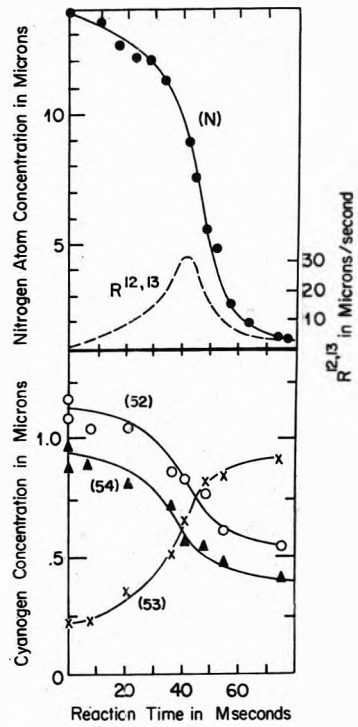

Figure 6. ^{12}C–^{13}C scrambling in cyanogen *vs.* reaction time. Top: solid line and ●, (N) in μ; broken line, $R^{12,13}$ in μ/sec. Bottom: O, (m/e 52) = ($^{12,12}C_2N_2$) in μ; X, (m/e 53) = ($^{12,13}C_2N_2$) in μ; ▲, (m/e 54) = ($^{13,13}C_2N_2$) in μ. Conditions: (N_2) = 3.00 Torr; $(C_2N_2)_0$ = 2.33 ± 0.2 μ; $(N)_0$ = 13.7 μ.

TABLE II: Carbon Scrambling in the ^{12}C–^{13}C Cyanogen Mixture *vs.* Initial Cyanogen Concentration[a]

$(N)_t/(N)_0$	$(C_2N_2)_0$, μ	Obsvd % scrambling	Obsvd amount of scrambled cyanogen Φ_s, μ	Calcd amount of scrambled cyanogen Φ_s, μ
0.82	1.0	52	0.5	
0.10	1.8	95	1.7	1.7
≤0.10	2.8	83	2.3	2.4
≤0.10	4.7	71	3.3	3.3
≤0.10	5.6	64	3.6	3.5
≤0.10	8.1	49	4.0	4.0

[a] Conditions: (N_2) = 3.00 Torr, $(N)_0$ = 13.8 μ, t = 75 msec. The consumption of nitrogen atoms is terminated by the observation time for $(C_2N_2)_0 > 2$ μ.

The use of the isotopic cyanogen mixture made it difficult to measure with accuracy the isotopic composition of C_4N_2 because its small amount was spread over five mass spectral peaks. Thus these findings must be regarded as only semiquantitative, but they do indicate (Table III) that ^{13}C and ^{12}C are completely scrambled (randomized) in C_4N_2. Excess cyanogen does not change this isotopic distribution in dicyanoacetylene. The sum of the five C_4N_2 peak heights indicates that 18.5 ± 5.0% of the C_2N_2 lost becomes C_4N_2. This figure compares well with the previously determined value of about 20%.

(b) Heavy Nitrogen. Isotopically enriched $C_2^{15,15}N_2$ was used as such. In the absence of active nitrogen the passage of $C_2^{15,15}N_2$ through a freshly cleaned Pyrex reactor or one with heavy polymer deposit (from ordinary cyanogen)

TABLE III: Isotopic Composition of Dicyanoacetylene Formed from the $^{12}C-^{13}C$ Cyanogen Mixture

	Relative mass peak heights, m/e				
	76	77	78	79	80
Experiment	7.2 ± 3.0	29.9 ± 4.0	32.1 ± 4.0	25.4 ± 4.0	5.5 ± 3.0
Predicted for complete scrambling	8.1	28.2	37.1	21.9	4.7

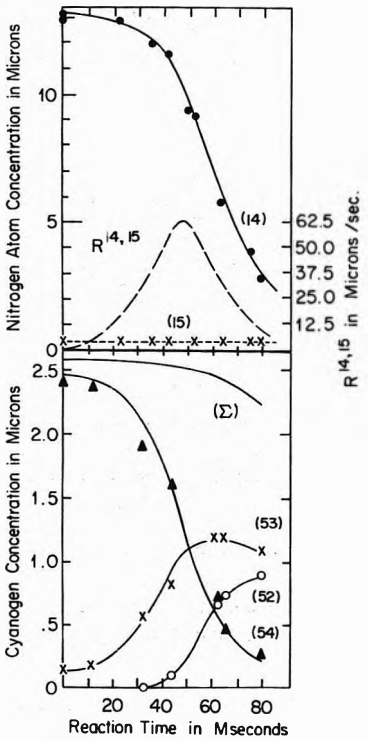

Figure 7. $^{14}N-^{15}N$ scrambling in cyanogen *vs.* reaction time. Top: solid line and ●, (^{14}N) in μ; dotted line and ×, (m/e 15); broken line, $R^{14,15}$ in μ/sec. Bottom: ○, (m/e 52) = ($C_2{}^{14,14}N_2$) in μ; ×, (m/e 53) = ($C_2{}^{14,15}N_2$) in μ; ▲, (m/e 54) = ($C_2{}^{15,15}N_2$) in μ; Σ, (m/e 52) + (m/e 53) + (m/e 54). Conditions: (N_2) = 3.00 Torr; ($C_2{}^{15,15}N_2$)$_0$ = 2.5 ± 0.2 μ; (N)$_0$ = 13.3 μ.

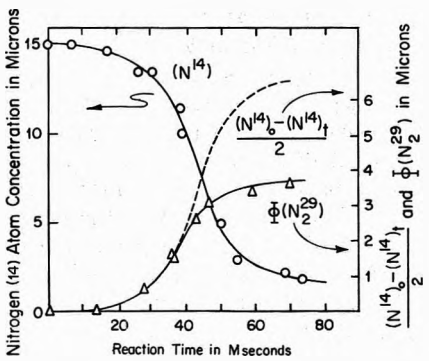

Figure 8. Formation of $^{29}N_2$, $\Phi(^{29}N_2)$, (^{14}N), and $\Phi(-^{14}N/2)$ *vs.* reaction time: ●, (^{14}N); △, $\Phi(^{29}N_2)$; dashed line, $\Phi(-^{14}N/2)$. Conditions: (N_2) = 3.05 Torr; ($C_2{}^{15,15}N_2$)$_0$ = 2.08 μ; (^{14}N)$_0$ = 15.1 μ.

TABLE IV: Yields of $^{28}N_2$, $^{29}N_2$, and $^{30}N_2$ *vs.* ($C_2{}^{15,15}N_2$)$_0$[a]

$\Phi(^{28}N_2)$,[b] μ	$\Phi(^{29}N_2)$, μ	$\Phi(^{30}N_2)$, μ	($C_2{}^{15,15}N_2$)$_0$, μ
2.60	3.95	0.05	2.0
2.02	4.40	0.18	3.3
1.18	5.20	0.22	6.0
0.20	6.10	0.30	10.0

[a] Conditions: (N_2) = 3.05 Torr, (^{14}N)$_0$ = 15.1 μ, (^{14}N)$_\infty$ = 1.9 μ, t = 70 msec. [b] $\Phi(^{28}N_2)$ is obtained by difference: $\Phi(^{28}N_2) = 6.6\mu - \Phi(^{29}N_2) - \Phi(^{30}N_2)$. The reaction is "complete" at the observation time for (C_2N_2)$_0$ > 2 μ.

resulted in no isotopic scrambling. Upon reaction with active nitrogen a large amount of nitrogen scrambling did occur in the cyanogen, the $^{14}N/^{15}N$ ratio increasing as the reaction progressed. The bottom section of Figure 7 illustrates the concentration *vs.* time profiles for $C_2{}^{14,14}N_2$ (52), $C_2{}^{14,15}N_2$ (53), and $C_2{}^{15,15}N_2$ (54), as well as for Σ, the total cyanogen concentration. Note that the replacement of ^{15}N by ^{14}N proceeds stepwise since as m/e (54) decreases (53) increases, but (52) begins to increase measurably only when much (53) has been formed.

M/e 15 did not increase above its level in absence of cyanogen. Hence, the remaining nitrogen atoms are the unreacted nitrogen atoms and not the re-formed N atoms as has been suggested elsewhere.[11]

The rate of nitrogen scrambling in cyanogen $R^{14,15}$, will be defined as $R^{14,15} = \frac{1}{2}(|d(52)| + |d(53)| + |d(54)|)/dt$. This function of time is plotted in the top section of Figure 7. The maximum rate of this scrambling also occurs when the nitrogen atom decay is most rapid.

The elucidation of the mechanism of N_2 production is paramount to understanding the entire cyanogen active nitrogen reaction; the use of $C_2{}^{15,15}N_2$ made it possible to monitor the products, $^{29}N_2$ and/or $^{30}N_2$. In Figure 8 the dashed line represents the total N_2 production expected if all nitrogen atoms eventually recombine to form N_2. Note that in the early part of the reaction (less than 40 msec) all the nitrogen formed is $^{29}N_2$, no $^{28}N_2$ being formed until later.

As ($C_2{}^{15,15}N_2$)$_0$ is increased, more $^{29}N_2$ is formed. In fact, if enough ($C_2{}^{15,15}N_2$)$_0$ is added, practically all of the molecular nitrogen formed is the mixed $^{29}N_2$. This is illustrated in Table IV which also shows a significant increase in m/e 30, $^{15,15}N_2$. For example, with ($C_2{}^{15,15}N_2$)$_0$ = 10 μ, ($^{29}N_2$) = 6.1 μ, ($^{30}N_2$) = 0.30 μ, and since the total new N_2 should be 6.6 μ, by difference ($^{28}N_2$) = 0.20 μ.

The peak at m/e 30 is believed to be $^{15,15}N_2$, since in the absence of nitrogen atoms no m/e 30 peak appeared when as much as 16 μ of cyanogen was added. The amount of $^{30}N_2$ produced is kinetically significant because only 0.022 μ of $^{30}N_2$ should be produced from ^{15}N atoms naturally occurring in normal active nitrogen. The observed concentration is 13.5 times greater and may be due to the process $CN + C_2N_2 \rightarrow N_2 + C_3N$ suggested by Boden and Thrush which occurs at higher temperatures (687°K) partly on the walls of the reaction vessel.[17] This four-center exothermic reaction (−44 kcal/mol) probably has a significant activation energy as a homogeneous gas-

phase process, but as a wall reaction it might be the source of $^{30}N_2$ at large concentrations of $C_2^{15,15}N_2$ in these experiments.

Discussion

Our results contain enough new information to make possible a meaningful examination of alternative reaction mechanisms. The extensive isotopic scrambling indicates that most cyanogen molecules are intimately involved in the reaction, but not *via* dissociation into two CN since these radicals recombine too slowly[27,28] to account for the observation that little cyanogen is consumed. In the ABK mechanism the CN radicals are alternately consumed and regenerated in reactions 1 and 2. This *cannot* be the major sequence for the recombination of nitrogen atoms because it predicts that $^{29}N_2$ must be less than 50% of the total N_2 produced even when $C_2^{15,15}N_2$ alone is present. Starting with $C^{15}N$ and ^{14}N, reaction 2 gives 50% ($^{29}N_2$ and $C^{14}N$) and 50% ($^{28}N_2$ and $C^{15}N$). In the next cycle then only 25% of $^{29}N_2$ would be formed and so on. However, Table IV shows that nearly 95% (equivalent to nearly 100%, if the cyanogen were 100% $C_2^{15,15}N_2$) of the N_2 produced is $^{29}N_2$ when enough $C_2^{15,15}N_2$ is added. This, and the facts that the polymer is carbon rich (and not nitrogen rich) and that C_4N_2 is formed, indicates that the ABK mechanism is incorrect.

The SJ mechanism (reactions 3–5) also does not explain the results, including the extensive isotopic scrambling in cyanogen. Also the predicted chain length is much too short. Finally the SJ mechanism predicts that only two-thirds of the nitrogen is produced as $^{29}N_2$ and one-third is $^{28}N_2$ (independent of the initial $C_2^{15,15}N_2$ concentration). This follows because if at the start of the reaction all cyanogen is $C_2^{15,15}N_2$ and somehow a trace of CN is formed, reactions 4 and 5 give a CN isotopic ratio of $(C^{15}N)/(C^{14}N) = 2$. However, our experiments show that the percentage of $^{29}N_2$ can reach almost 100% and that this percentage depends on the initial cyanogen concentration.

The reasoning in the previous paragraph is not valid if reaction 6

$$CN^* + C_2N_2 \longrightarrow CN + NC\text{-}CN^* \qquad (6)$$

is very much faster than reaction 3. Then, in the presence of an excess of $C_2^{15,15}N_2$, reaction 6 would convert $C^{14}N$ produced in reaction 5 to $C^{15}N$, and $^{29}N_2$ *via* reaction 3 would be the exclusive product. However, experimentally (Figures 6 and 7) the maximum rate of nitrogen atom recombination (600 μ/sec) is seen to be more than 10 times greater than the maximum rate of isotopic scrambling in cyanogen.

We reach the same conclusion by another approach. Assume reaction 3 is the rate-determining step. Then $(-d(N)/dt)_{max} = k_3(CN)_{max}(N)_t$. Substitution of appropriate values from Figure 6 yields $k_3 = 1 \times 10^{-11}$ cc/sec. This value for k_3 is consistent with the results of Slack and Fishburne,[29] who studied the decomposition of the CN radical in shock waves at 5500–10,000°K. They suggested that reaction 3 occurred in their system with a rate constant $k_3 > 7 \times 10^{-11}$ cc/sec with virtually no temperature dependence.

We now make an estimate for k_6, by assuming that the scrambling occurs *via* reaction 6. Then for carbon scrambling in cyanogen

$$d(53)/dt = k_6(54)(26) + k_6(52)(27) - \tfrac{1}{2}k_6(53)((26) + (27))$$

where (52) = $(^{12,12}C_2^{14,14}N_2)$, (53) = $(^{12,13}C_2^{14,14}N_2)$, (54) = $(^{13,13}C_2^{14,14}N_2)$, (26) = $(^{12}C^{14}N)$, (27) = $(^{13}C^{14}N)$. Since (^{12}C) very nearly equals (^{13}C) in the isotopic carbon cyanogen mixture, at all times (26) $\cong$ (27) $\cong$ (CN)/2 and thus

$$\frac{d(53)/dt}{((54) + (52) - (53)_t} = k_6((CN)/2)_t$$

Substitution of appropriate values from Figure 6 yields $k_6 = 7 \times 10^{-12}$ cc/sec. Using these values of k_3 and k_6, we calculate that even in the early part of the reaction (Figure 8) when $C_2^{15,15}N_2$ is nearly pure, reaction 3 is 15 times faster than reaction 6. Thus radical exchange reaction 6 is unimportant in converting $C^{14}N$ into $C^{15}N$. The SJ mechanism, even with reaction 6, does not explain the high yield of $^{29}N_2$.

Actually the above estimated value of k_6 is unreasonably large because the reaction probably requires at least a small activation energy[30,31] and therefore in the above estimate the preexponential factor must be nearly equal to hard-sphere collisional frequency. This is quite improbable for a reaction involving two stable multiatom molecules. We conclude, therefore, that CN radical exchange with molecular cyanogen is not important in our system.

A mechanism which explains many of the observations involves the following reactions

$$N_2(A^3\Sigma) + C_2N_2 \longrightarrow 2CN + N_2 \qquad (i)$$

$$N + CN \longrightarrow N_2 + C \qquad (3)$$

$$C + C_2N_2 \longrightarrow C_3N_2^* \qquad (7)$$

$$C_3N_2^* + N_2 \longrightarrow C_3N_2 + N_2 \qquad (8)$$

$$C_3N_2^* \longrightarrow C_2N + CN \qquad (9)$$

$$C_2N + N \longrightarrow 2CN \qquad (5)$$

$$C_3N_2 + N \longrightarrow C_2N_2 + CN \qquad (10)$$

$$C, C_3N_2, C_2N, CN \longrightarrow \text{polymer (wall)} \qquad (W)$$

$$2C_2N + N_2 \longrightarrow C_4N_2 + N_2 \qquad (D)$$

Reaction i of N_2 ($A^3\Sigma$) (produced by the recombination of N atoms) with cyanogen has been shown[26] to result in the C_2N_2 ($^3\Sigma_u^+ - {}^1\Sigma_g^+$) emission spectrum and some dissociation into CN radicals. Reaction 3 is the main pathway of N_2 production. Reaction 7 is assumed to result in the insertion of a carbon atom into the C–C bond of cyanogen to give $C_3N_2^*$, an excited dicyanocarbene radical.[32] Reaction 9, fragmentation of $C_3N_2^*$, followed by reaction 5, is the chain-branching step.

The preponderance of isotopic exchange in cyanogen without extensive loss of cyanogen means that chain-branching reactions 9 and 5 occur infrequently compared to the chain-propagating sequence 3, 7, 8, and 10. This sequence ensures that cyanogen is isotopically scrambled with respect to both carbon and nitrogen, without appealing to a massive dissociation of C_2N_2 into CN radicals.

The validity of this mechanism hinges on the supposition that $\Delta H_f°(C_2N) < +150$ kcal/mol; otherwise reaction 9 is endothermic. Since $\Delta H_f°(C_2N_2) = +74$ kcal/mol, the above value implies that ΔH for the reaction $C_2N_2 \rightarrow C_2N + N$ is $\leq +189$ kcal/mol. This is reasonable since the ΔH for the reaction $CN \rightarrow C + N$ is currently estimated[33] to be +180 kcal/mol. A recent determination of $\Delta H_f°(C_2N)$[34] places the limits $+149 < \Delta H_f°(C_2N) < +172$ kcal/mol; other workers have used values from +133 to +189 kcal/mol.

Reaction 7 also deserves comment. Thermalized radioactive carbon atoms formed by nuclear methods[35] insert into the C–H bond, attack the π bond of unsaturated hydrocarbons, and abstract hydrogen atoms from saturated hydrocarbons. Inorganic π bonded molecules (O_2, N_2O) react mainly by end-on attack with a large cross section (greater than 0.3 hard sphere).[36] However, Husain and Kirsh[20] have recently shown that carbon atoms in the ^1D state are far more reactive than those in the ^3P state in attacking C–C single bonds. Thermochemical considerations and total spin conservation require that reaction 3 result in C (^3P). Hence to assume that reaction 7 results in the insertion of the carbon atom into the C_2N_2 molecule, which is necessary to explain its isotopic scrambling, one must appeal to the large extent of π bond character in the C–C bond of cyanogen.[37] An alternative is that C (^3P) attacks C_2N_2 end-on and that this is followed by a rearrangement which internalizes the attacking carbon atom, analogously to the process in methyl isocyanide: CH_3–NC $\rightarrow$ CH_3–CN. It has been shown[36] that C (^3P) is an efficient reagent with molecules susceptible to end-on attack.

Reaction 10 which provides for nitrogen scrambling may be visualized as

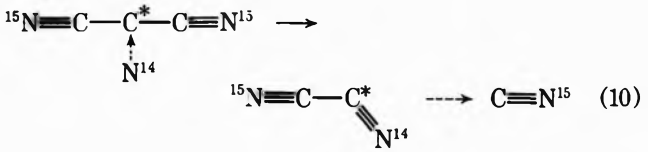

$$^{15}N{\equiv}C{-}C^{*}{-}C{\equiv}N^{15} \longrightarrow {}^{15}N{\equiv}C{-}C^{*} \dashrightarrow C{\equiv}N^{15} \quad (10)$$

where C* represents the inserted carbon atom. This reaction, followed by (3), predicts that N_2 will be produced predominantly as $^{29}N_2$ in the early stages of the reaction when $C_2{}^{15,15}N_2$ is the predominant species. The other alternative, reaction 6, followed by (3) has already been shown to be unimportant. It should be noted that the proposed chain sequence involving (10) provides also for the observed stepwise isotopic nitrogen scrambling in cyanogen

$$C_2{}^{15,15}N_2 \longrightarrow C_2{}^{14,15}N_2 \longrightarrow C_2{}^{14,14}N_2$$

If the proposed mechanism is correct and the wall accommodation coefficient in reaction W is near unity for all radical species, the composition of the wall polymer, $C_{1.16}N$, suggests that the volume concentration of CN radicals is much greater than those of the other reaction intermediates. Thus, reaction 3 of CN with N atoms must be slower than the reaction of C with cyanogen or of C_3N_2 with N and is rate determining.

Kley, *et al.*,[12] find that in the blue flame condition "a steady state equilibrium is rapidly established which lies completely on the side of the C atom." Our findings in the regular flame condition are that $(CN)_{ss} > (C)_{ss}$, and that a substantial induction period exists with little dissociation of cyanogen.

In terms of this mechanism, the expression for the instantaneous chain length is

$$\frac{-d(N)}{-d(C_2N_2)} = \frac{k_3(CN)(N) + k_{10}(C_3N_2)(N)}{k_7(C)(C_2N_2) - k_{10}(C_3N_2)(N)} \quad (I)$$

Expressing the steady-state concentrations, $(C)_{ss}$, $(C_3N_2)_{ss}$, and $(C_3N_2)_{ss}$, in terms of (CN), (C_2N_2), (N), and (N_2), we arrive at a steady-state equation

$$\frac{-d(N)}{-d(C_2N_2)} = \frac{2k_8(N_2) + k_9}{k_9} \quad (II)$$

Since the chain length is about 40, $k_8(N_2) = 20\ k_9$, the stabilization of the excited dicyanocarbene radical, $C_3N_2^*$, being apparently much more common than decomposition. This finding means that $k_9 < 10^7$ sec^{-1}, an improbably small value for such a simple molecule unless the internal energy in $C_3N_2^*$ is barely enough for reaction 9.

Equation II predicts that the chain length is independent of the cyanogen or nitrogen atom concentrations but depends on carrier gas pressure. This is roughly confirmed by the finding of SJ[11] that at their low pressures the chain length is very short. Moreover, the lack of dependence of the chain length on the nitrogen atom concentration suggests qualitatively that the chain length should also be independent of time. However, when the loss of CN and C_3N_2 on the walls is included in the steady-state treatment, the expression for the chain length becomes

$$\frac{-d(N)}{-d(C_2N_2)} = \frac{2k_{10}(N) + k_W}{k_{10}(N)(k_9/k_8(N_2)) + k_W} \quad (III)$$

This equation predicts that the chain length should decrease with (N). Indeed, the chain length does decrease slightly as (N) approaches $(N)_\infty$, see Table I. In order for the chain length to be constant to within 50% over the entire reaction (as observed), $k_{10}(N)_\infty(k_9/k_8(N_2)) \geq k_w \approx 200$ sec^{-1}, or $k_{10} \geq 1 \times 10^{-10}$ cc/sec.

The decrease in the chain length upon addition of oxygen atoms may be due to their reaction with C_3N_2 radicals

$$C_3N_2 + O \longrightarrow CO + 2CN \quad (11)$$

This reaction is spin allowed, exothermic by 40 kcal/mol, and explains the acceleration of the overall process, because the inefficient chain branching sequence (9) and (5) is replaced by a fast reaction 11. The expression for the chain length becomes

$$\frac{-d(N)}{-d(C_2N_2)} = \frac{2k_{10}(\bar{N}) + k_{11}(\bar{O})}{k_{10}(\bar{N})(k_9/k_8(N_2)) + k_{11}(\bar{O})} \quad (IV)$$

Using eq IV and choosing for best fit $k_{11} = 1.3 \times 10^{-10}$ cc/sec, the calculated dependence of the chain length on the oxygen atom concentration is found to describe well the experiments, as shown in Table V.

The observed effect of oxygen atoms suggests that perhaps reaction 9, being endothermic, does not occur and that $C_3N_2^*$ breaks up only by the reversal of (7). The chain branching could then be due to reactions of oxygen atoms formed in the electric discharge from the impurities in the nitrogen used. These impurities (H_2O, O_2) could produce up to 0.03–0.005% of oxygen atoms, *i.e.*, up to 5% of the atomic nitrogen concentration in our experiments. If reaction 11 is replaced by the sequence of reactions all of which are exothermic

$$C_3N_2 + O \longrightarrow NCO + C_2N \quad (11a)$$

$$NCO + N \longrightarrow CO + N_2 \quad (11b)$$

$$C_2N + N \longrightarrow 2CN \quad (5)$$

the net effect would be that of reactions 9 and 5. Since no experiments were performed to test this possibility we will not pursue the subject further.

When enough N atoms have been converted to O atoms by reaction with NO to reduce sufficiently their concentration in the reaction zone, the overall reaction becomes very slow, as it does also in the absence of O atoms when

TABLE V: Effect of Oxygen Atoms on the Chain Length, $\bar{\nu}$[a]

Chain length, $\bar{\nu}$			
Exptl	Calcd	$(O)_0$, μ	$(N)_0$, μ
40	40	0	13.3
16.7	17.2	0.675	12.6
11.2	11.4	1.28	12.0
7.7	7.9	2.10	11.2
5.6	5.6	3.00	10.3

[a] Conditions: (N_2) = 3.00 Torr, t = 60 msec.

$(N)_0$ is sufficiently small. The cause is that the N_2 $(A^3\Sigma)$ concentration becomes very low and hence the initiation reaction i nearly ceases. In virtual absence of C_3N_2 the O atoms cannot accelerate the reaction.

When both atomic concentrations are high, other reactions may become important. Thus oxygen atoms may retard the overall process *via* reaction 12[17]

$$CN + O \longrightarrow CO + N \qquad (12)$$

and the observations of SJ[23] that extremely intense CN emission results from addition of much atomic oxygen could be explained by reaction 13

$$C_2N + O \longrightarrow CO + CN^* \qquad (13)$$

where CN* is electronically excited.

The proposed mechanism correctly describes the dependence of the degree of carbon scrambling in cyanogen on the initial cyanogen concentration as shown in Table II. We write $d(\Phi_s)/dt = k_7(C)(\Phi_n)$ where (Φ_s) and (Φ_n) are the amounts of scrambled and unscrambled cyanogen, respectively, so that $(\Phi_s) + (\Phi_n) \simeq (C_2N_2)_0$. This ignores the small amount of cyanogen ($\sim$0.3 μ) consumed in the reaction and so introduces less than a 10% error. Combining the above expression with that for $(C)_{ss}$, one obtains

$$d(\Phi_s)/dt = k_3(N)(CN)[(C_2N_2)_0 - (\Phi_s)]/(C_2N_2)_0$$

and integrating

$$(\Phi_s) = (C_2N_2)_0[1 - e^{-(k_3(\bar{N})(\bar{CN})t)/(C_2N_2)_0}] \qquad (V)$$

where $(\bar{N})$ and $(\bar{CN})$ are the average concentrations during the reaction time t. The calculated values of Φ_s in Table II were obtained with eq V, using the values $k_3 = 1 \times 10^{-11}$ cc/sec, $(\bar{N})$ = 6 μ, $(\bar{CN})$ = 0.05 μ, and t = 68 msec.

We shall now derive an expression for $(CN)_{max}$, the peak CN radical concentration, and show that it is a measure of the maximum rate of the overall reaction. As noted earlier, additions of cyanogen to active nitrogen cause an increase in the maximum rate of nitrogen atom consumption until the "regular flame condition" is achieved. Further additions of cyanogen shorten the induction time, but do not change $(-d(N)/dt)_{max}$, see Figure 1. If the rate determining step is reaction (3), then $(-d(N)/dt)_{max} = \frac{1}{2}k_3(N)_0(CN)_{max}$. Since this quantity is independent of cyanogen concentration in the "regular flame condition," $(CN)_{max}$ also must remain constant. Setser and Thrush[38] report indeed that $(CN)_{ss}$ approached a constant value with increasing cyanogen addition in their study of CN emission from the cyanogen–active nitrogen flame.

According to the proposed mechanism, qualitatively, d(CN)/dt = (initial rate of production) + (rate of branching) − (rate of removal). The first term is independent of (CN), but the latter two terms are not, and thus

$$(CN)_{max} = k_i(N_2(A^3\Sigma))_0(C_2N_2)/[\text{quenching frequency} - (3k_3k_9(N)/k_8(N_2))]$$

If the chain breaking reactions are (W) and (Q), where (Q) is[30]

$$CN + C_2N_2 \longrightarrow \cdots\cdots \qquad (Q)$$

and $((N_2)\ A^3\Sigma)_0 \propto (N)_0(N_2)$ as Boden and Thrush have shown,[3a] then the above expression becomes

$$(CN)_{max} \propto \frac{(N)_0(N_2)(C_2N_2)}{k_Q(C_2N_2) + k_W - k_B(\bar{N})} \qquad (VI)$$

where $k_B = 3k_3k_9/(k_8(N_2))$ is the "chain-branching rate constant." This relation shows that in the "regular flame condition" the value of the term not dependent on (C_2N_2), namely, $(k_W - k_B(\bar{N}))$, must be small to make $(CN)_{max}$ independent of (C_2N_2). The "explosions," reported by others[3b,11] at low total pressures and low concentrations of cyanogen which we have observed also, can be understood in terms of eq VI; when the value of $k_B(\bar{N})$ approaches that of $k_Q(C_2N_2) + k_W$, (CN) becomes very large.

Dicyanoacetylene is formed by the combination of two C_2N radicals

$$d(C_4N_2)/dt = k_D(C_2N)^2(N_2) \qquad (VII)$$

The mechanism predicts $(C_2N)_{max} = k_9k_3(CN)/(k_5k_8(N_2))$. Combining this expression for $(C_2N)_{max}$ with eq VI and VII, we obtain for the yield of C_4N_2

$$\Phi(C_4N_2) \propto (N)_0^2(N_2)$$

which is the experimentally observed relation.

Since C_4N_2 reacts rapidly with N atoms,[39] its concentration should remain low until the N atoms are consumed, which explains the observed lag in its production.

The proposed mechanism, to be sure, is far from proven and it includes reaction 7 whose dynamics are questionable. But it describes very well the isotopic scrambling and overall features of this very complex chain reaction and is, we believe, preferable to other explanations.

Acknowledgment. We wish to thank the National Science Foundation for a grant which made this work possible.

References and Notes

(1) This paper is abstracted from the Doctoral Thesis by M. Berger presented to the Department of Chemistry, Harvard University, 1972.
(2) See A. N. Wright and C. A. Winkler, "Active Nitrogen," Academic Press, New York, N. Y., 1968. The major constituents of our active nitrogen are, roughly, 3.0 Torr N_2 $(X^1\Sigma)$, 0.03 Torr N (^4S), and 0.000001 Torr N_2 $(A^3\Sigma)$.
(3) (a) J. C. Boden and B. A. Thrush, *Proc. Roy. Soc., Ser. A*, **305**, 93 (1968); (b) K. Bayes, *Can. J. Chem.*, **39**, 1074 (1961).
(4) N. Kiess and H. P. Broida, *Symp. (Int.) Combust., [Proc.]*, 7th, (London), (1959) 207.
(5) D. Setser and B. Thrush, *Nature (London)*, **200**, 864 (1964).
(6) H. E. Radford and H. P. Broida, *J. Chem. Phys.*, **38**, 644 (1964).
(7) T. Iwa, M. Savadatti, and H. P. Broida, *J. Chem. Phys.*, **47**, 3861 (1967).
(8) G. M. Provencher and D. J. McKenny, *Chem. Phys. Lett.*, **10**, 365 (1971).
(9) C. Haggart and C. A. Winkler, *Can. J. Chem.*, **38**, 329 (1960).
(10) C. A. Arrington, O. O. Bernadini, and G. B. Kistiakowsky, *Proc. Roy. Soc., Ser. A*, **310**, 161 (1969).
(11) D. R. Safrany and W. Jaster, *J. Phys. Chem.*, **72**, 3305 (1968).
(12) D. Kley, N. Washida, K. H. Becker, and W. Groth, *Chem. Phys. Lett.*, **15**, 45 (1972).
(13) (a) L. Elias, *J. Chem. Phys.*, **44**, 3810 (1966); (b) H. von Weys-

senhoff and M. Patapoff, *J. Phys. Chem.*, **69**, 1756 (1965).
(14) C. A. Arrington, Ph.D. Thesis, Harvard University, 1965.
(15) D. Rapp and P. Englander-Golden, *J. Chem. Phys.*, **43**, 1464 (1965).
(16) D. A. Frank-Kamenetskii, "Diffusion and Heat Exchange in Chemical Kinetics," Princeton University Press, Princeton, N. J., 1955, p 78.
(17) J. C. Boden and B. A. Thrush, *Proc. Roy. Soc., Ser. A*, **305**, 107 (1968).
(18) A. B. Callear and P. M. Wood, *Trans. Faraday Soc.*, **67**, 272 (1971).
(19) G. B. Kistiakowsky and G. G. Volpi, *J. Chem. Phys.*, **28**, 665 (1958).
(20) D. Husain and L. Kirsh, *Trans. Faraday Soc.*, **67**, 3166 (1971).
(21) W. Braun, A. M. Brass, D. D. Davis, and J. D. Simmons, *Proc. Roy. Soc., Ser. A*, **312**, 417 (1969).
(22) N. Basco, *Proc. Roy. Soc., Ser. A*, **283**, 302 (1965).
(23) D. R. Safrany and W. Jaster, *J. Phys. Chem.*, **72**, 3318 (1968).
(24) G. B. Kistiakowsky and G. G. Volpi, *J. Chem. Phys.*, **27**, 1141 (1957).
(25) D. W. Setser and B. A. Thrush, *Proc. Roy. Soc., Ser. A*, **288**, 275 (1965).
(26) (a) J. A. Meyer, D. H. Klosterboer, and D. W. Setser, *J. Chem. Phys.*, **55**, 2084 (1971); (b) J. A. Meyer, D. W. Setser, and W. G. Clark, *J. Phys. Chem.*, **76**, 1 (1972); (c) D. Stedman, J. A. Meyer, and D. W. Setser, *J. Mol. Spectrosc.*, **44**, 206 (1972).
(27) N. Basco, J. E. Nicholas, R. G. W. Norrish, and W. H. J. Vickers, *Proc. Roy. Soc., Ser. A*, **272**, 147 (1963).
(28) M. Slack, E. S. Fishburne, and A. R. Johnson, *J. Chem. Phys.*, **54**, 1652 (1971).
(29) M. W. Slack and E. S. Fishburne, *J. Chem. Phys.*, **52**, 5830 (1970).
(30) (a) D. E. Paul and F. W. Dalby, *J. Chem. Phys.*, **37**, 592 (1962), report E_a = 2.1 kcal/mol, while (b) G. E. Bullock and R. Cooper, *J. Chem. Soc., Faraday Trans. 1*, 2175 (1972), give E_a = 2.7 kcal/mol. Both references give $k \approx 4 \times 10^{-15}$ cc/sec for CN + C_2N_2 → . . . at room temperature.
(31) S. Jaffee and F. Klein, *Trans. Faraday Soc.*, **62**, 3135 (1966).
(32) The C_3N_2 radical has been detected experimentally (W. Smith and G. Leroi, *Spectrochim. Acta, Part A*, **25**, 1917 (1969); E. Wasserman, L. Barash, and W. A. Yager, *J. Amer. Chem. Soc.*, **87**, 2075 (1965) and has recently been suggested as an intermediate in the reaction of C_4N_2 with oxygen atoms: J. Meyer and D. Setser, *J. Phys. Chem.*, **74**, 3454 (1970).
(33) Based on the H_f(CN) = 104 kcal/mol, H_f(N) = 113 kcal/mol and H_f(C) = 171 kcal/mol. "JANAF Thermodynamic Tables," D. R. Stull, Ed., Clearinghouse for Federal Scientific and Technical Information, Springfield, Va., 1968, Document No. PB-168,370. Tables issued as of Jan 1971.
(34) J. Wyatt and F. Stafford, *J. Phys. Chem.*, **76**, 1913 (1972).
(35) D. MacKay and R. Wolfgang, *Science*, **148**, 899 (1965).
(36) D. Husain and L. Kirsh, *Trans. Faraday Soc.*, **67**, 2025 (1971).
(37) G. W. Wheland, "Resonance in Organic Chemistry," Wiley, New York, N. Y., 1955, p 85.
(38) D. W. Setser and B. A. Thrush, *Proc. Roy. Soc., Ser. A*, **288**, 256 (1965).
(39) C. Hand and R. Obenauf, *J. Phys. Chem.*, **76**, 2643 (1972).

Arrhenius Parameters for the Reactions of Methyl Radicals with Silane and Methylsilanes

R. E. Berkley, I. Safarik, H. E. Gunning, and O. P. Strausz*

Department of Chemistry, University of Alberta, Edmonton, Canada *(Received December 27, 1972)*

Publication costs assisted by the University of Alberta

Arrhenius parameters have been measured for the hydrogen transfer reactions of methyl radicals with silane, methylsilanes, and their deuterated counterparts. The A factors all lie in the range of log A = 11.4–12.4 and the activation energies do not follow the trends in the Si–H bond energies. The bond-energy–bond-order method of estimating the potential energies of activation cannot be directly applied to these reactions.

Quantitative data on hydrogen atom transfer reactions between alkyl radicals and methylated silanes are sparse. For the reaction $CH_3 + HSi(CH_3)_3 \rightarrow CH_4 + Si(CH_3)_3$, Kerr, *et al.*,[1] found an activation energy of 7.00 kcal/mol and Morris and Thynne[2] reported a value of 7.92 kcal/mol. From these data it would appear that the activation energy for the trimethylsilane reaction is about the same or slightly higher than that for the monosilane reaction, in spite of the large difference, ~15 kcal/mol, in the values of the reported bond dissociation energies. Attempts by Glasgow, *et al.*,[3] to reproduce the experimental activation energy for the trimethylsilane reaction by the bond-energy–bond-order (BEBO) method were unsuccessful. However, a slightly modified BEBO method could be applied for the reactions of H atoms with methylated silanes and for the reactions of alkyl radicals with monosilane.[4]

In order to assess the effect of methyl substitution in the silane molecule on the Arrhenius parameters of the hydrogen transfer reactions, we have examined the reactions of methyl radicals with all the methyl-substituted monosilanes and their deuterated counterparts.

Experimental Section

Azomethane, azomethane-d_6, methylsilane, methylsilane-d_3, dimethylsilane-d_2, trimethylsilane-d, tetramethylsilane (Merck), dimethylsilane, trimethylsilane (Peninsular), and neopentane (Phillips) were purified by repeated low-temperature distillation. All deuterated compounds were shown by mass or nmr spectrometry to contain a maximum of 2.5% molecules with proton impurity. The materials used in calibrations, methane-d, methane-d_3, methane-d_4, ethane-d_6 (Merck), methane, and ethane

TABLE I: Reactions of Methyl Radicals with Tetramethylsilane and Neopentane[a]

Temp, °C	Time, min	[Azo] × 10^6 mol/cc	$[(CH_3)_4Si]$ × 10^6 mol/cc	Rate × 10^{12} mol/cc/sec						
				N_2	CH_4 (total)	CH_4 R_2	CH_4 R_4	C_2H_6 (total)	C_2H_6 R_3	$k_4/k_3^{1/2}$
58.0	10.00	1.361	6.033	40.82	1.79	1.10	0.69	29.12	28.80	0.02131
91.0	10.00	1.634	5.739	49.58	5.91	3.90	2.01	28.38	28.06	0.06612
119.0	10.00	1.274	16.814	42.93	17.09	4.98	12.11	14.87	14.56	0.1868
178.0	10.00	1.220	12.110	41.67	32.17	9.16	23.01	4.11	3.80	0.9747
214.0	10.00	1.416	13.711	54.43	53.91	14.10	39.81	2.11	1.69	2.233
61.0	10.00	1.209	13.057	36.71	2.64	1.07	1.57	26.90	26.69	0.02327
150.0	10.00	1.416	14.952	47.05	29.01	8.34	20.67	7.60	7.28	0.5124
			$[(CH_3)_4C]$				R_{4a}			$k_{4a}/k_3^{1/2}$
151.0	10.00	1.220	16.215	43.78	16.25	7.83	8.42	8.97	8.65	0.1766
92.0	11.00	1.383	33.617	44.40	6.43	3.33	3.10	26.76	26.47	0.01792
120.0	11.00	1.372	33.367	45.26	13.04	5.97	7.07	17.36	17.07	0.05128
183.0	10.00	1.220	31.777	45.04	32.49	9.60	22.89	3.59	3.27	0.3983
222.0	10.00	1.252	16.705	48.42	41.35	14.09	27.26	2.00	1.69	1.255

[a] Cell volume 186.5 cc, illuminated volume 158 cc.

(Phillips), were similarly purified by low-temperature distillation. The materials used were shown by gas chromatography to contain a maximum of 0.1% impurities.

The furnace, cell, temperature measurement, and analytical systems are described in the accompanying article.[5] All measurements of isotopic ratios were made using an AEI MS-10 mass spectrometer.

Results

The photolysis of azomethane, used as the source of methyl radicals, proceeds by the following sequence[6-11]

$$CH_3N{=}NCH_3 \longrightarrow 2CH_3 + N_2 \quad (1)$$

$$CH_3N{=}NCH_3 \longrightarrow C_2H_6 + N_2 \quad (1a)$$

$$CH_3 + CH_3N{=}NCH_3 \longrightarrow CH_4 + CH_2N{=}NCH_3 \quad (2)$$

$$2CH_3 \longrightarrow C_2H_6 \quad (3)$$

In the accompanying article the relative Arrhenius parameters of reaction 2 are reported to have the values

$$\log (k_2/k_3^{1/2}) = 4.49 \pm 0.25 - [(8050 \pm 440)/2.303RT]$$

When the photolysis of azomethane is carried out in the presence of tetramethylsilane, methane also forms in the reaction

$$CH_3 + (CH_3)_4Si \longrightarrow CH_4 + CH_2Si(CH_3)_3 \quad (4)$$

in addition to step 2. The rate constant, k_4, can then be evaluated from the following expression

$$k_4/k_3^{1/2} = (R_{CH_4} - R_2)/[(CH_3)_4Si]R_3^{1/2}$$

Least-mean-squares treatment of the data obtained in the temperature range 58–214° and compiled in Table I yield the following Arrhenius equation

$$\log (k_4/k_3^{1/2}) = 4.67 \pm 0.23 - [(9660 \pm 410)/2.303RT]$$

The Arrhenius plot is shown in Figure 1.

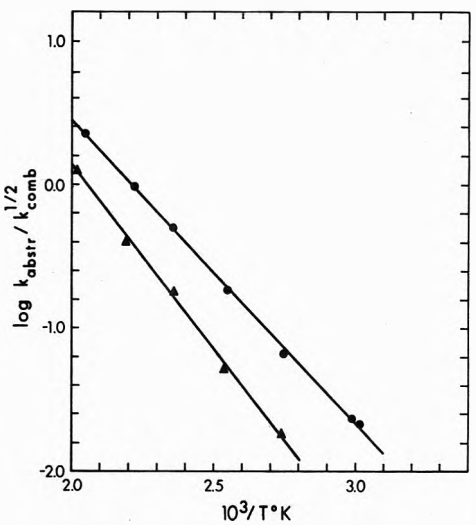

Figure 1. Arrhenius plots for reaction of methyl radicals with tetramethylsilane (●) and neopentane (▲).

Similar studies on the hydrogen abstraction reaction with neopentane

$$CH_3 + (CH_3)_4C \longrightarrow CH_4 + CH_2C(CH_3)_3 \quad (4a)$$

provided the Arrhenius equation

$$\log (k_{4a}/k_3^{1/2}) = 5.25 \pm 0.48 - [(11720 \pm 920)/2.303RT]$$

which is in good agreement with that reported by Kerr, *et al.*[12] These data are also presented in Table I and Figure 1.

When methyl radicals are allowed to react with partially methylated silanes abstraction may occur from either the Si–H or C–H bonds. In an attempt to assess the relative importance of the two reactions we have examined the reactions of methyl radicals with methylsilane-d_3

$$CH_3 + CH_3SiD_3 \longrightarrow CH_3D + CH_3SiD_2 \quad (5)$$

$$CH_3 + CH_3SiD_3 \longrightarrow CH_4 + CH_2SiD_3 \quad (5a)$$

TABLE II: Reactions of Methyl Radicals with Methylsilane-d_3[a]

Temp, °C	Time, min	[Azo] × 10⁶ mol/cc	[CH_3SiD_3] × 10⁶ mol/cc	Rate × 10^{12} mol/cc/sec							
						CH_4			C_2H_6		
				N_2	CH_4 (total)	R_2	Excess	CH_3D R_5	(total)	C_2H_6 R_3	$k_5/k_3^{1/2}$
24.0	40.00	1.158	2.834	11.52	0.46	0.14	0.320	0.59	10.31	10.22	0.06512
48.0	40.00	1.197	2.608	12.61	1.15	0.38	0.770	1.76	9.46	9.37	0.2205
61.0	40.00	1.070	2.637	11.00	1.58	0.48	1.100	2.52	7.10	7.01	0.3609
75.0	40.00	1.041	2.462	11.33	1.54	0.67	0.870	3.30	5.51	5.43	0.5752
92.0	45.00	1.041	1.829	10.51	1.99	0.92	1.070	4.05	3.65	3.57	1.172
103.0	40.10	1.158	1.965	11.00	2.36	1.21	1.150	5.17	2.66	2.58	1.638
117.0	40.00	1.080	1.508	10.76	2.37	1.36	1.010	5.36	1.76	1.69	2.734
135.0	43.00	1.119	1.343	13.02	3.29	1.86	1.430	6.40	1.25	1.15	4.444
150.0	42.00	1.070	1.187	13.10	3.76	2.08	1.680	6.97	0.87	0.79	6.606
167.0	40.00	1.070	1.323	13.26	3.84	2.15	1.690	8.94	0.50	0.41	10.55
184.0	40.00	1.051	0.983	13.28	4.54	2.60	1.940	8.22	0.41	0.33	14.56
201.0	40.00	1.099	1.041	13.41	4.84	2.98	1.860	10.61	0.28	0.20	22.79

[a] Cell volume 218 cc, illuminated volume 192 cc.

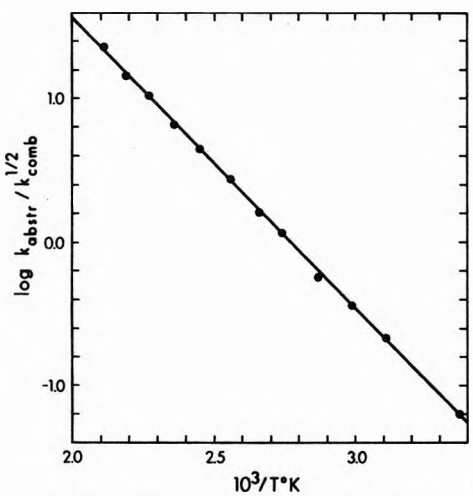

Figure 2. Arrhenius plot for reaction of methyl radicals with methylsilane-d_3.

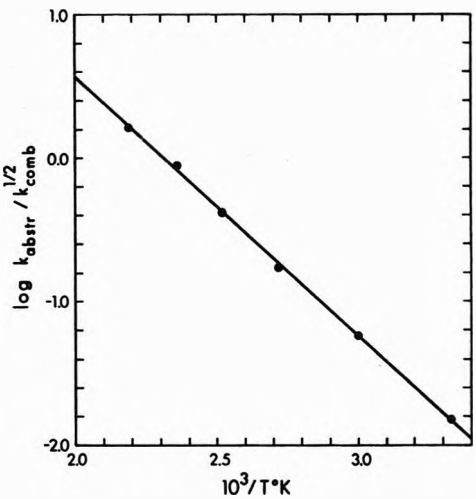

Figure 3. Arrhenius plot for reaction of trideuteriomethyl radicals with azomethane-d_6.

Methane is formed in reactions 2 and 5a, and methane-d in reaction 5. The rate constants for reaction 5 were calculated by the expression

$$k_5/k_3^{1/2} = R_{CH_3D}/[CH_3SiD_3]R_3^{1/2}$$

From temperature studies in the range 24–201° the following Arrhenius equation was derived

$$\log (k_5/k_3^{1/2}) = 5.58 \pm 0.09 - [(9220 \pm 150)/2.303RT]$$

The data are compiled in Table II and the Arrhenius plot is shown in Figure 2.

It can be seen from Table II that some excess CH_4 is produced in addition to that which could be accounted for by reaction 2. In order to establish whether this excess methane is formed by abstraction from the C–H bond of the silane we carried out further experiments using trideuteriomethyl radicals.

Reactions of Methyl-d_3 Radicals with Deuterated Methylsilanes. The methyl-d_3 radicals were generated by the photolysis of azomethane-d_6. It is reasonable to assume that the mechanism of the azomethane-d_6 photolysis is analogous to that of azomethane.

$$CD_3N{=}NCD_3 \longrightarrow 2CD_3 + N_2 \quad (6)$$

$$CD_3N{=}NCD_3 \longrightarrow C_2D_6 + N_2 \quad (6a)$$

$$CD_3 + CD_3N{=}NCD_3 \longrightarrow CD_4 + CD_2N{=}NCD_3 \quad (7)$$

$$2CD_3 \longrightarrow C_2D_6 \quad (8)$$

The rate constant for reaction 7 should be smaller than that of reaction 2 but the rate of reaction 8 is expected to be indistinguishable from that of reaction 3.

From the study of the photolysis of azomethane-d_6 in the temperature range 27–184°' the following Arrhenius equation was obtained

$$\log (k_7/k_8^{1/2}) = 4.15 \pm 0.15 - [(8210 \pm 250)/2.303RT]$$

Data for reaction 7 are listed in Table III and plotted in Figure 3.

The difference in activation energy for reactions 2 and 7 is smaller than expected, and may be due to experimental error. Indeed, the rate of reaction 7 was slow and rate measurements were difficult to reproduce. Nevertheless, the values obtained were used in the estimation of the correction term in methane formation. Since the values of

TABLE III: Reactions of Trideuteriomethyl Radicals with Azomethane-d_6[a]

Temp, °C	Time, min	[Azo] × 10⁶ mol/cc	Rate × 10¹² mol/cc/sec: N_2	CD_4 R_7	C_2D_6 (total)	C_2D_6 R_8	$k_7/k_8^{1/2}$
27.0	10.00	6.088	145.77	1.05	131.96	130.90	0.01507
94.0	7.00	5.652	152.80	8.44	73.69	72.63	0.1752
184.0	7.00	3.653	113.02	14.92	7.08	6.33	1.623
151.0	7.20	3.642	110.90	12.01	14.65	13.92	0.8839
123.0	7.20	4.229	122.62	9.96	33.26	32.38	0.4139
60.0	7.00	5.641	144.36	3.32	106.24	105.18	0.05739

[a] Cell volume 186.5 cc, illuminated volume 158 cc.

TABLE IV: Reactions of Trideuteriomethyl Radicals with Deuterated Methyl Silanes

Temp, °C	Time, min	[Azo] × 10⁶ mol/cc	$[CH_3SiD_3]$ × 10⁶ mol/cc	Rate × 10¹² mol/cc/sec: N_2	CD_4 Total	CD_4 R_7	CD_4 R_9	C_2D_6 total	C_2D_6 R_8	$k_9/k_8^{1/2}$
69.0	40.00	1.068	3.121	8.14	4.60	0.13	4.47	2.47	2.41	0.9226[a]
102.0	42.40	1.106	3.261	8.35	7.10	0.20	6.90	0.68	0.61	2.709[a]
131.0	40.00	0.994	1.709	8.61	7.60	0.29	7.31	0.39	0.33	7.446[a]
85.0	40.00	1.124	3.177	8.90	6.84	0.20	6.64	1.65	1.58	1.663[a]
115.0	40.00	1.096	2.397	10.35	9.72	0.28	9.44	0.67	0.61	5.042[a]
152.0	20.00	1.579	1.124	18.62	11.80	1.15	10.65	0.87	0.74	11.01[a]
22.0	40.10	1.339	6.100	37.94	3.76	0.09	3.67	31.91	31.65	0.1069[b]
49.0	21.50	1.406	3.797	41.36	7.06	0.29	6.77	28.45	28.16	0.3343[b]

Temp, °C	Time, min	[Azo] × 10⁶ mol/cc	$[(CH_3)_2SiD_2]$	R_{10}	$k_{10}/k_8^{1/2}$
22.0	10.00	1.339	4.904	1.60	0.05590[b]
49.0	10.00	1.209	5.020	4.94	0.1940[b]
69.0	10.50	1.209	4.759	8.95	0.3776[b]
89.0	10.00	1.317	4.871	16.46	0.8332[b]
111.0	10.00	1.198	4.748	23.39	1.729[b]
132.0	10.00	1.198	3.931	26.91	3.043[b]
152.0	10.00	1.296	2.396	25.29	5.741[b]

Temp, °C	Time, min	[Azo] × 10⁶ mol/cc	$[(CH_3)_3SiD]$	$\frac{CD_3H}{R_{12}}$	R_{11}	$k_{11}/k_8^{1/2}$	$k_{12}/k_8^{1/2}$
26.0	10.00	1.263	9.670	0.32	1.38	0.02563	0.00594[b]
61.0	11.40	1.361	9.725	1.20	5.87	0.1199	0.02451[b]
93.0	10.00	1.492	9.659	2.53	15.56	0.3827	0.06222[b]
124.0	10.00	1.350	5.271	3.06	17.60	1.049	0.1824[b]
157.0	10.00	1.361	3.561	3.59	19.66	2.563	0.4680[b]
184.0	10.00	1.361	2.352	3.59	18.81	4.922	0.9394[b]
216.0	10.00	1.307	1.503	4.43	20.22	11.06	2.423[b]

[a] Cell volume 218 cc, illuminated volume 192 cc. [b] Cell volume 186.5 cc, illuminated volume 158 cc.

the correction terms are rather small, possible errors in them would not significantly affect the results.

The reactions of trideuteriomethyl radicals with Si-deuterated methylsilanes provide a way of determining the relative importance of the hydrogen abstraction step from the methyl groups since this leads to the formation of methane-d_3, the mass spectrum of which features a mass 19 principal peak corresponding to the parent molecular ion. This peak is insignificant in the spectrum of CD_4 and therefore small concentrations of CD_3H in CD_4 can be measured.

The relative abundance of mass 19 in the mass spectrum of methane formed in the photolysis of azomethane-d_6 alone was compared to that of mass 19 in the mass spectrum of methane produced from the photolysis of azomethane-d_6 in the presence of methylsilane-d_3. From this it was apparent that the formation of methane-d_3 in the reaction of trideuteriomethyl radicals with methylsilane-d_3 was too small to measure, and the small amounts of methane-d_3 arise in part from isotopic impurities in the methylsilane-d_3.

From the studies of the reaction of the trideuteriomethyl radical with methylsilane-d_3

$$CD_3 + CH_3SiD_3 \longrightarrow CD_4 + CH_3SiD_2 \qquad (9)$$

over the temperature range 22–152° the following Arrhenius equation was obtained

TABLE V: Reactions of Methyl Radicals with Methyl Silanes

Temp, °C	Time, min	[Azo] × 10^5 mol/cc	[CH_3SiH_3] × 10^6 mol/cc	Rate × 10^{12} mol/cc/sec: N_2	CH_4 (total)	CH_4: R_2	CH_4: R_{15}	C_2H_6 (total)	C_2H_6 R_3	$k_{15}/k_3^{1/2}$
25.0	30.00	0.983	2.549	11.20	3.68	0.11	3.57	8.51	8.42	0.4827[a]
47.0	30.00	1.090	2.578	13.63	8.45	0.29	8.16	7.06	6.97	1.199[a]
62.0	30.00	1.099	2.491	13.31	10.59	0.42	10.17	4.72	4.63	1.897[a]
76.0	30.00	1.012	1.732	12.39	10.62	0.51	10.11	3.15	3.07	3.331[a]
93.0	31.00	1.022	1.693	13.13	12 29	0.66	11.53	1.85	1.76	5.178[a]
105.0	31.20	1.177	1.469	14.66	14 63	0.97	13.56	1.50	1.39	7.887[a]
121.0	25.00	0.834	1.148	10.24	12 57	0.69	11.88	0.69	0.62	13.14[a]
151.0	25.00	1.051	1.051	13.30	16.53	1.12	15.41	0.35	0.24	29.93[a]
137.0	20.00	1.090	1.158	13.50	16.01	1.19	14.82	0.56	0.48	18.47[a]
			[$(CH_3)_3SiH_2$]				R_{16}			$k_{16}/k_3^{1/2}$
27.0	10.00	1.535	5.380	41.35	7.81	0.37	7.44	31.86	31.54	0.2462[b]
60.0	12.00	1.394	4.737	40.35	19.87	1.05	18.82	21.27	21.01	0.8668[b]
91.0	10.00	1.372	3.855	41.14	31.54	1.84	29.70	9.18	8.86	2.588[b]
119.0	10.00	1.492	3.136	45.99	45.15	3.54	41.61	5.80	5.49	5.663[b]
151.0	10.00	1.198	2.581	38.08	45.47	2.95	45.52	1.58	1.27	14.62[b]
183.0	10.00	1.361	1.459	43.15	48.34	6.10	42.24	1.37	1.05	28.25[b]
212.0	5.00	2.548	1.285	79.32	86.08	21.19	64.89	1.90	1.27	44.81[b]
			[$(CH_3)_3SiH$]				R_{14} R_{13}			$k_{13}/k_3^{1/2}$
29.0	10.00	1.274	6.970	43.78	4.64	0.30	0.18 4.16	26.90	26.58	0.1158[b]
150.0	10.00	1.350	3.757	46.94	41.99	5.07	3.17 33.75	3.27	2.95	5.230[b]
120.0	10.00	1.307	3.670	44.41	30.70	4.05	2.21 24.44	8.97	8.65	2.264[b]
91.0	11.40	1.361	3.855	44.14	19.62	2.58	1.20 15.84	18.04	17.77	0.9747[b]
57.0	10.20	1.361	6.022	41.88	11.27	0.97	0.56 9.74	24.30	23.99	0.3302[b]
183.0	10.30	1.427	1.557	48.24	37.90	8.87	2.49 26.54	2.36	2.05	11.91[b]
213.0	7.00	2.124	1.350	72.63	60.28	20.16	3.66 36.46	2.11	1.66	20.96[b]

[a] Cell volume 218 cc, illuminated volume 192 cc. [b] Cell volume 186.5 cc, illuminated volume 158 cc.

$$\log (k_9/k_8^{1/2}) = 5.82 \pm 0.34 - [(9200 \pm 550)/2.303RT]$$

A similar investigation of the reaction of trideuteriomethyl radicals with dimethylsilane-d_2

$$CD_3 + (CH_3)_2SiD_2 \longrightarrow CD_4 + (CH_3)_2SiD \quad (10)$$

resulted in the Arrhenius equation

$$\log (k_{10}/k_8^{1/2}) = 5.25 \pm 0.24 - [(8820 \pm 390)/2.303RT]$$

In the case of dimethylsilane-d_2, again no significant abstraction from the methyl groups could be detected.

The reaction of CD_3 with trimethylsilane-d led to the production of a measurable amount of CD_3H indicating the occurrence of both reactions

$$CD_3 + (CH_3)_3SiD \longrightarrow CD_4 + (CH_3)_3Si$$

$$CD_3 + (CH_3)_3SiD \longrightarrow CD_3H + CH_2SiD(CH_3)_2 \quad (12)$$

From the determined amounts of methane-d_4 and methane-d_3 the following Arrhenius equations were derived for reactions 11 and 12

$$\log (k_{11}/k_8^{1/2}) = 5.11 \pm 0.19 - [(9210 \pm 330)/2.303RT]$$

$$\log (k_{12}/k_8^{1/2}) = 4.31 \pm 0.53 - [(9070 \pm 920)/2.303RT]$$

The experimental data for the reactions of the trideuteriomethyl radicals with the series of the Si-deuterated methyl-substituted silanes are compiled in Table IV and the Arrhenius plots are shown in Figure 4.

The Arrhenius parameters obtained for reaction 12 do not differ significantly from those obtained for tetramethylsilane. Since the rate of reaction 12 is small compared to that of reaction 13 (*vide infra*), then at lower temperatures the small quantity of undeuterated trimethylsilane present as isotopic impurity makes a significant contribution to the methane-d_3 formed. Inspection of the Arrhenius plot for reaction 12 indeed reveals the expected curvature. Also, because of this curvature, the statistical error limits for this set of rate constants are larger than for most of the other reactions in this study. In view of the uncertainty inherent in the treatment of these results, we decided to use the Arrhenius parameters obtained for tetramethylsilane in calculating the rate of abstraction from the methyl groups of the undeuterated trimethylsilane.

Reactions of Methyl Radicals with Methylsilanes. Rate constants for the reaction

$$CH_3 + HSi(CH_3)_3 \longrightarrow CH_4 + Si(CH_3)_3 \quad (13)$$

were calculated by the relation

$$k_{13}/k_3^{1/2} = (R_{CH_4} - R_2 - R_4)/[(CH_3)_3SiH]R_3^{1/2}$$

TABLE VI: Arrhenius Parameters for Hydrogen Atom Abstraction by Methyl Radicals

Temp range, C°	Reactant	Log A,[a] cm^3 mol^{-1} sec^{-1}	E, kcal mol^{-1}	Log k(200°), cm^3 mol^{-1} sec^{-1}	Ref
28–48	SiH_4	12.26	7.47	8.81	5
29–213	SiH_4	11.80	6.99	8.57	13
49–203	SiH_4	11.82	6.89	8.64	2
25–151	CH_3SiH_3	12.28 ± 0.24	8.13 ± 0.39	8.53	*b*
24–201	CH_3SiD_3	12.25 ± 0.09	9.22 ± 0.15	7.99	*b*
22–152	CH_3SiD_3[c,d]	12.49 ± 0.34	9.20 ± 0.55	8.24	*b*
27–212	$(CH_3)_2SiH_2$	12.07 ± 0.18	8.30 ± 0.31	8.24	*b*
22–152	$(CH_3)_2SiD_2$[c,d]	11.92 ± 0.24	8.82 ± 0.39	7.85	*b*
29–213	$(CH_3)_3SiH$	11.69 ± 0.27	8.31 ± 0.47	7.85	*b*
26–216	$(CH_3)_3SiD$[c,e]	10.98 ± 0.53	9.07 ± 0.92	6.79	*b*
50–200	$(CH_3)_3SiH$	11.42	7.92	7.76	2
57–172	$(CH_3)_3SiH$	11.1	7.0	7.87	1
58–214	$(CH_3)_4Si$	11.34 ± 0.23	9.66 ± 0.41	6.88	*b*
50–200	$(CH_3)_4Si$	11.53	10.30	6.77	2
~140	$(CH_3)_4Si$	12.6	11.0	7.52	14
123–203	$(CH_3)_4Si$	11.55	10.23	6.83	12
150–300	$(CH_3)_4Si$	12.00	10.79	7.02	15
200–350	CH_4	11.83	14.65	5.06	16
260–490	C_2H_6[c]	12.17	11.73	6.75	17
290–460	C_3H_8[c]	11.82	10.13	7.14	18
290–460	$(CH_3)_3CH$[c]	11.38	8.03	7.67	18
92–222	$(CH_3)_4C$	11.92 ± 0.48	11.72 ± 0.92	6.51	*b*
185–309	$(CH_3)_4C$	12.30	12.0	6.76	19
138–292	$(CH_3)_4C$	11.17	10.0	6.55	20

[a] Assuming log (k_{comb}) = 13.34 and E_a = 0 in all cases.[21] [b] This work. [c] CD_3 radicals. [d] D abstraction. [e] H abstraction.

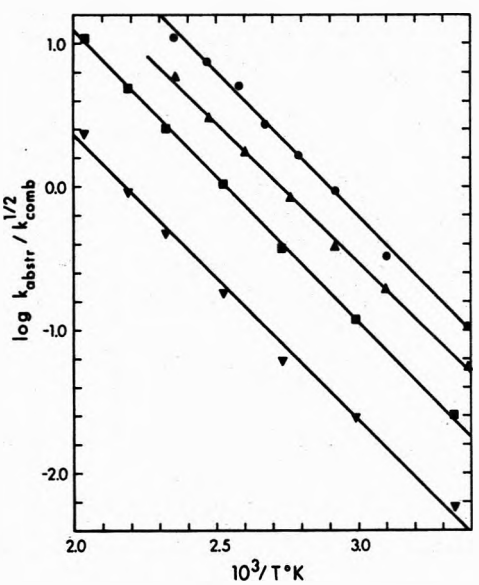

Figure 4. Arrhenius plots for reaction of trideuteriomethyl radicals with methylsilane-d_3 (●), dimethylsilane-d_2 (▲), the silyl group of trimethylsilane-d (■), and the methyl groups of trimethylsilane-d (▼).

assuming that the rate of the reaction

$$CH_3 + CH_3SiH(CH_3)_2 \longrightarrow CH_4 + CH_2SiH(CH_3)_2 \quad (14)$$

is approximately equal to that of reaction 4. Least-squares treatment of the experimental data yielded the Arrhenius equation

$$\log (k_{13}/k_3^{1/2}) = 5.02 \pm 0.27 - [(8310 \pm 470)/2.303RT]$$

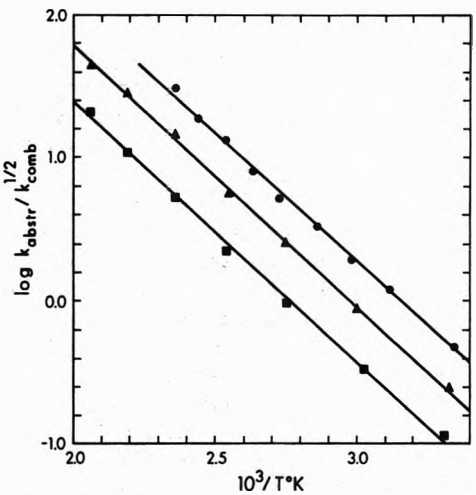

Figure 5. Arrhenius plots for reaction of methyl radicals with methylsilane (●), dimethylsilane (▲), and trimethylsilane (■).

TABLE VII: Experimental Kinetic Isotope Effects for Hydrogen Abstraction by Methyl Radicals

Substrate	k_H/k_D (100°)	Ref
SiH_4	3.3	13
CH_3SiH_3	3.7	*a*
$(CH_3)_2SiH_2$	2.9	*a*
$(CH_3)_3SiH$	2.8	a
CH_4	12.6	16
CH_3CH_3	7.6	17
$CH_3CH_2CH_3$ (secondary H)	6.9	18
i-C_4H_{10} (tertiary H)	6.9	18

[a] This work.

The reactions of methyl radicals with methylsilane and dimethylsilane

$$CH_3 + CH_3SiH_3 \longrightarrow CH_4 + CH_3SiH_2 \quad (15)$$

$$CH_3 + (CH_3)_2SiH_2 \longrightarrow CH_4 + (CH_3)_2SiH \quad (16)$$

were also studied. On the basis of the results obtained from the studies of the trideuteriomethyl radical reactions with methylsilane-d_3 and dimethylsilane-d_2 it was assumed that no significant reaction with the methyl groups of methylsilane and dimethylsilane took place. Temperature studies yielded the following Arrhenius equations

$$\log (k_{15}/k_3^{1/2}) = 5.61 \pm 0\text{-}24 - [(8130 \pm 390)/2.303RT]$$

$$\log (k_{16}/k_3^{1/2}) = 5.40 \pm 0.18 - [(8300 \pm 310)/2.303RT]$$

The experimental data for the methyl radical reactions with the methyl-substituted silanes are listed in Table V and the Arrhenius plots are shown in Figure 5.

Discussion

The Arrhenius parameters obtained for the hydrogen abstraction reactions of methyl radicals with the methylated silanes and the azomethanes are summarized in Table VI along with the available literature data.[13-21] For comparison, related rate parameters for the methyl plus paraffin systems are also included. The data from the different laboratories are in reasonable agreement. The small changes in the reactivity of the various silane molecules are apparently due to changes in both the activation energies and the A factors.

The A factors listed in the table all lie in a narrow range, $\log A \sim 11.4 - 12.4$ (cc mol^{-1} sec^{-1}). Nevertheless, a subtle trend can be observed for both the Si–H and Si–D abstraction reactions; with decreasing number of Si–H or Si–D bonds in the molecule, the value of log A decreases slightly by about 0.2–0.3 per methyl.

The activation energies are generally lower for the abstraction of hydrogen from the Si–H than from the C–H bond, presumably owing to the lower strength of the former. Introduction of a single methyl group results in a slight increase in the activation energy which then remains unaffected by further methylation.

Si–H bond dissociation energies are available in the literature only for monosilane, $D(H_3Si\text{–}H)$ = 95.2 kcal/mol,[22] and trimethylsilane, $D((CH_3)_3Si\text{–}H)$ = 81 kcal/mol.[23] These values indicate a decrease in bond strength with an increasing number of methyl groups on the Si atom by analogy with the paraffins. However, the experimental activation energies do not reflect this trend. The bond-energy–bond-order method of calculating activation energies is evidently not applicable for the CH_3 plus methyl silane systems although as has been shown it could be applied to the D plus silanes and methyl silanes[4] and possibly to the CH_3, C_2H_5 n-C_3H_7, and i-C_3H_7 plus silanes systems.[5]

At present we are unable to offer an explanation as to the cause of these peculiarities in the trend of the measured activation energies. Undoubtedly further work will be required for the elucidation of this problem.

In Table VII the experimental H/D kinetic isotope effects, at one selected temperature, 100°, are tabulated in comparison with related data on paraffins. The k_H/k_D values are all smaller for silanes than for paraffins and they feature a temperature coefficient corresponding to an activation energy of 0.5–1.1 kcal/mol. The A factors of the silane reactions are not affected by deuteration.

Acknowledgments. The authors are indebted to the National Research Council of Canada for financial support and Dr. E. M. Lown for reading the manuscript.

References and Notes

(1) J. A. Kerr, D. H. Slater, and J. C. Young, *J. Chem. Soc. A*, 134 (1967).
(2) E. R. Morris and J. C. J. Thynne, *J. Phys. Chem.*, **73**, 3294 (1969).
(3) L. C. Glasgow, G. O'brich, and P. Potzinger, *Chem. Phys. Lett.*, **14**, 466 (1972).
(4) K. Obi, H. S. Sandhu, H. E. Gunning, and O. P. Strausz, *J. Phys. Chem.*, **76**, 3911 (1972).
(5) R. E. Berkley, I. Safarik, O. P. Strausz, and H. E. Gunning, *J. Phys. Chem.*, **77**, 1741 (1973).
(6) S. Toby and B. H. Weiss, *J. Phys. Chem.*, **66**, 2681 (1962).
(7) R. Rebbert and P. Ausloos, *J. Phys. Chem.*, **67**, 1925 (1963).
(8) P. Gray and J. C. J. Thynne, *Trans. Faraday Soc.*, **59**, 2275 (1963).
(9) P. Gray, A. Jones, and J. C. J. Thynne, *Trans. Faraday Soc.*, **61**, 474 (1965).
(10) S. Toby and J. Nimoy, *J. Phys. Chem.*, **70**, 867 (1966).
(11) S-L. Cheng, J. Nimoy, and S. Toby, *J. Phys. Chem.*, **71**, 3075 (1967).
(12) J. A. Kerr, A. Stephens, and J. C. Young, *Int. J. Chem. Kinet.*, **1**, 339 (1969).
(13) O. P. Strausz, E. Jakubowski, H. S. Sandhu, and H. E. Gunning, *J. Chem. Phys.*, **51**, 552 (1969).
(14) A. U. Chaudhry and B. G. Gowenlock, *J. Organometal. Chem.*, **16**, 221 (1969).
(15) T. N. Bell and A. E. Platt, *J. Phys. Chem.*, **75**, 603 (1971).
(16) F. S. Dainton, K. J. Ivin, and F. Wilkinson, *Trans. Faraday Soc.*, **55**, 929 (1959).
(17) J. R. McNesby, *J. Phys. Chem.*, **64**, 1671 (1960).
(18) W. M. Jackson, J. R. McNesby, and B. deB. Darwent, *J. Chem. Phys.*, **37**, 1610 (1962).
(19) J. A. Kerr and D. Timlin, *J. Chem. Soc. A*, 1241 (1969).
(20) A. F. Trotman-Dickenson, J. R. Birchard, and E. W. R. Steacie, *J. Chem. Phys.*, **19**, 163 (1951).
(21) A. Shepp, *J. Chem. Phys.*, **24**, 939 (1956).
(22) F. E. Saalfeld and H. J. Svec, *J. Phys. Chem.*, **70**, 1753 (1966).
(23) S. J. Band, I. M. T. Davidson, and C. A. Lambert, *J. Chem. Soc. A*, 2068 (1968).

Arrhenius Parameters for the Reactions of Higher Alkyl Radicals with Silanes

R. E. Berkley, I. Safarik, O. P. Strausz,* and H. E. Gunning

Department of Chemistry, University of Alberta, Edmonton, Canada *(Received December 27, 1972)*

Publication costs assisted by the University of Alberta

Arrhenius parameters have been measured for the hydrogen abstraction reactions of the ethyl radical with silane, silane-d_4, disilane, and disilane-d_6 and for the reactions of the *n*-propyl and isopropyl radicals with silane and silane-d_4 molecules. The *A* factors exhibit little variation and the activation energies follow the trend predicted by BEBO calculations only if it is assumed that the combination–disproportionation reactions of these radicals possess a small activation energy, ~3.6 kcal/mol for the ethyl, *n*-propyl, and the isopropyl radicals.

Introduction

Hydrogen abstraction reactions of higher alkyl radicals are expected to be similar to those of methyl radicals except that the activation energies involved would show a definite variation with the C–H bond energies of the abstracting radicals. However, the few experimental data available in the literature do not seem to support the validity of this expectation. For example, the activation energies for abstraction of hydrogen from aldehydes by different butyl radicals were found to be considerably lower than those for abstraction by methyl. On the other hand, the hydrogen abstraction reactions of ethyl radicals with paraffins feature activation energies about 0.8 kcal larger than the analogous methyl radical reactions.[1]

In a previous publication from this laboratory[2] an activation energy of 8.9 kcal/mol was reported for hydrogen abstraction from propane by *n*-propyl radicals. This is somewhat lower than the activation energy of 10.2 kcal/mol previously reported for the reaction between methyl and propane.[1]

In order to gain more information about the hydrogen abstraction reactions of higher alkyl radicals we have examined the reactions of ethyl, *n*-propyl, and isopropyl radicals with silane and disilane. Silanes offer the advantage that the products of the reaction can be measured directly and interference by competing side reactions is minimal.

Kerr, *et al.*,[3,4] in their studies of hydrogen abstraction reactions from tetramethylsilane and from trichlorosilane, found that the activation energies for abstraction by ethyl radicals were about 1 kcal/mol higher than those for abstraction by methyl radicals.

Experimental Section

Azoethane, azo-*n*-propane, azobis(*n*-propane-2,2,d_2), and azoisopropane (Merck) were purified by gas–liquid chromatography, and azomethane, monosilane, monosilane-d_4, disilane, and disilane-d_6 (Merck) by repeated low-temperature distillation. All deuterated compounds were shown by mass spectrometry or by nmr to contain a maximum of 2.5% protonated molecules except for disilane-d_6, which contained 6.5%. The materials used in calibrations, methane, ethane, propane, *n*-butane, *n*-hexane, and 2,3-dimethylbutane (Phillips), were similarly purified by low-temperature distillation and were shown by gas chromatography to contain a maximum of 0.1% impurities.

Photolyses were carried out in a cylindrical quartz cell equipped with a cold finger and attached to a high vacuum system. The cell was mounted inside an aluminum block furnace with double quartz windows at each end. Temperature measurements were made with an internal standard pyrometer (Assembly Products). Calibration was checked regularly against ice, room temperature (as measured by a calibrated mercury thermometer), and boiling water. The temperatures measured in this manner are considered to be accurate to ±1°. Light was isolated from a Hanovia Utility medium-pressure mercury arc by a Kodak Wratten 18A filter. In the photolysis of azomethane and azoethane, window glass was used instead, m order to obtain higher light intensity and higher radical concentration.

Product analyses were accomplished by low-temperature distillation, gas chromatography, and mass spectrometry. The fraction volatile at −210° was measured in a gas buret. Where nitrogen was the only expected noncondensable product, this fraction was occasionally analyzed by mass spectrometry. In runs where methane was produced, the −210° fraction was analyzed by gas chromatography (1 ft × 0.25 in., 13X molecular sieves, 0°), or by mass spectrometry (AEI MS-10). Condensable products were separated by low-temperature distillation and analyzed by gas chromatography. Ethane and ethylene were normally analyzed on a 15 ft × 0.25 in. medium activity silica gel column at room temperature. Ethane and ethylene in the presence of monosilane were analyzed on a 15 ft × 0.25 in. high-activity silica gel column at 60°. Butane was normally analyzed on a 20 ft × 0.25 in. silicone gum rubber column at room temperature. Condensable products from the reaction of ethyl radicals with disilane were distilled off at −117° and passed through the medium activity silica gel column at room temperature. After ethane and ethylene were eluted, the temperature of the column was rapidly increased to 70°, after which disilane and butane distilled off.

After photolysis of azobis(*n*-propane-2,2-d_2) in the presence of a mixture of silane and silane-d_4, the noncondensables were pumped off through a liquid nitrogen trap, monosilane was distilled off at −161°, and the fraction containing propane was distilled off at −126°. Propane was recovered by gas chromatography using the medium activity silica gel column at 50°. The relative amounts of propane-2,2-d_2 and propane-1,2,2-d_3 were determined by mass spectrometry. Use of *n*-propyl radicals which were

deuterated on the second carbon atom was found to be very advantageous for mass spectrometric analysis, since the resulting propane molecules have an $(M - 1)$ peak which is quite small compared to the parent peak. The reactions of isopropyl radicals with disilane and disilane-d_6 were carried out in the same manner, except that light isopropyl radicals were used.

Propane-2,2-d_2 used in the mass spectrometer calibration was synthesized by photolysis of azobis(*n*-propane-2,2-d_2) in the presence of a high pressure of monosilane. Propane-2-d and propane-1,2,2-d_3 were similarly obtained by photolysis of the appropriate azoalkane in the presence of disilane-d_6. These syntheses were carried out at 220°.

Some polymer was formed in each run. This was particularly true of the relative rate runs involving disilane. It is probable that this polymer is of the same $(SiH_x)_n$ composition which has been reported previously.[5] Most of the heavy products were driven out of the reaction cell by the heat of the furnace, and the buildup of a brownish-yellow material in the lines and traps outside the cell necessitated occasional cleaning by washing with dilute HF solution. Eventually, however, a golden brown deposit built up in the cell itself, especially in the cold trap and entrance line, which could not be heated as strongly as the body of the cell. This deposit severely decreased the transmittance of the cell windows and finally began to cause dark decomposition of the azoalkanes in a rather unusual manner (azoisopropane yielded methane). At this point it became impossible to obtain consistent results and the cell was replaced, efforts to clean it with dilute HF having proven futile.

Results

It has been established that the photolysis of azomethane proceeds *via* the following sequence[6-11]

$$CH_3N{=}NCH_3 \xrightarrow{h\nu} 2CH_3 + N_2 \quad (1)$$

$$CH_3N{=}NCH_3 \xrightarrow{h\nu} C_2H_6 + N_2 \quad (1a)$$

$$CH_3 + CH_3N{=}NCH_3 \longrightarrow CH_4 + CH_2N{=}NCH_3 \quad (2)$$

$$2CH_3 \longrightarrow C_2H_6 \quad (3)$$

The quantum yield of ethane in reaction 1a was found to be 0.007 and allowance has been made for it in determining the ethane produced in reaction 3. Assuming steady-state conditions, the rate constant for the abstraction reaction, k_2, can be calculated by the equation

$$k_2/k_3^{1/2} = R_2/R_3^{1/2}[(CH_3)_2N_2] \quad (I)$$

where R_2 and R_3 are the rates of reactions 2 and 3, respectively, and the square brackets denote the initial concentration of the reactant. From seven runs between 25 and 218° the following Arrhenius equation was obtained by least-squares treatment

$$\log (k_2/k_3^{1/2}) = 4.49 \pm 0.25 - [(8050 \pm 440)/2.303RT]$$

This is in satisfactory agreement with several previously reported values in the literature,[3,9,12] and has been used in the evaluation of kinetic data for methyl radicals.

When azomethane is photolyzed in the presence of silane, methane is formed in the reaction

$$CH_3 + SiH_4 \longrightarrow CH_4 + SiH_3 \quad (4)$$

The rate constant for reaction 4 can be calculated from the expression

$$k_4/k_3^{1/2} = (R_{CH_4} - R_2)/R_3^{1/2}[SiH_4] \quad (II)$$

where R_2 can be determined from eq I. Experimental data for reaction 4 are summarized in Table I and the Arrhenius plot of $k_4/k_3^{1/2}$ is shown in Figure 1. Least-squares

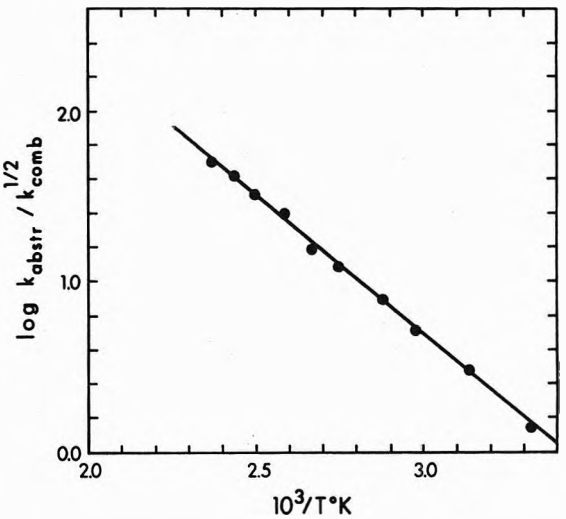

Figure 1. Arrhenius plot for the reaction of methyl radicals with silane.

TABLE I: Reactions of Methyl Radicals with Silane[a]

				Rate × 10^{12} mol/cc sec						
					CH_4					
Temp, °C	Time, min	[Azo] × 10^6 mol/cc	[SiH_4] × 10^6 mol/cc	N_2	Total	R_2	R_4	C_2H_6 (total)	C_2H_6 R_3	$k_4/k_3^{1/2}$
113.0	5.10	2.016	0.307	40.17	24.34	1.90	22.44	8.85	8.51	24.06
148.0	5.00	1.849	0.269	39.58	27.60	2.68	24.92	3.82	3.47	49.73
137.0	5.00	1.895	0.320	40.62	28.47	2.20	26.27	4.17	3.82	42.00
127.0	6.00	1.858	0.375	38.05	27.34	1.81	25.53	4.63	4.34	32.68
101.0	6.00	1.867	0.536	36.31	24.45	1.34	23.11	7.96	7.67	15.57
91.0	6.00	1.895	0.412	38.77	18.81	1.18	17.63	13.02	12.73	11.99
74.0	7.00	1.756	0.428	35.22	14.14	0.73	13.41	16.00	15.75	7.895
28.0	10.00	1.375	0.670	22.66	3.99	0.11	3.88	17.01	16.84	1.411
45.0	10.00	1.459	0.501	28.04	6.86	0.24	6.62	18.49	18.32	3.087
62.0	10.00	1.607	0.481	27.78	10.16	0.44	9.72	15.10	14.93	5.230

[a] Cell volume 218 cc, illuminated volume 192 cc.

TABLE II: Reactions of Ethyl Radicals with Silane[a]

Temp, °C	Time, min	[Azo] × 10^6 mol/cc	[SiH_4] × 10^6 mol/cc	Rate × 10^{12} mol/cc sec						
				N_2	C_2H_6 Total	C_2H_6 R_6	C_2H_6 R_7	C_2H_6 R_9	C_4H_{10} R_8	$k_9/k_8^{1/2}$
45.0	10.00	1.997	0.578	55.21	11.72	1.27	6.06	4.39	43.32	1.154
63.0	10.00	1.812	0.496	15.10	5.38	0.96	1.07	3.35	7.64	2.444
76.0	10.00	1.784	0.472	56.86	17.97	3.40	4.86	9.71	34.72	3.491
89.0	10.00	1.942	0.706	58.86	25.87	5.17	3.99	16.71	28.47	4.436
120.0	10.00	1.468	0.506	57.03	35.85	8.53	2.84	24.48	20.31	10.740
149.0	10.00	1.793	0.554	68.32	57.82	16.82	1.70	39.30	12.15	20.350
180.0	10.50	1.997	0.692	90.36	91.10	26.60	0.87	63.63	6.20	36.930
103.0	10.00	1.774	0.589	63.72	35.51	7.33	4.07	24.11	29.08	7.591
			[SiD_4]					C_2H_5D R_{10}		$k_{10}/k_8^{1/2}$
92.0	10.00	2.025	1.031	61.37	19.27	6.27	4.55	8.45	32.47	1.438
123.0	10.00	1.375	1.096	52.87	31.51	8.56	2.75	20.20	19.62	4.161
148.0	10.00	1.022	1.189	48.70	37.07	8.86	1.46	26.75	10.42	6.970
179.0	10.00	1.031	1.189	54.60	54.60	12.13	0.68	41.79	4.86	15.940
212.0	10.00	0.640	1.022	40.28	47.70	8.64	0.24	38.82	1.74	28.800
105.0	15.00	0.546	1.096	25.69	12.27	1.50	1.51	9.26	10.82	2.569
232.0	10.00	0.598	0.807	44.10	49.05	11.39	0.24	37.42	1.74	35.150

[a] Cell volume 218 cc, illuminated volume 192 cc.

treatment has given the equation

$$\log (k_4/k_3^{1/2}) = 5.59 \pm 0.17 - [(7470 \pm 290)/2.303RT]$$

in reasonable agreement with previously reported values.[12,13]

Reactions of Ethyl Radicals with Silanes. Ethyl radicals were generated by the photolysis of azoethane which follows the mechanism[14,15]

$$C_2H_5N{=}NC_2H_5 \xrightarrow{h\nu} 2C_2H_5 + N_2 \quad (5)$$

$$C_2H_5 + C_2H_5N{=}NC_2H_5 \rightarrow C_2H_6 + CH_3CHN{=}NC_2H_5 \quad (6)$$

$$2C_2H_5 \rightarrow C_2H_4 + C_2H_6 \quad (7)$$

$$2C_2H_5 \rightarrow n\text{-}C_4H_{10} \quad (8)$$

Taking the ratio $k_7/k_8 = 0.14$,[16] the rate constants may be calculated by an expression analogous to eq I. The Arrhenius parameters of this reaction were determined from eight runs between 26 and 149° to have the value

$$\log (k_6/k_8^{1/2}) = 4.87 \pm 0.35 - [(8570 \pm 590)/2.303RT]$$

in satisfactory agreement with literature data.[4,15]

Rate constants as the function of temperature have been determined for the reactions of ethyl radicals with silane, silane-d_4, disilane, and disilane-d_6.

$$C_2H_5 + SiH_4 \rightarrow C_2H_6 + SiH_3 \quad (9)$$

$$C_2H_5 + SiD_4 \rightarrow C_2H_5D + SiD_3 \quad (10)$$

$$C_2H_5 + Si_2H_6 \rightarrow C_2H_6 + Si_2H_5 \quad (11)$$

$$C_2H_5 + Si_2D_6 \rightarrow C_2H_5D + Si_2D_5 \quad (12)$$

The rate constants were calculated by the equation

$$k_x/k_8^{1/2} = (R_{C_2H_6} - 0.14R_8 - R_6)/R_8^{1/2}[\text{silane}] \quad (III)$$

The experimental data for these reactions are summarized in Tables II and III, and the respective Arrhenius plots are shown in Figure 2.

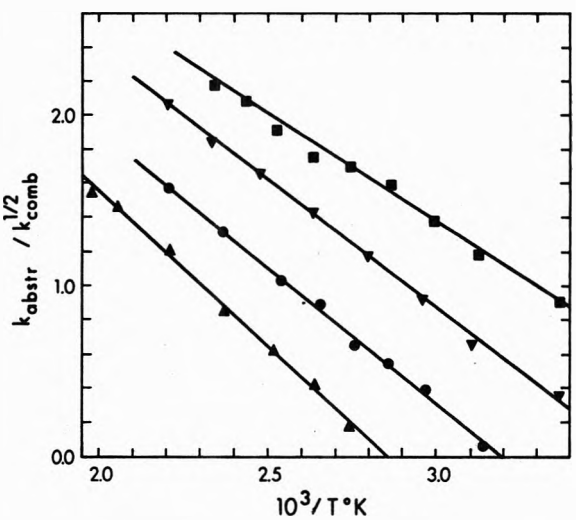

Figure 2. Arrhenius plots for the reaction of ethyl radicals with silane (●), silane-d_4 (▲), disilane (■), and disilane-d_6 (▼).

Least-squares treatment of the data yield the following Arrhenius equations

$$\log (k_9/k_8^{1/2}) = 5.06 \pm 0.23 - [(7250 \pm 380)/2.303RT]$$

$$\log (k_{10}/k_8^{1/2}) = 5.20 \pm 0.35 - [(8350 \pm 670)/2.303RT]$$

$$\log (k_{11}/k_8^{1/2}) = 5.08 \pm 0.28 - [(5650 \pm 450)/2.303RT]$$

$$\log (k_{12}/k_8^{1/2}) = 5.36 \pm 0.16 - [(6840 \pm 270)/2.303RT]$$

Reactions of Propyl Radicals with Silanes. The photolysis of azo-*n*-propane and azoisopropane proceeds analogously with the photolysis of azoethane and provides a good source for *n*-propyl and isopropyl radicals. For the hydrogen abstraction reactions of the radicals from the parent azo compounds the Arrhenius parameters have been reported previously from this laboratory[2]

ห้องสมุด กรมวิทยาศาสตร์

TABLE III: Reactions of Ethyl Radicals with Disilane[a]

Temp, °C	Time, min	[Azo] × 10^6 mol/cc	[Si_2H_6] × 10^6 mol/cc	Rate × 10^{12} mole/cc sec: N_2	C_2H_6 Total	C_2H_6 R_6	C_2H_6 R_7	C_2H_6 R_{11}	C_4H_{10} R_8	$k_{11}/k_8^{1/2}$
24.0	10.00	1.096	0.855	40.02	27.26	0.14	1.82	25.30	13.02	8.201
46.0	10.00	1.031	0.746	33.86	31.25	0.27	0.94	30.04	6.68	15.580
60.0	10.00	1.013	0.406	34.55	31.25	0.54	1.26	29.45	9.03	24.140
75.0	10.00	1.161	0.676	41.50	52.43	0.69	0.51	51.23	3.65	39.670
90.0	10.00	1.115	0.546	41.58	51.48	1.07	0.47	49.94	3.39	49.680
106.0	10.00	0.743	0.647	31.69	43.23	0.71	0.18	42.34	1.30	57.400
122.0	10.00	1.050	0.780	45.14	68.06	1.44	0.15	66.47	1.04	83.560
137.0	10.00	1.096	0.657	59.20	89.15	2.30	0.16	86.69	1.13	124.100
152.0	10.00	1.078	0.655	48.35	85.77	2.62	0.10	83.05	0.69	152.600
			[Si_2D_6]					C_2H_5D R_{12}		$k_{12}/k_8^{1/2}$
24.0	10.00	1.210	0.945	36.55	13.80	0.21	3.18	10.41	22.74	2.310
48.0	10.00	1.031	1.059	34.98	22.05	0.45	2.20	19.40	15.71	4.622
64.0	10.00	1.152	1.013	42.02	34.90	0.86	1.94	32.10	13.89	8.502
84.0	10.00	1.087	1.003	39.50	42.28	1.24	0.98	40.06	7.03	15.060
105.0	10.50	1.078	0.929	39.60	52.50	1.78	0.54	50.18	3.89	27.390
130.0	10.00	1.106	1.068	44.97	63.46	2.31	0.22	60.93	1.56	45.680
154.0	10.00	1.115	0.676	43.41	60.68	4.02	0.19	56.47	1.39	70.850
180.0	10.00	1.078	0.535	45.84	83.68	7.04	0.21	76.43	1.48	117.400

[a] Cell volume 218 cc, illuminated volume 192 cc.

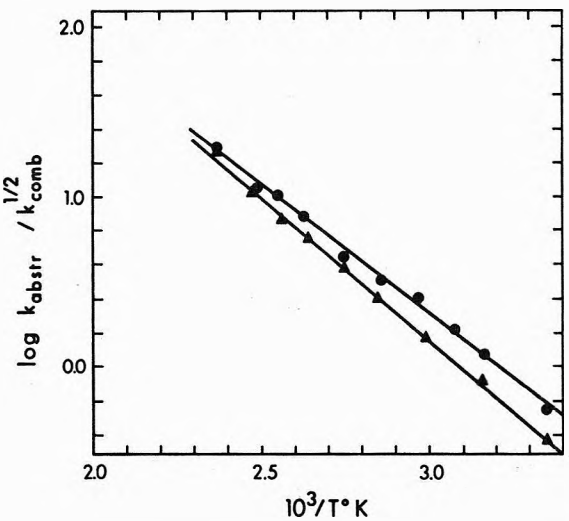

Figure 3. Arrhenius plots for the reaction of *n*-propyl radicals (●) and isopropyl radicals (▲) with silane.

$$\log (k_{abstr}/k_{comb}^{1/2}) = 4.8 - (8000/2.303RT)$$

for *n*-propyl radicals, and

$$\log (k_{abstr}/k_{comb}^{1/2}) = 4.0 - (7080/2.303RT)$$

for isopropyl radicals. The ratio of disproportionation to combination was taken as 0.15 for *n*-propyl and 0.55 for isopropyl radicals.[17,18]

In the photolysis of azo-*n*-propane and azoisopropane in the presence of silane, reactions 13 and 14 take place.

$$n\text{-}C_3H_7 + SiH_4 \rightarrow C_3H_8 + SiH_3 \quad (13)$$

$$i\text{-}C_3H_7 + SiH_4 \rightarrow C_3H_8 + SiH_3 \quad (14)$$

The following Arrhenius equations were derived from measurements of the abstraction/recombination rate ratios as a function of temperature:

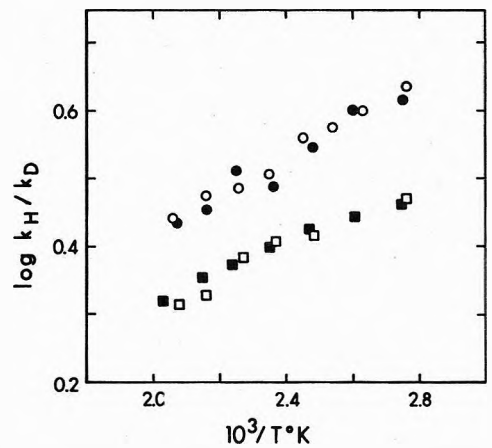

Figure 4. Kinetic isotope effect in the reaction of *n*-propyl radicals with silane (○), and disilane (□), and in the reaction of isopropyl radicals with si ane (●) and disilane (■).

$$\log (k_{13}/k_{comb}^{1/2}) = 4.85 \pm 0.21 - [(6910 \pm 340)/2.303RT]$$

$$\log (k_{14}/k_{comb}^{1/2}) = 5.17 \pm 0.21 - [(7640 \pm 330)/2.303RT]$$

The experimental data for reactions 13 and 14 are summarized in Table IV and the Arrhenius plots are given in Figure 3.

When azo-*n*-propane is photolyzed at 90–220° in the presence of a large concentration of silane and silane-d_4, the following reactions take place

$$n\text{-}C_3H_7 + SiH_4 \rightarrow C_3H_8 + SiH_3$$

$$n\text{-}C_3H_7 + SiD_4 \rightarrow C_3H_7D + SiD_3$$

The rate constant ratio is then given by the expression

$$k_H/k_D = R_H P_D / R_D P_H$$

The isotope effect k_H/k_D can be calculated from the rela-

TABLE IV: Reactions of Propyl Radicals with Silane[a]

Temp, °C	Time, min	[Azo] × 10^6 mol/cc	[SiH_4] × 10^6 mol/cc	Rate × 10^{12} mole/cc sec: N_2	C_3H_8: Total	C_3H_8: Abstr. from azo	C_3H_8: Disp.	R_{13}	C_6H_{14} R_{comb}	$k_{13}/k_{comb}^{1/2}$
				(1) *n*-Propyl Radicals						
90.0	165.00	0.466	2.930	5.11	6.05	0.18	0.03	5.84	0.20	4.4570
119.0	160.00	0.284	1.280	4.81	5.97	0.25	0.03	5.69	0.19	10.2000
149.0	160.00	0.285	0.514	5.47	6.08	0.63	0.04	5.41	0.29	19.5400
63.0	160.00	0.392	3.560	4.05	4.76	0.09	0.04	4.63	0.26	2.5510
76.0	160.00	0.420	2.290	4.53	4.98	0.15	0.06	4.77	0.41	3.2530
42.0	80.00	0.519	2.330	4.24	3.23	0.09	0.16	2.98	1.18	1.1770
107.0	60.00	0.403	0.853	5.99	6.08	0.49	0.11	5.48	0.72	7.5710
128.0	94.00	0.363	1.340	4.85	6.65	0.37	0.03	6.25	0.17	11.3100
25.0	67.00	0.509	4.160	2.90	2.22	0.04	0.12	2.06	0.78	0.5607
52.0	62.00	0.434	4.350	3.40	3.89	0.05	0.04	3.80	0.27	1.6810
								C_3H_8 R_{14}	C_6H_{14} R_{comb}	$k_{14}/k_{comb}^{1/2}$
				(2) Isopropyl Radicals						
25.0	30.00	1.014	6.762	8.97	4.95	0.11	1.19	3.65	2.17	0.3664
90.0	51.20	1.072	3.454	15.31	13.14	0.61	0.48	12.05	0.88	3.7190
118.0	40.00	0.595	1.537	10.20	9.29	0.53	0.30	8.46	0.54	7.4900
149.0	42.05	0.559	0.961	10.79	11.50	0.78	0.19	10.53	0.35	18.5200
132.0	40.00	0.540	1.041	9.70	9.09	0.67	0.31	8.11	0.56	10.4100
105.0	40.00	0.724	1.820	11.00	10.16	0.58	0.44	9.14	0.80	5.6150
78.0	40.00	0.739	3.707	10.29	8.90	0.28	0.43	8.19	0.78	2.5020
61.0	40.00	0.656	3.279	8.48	6.42	0.19	0.72	5.51	1.30	1.4740
43.0	40.00	0.630	3.454	7.27	4.73	0.11	0.92	3.70	1.67	0.8289

[a] Cell volume 218 cc, illuminated volume 192 cc.

TABLE V: Relative Rates of Reaction of *n*-Propyl Radicals with Nondeuterated and Deuterated Silanes

Temp, °C	Time, min	Pressure, Torr: Azo	SiH_4	SiD_4	R_H/R_D	k_H/k_D
			Silane and Silane-d_4			
120.0	250.00	7.6	51.9	150.9	1.289	3.75
135.0	181.00	7.6	54.6	162.3	1.218	3.62
170.0	210.00	6.2	49.8	152.8	0.992	3.04
152.0	142.00	7.0	41.4	160.6	0.822	3.19
191.0	150.00	7.9	58.7	165.4	1.054	2.97
213.0	131.00	6.5	61.3	150.2	1.124	2.75
107.0	200.00	7.0	32.2	175.5	0.730	3.98
89.0	173.00	7.7	44.1	159.4	1.193	4.31
			Si_2H_6	Si_2D_6		
			Disilane and Disilane-d_6			
130.0	250.00	9.5	49.7	147.4	0.883	2.62
149.0	153.00	8.2	57.7	149.9	0.977	2.54
168.0	226.00	7.7	50.8	150.0	0.815	2.41
189.0	202.00	8.1	52.6	149.9	0.749	2.13
208.0	325.00	8.0	48.3	145.9	0.686	2.07
89.0	300.00	6.8	52.8	152.4	1.016	2.93

TABLE VI: Relative Rates of Reaction of Isopropyl Radicals with Nondeuterated and Deuterated Silanes

Temp, °C	Time, min	Pressure, Torr: Azo	SiH_4	SiD_4	R_H/R_D	k_H/k_D
			Silane and Silane-d_4			
209.0	170.00	7.4	106.3	302.6	0.956	2.72
191.0	236.00	7.6	106.4	300.2	1.009	2.85
172.0	452.00	6.7	105.8	301.8	1.142	3.26
150.0	120.00	8.1	106.2	304.0	1.081	3.10
131.0	277.00	4.8	102.3	303.1	1.176	3.49
112.0	244.00	5.8	102.5	306.6	1.323	3.96
90.0	336.00	4.3	102.5	299.6	1.414	4.13
			Si_2H_6	Si_2D_6		
			Disilane and Disilane-d_6			
90.0	174.00	5.9	36.8	122.4	0.877	2.92
193.0	150.00	5.1	43.5	101.9	0.963	2.26
174.0	150.00	4.8	40.2	109.8	0.864	2.36
151.0	187.00	6.0	40.4	107.1	0.944	2.50
132.0	140.00	3.6	38.5	90.1	1.132	2.65
110.0	234.00	4.3	42.1	111.3	1.047	2.77
220.0	201.00	5.8	47.5	104.3	0.951	2.09

tive pressures of the silanes and the measured rates of formation of the deuterated and nondeuterated propane.

The isotope effect in the reactions of *n* and isopropyl radicals has been determined as a function of temperature in mixtures of silane and silane-d_4, and in mixtures of disilane and disilane-d_6 as well. The experimental data are compiled in Tables V and VI. The isotope effect as a function of temperature is shown in Figure 4.

TABLE VII: Input Parameters for BEBO Calculations

		Ref
Bond dissociation energies,[a] kcal mol^{-1}		
$D(CH_3-H)$	108.3	20
$D(CH_3CH_2-H)$	102.1	20
$D(C_2H_5CH_2-H)$	102.1	20
$D[(CH_3)_2CH-H]$	98.6	20
$D(SiH_3-H)$	98.3	21
$D(CH_3-SiH_3)$	85.1	22
Bond distances, Å		
Si–H	1.48	23
C–H	1.09	23
C–Si	1.87	23
Stretching frequency, cm^{-1}		
C–Si	701	23

[a] Includes zero-point energy.

The bond-energy–bond-order (BEBO) method, developed by Johnston and Parr,[19] has been widely used for estimating the activation energies of hydrogen abstraction reactions and the calculated values have generally been found to agree with experiment to within 2 kcal/mol. We have performed calculations with this method in order to establish the predicted trend in the activation energies of the hydrogen abstraction reactions of higher alkyl radicals. The input data and the results obtained are summarized in Tables VII[20-23] and VIII, respectively.

TABLE VIII: Potential Energies of Activation and Experimental Activation Energies of Hydrogen Abstraction by Alkyl Radicals

Reaction	V, kcal/mol	E_a, kcal/mol
$CH_3 + SiH_4$	10.2	7.47
$C_2H_5 + SiH_4$	10.8	9.05
n-$C_3H_7 + SiH_4$	10.4	8.71
i-$C_3H_7 + SiH_4$	11.8	9.44
$CH_3 + CH_4$	15.8	14.8
$C_2H_5 + CH_4$	18.3	
i-$C_3H_7 + CH_4$	20.7	

Discussion

The Arrhenius parameters and log k values calculated at 200° are summarized in Table IX[24-26] as well as those of other analogous reactions. It is seen that the values of the A factors for the reactions of higher alkyl radicals with silane are similar, and they are not very different from those reported for hydrogen abstraction from hydrocarbons. The activation energies for the silane reactions are generally lower than for the hydrocarbon reactions and this is clearly the reason why abstraction is faster from silanes. On the other hand, the activation energies for different radicals attacking the same silane molecule are all about the same in spite of the difference in the energies of the bonds being formed.

The Arrhenius parameters in Table IX were calculated assuming log A = 13.34[27] and E_a = 0 for alkyl radical combination. However, an activation energy of 2 kcal/mol and a rather high A factor of $10^{14.65}$ (cc mol^{-1} sec^{-1}) has

TABLE IX: Arrhenius Parameters for Hydrogen Abstraction Reactions of Alkyl Radicals[a]

Temp range, °C	Reaction	Log A,[b] cm^3 mol^{-1} sec^{-1}	E, kcal mol^{-1}	Log k(200°), cm^3 mol^{-1} sec^{-1}	Ref
28–148	$CH_3 + SiH_4$	12.26 ± 0.17	7.47 ± 0.29	8.81	c
45–180	$C_2H_5 + SiH_4$	11.73 ± 0.23	7.25 ± 0.38	8.38	c
92–232	$C_2H_5 + SiD_4$	11.87 ± 0.35	8.35 ± 0.67	8.01	c
24–152	$C_2H_5 + Si_2H_6$	11.75 ± 0.28	5.65 ± 0.45	9.14	c
24–180	$C_2H_5 + Si_2D_6$	12.03 ± 0.16	6.84 ± 0.27	8.87	c
25–149	n-$C_3H_7 + SiH_4$	11.52 ± 0.21	6.91 ± 0.34	8.33	c
89–213	n-$C_3H_7 + SiD_4$	11.52 ± 0.30	7.90 ± 0.51	7.87	c,d
25–149	i-$C_3H_7 + SiH_4$	11.84 ± 0.21	7.64 ± 0.33	8.31	c
90–209	i-$C_3H_7 + SiD_4$	11.84 ± 0.41	8.63 ± 0.72	7.85	c,d
29–213	$CH_3 + SiH_4$	11.80	6.99	8.57	13
30–215	$CH_3 + SiD_4$	11.98	8.19	8.20	13
33–202	$CH_3 + Si_2H_6$	11.96	5.65	9.36	13
37–189	$CH_3 + Si_2D_6$	12.19	6.96	8.98	13
49–203	$CH_3 + SiH_4$	11.82	6.89	8.64	12
200–350	$CH_3 + {}^{14}CH_4$	11.83	14.65	5.06	24
200–350	$CD_3 + {}^{14}CD_4$	12.61	17.80	4.39	25
260–490	$CD_3 + C_2H_6$	12.17	11.73	6.75	26
260–490	$CD_3 + C_2D_6$	12.17	13.23	6.06	26
25–218	$CH_3 + (CH_3)_2N_2$	11.16 ± 0.25	8.05 ± 0.44	7.44	c
59–197	$CH_3 + (CH_3)_2N_2$	11.13	7.85	7.50	3
120–180	$CH_3 + (CH_3)_2N_2$	11.03	8.20	7.24	9
71–253	$CH_3 + (CH_3)_2N_2$	11.10	7.60	7.59	12
26–149	$C_2H_5 + (C_2H_5)_2N_2$	11.54 ± 0.35	8.57 ± 0.59	7.58	c
27–175	$C_2H_5 + (C_2H_5)_2N_2$	12.20	8.00	8.51	15
41–140	$C_2H_5 + (C_2H_5)_2N_2$	11.30	8.13	7.55	4
27–160	n-$C_3H_7 + (n$-$C_3H_7)_2N_2$	11.47	8.00	7.78	2
27–160	i-$C_3H_7 + (i$-$C_3H_7)_2N_2$	10.67	7.08	7.40	2

[a] Error limits are for 95% confidence level. [b] Assuming log (k_{comb}) = 13.34 and E_a = 0 in all cases.[27] [c] This work. [d] Calculated from isotope effect.

TABLE X: Arrhenius Parameters for Hydrogen Abstraction Reactions of Alkyl Radicals

Reaction	Log A,[a] cm^3 mol^{-1} sec^{-1}	E,[a] kcal/mol	Log A,[b] cm^3 mol^{-1} sec^{-1}	E,[b] kcal/mol	Log A,[c] cm^3 mol^{-1} sec^{-1}	E,[c] kcal/mol
$CH_3 + SiH_4$	12.26	7.47	12.26	7.47	12.26	7.47
$C_2H_5 + SiH_4$	11.73	7.25	10.86	7.25	11.73	9.05
n-$C_3H_7 + SiH_4$	11.52	6.91	10.65[d]	6.91[d]	11.52[d]	8.71[d]
i-$C_3H_7 + SiH_4$	11.84	7.64	10.97	7.64	11.84	9.44
$CH_3 + Si_2H_6$	11.96	5.63	11.96	5.63	11.96	5.63
$C_2H_5 + Si_2H_6$	11.75	5.65	10.88	5.65	11.75	7.45

[a] Assuming log k_{comb} = 13.34 and E_{comb} = 0 in all cases. [b] Using the rate constant values from ref 30 and 31 and assuming that E_{comb} = 0 in all cases. [c] Using the rate constant values from ref 30 and 31 and assuming that log A_{comb} = 13.34 in all cases. [d] Assuming that log k_{comb} = 11.6.

TABLE XI: Experimentally Determined Kinetic Isotope Effects at 100°

Reaction	k_H/k_D
CH_3 + silane[a]	3.3
CH_3 + disilane[a]	3.6
C_2H_5 + silane[b]	3.2
C_2H_5 + disilane[b]	2.7
n-C_3H_7 + silane[b]	3.9
n-C_3H_7 + disilane[b]	2.9
i-C_3H_7 + silane[b]	4.0
i-C_3H_7 + disilane[b]	2.8
CH_3 + methane[c]	12.6
CH_3 + ethane[d]	7.4

[a] Reference 13. [b] This work. [c] Reference 24 and 25. [d] Reference 26.

been reported by Shepp and Kutschke[28] for the combination of ethyl radicals. More recently Hiatt and Benson[29-31] obtained log k = 11.6 (cc mol^{-1} sec^{-1}) for the combination of ethyl and isopropyl radicals and their data indicate that the activation energy for ethyl radical recombination is zero. But this rate constant, together with log A = 13.34, yields an activation energy of 3.6 kcal/mol for the combination of ethyl and isopropyl radicals.

The Arrhenius parameters for the hydrogen abstraction reactions from silanes were recalculated from these data and are presented in Table X. It is seen that the activation energies show a definite upward trend with decreasing C–H bond energies of the reacting alkyl radicals if an activation energy of 3.6 kcal/mol is assumed for the combination of ethyl, n-propyl, and isopropyl radicals.

Potential energies of activation calculated by the BEBO method are tabulated in Table VIII. They are all higher than the experimental activation energies, but also follow an upward trend corresponding to the decreasing strength of the newly formed C–H bonds from SiH_4 as well as CH_4.

Experimental kinetic isotope effects are listed in Table XI. They are generally lower for disilane than for silane, in accordance with the lower zero-point energies involved. Arrhenius type curves of the temperature dependence of the isotope effect for n-propyl and isopropyl radicals, plotted in Figure 4, show little difference. Extrapolation of the curves to infinite temperatures results in a limiting value of about 0.75 for k_H/k_D. This is much too low in comparison with the expected value of about 1.35 for the high-temperature limit and appears to indicate a considerable tunneling effect.

In the absence of reliable activation energies for the recombination–disproportionation reactions of the alkyl radicals involved in the present study, the precise values of the Arrhenius parameters of the hydrogen abstraction reactions cannot be determined. If a simple correlation between the C–H bond strength in the abstracting radical and the magnitude of the activation energy for hydrogen transfer does exist, as predicted by the BEBO method, then our results would seem to favor the existence of a small activation energy for the ethyl, n-propyl, and isopropyl radical recombination–disproportionation reactions. However, because of the rather low temperatures of the experiments, tunneling effects could also contribute to a distortion of the expected trend in the activation energies.

Acknowledgments. We thank the National Research Council of Canada for financial support and Dr. A. M. Hogg for assistance in the mass spectrometric analysis.

References and Notes

(1) A. F. Trotman-Dickenson, *Advan. Free Radical Chem.*, **1**, 1 (1965).
(2) R. E. Berkley, G. N. C. Woodall, O. P. Strausz, and H. E. Gunning, *Can. J. Chem.*, **47**, 3305 (1969).
(3) J. A. Kerr, A. Stephens, and J. C. Young, *Int. J. Chem. Kinet.*, **1**, 339 (1969).
(4) J. A. Kerr, A. Stephens, and J. C. Young, *Int. J. Chem. Kinet.*, **1**, 371 (1969).
(5) J. H. Purnell and R. Walsh, *Proc. Roy. Soc., Ser. A.*, **293**, 543 (1966).
(6) S. Toby and B. H. Weiss, *J. Phys. Chem.*, **66**, 2681 (1962).
(7) R. Rebbert and P. Ausloos, *J. Phys. Chem.*, **67**, 1925 (1963).
(8) P. Gray and J. C. J. Thynne, *Trans. Faraday Soc.*, **59**, 2275 (1963).
(9) P. Gray, A. Jones, and J. C. J. Thynne, *Trans. Faraday Soc.*, **61**, 474 (1965).
(10) S. Toby and J. Nimoy, *J. Phys. Chem.*, **70**, 867 (1966).
(11) S-L. Cheng, J. Nimoy, and S. Toby, *J. Phys. Chem.*, **71**, 3075 (1967).
(12) E. R. Morris and J. C. J. Thynne, *J. Phys. Chem.*, **73**, 3294 (1969).
(13) O. P. Strausz, E. Jakubowski, H. S. Sandhu, and H. E. Gunning, *J. Chem. Phys.*, **51**, 552 (1969).
(14) P. Ausloos and E. W. R. Steacie, *Bull. Soc. Chim. Belg.*, **63**, 87 (1954).
(15) H. Cerfontain and K. O. Kutschke, *Can. J. Chem.*, **36**, 344 (1958).
(16) W. E. Falconer and W. A. Sunder, *Int. J. Chem. Kinet.*, **3**, 523 (1971).
(17) R. W. Durham and E. W. R. Steacie, *Can. J. Chem.*, **31**, 377 (1953).
(18) R. H. Riem and K. O. Kutschke, *Can. J. Chem.*, **38**, 2332 (1960).
(19) H. S. Johnston, "Gas Phase Reaction Rate Theory," Ronald Press, New York, N. Y., 1966.
(20) J. A. Kerr, *Chem. Rev.*, **66**, 465 (1966).
(21) F. E. Saalfeld and H. J. Svec, *J. Phys. Chem.*, **70**, 1753 (1966).
(22) W. C. Steele, L. D. Nichols, and F. G. A. Stone, *J. Amer. Chem. Soc.*, **84**, 4441 (1962).
(23) R. E. Wilde, *J. Mol. Spectrosc.*, **8**, 427 (1962).
(24) F. S. Dainton, K. J. Ivin, and F. Wilkinson, *Trans. Faraday Soc.*, **55**, 929 (1959).
(25) G. A. Creak, F. S. Dainton, and K. J. Ivin, *Trans. Faraday Soc.*, **58**, 326 (1962).
(26) J. R. McNesby, *J. Phys. Chem.*, **64**, 1671 (1960).
(27) A. Shepp, *J. Chem. Phys.*, **24**, 939 (1956).
(28) A. Shepp and K. O. Kutschke, *J. Chem. Phys.*, **26**, 1020 (1957).
(29) R. Hiatt and S. W. Benson, *J. Amer. Chem. Soc.*, **94**, 25 (1972).
(30) R. Hiatt and S. W. Benson, *Int. J. Chem. Kinet.*, **4**, 151 (1972).
(31) R. Hiatt and S. W. Benson, *J. Amer. Chem. Soc.*, **94**, 6886 (1972).

Kinetics and Mechanisms of the Reactions of Atomic Fluorine with CF_3I and CCl_3Br

Joseph W. Bozzelli and M. Kaufman*[1]

Frick Chemical Laboratory, Princeton University, Princeton, New Jersey 08540 *(Received February 20, 1973)*

Publication costs assisted by The Office of Naval Research

Using molecular beam analysis, the kinetics and mechanisms of the reactions of atomic fluorine with CF_3I and CCl_3Br have been investigated in a fast-flow reactor. Direct observation of perhalomethyl radicals and lack of detection of displaced halogen atoms proves conclusively that both of these reactions proceed primarily by abstraction, rather than displacement, of a halogen atom. In the CCl_3Br system, successive "atom-switching" reactions rapidly convert CCl_3 to its fluorinated analogs. The rate constants are $k(F + CF_3I) = 7.2 \pm 3.6 \times 10^{13}$ cm^3/mol sec and $k(F + CCl_3Br) = 5.6 \pm 2.8 \times 10^{13}$ cm^3/mol sec.

Introduction

The attack of an atom on an unstrained sp^3-hybridized carbon usually results in the *abstraction* of some group from the carbon. For only a few thermal reactions, has it been proposed that the principle mechanism is *displacement* of a group from the carbon.[2] Such displacement reactions are strongly exothermic for the reactions of atomic fluorine with perhalomethanes, and have, in fact, been observed in the hot-atom regime.[3] However, it is still somewhat unclear whether *displacement* occurs at thermal energies in this series of reactions, especially since their rates seem to correlate with the energetics of the *abstraction* mechanism. The reactions of this group for which abstraction is endothermic are all found to be very slow. However, while abstraction has been indicated for F + CCl_4 (at 298°K)[4] and F + CCl_3F (at 491–586°K),[5] the displacement pathway has been strongly favored for F + CCl_2F_2 and F + CF_3Cl at flame temperatures (1500°K).[6] Abstraction is exothermic for F + CF_3I; this reaction has been found to be very rapid, and evidence has been obtained that it proceeds by the abstraction mechanism.[7]

In the present work, we investigate the reactions of atomic fluorine with CF_3I and CCl_3Br, using an instrument which is capable of direct observation of transient intermediates.[8] Detection of CX_3 radicals and lack of detection of displaced halogen atoms proves conclusively that these reactions follow primarily the abstraction pathway, which is exothermic in both cases. The room temperature rate constants of these two reactions are measured.

Experimental Section

The reactions of atomic fluorine with CF_3I and CCl_3Br are studied by molecular beam analysis, a new method, in which molecular beam techniques are employed to preselect the neutral species entering a mass spectrometer.[8,9] With the beam measurements helping to identify the neutral parent of each ion observed in the mass spectrometer, there is no need to carefully control the energy of the ionizing electrons, in order to achieve "appearance potential discrimination." Thus 100–250 mA of ionizing electrons can be employed, giving ionization efficiencies several orders of magnitude larger than those generally attained in free-radical mass spectrometry. The use of phase sensitive detection of the modulated beam and total pressures of the order of 10^{-9} Torr in the ionization region allows very low concentrations of transient intermediates to be detected by this method.

In this work, we have employed only the magnetic deflection mode of molecular beam analysis,[8,9] which consists of blocking the entrance to the mass spectrometer with an obstacle, and then using a small permanent (hexapolar) magnet to deflect particles into the ionization region. Paramagnetic atoms and free radicals are effectively "focused" by such a magnetic lens, while diamagnetic molecules are hardly affected by the field. The observation of *net* magnetic focusing at any m/e in the mass spectrum indicates that at least a few per cent of these ions arise from paramagnetic neutrals, since the focusing effect must overcome the decrease in signal resulting from blockage of some of the scattered beam by the permanent magnet.

Except for addition of liquid nitrogen cryopumping to the detector chamber, the molecular beam analyzer was physically as described previously.[8] An additional change consists of maintaining the exit electrode of the Weiss-type ionizer[10] at *ca.* 300-V negative with respect to the grids and anode. This has proved to be a more efficient means of collecting ions than the application of a similar positive voltage to the entrance electrode.

The F + CF_3I and F + CCl_3Br reactions were studied in a fast flow system at total pressures of *ca.* 1 Torr. Atomic fluorine was generated by a microwave discharge in dilute (0.1%) mixtures of F_2 in He or Ar, using an alumina discharge tube[11] and alumina, Teflon or Teflon-coated 19-mm diameter flow tubes. The perhalomethanes were added through a Teflon inlet, whose position could be varied with respect to the 0.1–0.2-mm diameter sampling orifice of the molecular beam analyzer. In such systems, no products of the reaction of atomic fluorine with surfaces could be observed mass spectrometrically.

Both reactions were found to be very rapid. In order to achieve the flow speeds of 20–50 m/sec necessary for spacial resolution of the reaction in convenient ranges of concentrations, it was necessary to modify the flow reactor used in ref 4 by increasing the diameter of the tubing in the trapping system to 5 cm and using only a single trap at liquid N_2 temperature. Since F_2 is not removed by such a trap, the oil in the Welch 1397 pump was changed every 3 days.

Gas flow rates are determined by timing pressure increases in calibrated volumes or volume changes at known

pressures. Halocarbon oil (Halocarbon Products Corp., Series 13-21) manometers are employed for these measurements. The very small flows of the perhalomethanes are controlled by a Granville-Phillips Series 203 variable leak valve. Pressure is measured with a McLeod gauge and generally varies less than 10% across the reaction zone. The average pressure is used to convert flow rate measurements to partial pressures.

Initiation of the discharge reduces the m/e 38 (F_2^+) signal to less than 3% of its original intensity. Simultaneously, m/e 19 (F^+) increases greater than threefold and shows 25–30% magnetic focusing, indicating that F_2 is efficiently dissociated by the discharge. This result is obtained with as little as 10 W of 2450-MHz power. However, measurements are generally made with 40 W, at which power it is somewhat easier to stabilize the discharge and minimize the radiation reflected from the Evenson-type cavity.[12] The almost complete dissociation of F_2 observed here contrasts with dissociations of 20–40% achieved in our earlier $F + CCl_4$ studies,[4] where the low rate constant required the use of high atomic fluorine concentrations and low flow velocities. Since the microwave power per input F_2 molecule is similar in the two experiments, the difference must undoubtedly be due to the greater importance of atomic fluorine recombination in the CCl_4 case. In Rosner's work,[11] intermediate (*ca.* 1%) concentrations of F_2 were employed and 78% dissociation was attained.

Absolute concentrations of atomic fluorine are determined by titration with H_2. However, the interpretation of the titration curves is somewhat different from that appropriate to our $F + CCl_4$ studies,[4] due to the higher flow rates and lower F_2 concentration in the present work. The fall off of the magnetically focused m/e 19 (atomic fluorine) signal, as H_2 is added to the gas stream, is shown for three titrations in Figure 1. Although the initial decrease of this signal is linear with added H_2, some tailing can be observed in the latter part of the titration curve. This results from the fact that the titration reaction

$$F + H_2 \longrightarrow HF + H \qquad (1)$$

does not have sufficient time to go to completion while the gas is flowing the 20 cm from the H_2 inlet to the sampling orifice. Corrections for this effect, which becomes relatively more important toward the end point of the titration, are made by using the known rate constant of reaction 1, as illustrated in Appendix I. The corrected titration curves are linear to the equivalence point. In the current work, regeneration of atomic fluorine by the reaction

$$H + F_2 \longrightarrow HF + F \qquad (2)$$

is negligible, due to the low F_2 concentration and the short time available for this reaction, which has been reported to be somewhat slower than reaction 1.[13]

Table I shows that the atomic fluorine flow measured by H_2 titration corresponds to dissociation of between 80 and 100% of the added F_2. Considering the other indications that F_2 is efficiently dissociated under these conditions, we feel that the titration values can be trusted to within ±10%.

Ion intensities at m/e 196 (CF_3I^+) and 163 (CCl_2Br^+) were taken as proportional to the concentrations of CF_3I and CCl_3Br, respectively. The latter compound has a very low parent ion intensity, which is generally characteristic of totally halogenated alkanes. At each inlet position, the ratio of the ion signals with the discharge on to that with it off was assumed equal to the fraction of the perhalomethane unreacted at that position.

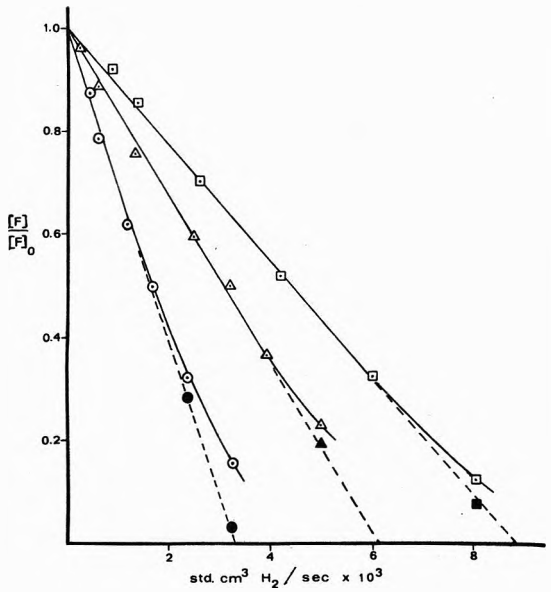

Figure 1. Three typical titrations of atomic fluorine with molecular hydrogen. The solid curve is through the experimental points; the dased line is corrected for incompleteness of the titration reaction by the method given in Appendix I.

TABLE I: Comparison of Atomic Fluorine Titration with Total F_2 Input

Pressure, Torr	Atomic fluorine flow (by titration), std cc/sec × 10^3	F_2 input (flowmeter), std cc/sec × 10^3	F flow / 2 × F_2 input
0.79	8.84	5.05	0.88
0.90	4.90	2.47	0.99
1.14	3.70	2.27	0.81
0.90	8.47	4.63	0.91
1.13	1.84	1.08	0.85
0.92	1.84	10.9	0.84
0.92	3.24	2.01	0.81
0.78	4.30	2.60	0.83
0.85	4.18	2.10	1.00
1.16	6.38	3.26	0.98
0.84	3.37	1.97	0.86
0.82	5.28	2.80	0.94

All the gases used in these experiments are purchased from Matheson Gas Products, except for CF_3I, which is obtained from Peninsular Chemresearch, Inc. Helium and hydrogen are ultrapure grade and are used without further purification. Argon was dried by passing it through a P_2O_5 trap. Fluorine was passed through a NaF trap to remove HF. The molecular beam analyzer indicated that it contained less than 1% of air impurity. CF_3I was used without further purification. CCl_3Br was subjected to several cycles of freezing, pumping, and thawing, and stored in a 3-l. bulb. In some experiments it was diluted with He to improve the mixing at the inlet.

Results and Discussion

$F + CF_3I$. Reaction Mechanism. In the $F + CF_3I$ reaction, magnetic focusing is observed for the ions listed in Table II. The paramagnetic neutral parent of CF_3^+ is un-

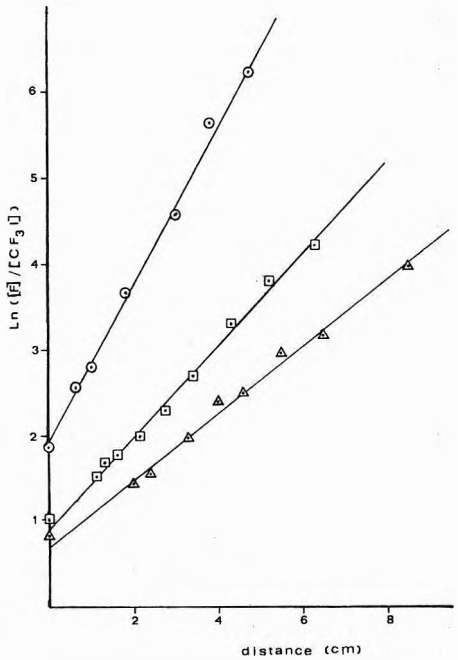

Figure 2. Linear least-squares fit to data for the F + CF_3I reaction: Upper curve, run 3; middle curve, run 4; lower curve, run 1; linear flow velocities 2690, 2940, and 4300 cm/sec, respectively (see Table III).

doubtedly the CF_3 radical. This species probably alsc produces the observed focusing at CF_2^+, due to dissociative ionization by the 70–110-V electrons used in the ionizer. CF_2 could not cause this focusing, since it has a singlet ground state[14] and there is no reasonable mechanism for its formation in this system. The focusing at CF_2^+ is considerably larger than that at CF_3^+, indicating that the CF_3 radical, much like all perhalomethane molecules, shows a pronounced tendency to fragment one carbon–halogen bond when it is ionized. Thus, when the direct beam is monitored, initiation of the reaction results in a marked increase in the CF_2^+ peak and a decrease in the CF_3^+ peak. This latter effect can also be observed in Leipunskii's data.[7]

No magnetic focusing is detected for the I^+ ion in this system, and the defocusing observed when the magnet is lowered is typical of that obtained for ions from diamagnetic species. The presence of CF_3 radicals and absence of detectable concentrations of atomic iodine proves that this reaction proceeds primarily by iodine abstraction

$$F + CF_3I \longrightarrow CF_3 + IF \quad \Delta H = -11 \pm 5\ \text{kcal/mol}^{15} \tag{3}$$

rather than by displacement

$$F + CF_3I \longrightarrow CF_4 + I \quad \Delta H = -69 \pm 8\ \text{kcal/mol}^{15} \tag{4}$$

A similar inference was made by Leipunskii, *et al.*,[7] based upon the decrease in I^+ and increase in IF^+ upon initiation of the reaction. However, our conclusion is based upon direct observation of CF_3, rather than assumptions regarding fragmentation patterns and the importance of subsequent steps in the mechanism.

With fast flows, the only new ion produced by the reaction is IF^+. However, at slower flows IF_2^+, IF_3^+, IF_4^+, IF_5^+, and $C_2F_n^+$ appear in the mass spectrum. These ions no doubt arise from recombination of CF_3 radicals and from successive reactions of IF with atomic fluorine and residual F_2 in the system.

TABLE II: Magnetic Focusing in the F + CF_3I Reaction

Ion	% magnetic focusing[a]	Relative focused signal[b]	Paramagnetic netural parent
CF_3^+	1.3	0.025	CF_3
CF_2^+	6.6	0.127	CF_3
F^+	28.5	1.00	F

[a] [Increase in intensity when magnet is lowered (direct beam blocked by obstacle)/direct beam] × 100. [b] Increase in ion signal when magnet is lowered/increase at *m/e* 19 (at same multiplier voltage and amplifier gain).

TABLE III: Rate Data for F + CF_3I

Run	Pressure, Torr	[He] × 10^8, mol/cm³	$[F]_0$ × 10^{11}, mol/cm³	$[CF_3I]_0$ × 10^{11}, mol/cm³	$k \times 10^{-13}$, cm³/mol sec[a]
1	1.40	8.2	3.4	1.38	8.1
2	0.98	5.7	7.3	6.00	7.6
3	1.03	6.0	7.4	1.20	4.0
4	0.90	5.3	4.5	1.60	5.4
5	0.90	5.3	4.5	0.48	5.1
6	1.14	6.7	3.2	0.50	5.9
7	1.14	6.7	3.2	0.92	10.0
8	1.14	6.7	3.2	1.05	8.9
9	0.91	5.3	7.8	1.15	6.4
10	1.13	6.6	1.5	0.81	10.6

[a] $k_{av} = 7.2 \times 10^{13}$ cm³/mol sec.

F + CF_3I. Rate Constant. The data for ten kinetic runs for the F + CF_3I reaction are given in Table III. Atomic fluorine was always in excess, but its concentration could not be made large enough to be considered constant, without having the reaction proceed inconveniently fast. However, the ratio of CF_3I consumed to atomic fluorine consumed was consistently measured to be 1.0, allowing the rate equation to be expressed in terms of a single concentration variable, the amount of either reagent that has reacted (x)

$$dx/dt = k_3([CF_3I]_0 - x)([F]_0 - x) \tag{5}$$

Integrating this expression by the method of partial fractions gives

$$\ln \frac{[F]}{[CF_3I]} = ([F]_0 - [CF_3I]_0)k_3t + \ln \frac{[F]_0}{[CF_3I]_0} \tag{6}$$

Figure 2 shows that plots of the kinetic data have this form. Each set of data is fit by a linear least-squares analysis, and the rate constants so determined are given in Table III. The average rate constant is 7.2×10^{13} cm³/mol sec, with a standard deviation of the mean of 0.7×10^{13} cm³/mol sec. No obvious dependence of the measured rate constant on the initial concentration of F or CF_3I, or on the ratio of these concentrations, can be discerned.

Although the random scatter of the results is quite small, there are difficulties involved in measuring very large rate constants in a flow system such as ours, which introduce numerous possibilities for systematic errors. Probably the most important of these is a somewhat poorly defined flow pattern for a reaction that approaches completion in a distance of three–five tube diameters,

TABLE IV: Magnetic Focusing in the F + CCl_3Br Reaction

Ion	% magnetic focusing[a]	Relative focused signal[b]	Paramagnetic neutral parent
CCl_3^+	1.2	0.03	CCl_3
CCl_2^+	4.1	0.04	CCl_3, (CCl_2F)
$CClF^+$	5.5	0.05	CCl_2F, ($CClF_2$)
CF_2^+	5.5	0.04	CF_2Cl, CF_3
Cl^+	19.2	0.24	Cl, CCl_3, CCl_2F, $CClF_2$
F^+	28.5	1.0	F

[a,b] See corresponding footnotes to Table II.

with possibilities of incomplete mixing and radial concentration gradients. However, the good fit of the experimental data to the theoretical form tends to indicate that these effects are not of overwhelming importance. Making allowance for errors in the titration (±10%), errors introduced by the pressure drop (<10%) over the reaction zone, and the unknown flow pattern, we consider our result accurate to within 50%, and thus report $k_3 = 7.2 \pm 3.6 \times 10^{13}$ cm³/mol sec.

Leipunskii, *et al.*, determined that the rate constant is $1.0 \pm 0.4 \times 10^{14}$ cm³/mol sec for this reaction, using a diffusion rather than a flow system.[7] The good agreement between the two results gives us additional confidence in our technique. The measured rate constant is close to the collision rate for fluorine atoms hitting the iodine part of CF_3I, and indicates a reaction that has essentially zero activation barrier.

F + CCl_3Br. Reaction Mechanism. Table IV summarizes the magnetic focusing data for the F + CCl_3Br reaction. The radicals in parentheses are thought to contribute very little to the respective focusing, since this would involve their fragmenting a strong C–F bond, rather than a much weaker C–Cl bond. The focusing for Cl^+ is much too strong to be accounted for by CX_3 radicals, and must be primarily due to chlorine atoms.

Conspicuously absent in Table IV is any magnetic focusing observed for Br^+. Once again, the major pathway is abstraction

$$F + CCl_3Br \longrightarrow BrF + CCl_3 \quad \Delta H = -3 \pm 4 \text{ kcal/mol}^{16} \quad (7)$$

rather than displacement

$$F + CCl_3Br \longrightarrow CCl_3F + Br \quad \Delta H = -54 \pm 8 \text{ kcal/mol}^{16} \quad (8)$$

The presence of the fluorinated trihalomethyl radicals $CFCl_2$, CF_2Cl, and CF_3 in the reaction mixture is explained by rapid atom-switching reactions of the type

$$F + CCl_3 \longrightarrow CCl_3F^* \longrightarrow CCl_2F + Cl \quad \Delta H \approx -30 \text{ kcal/mol} \quad (9)$$

where stabilization of the excited CCl_3F would be negligible at our operating pressures. (Elimination of ClF or Cl_2 from CCl_3F^* is not energetically feasible.) In our earlier work on the reaction F + CCl_4,[4] the occurrence of atom-switching reactions was postulated on the basis of the observation of chlorine atoms and end products in which more than one chlorine had been substituted by fluorine. In the present work however, the primary reaction, (7), is fast enough so that the extremely reactive trihalomethyl radicals reach concentrations of 10^{11}–10^{12} cm^{-3} (estimated from the magnitude of the focusing). Their observation by molecular beam analysis constitutes a more direct proof of the atom-switching mechanism.

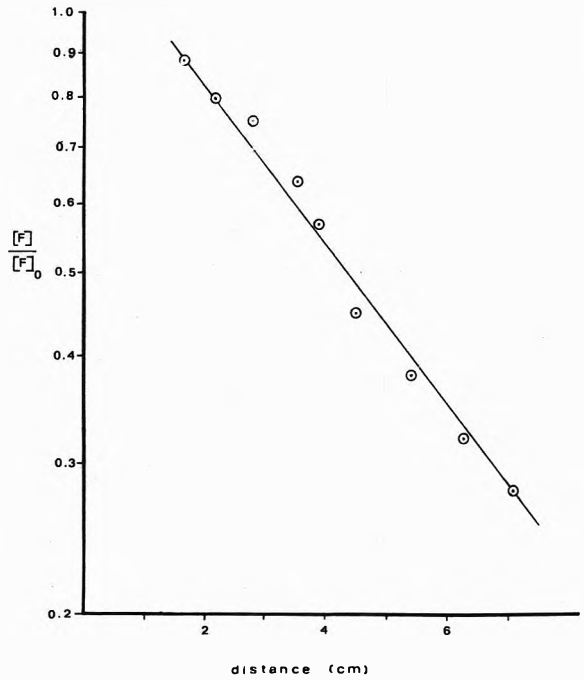

Figure 3. First-order plot of the decay of atomic fluorine in the F + CCl_3Br reaction, linear flow velocity 3280 cm/sec.

At fast flows, in addition to the ions listed in Table IV, a large diamagnetic BrF^+ signal is produced by the reaction. $BrCl^+$ ions are not observed, indicating that the reaction of CCl_3Br with atomic chlorine must be considerably slower than its reaction with atomic fluorine. At slower flow rates, many ions containing two carbon atoms are observed, indicating that some recombination of CX_3 radicals is occurring. Also, under these conditions, the presence of BrF_2^+, BrF_3^+, BrF_4^+, and BrF_5^+ points to successive reactions of BrF with atomic and molecular fluorine.

F + CCl_3Br. Rate Constant. To determine the rate constant for the F + CCl_3Br reaction, CCl_2Br^+ (*m/e* 163) and the magnetically focused F^+ signals were monitored as a function of inlet position. This reaction, unlike F + CF_3I, definitely does not follow 1:1 stoichiometry. The consumption of atomic fluorine increases from one to three times the consumption of CCl_3Br during the course of the reaction, due to the occurrence of the atom-switching reactions. The rate data could be most easily analyzed by making use of the observation, illustrated in Figure 3, that the decay of atomic fluorine was approximately first order. This finding is unexpected for the *reagent present in excess* in a second-order reaction, and means that the atom-switching reactions (9) must have rate constants very similar to the initial reaction (7), so that, in effect, the fluorine atoms are reacting with a constant concentration of reactant throughout the reaction. Using[17]

$$\ln([F]/[F]_0) = a + bt \quad (10)$$

in the differential rate expression

$$d[CCl_3Br]/dt = -k_7[F][CCl_3Br] \quad (11)$$

and integrating, gives

$$\ln([CCl_3Br]_t/[CCl_3Br]_0) = k_7[F]_0 e^a(1 - e^{bt})/b \quad (12)$$

TABLE V: Rate Data as a Function of Time for one F + CCl_3Br Experiment[a]

Time, msec	$k \times 10^{-13}$, cm^3/mol sec[b]	Time, msec	$k \times 10^{-13}$, cm^3/mol sec[b]
0.38	4.64	1.41	5.51
0.51	6.47	1.70	5.01
0.72	5.09	2.02	6.85
0.99	5.65	2.37	6.60
1.23	4.38		

[a] Run 6, see Table VI. [b] $k_{av} = 5.58 \times 10^{13}$ cc/mol sec.

TABLE VI: Rate Data for F + CCl_3Br

Run	Pressure, Torr	[He] $\times 10^6$, mol/cm^3	$[F]_0$ $\times 10^{11}$, mol/cm^3	$[CCl_3Br]_0$ $\times 10^{11}$, mol/cm^3	$k \times 10^{-13}$, cm^3/mol sec[b]
1	0.84	4.96	7.32	1.47	5.59
2	0.84	4.92	7.26	1.46	5.79
3	1.46	8.56	7.97	1.60	4.35
4	1.04	6.10	6.54	0.67	6.98
5	0.92	5.40	1.71	0.53	5.31
6	0.92	5.40	1.71	0.53	5.58
7	0.92	5.40	2.96	1.01	7.81
8	0.78	4.57[a]	3.45	0.84	5.07
9	0.85	4.99[a]	3.44	0.97	5.76
10	1.09	6.39	5.71	0.77	3.84

[a] Ar substituted for He. [b] $k_{av} = 5.6 \times 10^{13}$ cm^3/mol sec.

Thus, by determining a and b from a least-squares fit to the atomic fluorine decay data, a rate constant can be calculated for each time in an experiment. As can be seen in Table V, the calculated rate constant exhibits no systematic variation as a function of time. The time-averaged rate constant from ten different experiments, given in Table VI, agree surprisingly well and show no systematic changes with the concentration of atomic fluorine or of CCl_3Br, with the ratio of these concentrations, or with the substitution of Ar for He as the carrier gas.

The average rate constant for reaction 7 is 5.6×10^{13} cm^3/mol sec, with a standard deviation of the mean of 0.4×10^{13} cm^3/mol sec. Once again the uncertainty in the result is dominated by the possibility of systematic errors. Although more spacial resolution can be obtained than with the somewhat faster F + CF_3I reaction, this is balanced by a more complicated analysis due to the variable stoichiometry, so that we again estimate the overall accuracy to be ±50%. The rate constant is $k_7 = 5.6 \pm 2.8 \times 10^{13}$ cm^3/mol sec, which is close to the collision rate, indicating negligible activation barrier for this reaction. The reduction in the rate constant compared to that for F + CF_3I, if significant, could be explained by the smaller size of the atom being abstracted in the F + CCl_3Br reaction.

A rate constant close to the collision rate for F + CCl_3Br lends some credence to our explanation for the first-order decay of the atomic fluorine concentration. The atom-switching reactions, being between two species with unsaturated valences, would be very fast and might have rate constants quite similar to k_7. Eventually CF_3 is formed, which no longer will undergo atom switching. However, during the period over which we study the reaction, very little of the CCl_3Br will have time to undergo the four successive reactions necessary for its conversion to CF_3.

Acknowledgment. The authors would like to acknowledge research support by the Office of Naval Research under Contract No. NOO14-67-A-0151-0013. Many helpful discussions with Barry Hertzler are greatly appreciated.

Appendix I

In order to account for incompleteness of the titration reaction, we solve the rate expression for this reaction

$$-d[F]/dt = k_1[F][H_2] \quad (13)$$

Letting x = the concentration of atomic fluorine that has reacted and $y = [H_2]_0/[F]_0$, this becomes

$$dx/dt = k_1([F]_0 - x)(y[F]_0 - x) \quad (14)$$

which may be rearranged and integrated by the method of partial fractions, to give

$$\ln [y([F]_0 - x)/y[F]_0 - x] = [F]_0(1 - y)k_1t \quad (15)$$

Further rearrangement produces

$$\frac{x}{[F]_0} = \frac{y[1 - \exp([F]_0(1 - y)k_1t)]}{y - \exp([F]_0(1 - y)k_1t)} = 1 - \frac{[F]}{[F]_0} \quad (16)$$

Using the measured time available for reaction 1 and $k_1 = 1 \times 10^{13}$ cm^3/mol sec,[13] equation 16 is solved by computer to provide a table of corresponding values of x and y. Thus, for a measured value of $[F]/[F]_0$, one can obtain y, which is the fraction of the atomic fluorine that would have been removed if the titration had gone to completion.

References and Notes

(1) Correspondence should be addressed to Department of Chemistry, Emory University, Atlanta, Ga. 30322.
(2) K. U. Ingold and B. P. Roberts, "Free-Radical Substitution Reactions," Wiley-Interscience, 1971, p 72; F. Wright, *Symp. (Int.) Combust., [Proc.], 10th, 1964*, 386 (1965); A. Ung and H. I. Schiff, *Can. J. Chem.*, **40**, 486 (1962).
(3) W. J. Parks, K. A. Krohn, and J. Root, *J. Chem. Phys.*, **55**, 2690, 5771, 5785 (1971); D. T. Smail and F. S. Rowland, *J. Phys. Chem.*, **74**, 1866 (1970).
(4) C. E. Kolb and M. Kaufman, *J. Phys. Chem.*, **76**, 947 (1972).
(5) R. Foon and K. B. Tait, *Trans. Faraday Soc.*, **67**, 3038 (1971); **68**, 104 (1972).
(6) K. H. Homann and D. I. MacLean, *Combust. Flame*, **14**, 409 (1970); *J. Phys. Chem.*, **75**, 3645 (1971).
(7) I. O. Leipunskii, I. I. Morosov, and V. L. Tal'rose, *Dokl. Akad. Nauk SSSR*, **198**, 1367 (1971).
(8) C. E. Kolb and M. Kaufman, *Chem. Instrum.*, **3**, 175 (1971).
(9) V. L. Tal'rose, A. F. Dodonov, I. O. Leipunskii, and I. I. Morozov, *Int. J. Mass Spectrom. Ion Phys.*, **7**, 363 (1971).
(10) R. Weiss, *Rev. Sci. Instrum.*, **32**, 397 (1961).
(11) D. E. Rosner and H. D. Allendorf, *J. Phys. Chem.*, **75**, 308 (1971).
(12) F. C. Fehsenfeld, K. M. Evenson, and H. P. Broida, *Rev. Sci. Instrum.*, **36**, 294 (1965).
(13) K. H. Homann, W. C. Solomon, J. Warnatz, H. G. Wagner, and C. Zetzsch, *Ber. Bunsenges. Phys. Chem.*, **74**, 585 (1970); R. G. Albright, A. F. Dodonov, G. K. Lavrovskaya, I. I. Morosov, and V. L. Tal'rose, *J. Chem. Phys.*, **50**, 3632 (1969); S. W. Rabideau, H. G. Hecht, and W. Burton Lewis, *J. Mag. Resonance*, **6**, 384 (1972).
(14) F. X. Powell and D. R. Lide, *J. Chem. Phys.*, **45**, 1067 (1966).
(15) $D°_{298}$: I–F, 67 ± 1; CF_3–I, 56 ± 4 (taken as equal to CH_3–I, by analogy to CF_3Br *vs.* CH_3Br); CF_3–F, 125 ± 4, *Nat. Stand. Ref. Data Ser., Nat. Bur. Stand.*, **No. 31** (1970).
(16) $D°_{298}$: CCl_3–Br, 52 ± 3; CCl_3–F, 106 ± 5, see ref 15; Br–F, 55 ± 1, B. Rosen, "Spectroscopic Data Relative to Diatomic Molecules," Pergamon Press, New York, N. Y., 1970.
(17) The inclusion of the constant a in this expression allows for the experimentally observed mixing distance (see Figure 3), which appears to be *ca.* 1 cm.

Raman Spectroscopy of Alkali Metal–Ammonia Solutions

Billie L. Smith and William H. Koehler*

Department of Chemistry, Texas Christian University, Fort Worth, Texas 76129 *(Received February 5, 1973)*

Publication costs assisted by The Robert A. Welch Foundation

A laser Raman spectrometer has been constructed which readily accepts a specially designed dewar assembly. After the resolution and polarization performance characteristics of the spectrometer were determined, polarization studies on liquid ammonia were undertaken. Depolarization ratios for the fundamental modes of ammonia are reported, and a doublet has been observed for the ν_2 band. Alkali metal–ammonia solutions in the concentration range 0–50 × 10^{-4} M were studied. No scattering center attributed to the solvated electron was found, nor were the positions of the bands altered by the presence of the solute in this concentration region. The intensity of the scattered radiation was found to decrease with increasing metal concentration and has been attributed to the absorbance of these solutions. The Raman effect in F centers is discussed and compared to alkali metal–ammonia solutions.

Introduction

The nature of the species present in a very dilute metal–ammonia solution continues to be a matter of speculation. Numerous models have been proposed, but as yet no single theory is clearly superior. A discussion of the various models will not be attempted in this work because numerous review articles are available.[1] Copeland, Kestner, and Jortner[2] have proposed a model for localized excess electron states in ammonia, and this model has a particular bearing on the present work. According to Copeland, *et al.*, very dilute solutions may be described in terms of unassociated solvated cations and electrons. The electron is envisioned as existing in a cavity created by some number of preferentially oriented ammonia molecules.

The proposed model predicts a totally symmetric vibration in the ground state with a frequency given by

$$\nu = (1/2\pi)[K/\mu]^{1/2}$$

where K is $\frac{1}{2}(\partial^2 E_t/\partial R^2)_{R=R_0}$, and $\mu = N m_{NH_3}$ E_t is the total energy of the ground state, R is the cavity radius, N is the number of solvent molecules in the primary solvation shell, and m_{NH3} is the reduced mass of the ammonia molecule. Depending on the value of N and V_0, the electronic energy of the quasifree electron state, the totally symmetric vibration is predicted to be between 25 and 60 cm^{-1}.

Rusch,[3] applying the treatment of Klick and Schulman[4] to metal–ammonia solutions, has suggested that the symmetric "breathing" mode may be in the 400- to 700-cm^{-1} region. These results were obtained using the formulation for the frequency of the "breathing" mode which is given by

$$\nu_g = (2kT/h)[W_{h/2}(LT)/W_{h/2}(HT)]^2$$

where ν_g is the frequency of the ground-state vibration, $W_{h/2}$ is the width at half-height of the absorption band, and LT and HT refer to the low- and high-temperature limits, respectively.

Regardless of the model used to explain the observed properties of these solutions, the effect of the metal on the solvent structure is of primary importance. Several investigators have addressed themselves to this problem, but at present the results are incomplete and appear contradictory. Beckman and Pitzer,[5] using external reflection techniques, studied the intermediate and concentrated solutions in the infrared. Burow and Lagowski,[6] using internal reflection techniques, addressed themselves to much the same problem. Rusch,[7] using transmission techniques, studied the effect of metal concentration on the 3300-cm^{-1} envelope of ammonia. The results of the aforementioned investigations are summarized in Table I.

In addition to the effect of metal on the solvent structure, the assignment of the Raman bands of liquid ammonia is contradictory and still speculative. It is not the purpose of this work to review all the vibrational data reported on ammonia; however, the Raman data available on liquid ammonia are summarized in Table II.[8-16]

Experimental Section

A laser Raman spectrometer was constructed from three basic components: (1) Control Laser Corporation Ar^+ laser, (2) Spex 1401 double monochromator, and (3) Solid State Research photon-counting detection system. The spectrometer utilized the conventional 90° geometry and is shown schematically in Figure 1.

Radiation of appropriate frequency and intensity was focused on the sample cell (Figure 2) and the scattered radiation collected at right angles. Both the 4880- (50–350 mW) and the 4579-Å lines (maximum power 100 mW) were used in this work. The beam was focused to a diameter of approximately 0.2 mm at the sample cell.

The scattered radiation was collected and collimated with a conventional camera lens (55 mm $f/2$), passed through an analyzer, and focused on the entrance slit with a lens compatible with the f number of the monochromator. Prior to the slit assembly, a dove prism was used to rotate the image 90° (this rendered the image compatible with the vertical entrance slit), and a calcite wedge scrambler was inserted to remove the polarization dependence of the monochromator.

An SSRI photocounting detection system was employed with the Spex 1401 monochromator. This detection system incorporates a Bendix Channeltron photomultiplier tube which has a dark count of 10 counts/sec at room temperature.

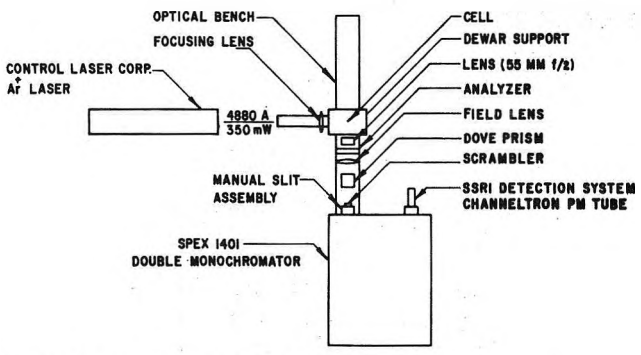

Figure 1. Laser Raman spectrometer.

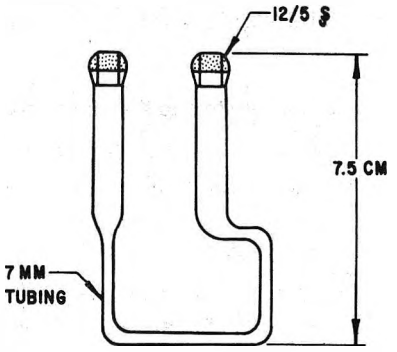

Figure 2. Sample cell.

TABLE I: Infrared Spectroscopy of Metal–Ammonia Solutions[a]

Ref	Assignment	Solvent	Concentration				
5			(MPM > 0.5)				
	ν_2		1030–1050				
	ν_1		3190				
	ν_3		3370				
			2×10^{-3} *M* Na	1.7×10^{-2} *M* Na	1.3×10^{-1} *M* Na	1.4 *M* Na	10.3 *M* Na
6	$2\nu_4$	3220	3220	3220	3230	3240	3220
	ν_1	3280	3280	3280	3230		3300
	ν_3	3410	3410	3410	3410	3410	3410
			1.0×10^{-2} *M* Li	1.0×10^{-2} *M* K	1.0×10^{-1} *M* Li	1.0×10^{-1} *M* K	
			3170	3230	3220	3240	
			3280	3280	3280	3280	
			3380	3420	3410	3400	
			5×10^{-3}[Li]	5×10^{-3}[K]	5×10^{-2}[Li]	5×10^{-2}[K]	
7	$2\nu_4$	3155	3158	3156	3153	3152	
	ν_1	3286	3265	3268	3250	3252	
	ν_3	3453	3429	3426	3409	3413	

[a] All values in cm^{-1}.

TABLE II: Raman Spectroscopy of Liquid Ammonia

Date	Observed bands and assignments					*t*, °C	Ref
1929			3210( )	3310( )	3380( )	−40	8
1930	1070($\nu_2\nu$)		3216( )	3304(ν_1)	3380(ν_3)	+25	9
1930		1594(ν_4)	3208( )	3296(ν_1)	3388(ν_3)		10
1936	1070( )	1580( )	3210( )	3300( )	3380( )	−40	11
1953	1031_{1054}	1624(ν_4)	3212( )	3303(ν_1)	3384(ν_3)	+25	12
	1077(ν_2)						
1954			3218($2\nu_4$)	3300(ν_1)	3373(ν_3)	−34 to −70	13
1968			3215($2\nu_4$)	3301(ν_1)	3384(ν_3)	+25	14
1970	1070(ν_2)	1641(ν_4)	3206(ν_1)	3296($2\nu_4$)	3363(ν_3)	−55	15
1970	1061(ν_2)	1645(ν_4)	3218( )	3303( )	3386(ν_3)	+40 to −80	16
1972	1060 ± 5	1634 ± 5	3215 ± 2	3301 ± 2	3380 ± 2	−67	Present work
	1060 ± 5		3214 ± 2	3300 ± 2	3377 ± 2	+25	

The Raman cell itself was little more than a U-tube. The extrusion permitted the closest approach of the scattering center to the collection lens within the confines of the dewar. This design also enabled the focal point of the collection lens to be set at the scattering center which resulted in good collimation. The dewar design permitted two passes of the laser when a mirror was placed at the exit window.

The solutions were prepared and studied in a modified version of the dewar assembly described by Quinn.[17] Prior to solution preparation, the assembly was subjected to a cleaning procedure previously described.[18] To prepare a solution, a quantity of ammonia was distilled off sodium and condensed in the insert. The volume was determined from the calibrated pipet and was known to within ±1%. A known weight of high-purity metal (Alfa Inorganics,

Inc.) was added using a winch assembly previously described.[18] Temperature of the solutions was monitored with a thermistor which extended into the optical cell. Room temperature spectra were recorded with the ammonia in sealed tubes.

In general, spectra were recorded without the analyzer in the fore optics and then with the analyzer set first parallel and then perpendicular. The spectra were recorded at constant slit width (usually 300 μ) which corresponded to spectral band widths in the order of 4–6 cm^{-1}. The spectrum was generally scanned at 10 cm^{-1}/min for the first several hundred wave numbers then increased to 50 cm^{-1}/min.

Results and Discussion

Prior to initiating the metal–ammonia studies, the resolution and polarization performance of the spectrometer were determined. The 459-cm^{-1} line of carbon tetrachloride was investigated and the three most prominent bands occurred at 456.1, 458.8, and 460.6 cm^{-1}. These three bands arise from the isotopic distribution of chlorine and have been reported by Herzberg[19] at 455.1, 458.4, and 461.5 cm^{-1}.

No attempt was made in the present study to eliminate all the errors generally associated with quantitative polarization measurements. The design of the spectrometer and cell assembly was predicted on obtaining Raman spectra of metal–ammonia solutions rather than absolute depolarization ratios. Consideration was given to such factors as monochromator polarization efficiency, image magnification, and cell design, but when necessary these parameters were compromised. For a detailed discussion concerning the effect of these parameters on polarization measurements, the reader is referred to several excellent papers on the subject.[20,21]

Carbon tetrachloride was used to determine the accuracy of the polarization measurements reported in this work. Depolarization ratios of 0.79, 0.78, and 0.01 were determined for the 225-, 312-, and 459-cm^{-1} bands, respectively. Comparison of these results reveals that the depolarization ratios are higher than the predicted and experimental values previously reported.[22-24] Although not absolute, the measurements were generally in error by no more than 10%.

The Raman spectrum of liquid ammonia was determined and salient features of a typical spectrum are shown in Figures 3 and 4. With reference to Figure 3, a broad structureless band centered around 200 cm^{-1} is evident and is attributed to solvent–solvent interaction. Figure 4 shows bands at 3380, 3301, and 3215 cm^{-1} which have been assigned to ν_3, ν_1, and $2\nu_4$, respectively. Although the ν_3 assignment is well accepted, the assignments of the $2\nu_4$ and ν_1 are not as certain. The bands observed at 1060 and 1634 cm^{-1} have been assigned as ν_2 and ν_4, respectively.

A relatively high resolution spectrum of the 1060-cm^{-1} (ν_2) band reveals an unresolved doublet which is shown in Figure 5. This doublet has been previously reported[12] and arises from inversion. Based on numerous runs, the best estimate of the splitting is 10–15 cm^{-1}. Attempts were made to resolve the remaining bands in the spectrum, but no other doublet structure was found.

Depolarization ratios are presented in Table III, and inspection reveals that the results are in qualitative agreement with those previously reported. The depolarization

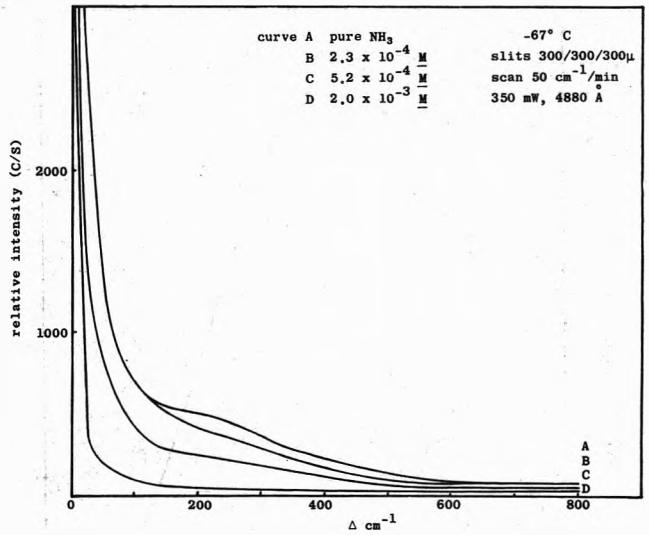

Figure 3. Raman spectra of sodium–ammonia solutions.

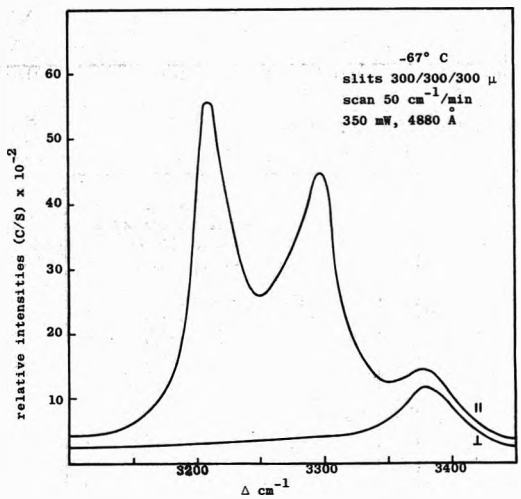

Figure 4. (ν_1, ν_2, $2\nu_4$) bands of liquid ammonia.

ratios for ν_2 and ν_4 are probably the most quantitative to date.

Typical Raman spectra of metal–liquid ammonia solutions are shown in Figures 3, 6, and 7. The broad band ($\bar{\nu}$ = 200 cm^{-1}) observed in pure ammonia was not observed in the metal solutions. Careful attention was given to the region 0–1000 cm^{-1} because of the predicted "breathing" mode vibration; however, no new scattering center was observed. In fact, the spectrum of pure ammonia was indistinguishable from that of a 2.3 × 10^{-4} M solution in the region 0–100 cm^{-1}. The only essential difference between the spectrum of pure ammonia and any solution in the concentration region (2–50 × 10^{-4} M) was in intensity. As is evident in Figures 3, 6, and 7, the scattered intensity decreases with increasing metal concentration.

Figure 8 is a plot of band maxima as a function of metal concentration and reveals that in the concentration range 0–5 × 10^{-3} M there are no shifts in band positions. Although the data are not shown, the 1060- and 1640-cm^{-1} bands were also unaffected by metal up to 5 × 10^{-4} M. At higher concentrations, the intensity of the ν_2 and ν_4 bands was too low to be observed. It is perhaps important to note that three concentrations (2.3, 5.2, and 20 × 10^{-4} M) represent sequential addition of metal, whereas the other

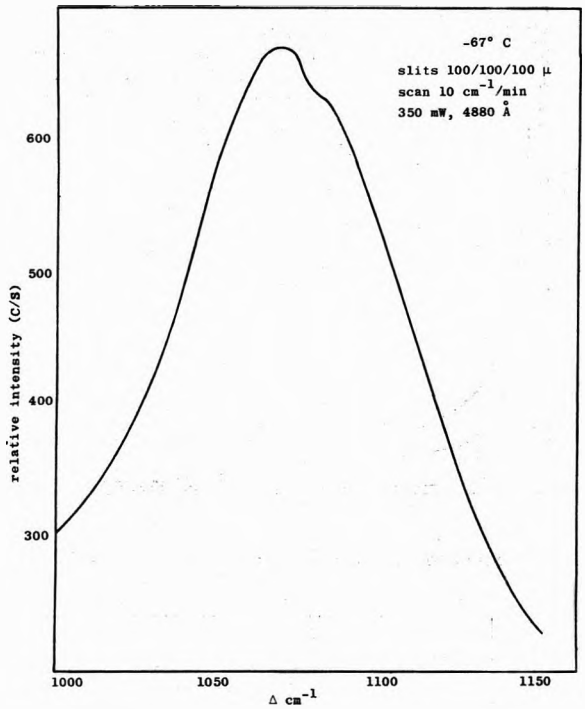

Figure 5. ν_2 band of liquid ammonia.

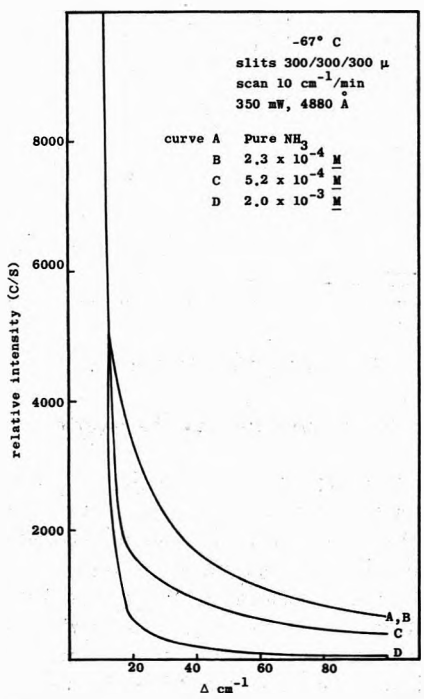

Figure 6. Raman spectrum of sodium–ammonia solutions.

three concentrations represent three different solution preparations.

These results are in disagreement with the infrared work of Rusch[7] who reported a shift in the positions of ν_1 and ν_3 with increasing metal concentration (Table I). Some caution must be exercised in comparing the two sets of data because the band positions reported by Rusch were obtained from computer-resolved infrared spectra and the band positions reported in this work are based on unresolved Raman data; however, the spectra presented in Figure 7 are of sufficiently high resolution that very little uncertainty exists in band positions.

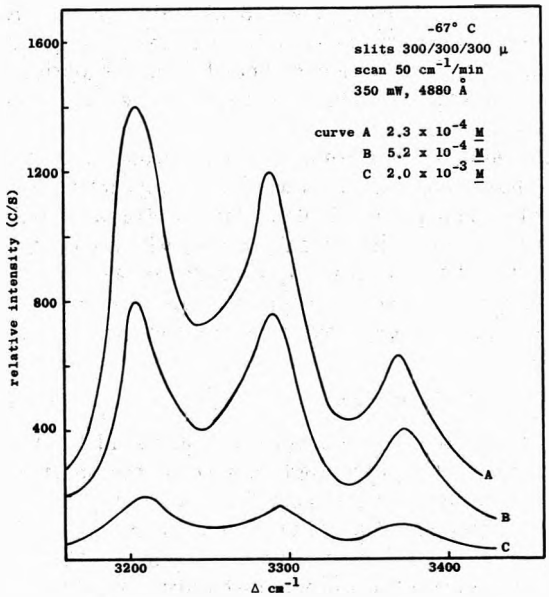

Figure 7. (ν_1, ν_2, $2\nu_4$) bands of ammonia in sodium–ammonia solutions.

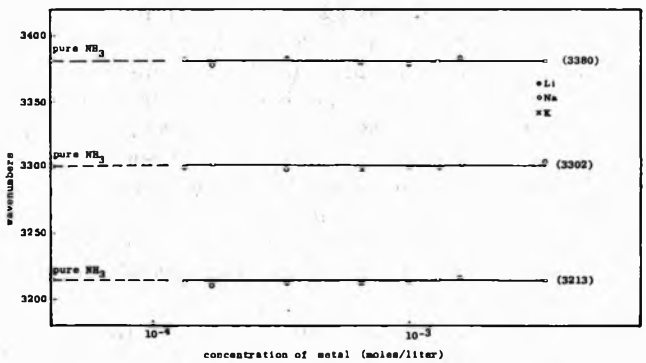

Figure 8. Band positions as a function of metal concentration.

The decrease in scattered intensity with increasing metal concentration is readily explained by considering the absorption spectrum of the solutions; the spectrum is asymmetric and tails into the visible region of spectrum. Using the optical data of Gold and Jolly,[25] a plot was made of (A/l) as a function of concentration at 5830 Å. Absorbance/pathlength, A/l, was used rather than absorbance to eliminate the pathlength dependency; 5830 Å corresponds to $\Delta\nu$ = 3300 cm^{-1}. Figure 9 shows at least a qualitative relationship between absorbance and Raman scattering intensity. Using 4880-Å excitation, $\Delta\nu$ = 3300 cm^{-1} corresponds to 5830 Å and the absorbance at this wavelength increases with concentration. There is also appreciable absorption at 4880 Å so that two effects are operative which tend to diminish the scattered intensity. First the excitation line energy is reduced due to absorption and secondly the scattered radiation is subject to absorption. At concentrations greater than 10^{-2} M, the 4880-Å line was completely absorbed and severe heating resulted. The spectrum of the 5.5 × 10^{-3} M solution was obtained using 4580-Å excitation. Although the power of this line was less than the 4880-Å line, the decreased absorption at 4580 Å, the ν^4 dependence, and the decreased absorption at 5390 ($\Delta\nu$ = 3300 cm^{-1}) resulted in a meaningful spectrum. Attempts to study concentrations greater than 5.5 × 10^{-3} M with the 4580-Å line were unsuccessful

TABLE III: Polarization Studies of Liquid Ammonia

Ref	1060 cm^{-1}	1640 cm^{-1}	3215 cm^{-1}	3300 cm^{-1}	3380 cm^{-1}
8			Polarized	Polarized	Depolarized
9			Polarized	Polarized	Depolarized
14			$\rho = 0.08$	$\rho = 0.08$	$\rho = 0.4$
15	50% polarization	0%	>95%	>95%	0
Present work	$\rho = 0.15$	$\rho = 0.5$	$\rho \approx 0.01$	$\rho \approx 0.01$	$\rho = 0.5$

due to absorption of both the excitation and emission frequencies.

Unfortunately it is impossible to state absolutely whether the predicted scattering center is or is not present. Arguments can be raised that the concentration of these centers was too low to be detected. Increasing the concentration is of little value because of the corresponding loss in intensity and the certainty of association in the solutions.

Since the analogy is often made between F centers and metal–ammonia solutions and since much of the theoretical treatment of these solutions has as its origin F center theory, it is interesting to extend the treatment of the Raman effect in F centers to metal–ammonia solutions. Kleinman[26] has calculated the Raman polarizability tensor using the expression

$$\alpha_R = f\frac{e^2}{m(\omega_{GF}^2 - \omega_0^2)}\frac{\beta - 1}{\beta}\left[\frac{2h/M\omega_G}{(X_G - X_F)^2}\right]^{1/2}$$

where α_R is the polarizability tensor, f the oscillator strength, ω_{GF} the angular frequency of the electronic absorption, ω_0 the angular frequency of the excitation energy, M the reduced mass, ω_G the angular frequency of the lattice vibration, and X_G and X_F the positions of the energy minimum of the ground and excited states, respectively. β is the "absorption–emission discrepancy" as shown in the relationship

$$(\psi_{GI}M_{GF}(X)^2\psi_{GI}) = \beta^2(\psi_{FI}M_{GF}(X)^2\psi_{FI})$$

when ψ_{GI} and ψ_{FI} represent the lowest vibrational states associated with the ground electronic state and the first excited electronic state, and $M_{GF}(X)$ is the matrix element of the dipole moment operator between electronic states G and F.

Kleinman calculated $\alpha_R = 9 \times 10^{-25}$ cm^3 for an F center using He–Ne excitation. This value is very close to the value of $\alpha_R = 2 \times 10^{-25}$ cm^3 reported[27] for the strong lines of carbon tetrachloride.

Worlock and Porto[28] reported observing Raman scattering from F centers in KCl and NaCl. The Raman line was broad (~200 cm^{-1}) and centered at $\Delta\nu = 200$ cm^{-1}. In these experiments the concentration of scattering centers was approximately 10^{16}–10^{17} centers/cm^3. Radhakrishna and Sehgal[29] reported similar spectra of F centers in KCl and KBr at densities of 10^{18} centers/cm^3.

Kleinman's equation was applied to metal–ammonia solutions using the following data: $f = 0.77$; $\omega_{GF} = 1.26 \times 10^{15}$ (1.5 μ); $\omega_0 = 3.68 \times 10^{15}$ (4880 Å); β varies from 1 to 10; $M = 1.7 \times 10^{-22}$ g (six NH_3 molecules); $\omega_G = 6.4 \times 10^{12}$ (35 cm^{-1}); $X_G = 2.2$ Å; $X_F = 2.6$ Å. The following result was obtained

$$\alpha_R = 6 \times 10^{-24}[(\beta - 1)/\beta]$$

If $\beta = 1$, then $\alpha_R = 0$, but as β becomes large α_R approaches 6×10^{-24} as a limit. Unfortunately, little is known about the excited state and consequently β is

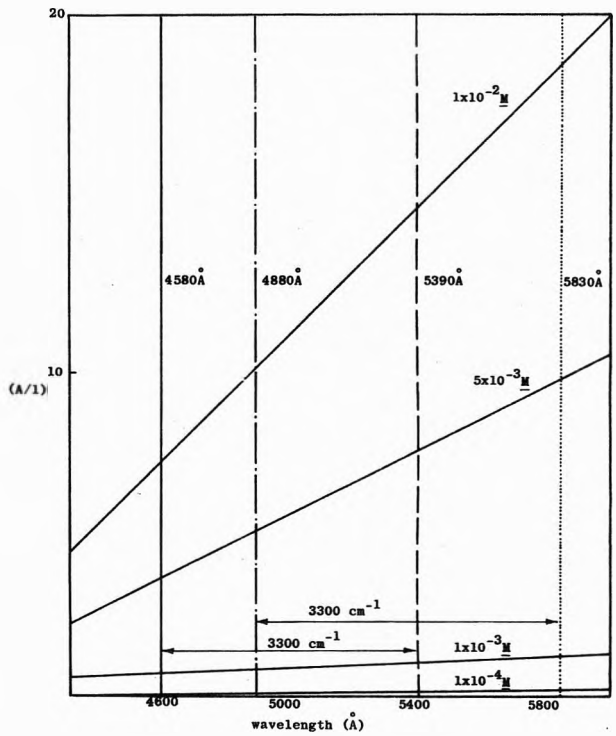

Figure 9. Absorbance and Raman excitation/emission.

indeterminate, but unless β is very small α_R is of the same magnitude as that obtained for F centers. It should also be pointed out that concentrations in the range 5×10^{-4}–5×10^{-3} M correspond to 3×10^{17}–3×10^{18} electrons/cm^3 (assuming no association).

In view of these results it is perhaps surprising that no Raman effect was observed in the metal–ammonia solutions; however, caution must be exercised in carrying the analogy too far. Several factors could be operative which could reduce the scattering below detectable limits. The interactions in this system may be much less localized than in F centers which would produce broad and continuous Raman shifts. Certainly the difference in lifetimes of the centers must be considered because F centers are very long lived compared to the lifetime of a given cavity (as deduced from nuclear magnetic resonance relaxation times).[30] The relative ease of reforming cavities coupled with the low cavity concentration may reduce the concentration of cavities at any instant below detectable limits. The high radiation density is another factor whose effect is difficult to predict. Localized heating might possibly reduce the concentration of cavities through density effects or even destroy cavities. In this context it should be mentioned that spectra were determined with and without focusing the laser and at very low laser power outputs. There was no discernible difference (other than intensity) between these spectra and those observed at high power outputs. There is also the possibility that a cavity as has

been described does not exist. Although no scattering center was found, the conclusion must be reached that alkali metals do not perturb the solvent structure in a detectable manner in the concentration region studied.

Acknowledgment. We gratefully acknowledge the financial support of The Robert A. Welch Foundation. We are indebted to the University of Dallas for the loan of the Spex 1401.

References and Notes

(1) *Metal–Ammonia Solutions, Physicochem. Prop., Colloq. Weyl II, 1970,* 1 (1971).
(2) D. A. Copeland, N. R. Kestner, and J. Jortner, *J. Chem. Phys.*, **53,** 1189 (1970).
(3) P. F. Rusch, Université Catholique de Lille, France, private communication.
(4) C. C. Klick and J. H. Schulman, "Solid State Physics," Vol. 5, Academic Press, New York, N. Y., 1957, p 97.
(5) T. A. Beckman and K. S. Pitzer, *J. Phys. Chem.*, **65,** 1527 (1961).
(6) D. F. Burow and J. J. Lagowski, *J. Phys. Chem.*, **72,** 169 (1968).
(7) P. F. Rusch, Ph.D. Dissertation, The University of Texas at Austin, 1971.
(8) P. Daure, *Ann. Phys.*, **12,** 375 (1929).
(9) S. Bhagavantam, *Indian J. Phys.*, **5,** 54 (1930).
(10) A. Dadieu and K. W. Kohlrausch, *Naturwissenschaften*, **18,** 154 (1930).
(11) M. G. Costeanu, *C. P. Acad. Sci.*, **207,** 285 (1938).
(12) S. Kinumaki and K. Aida, *Sci. Rep. Res. Inst. Tokohu Univ.*, **6,** 186 (1954).
(13) C. A. Plint, R. M. B. Small, and H. L. Welsh, *Can. J. Phys.*, **32,** 653 (1954).
(14) G. Seillier, M. Ceccaldi, and J. P. Leicknam, *Method. Phys. Anal. (GAM),* **4,** 388 (1968).
(15) T. Birchall and I. Drummond, *J. Chem. Soc. A,* 1859 (1970).
(16) B. Bettignies and F. Wallart, *C. R. Acad. Sci.*, **271,** 640 (1970).
(17) R. Quinn and J. J. Lagowski, *J. Phys. Chem.*, **73,** 2326 (1969).
(18) D. F. Burow and J. J. Lagowski, *Advan. Chem. Ser.*, **No. 50,** 1 (1965).
(19) G. Herzberg, "Infrared and Raman Spectra," Van Nostrand, New York, N. Y., 1966.
(20) H. H. Claasen, H. Selig, and J. Shanier, *Appl. Spectrosc.*, **23,** 8 (1969).
(21) C. D. Allemand, *Appl. Spectrosc.*, **24,** 348 (1970).
(22) W. F. Murphy, M. V. Evans, and P. Bender, *J. Chem. Phys.*, **47,** 1836 (1967).
(23) A. F. Slomba, C. D. Hinman, and E. H. Siegler, *Proc. Cont. Anal. Chem. Appl. Spectrosc.*, (1965).
(24) A. E. Douglas and D. H. Hank, *J. Opt. Soc. Amer.*, **38,** 281 (1948).
(25) M. Gold and W. L. Jolly, *Inorg. Chem.*, **1,** 818 (1962).
(26) D. A. Kleinman, *Phys. Rev. A,* **134,** 423 (1964).
(27) J. Brandmüller and H. Moser, "Einführung in die Raman-spektroskopie," Dr. Dietrich Steinkopff Verlag, Darmstadt, 1962
(28) J. M. Worlock and S. P. S. Porto, *Phys. Rev. Lett.*, **15,** 697 (1965).
(29) S. Radhakrishna and H. K. Sehgal, *Phys. Lett. A,* **29,** 286 (1969).
(30) R. Catterall, *Metal–Ammonia Solutions; Physicochem. Prop., Colloq. Weyl II, 1970,* 1 (1971).

Effects of Solvent and Substituents on the Absorption Spectra of Triplet Acetophenone and the Acetophenone Ketyl Radical Studied by Nanosecond Laser Photolysis

Hanspeter Lutz,[1] Emilienne Bréhéret, and Lars Lindqvist*

Laboratoire de Photophysique Moléculaire du C.N.R.S., Université de Paris-Sud, 91405 Orsay, France
(Received December 8, 1972)

Publication costs assisted by the Centre National de la Recherche Scientifique

The triplet absorption spectra of *p*-trifluoromethylacetophenone, acetophenone, and *p*-methyl- and *p*-methoxyacetophenone in nonpolar solvents were measured by nanosecond laser photolysis using the third and fourth harmonics of a Nd glass laser. Acetophenone was also studied in acetonitrile and water. In the cases where the energy of the lowest $^3(n,\pi^*)$ state is lower than that of the lowest $^3(\pi,\pi^*)$ state, the triplet absorption spectra are characterized by two weak absorption bands at about 410 and 450 nm and by a strong absorption appearing below 330 nm. When the $^3(\pi,\pi^*)$ state is lowest, the triplet has a structureless, weak absorption in the visible and a strong maximum at about 350 nm. The spectra of the ketyl radicals of *p*-trifluoromethylacetophenone, acetophenone, and *p*-methylacetophenone were determined in cyclohexane. The spectra are all very similar and resemble the triplet absorption spectra of the ketones which have lowest triplets of $^3(n,\pi^*)$ nature. The rate constants of hydrogen abstraction from 2-propanol by the triplet state of these latter ketones in benzene solutions containing 2 *M* 2-propanol are 6.2×10^6, 1.2×10^6, and 1.3×10^5 M^{-1} sec^{-1}, respectively. The results indicate that measurements of triplet absorption spectra may be useful in determining the $^3(\pi,\pi^*)$ *vs.* $^3(n,\pi^*)$ nature of the lowest triplet state of alkyl phenyl ketones.

Introduction

It is known that many alkyl phenyl ketones have almost isoenergetic lowest $^3(n,\pi^*)$ and $^3(\pi,\pi^*)$ states, a property leading to interesting spectroscopic and chemical consequences. Information about the nature of the lowest triplet state of these compounds has been obtained mainly from studies of phosphoresence,[2-6] singlet–triplet absorption,[7,8] and zero-field splitting.[9,10] Triplet absorption spectra are expected also to be of value in characterizing the triplet state; however, only few measurements of triplet absorption spectra of alkyl phenyl ketones have been reported previously.[11,12]

In the present study the triplet absorption spectra of acetophenone and a number of acetophenone derivatives were determined using the nanosecond laser photolysis method. The lowest triplet state of acetophenone in nonpolar solvents is considered to be a $^3(n,\pi^*)$ state;[2,3a] the second triplet, situated only a few hundred wave numbers above the lowest triplet state, is considered to be a $^3(\pi,\pi^*)$ state.[9] Vibronic coupling between these two states is efficient and produces a mixed character of the lowest triplet state.[13] A consequence of the energetic proximity of the triplet levels is that even small perturbations, *e.g.*, substituent[5,14] or solvent[9] effects, may produce level inversion or changes in the extent of vibronic coupling between the two lowest lying triplet states. The effects of such perturbations on the triplet absorption spectrum were determined in the present study by comparing the absorption spectrum of triplet acetophenone in nonpolar solvents to those of para-substituted acetophenones containing electron-withdrawing (CF_3^-) or electron-donating groups (CH_3^-, CH_3O^-). Solvent effects were determined from measurements of the acetophenone triplet absorption spectrum in solvents of varying polarity (cyclohexane, acetonitrile, and water). By the use of these solvents and substituents, it was possible to vary the nature of the triplet state progressively from a predominantly $^3(n,\pi^*)$ to a predominantly $^3(\pi,\pi^*)$ configuration.

Experimental Section

Materials. Acetophenone (Eastman) and *p*-methylacetophenone (Fluka) were doubly vacuum distilled; *p*-trifluoromethyl- and *p*-methoxyacetophenone (Fluka) were purified by sublimation. Benzene, cyclohexane, 2-propanol, acetonitrile (Merck Uvasol), and perfluoromethylcyclohexane (Peninsular Chemresearch) were used without further purification. Water was doubly distilled. Solutions were degassed by three freeze–thaw cycles with intermittent saturation by argon.

Laser Photolysis Equipment. The excitation light source was a Q-switched Nd glass laser (Compagnie Générale d'Electricité, Model VD 231, maximum energy 60 J) emitting at 1058 nm; the pulse half-width was 35 nsec. The third (353 nm) and fourth (265 nm) harmonics, generated by means of KDP crystals, were used in the present study, at energies in the order of 1–20 mJ. Relative values of the laser energy were obtained by measuring the integrated photocurrent from a photomultiplier tube (EMI 9781 B) exposed to a small fraction of the ultraviolet laser beam.

An optical system projected the laser beam, reduced to a height of 4 mm and a width of 8 mm, on one side of a 10-mm square silica cell with polished sides, containing the sample. The monitoring light was obtained by discharging a 320-μF capacitor (1–1.8 kV) across a xenon flash tube (Verre et Quartz, VQX 65 N) in series with an inductance of approximately 100 μH; the flash half-width was 650 μsec. Triggering was made such that the laser pulse occurred during the period of maximum intensity of the analysis flash. The analyzing light passed in a crossed-beam arrangement through a 2 mm wide section of the sample cell, close to the laser entrance window. A narrow wavelength band (2 nm) of the transmitted light was selected by means of a monochromator (Jarrell-Ash, Model 82-410, $f/3.5$, f = 25 cm); the intensity in this band was measured using a photomultiplier tube (Radiotechnique, 150 UVP or 150 CVP). The output of the seventh dynode, terminated by 75 Ω, was displayed on an oscilloscope (Fairchild, Model 777, 100 MHz). The overall time resolution of the detector system was *ca.* 10 nsec.

Transient absorption spectra were obtained from oscilloscope recordings over a range of wavelengths (every 3–10 nm). A linear correction of the transient optical densities was applied for variations in the laser energy.

Results and Discussion

(A) Effect of Substituents on the Acetophenone Triplet Absorption. Laser excitation of acetophenone and some of its para-substituted derivatives in nonpolar solvents produced the end-of-pulse transient absorption spectra shown in Figure 1. The ultraviolet part of the spectra was obtained after excitation by the 265-nm harmonic. The solute concentration was chosen such that an OD of 1 to 2 was obtained across a 1-cm path (0.002–0.006 *M*). The transient absorption in the visible is very weak and it was for this reason found necessary to use the higher output of the 353-nm harmonic and higher solute concentrations (0.1–0.2 *M*) to obtain measurable absorptions in this spectral range. Aerated solutions gave the same end-of-pulse spectra as the degassed solutions. Measurements between 600 and 1000 nm did not reveal any perceptible absorption in this spectral range. Our previous study[12] established that the transient spectrum observed immediately after laser irradiation of acetophenone is due to the triplet state. The spectra in Figure 1 are by analogy attributed to the lowest triplet state of the corresponding compounds.

In the case of *p*-trifluoromethylacetophenone, measurements of the triplet spectrum in hydrogen-donating solvents was impracticable due to the high triplet reactivity of this compound. Perfluoromethylcyclohexane was chosen as solvent in the determination of the ultraviolet part (Figure 1a, dotted line) and benzene, because of the higher solubility of the ketone in this solvent, in the determination of the visible part (Figure 1a, full line) of the triplet spectrum of this ketone.

Estimates of the extinction coefficients given in Figures 1 and 2 were obtained by comparison of the triplet absorption intensities of the acetophenone derivatives with the intensity of the benzophenone triplet absorption,[12] measured at equal laser excitation energies. It was assumed that the extinction coefficient of triplet benzophenone in cyclohexane has the same value at 533 nm as that determined in benzene solution[15] (7630 M^{-1} cm^{-1}). It was also assumed that the triplet yield was unity for all the compounds studied.

It is seen from Figure 1 that substitution in the benzene nucleus leads to pronounced changes in the triplet absorption of acetophenone. Substitution by the electron-withdrawing trifluoromethyl group produces a shift of the strong ultraviolet absorption to shorter wavelengths. The electron-donating methyl and methoxy groups instead lead to complete disappearance of the structure of the absorption in the visible while a high-intensity absorption band shows up in the near ultraviolet around 350 nm. These spectral changes may be discussed by considering the effect of substituents on the electronic nature of the lowest triplet state.

Low-temperature studies of the lifetime, structure, and polarization of the phosphorescence of acetophenone in hydrocarbons indicate that the lowest triplet state of the ketone is of $^3(n,\pi^*)$ nature under these conditions.[13,2,3] This state is expected to be strongly perturbed by a nearby $^3(\pi,\pi^*)$ state. The closeness of the two states is demon-

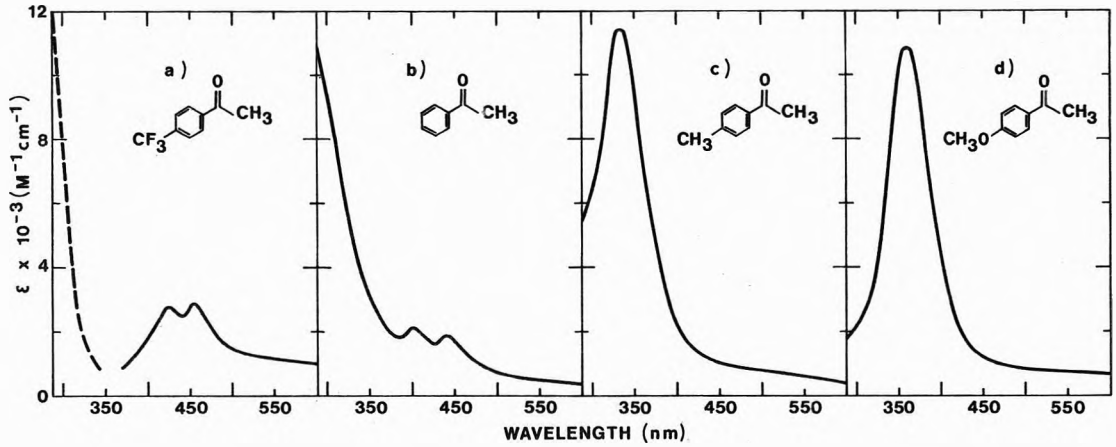

Figure 1. Triplet absorption spectra of para-substituted acetophenones in aerated solutions determined by nanosecond laser photolysis (end-of-pulse spectra): (a) *p*-trifluoromethylacetophenone in perfluoromethylcyclohexane (- - - -) and in benzene (——); (b) acetophenone in cyclohexane; (c) *p*-methylacetophenone in cyclohexane; and (d) *p*-methoxyacetophenone in cyclohexane.

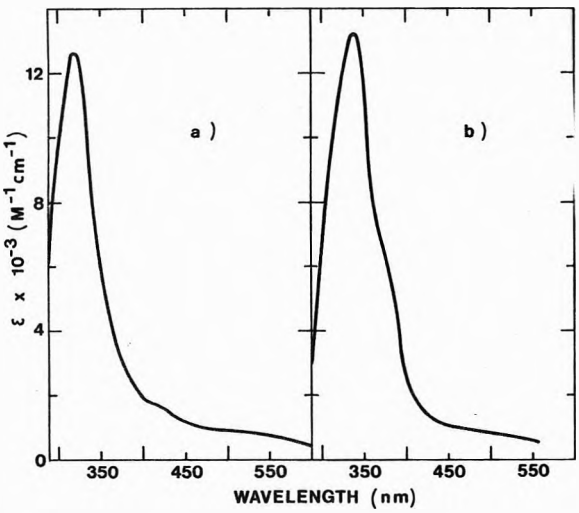

Figure 2. Triplet absorption spectra of acetophenone in aerated polar solvents determined by nanosecond laser photolysis (end-of-pulse spectra): (a) acetophenone in acetonitrile and (b) acetophenone in water.

strated by the ease of inversion of the states with change of solvent; in the more polar EPA glass the lowest triplet is a $^3(\pi,\pi^*)$ state according to a study of the polarization of the phosphorescence.[13] The appearance of vibrations assigned to nonplanar modes in the $^3(\pi,\pi^*)$ phosphorescence of acetophenone in EPA[13] and some substituted acetophenones[16] reveals a strong vibronic coupling between the $^3(n,\pi^*)$ and $^3(\pi,\pi^*)$ configurations.

p-Trifluoromethylacetophenone has been studied using phosphorescence excitation techniques.[14] It was found that the energy of the $^3(n,\pi^*)$ state of acetophenone is decreased by the substituent; no evidence was obtained as to the location of the upper $^3(\pi,\pi^*)$ state. From the fact that trifluoromethyl substitution produces a blue shift of the absorption maximum of the $^1L_a \leftarrow {}^1A$ transition,[17] one may expect a similar increase in energy of the corresponding $^3(\pi,\pi^*)$ state ^3L_a. It follows that the energy spacing between the low-lying $^3(n,\pi^*)$ and $^3(\pi,\pi^*)$ levels should increase when a trifluoromethyl group is introduced in the acetophenone molecule, thus bringing about a reduction in the vibronic coupling between the two states. The enhancement of the $^3(n,\pi^*)$ character of the lowest triplet state is further supported by the very short phosphorescence lifetime of *p*-trifluoromethylacetophenone.[14]

Triplet state assignments have been made for *p*-methylacetophenone in 3-methylpentane glass at 77°K.[13] It is concluded from the results that the lowest triplet state in this case is a $^3(\pi,\pi^*)$ state, coupled vibronically to a close-lying $^3(n,\pi^*)$ state. The $^3(\pi,\pi^*)$ assignment of the lowest triplet state of *p*-methylacetophenone is also supported by its phosphorescence excitation spectrum.[14]

The lowest triplet of *p*-methoxyacetophenone in a moderately polar solvent is considered to be a $^3(\pi,\pi^*)$ state.[5,16] The $^3(n,\pi^*)$ state was located 2100 cm^{-1} above this state.[5] Due to the large energy gap between the two states, vibronic interactions are expected to be small, and variations in the solvent polarity thus should not have a great influence on the orbital character of the triplet state. Indeed, it has been shown that the phosphorescence lifetime of this ketone is almost the same in 3-methylpentane glass as in EPA, demonstrating the lack of influence of the solvent on the triplet state character in this case.[13]

Making use of the assignments cited above in discussing the absorption spectra given in Figure 1, we note that the absorption spectra of the ketones with lowest triplet states of $^3(n,\pi^*)$ nature (*p*-trifluoromethylacetophenone and acetophenone) show two absorption bands in the visible. The presence of these bands seems to be directly connected with the $^3(n,\pi^*)$ nature of the triplet state since no such bands are observed in the cases where the $^3(\pi,\pi^*)$ state is lowest. It may also be noted that the visible band system is most pronounced in the triplet absorption spectrum of *p*-trifluoromethylacetophenone in which vibronic perturbation of the lowest $^3(n,\pi^*)$ state is expected to be weak. The ketones with lowest triplet state of $^3(\pi,\pi^*)$ nature (*p*-methyl- and *p*-methoxyacetophenone) have triplet absorption spectra showing a strong maximum at about 350 nm and weak structureless absorption in the visible.

The triplet absorption spectra in the present study were obtained at room temperature whereas the triplet state assignments discussed above were obtained from low-temperature studies. It has been shown,[3b,18] that the overall orbital character may vary with the temperature when the triplet states are closely spaced. In the absence of quantitative estimates of such effects, their possible influence on the triplet nature was neglected in the interpretation of the results. A verification of the above assignments and of their validity at room temperature conditions may be obtained by determining the hydrogen-abstracting power of the triplet state, since it is known that hydrogen abstrac-

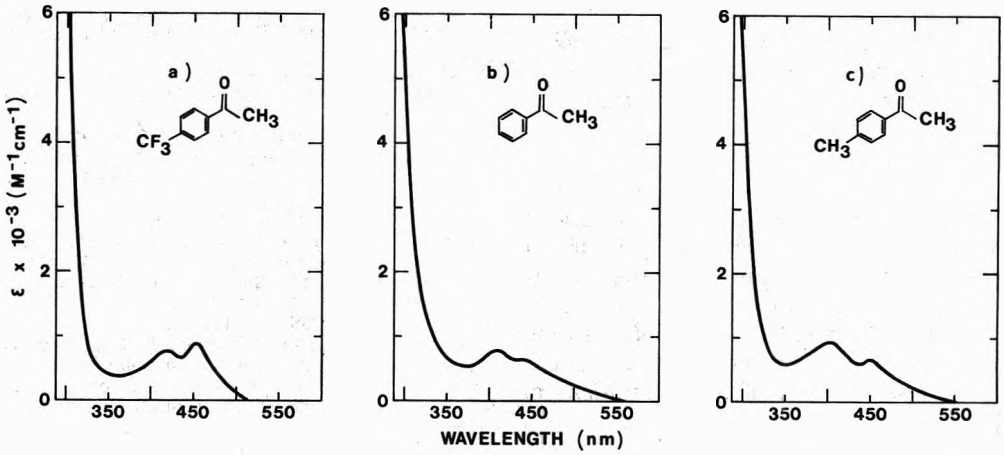

Figure 3. Ketyl radical absorption spectra of para-substituted acetophenones in degassed cyclohexane; (a) *p*-trifluoromethylacetophenone (measured 1 μsec after laser excitation); (b) acetophenone (measured 1.4 μsec after laser excitation); and (c) *p*-methylacetophenone (measured 10 μsec after laser excitation).

tion from the solvent by an aromatic ketone in the triplet state will be efficient only if the state has $^3(n,\pi^*)$ orbital character. The hydrogen-abstracting efficiency is obtained conveniently by the nanosecond laser technique from measurements of the triplet decay rate. We determined in this manner the rate constants of photoreduction, k_r, of *p*-trifluoromethylacetophenone, acetophenone, and *p*-methylacetophenone. Details of the procedure have been described elsewhere.[19] The measurements were made in degassed solutions of these compounds (0.1 *M*) in benzene solutions that were 2 *M* in 2-propanol. The following values were obtained

Compound	k_r, M^{-1} sec^{-1}
p-Trifluoromethylacetophenone	6.2×10^6
Acetophenone	1.2×10^6
p-Methylacetophenone	1.3×10^5

Information regarding the effect of ring substituents on the triplet state reactivity of acetophenone was obtained by Yang and Dusenbery[14] from quantum yield studies. These authors reported somewhat lower values of k_r than those obtained in the present work; the relative importance of k_r is about the same, however.

The strong decrease of k_r in going from *p*-trifluoromethylacetophenone to *p*-methylacetophenone is consistent with the proposed change of the orbital character of the lowest triplet state from $^3(n,\pi^*)$ to $^3(\pi,\pi^*)$. The high reactivity of triplet *p*-trifluoromethylacetophenone compared to that of acetophenone may be attributed to the reduced perturbation of the lowest $^3(n,\pi^*)$ by the upper $^3(\pi,\pi^*)$ state. The lowest triplet state of *p*-methylacetophenone is expected to be a $^3(\pi,\pi^*)$ state, yet *p*-methylacetophenone shows significant photoreactivity. This behavior has been attributed to the vibronic coupling of the lowest $^3(\pi,\pi^*)$ with the closely spaced $^3(n,\pi^*)$ state.[14]

(B) Effect of Solvent Polarity on the Acetophenone Triplet Absorption. Figure 2 shows the triplet absorption spectra of acetophenone in the polar solvents acetonitrile (a) and water (b). The triplet absorption spectrum of acetophenone in ethanol has been given elsewhere.[12] The spectra were measured under the same experimental conditions as the spectra shown in Figure 1. The wavelength of the triplet absorption peak in water is in agreement with recent flash photolysis results.[20] It is seen that the absorption spectra of triplet acetophenone in polar solvents are similar to those found in acetophenone containing an electron-donating substituent in the benzene ring. The band structure in the visible observed in cyclohexane (Figure 1b) does not appear in the more polar solvents, but instead, a strong absorption maximum is found at about 330 nm.

This change may be interpreted as being due to the change from $^3(n,\pi^*)$ to $^3(\pi,\pi^*)$ nature of the lowest triplet with increasing solvent polarity. Lamola[9] predicted the $^3(n,\pi^*)$ and $^3(\pi,\pi^*)$ states of acetophenone to have nearly the same energy in ethanol. This prediction is supported by the observation of dual phosphorescence from acetophenone in ethanol and solvents of similar polarity, such as EPA.[21] It appears from recent phosphorescence studies that the $^3(\pi,\pi^*)$ state of acetophenone is located even below the $^3(n,\pi^*)$ state in ethanol-containing glass.[13]

In a previous study we have presented evidence for a strong solvent dependence of the acetophenone triplet state reactivity and explained this in terms of the extent of mixing of the lowest $^3(n,\pi^*)$ and $^3(\pi,\pi^*)$ states.[19] The dependence of the acetophenone triplet absorption on the solvent polarity observed in the present study lends further support to this conclusion.

(C) Effects of Substituents on the Acetophenone Ketyl Radical Absorption. In the preceding discussion, the variations in triplet absorption due to substitution were interpreted as being due to changes in the relative positions of the $^3(n,\pi^*)$ and $^3(\pi,\pi^*)$ levels. If other specific substituent effects produce the observed variations one would expect to find similar effects on the acetophenone ketyl radicals. To examine this possibility the ketyl radical spectra of acetophenone and *p*-trifluoromethyl- and *p*-methylacetophenone were determined and compared. The ketyl radicals were obtained by laser excitation of the ketones in degassed cyclohexane. Figure 3 shows the transient spectra due to this radical, measured after disappearance of the triplet absorption. The extinction coefficients of the radicals were estimated roughly assuming that the corresponding triplet disappears exclusively to produce the radical.

The similarity of the spectra indicates that substitution does not specifically change the electronic configuration of the acetophenone ketyl radical. This observation strengthens the hypothesis that the spectral changes in the triplet absorption arising by substitution are indeed due to $^3(n,\pi^*)$–$^3(\pi,\pi^*)$ level inversion.

It is seen that the ketyl radicals have spectra very similar to those of the triplet state of $^3(n,\pi^*)$ nature. Such a relation was already found for benzophenone and was attributed to the similarity in the π electron configuration of the $^3(n,\pi^*)$ state and the ketyl radical.[22]

Conclusions

The present study provides evidence of strong solvent and substituent effects on the absorption spectrum of triplet acetophenone. These effects are shown to be related to variations in the extent of $^3(n,\pi^*)$ *vs.* $^3(\pi,\pi^*)$ orbital nature of the lowest triplet state. One may conclude from these results that triplet absorption spectra are useful criteria in determining the lowest triplet configurations of alkyl phenyl ketones.

Measurements of the decay of the triplet in hydrogen-donating solvents show that the changes in the triplet absorption spectra due to solvent and substituent effects are associated with significant changes in the reactivity of the triplet state. These findings are direct evidence that the variations in the acetophenone photoreactivity are due to variations of the electronic configuration of the lowest triplet state.

References and Notes

(1) Present address, Laboratory for Research on the Structure of Matter, The University of Pennsylvania, Philadelphia, Pa. 19174.
(2) V. G. Krishna, *J. Mol. Spectrosc.*, **13**, 296 (1964).
(3) (a) R. Shimada and L. Goodman, *J. Chem. Phys.*, **43**, 2027 (1965); (b) M. Koyanagi, R. J. Zwarich, and L. Goodman, *ibid.*, 56, 3044 (1972).
(4) T. F. Hunter, *Trans. Faraday Soc.*, **66**, 300 (1970).
(5) D. R. Kearns and W. A. Case, *J. Amer. Chem. Soc.*, **88**, 5087 (1966).
(6) W. A. Case and D. R Kearns, *J. Chem. Phys.*, **52**, 2175 (1970).
(7) S. Dym and R. M. Hochstrasser, *J. Chem. Phys.*, **51**, 2458 (1969).
(8) Y. Tanimoto, H. Kobayashi, S. Nagakura, and T. Azumi, *Chem. Phys. Lett.*, **16**, 10 (1972).
(9) A. A. Lamola, *J. Chem. Phys.*, **47**, 4810 (1967).
(10) (a) N. Hirota, *Chem. Phys. Lett.*, **4**, 305 (1969); (b) J. B. Gallivan and J. S. Brinen, *ibid.*, **10**, 455 (1971); (c) T. H. Cheng and N. Hirota, *ibid.*, **13**, 194 (1972); (d) S. W. Mao, T. C. Wong, and N. Hirota, *ibid.*, **13**, 199 (1972); (e) T. H. Cheng and N. Hirota, *J. Chem. Phys.*, **56**, 5019 (1972).
(11) D. S. McClure and P. L. Hanst, *J. Chem. Phys.*, **23**, 1772 (1955).
(12) H. Lutz and L. Lindqvist, *Chem. Commun.*, 493 (1971).
(13) Y. H. Li and E. C. Lim, *Chem. Phys. Lett.*, **7**, 15 (1970).
(14) N. C. Yang and R. L. Dusenbery, *J. Amer. Chem. Soc.*, **90**, 5899 (1968).
(15) R. Bensasson and E. J. Land, *Trans. Faraday Soc.*, **67**, 1904 (1971).
(16) E. C. Lim, Y. H. Li, and R. Li, *J. Chem. Phys.*, **53**, 2443 (1970).
(17) N. C. Yang and R. L. Dusenbery, *Mol. Photochem.*, **1**, 159 (1969).
(18) E. Migirdicyan, *Chem. Phys. Lett.*, **12**, 473 (1972).
(19) H. Lutz, M. C. Duval, E. Bréhéret, and L. Lindqvist, *J. Phys. Chem.*, **76**, 821 (1972).
(20) M. B. Ledger and G. Porter, *J. Chem. Soc., Faraday Trans. 1*, **68**, 539 (1972).
(21) (a) N. C. Yang and S. Murov, *J. Chem. Phys.*, **45**, 4358 (1966); (b) P. Gacoin and Y. Meyer, *C. R. Acad. Sci.*, **267**, 149 (1968); (c) R. N. Griffin, *Photochem. Photobiol.*, **7**, 159, 175 (1968); (d) P. J. Wagner, M. J. May, A. Haug, and D. R. Graber, *J. Amer. Chem. Soc.*, **92**, 5269 (1970); (e) M. E. Long, Y. H. Li, and E. C. Lim, *Mol. Photochem.*, **3**, 221 (1971).
(22) H. Tsubomura, N. Yamamoto, and S. Tanaka, *Chem. Phys. Lett.*, **1**, 309 (1967).

Vapor-Phase Dissociation Energy of $(HCN)_2$

Howard D. Mettee

Department of Chemistry, Youngstown State University, Youngstown, Ohio 44503

(Recieved April 2, 1973)

Publication costs assisted by The Graduate School, Youngstown State University

The temperature dependence of fundamental infrared absorbance intensities of ν_1 in monomeric and dimeric forms of HCN vapor is used to calculate a $\Delta E_D = -3.80 \pm 0.16$ kcal/mol. This value is somewhat greater than the earlier experimental value of -2.6 kcal/mol, determined by classical vapor density measurements, and compares more favorably with a recently theoretically computed value of $\Delta E_D^\circ = -3.7$ kcal/mol, based on *a priori* methods.

With the exceptions of the work of Inskeep,[1] Bernstein,[2] and Dunken and Winde,[3] very few measurements of the thermodynamic properties of small, hydrogen-bonded complexes in the vapor phase are currently being reported. Since recent theoretical methods have advanced to the point where *a priori* calculations may now be performed on such systems,[4] there exists a need to have reliable experimental data at hand for comparison.

The recent calculations of Kollman, *et al.*,[5] on the HCN dimer illustrates the problem rather nicely. For the reaction

$$2HCN \rightleftharpoons (HCN)_2$$

the calculated energy of reaction ($\Delta E_D^\circ = -3.7$ kcal/mol of bonds) could only be compared with an experimental value ($\Delta E_D = -2.6$ kcal/mol of bonds) determined 34 years ago by Giauque and Ruehrwein[6] using vapor density data which were still 10 years older. In view of the acknowledged occurence of higher polymers in HCN vapor such data are somewhat suspect. In fact, the above authors[6] caution against taking equilibrium constants based on such measurements too seriously.

In the case of HCN the infrared measurements of Hyde and Hornig[7] provide an independent means of checking the earlier vapor density value and the more recent calculated one. The ν_1 mode of monomeric HCN is an example

of a classical infrared anomaly in which a molecule with a large dipole (~2.9 D), and with a symmetry allowed transition moment, produces an extremely weak absorption compared to the other fundamental modes.[8] Hyde and Hornig describe this band and show the existence of a companion band assignable to this mode in the hydrogen-bonded dimer.

It is then a relatively simple matter to measure the temperature dependence of the absorptions due to the monomeric (M) and dimeric (D) forms of HCN, and to determine the energy difference between these two forms according to the integrated van't Hoff equation[9]

$$\ln K_c = -\Delta E_D/RT + \text{constant} \quad (1)$$

where

$$K_c = C_D/C_M^2$$

and C_M and C_D are the concentrations of monomer and dimer, respectively. In the present case K_c was taken as

$$K_c = (I_D/I_M^2)(\alpha_M^2/\alpha_D)(\beta_M^2/\beta_D) \quad (2)$$

where I's refer to peak optical densities, α's are integrated extinction coefficients, and β's are proportionality constants between the peak optical densities and the integrated band areas. Thus the limiting accuracy of the method hinges upon two related assumptions: (i) that the extinction coefficient ratio be temperature independent and (ii) that the proportionality constant ratio also be temperature independent. Neither are severely doubtful over the limited temperature range (25–95°) of this work. With these assumptions

$$\ln(I_D/I_M^2) = -\Delta E_D/RT + \text{constant} \quad (3)$$

It would have been more nearly correct to use band areas themselves, rather than peak intensities, in eq 2 but the problem of band overlapping opens such a procedure to some doubt and little if any neighboring contribution to peak intensities was observed in this work.

For this study, HCN was synthesized according to Ziegler,[10] with the exception that 50% H_2SO_4 was dripped directly onto solid NaCN, rather than mixed with an aqueous solution. All measurements were made in a standard cylindrical 10-cm path demountable gas cell, fitted with rock salt windows, uniformly wrapped with asbestos tape and nichrome heating wire, and fitted with a calibrated pyrometer lead (3M) in a small glass capillary placed so as to avoid direct contact with the nichrome. After filling the cell with about 700 mm pressure of HCN at room temperature, the cell temperature was varied without opening the cell stopcock so that the experiment was performed at *constant volume* rather than *constant pressure*. A dry-air-purged Beckmann IR-12 was used to measure all spectra, with due precautions taken to ensure that the spectrum obtained was not an artifact of either slit width or scanning speed. Frequencies were calibrated using CO as a reference according to the IUPAC tables.[11]

Since the cell windows were not directly heated the true temperature of the gas is probably the least certain measurement of the present experiment. This temperature was computed from the measured wall and window temperatures (the latter were found by direct contact of the pyrometer couple to the window surface), where each was weighted according to the fraction of the normalized surface area presented to the enclosed gas. Elementary thermal transfer equations may be used to show that convection plays a minimal role here.[12]

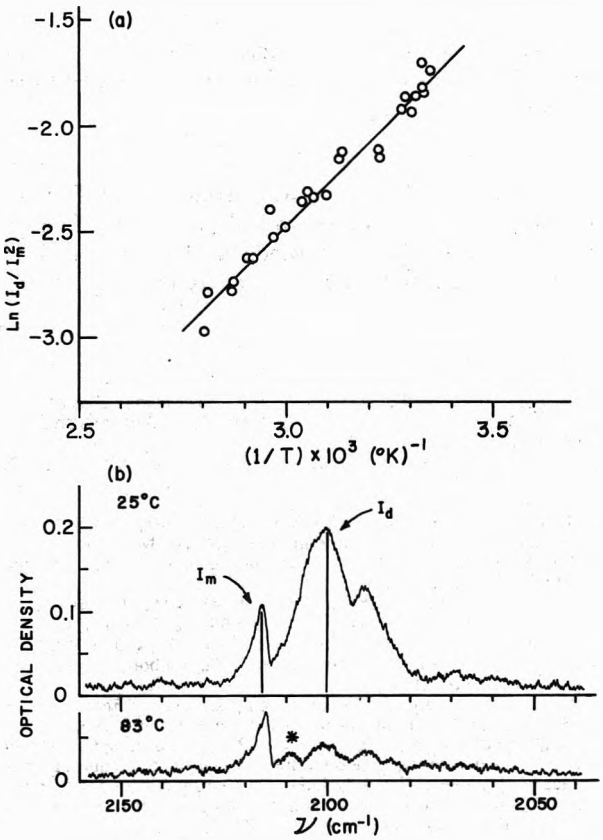

Figure 1. (a) Van't Hoff plot of eq 3. (b) Infrared spectra of the ν_1 region of 700 mm pressure of HCN (path length 10 cm) showing the disappearance of the band assigned to the dimer (I_d) at high temperatures. The reproducible band marked by an asterisk is probably the P branch of the monomer. Corrected frequencies (to vacuum) of maximum absorbances are for monomer R branch (I_m), 2115 cm^{-1}; for dimer R branch (I_d), 2100 cm^{-1}; for monomer P branch (asterisk), 2107 cm^{-1}; and for dimer P branch, 2089 cm^{-1}. The central minima are at 2111 and 2095 cm^{-1} for ν_1 of the monomer and dimer, respectively.

Figure 1 summarizes the experimental findings. A standard least-squares treatment of the 27 data points gives a value of $\Delta E_D = -3.80 \pm 0.16$ kcal/mol of intermolecular bonds, where the uncertainty is the standard deviation. It is seen that this value is in better agreement with that calculated by Kollman, and is larger than the earlier measurement of Giauque and Ruehrwein. It is worth noting the magnitude of the error encountered if the window temperature correction is ignored. Using the wall temperature alone as the gas temperature to calculate ΔE_D the resulting value is -3.47 ± 0.14 kcal/mol. This is probably a lower limit and it is still somewhat larger than the earlier vapor density based value, even though some 10% lower than the corrected result.

Since a ΔS_D estimate of -16.5 eu/mol is provided by Giauque and Ruehrwein, one may use this and the present infrared based ΔH_D value of -4.45 ± 0.16 kcal/mol (see footnote 6) to compute a revised equilibrium constant at 303°K. Comparison with the earlier value of the above authors gives the following result.

$$K_p(\text{revised}) = 0.40; \; K_p(\text{ref } 6) = 0.056$$

This comparison suggest that the dimer makes a somewhat larger contribution to the overall species distribution with the result that the population of higher polymers may have been overestimated in fitting the earlier vapor

density data. Alternatively, the correction for departure from ideality may have been imperfect since it was based on HCl. The value of ΔS_D is relatively insensitive to this correction.

Acknowledgments. The assistance of the Youngstown State University Chemistry Department and Professor Janet Del Bene, whose theoretical work prompted this project, are gratefully acknowledged. The author is also indebted to a referee for pointing out some of the thermodynamic relationships.

References and Notes

(1) (a) R. G. Inskeep, F. E. Dickson, and J. J. Kellihei, *J. Mol. Spectrosc.*, **4**, 477 (1960); (b) R. G. Inskeep, F. E. Dickson, and H. M. Olson, *ibid.*, **5**, (1960).
(2) (a) A. D. H. Clague and H. J. Bernstein, *Spectrochim. Acta., Part A*, **25**, 593 (1969); (b) A. D. H. Clague, G. Govil, and H. J. Bernstein, *Can. J. Chem.*, **47**, 625 (1969).
(3) H. Dunken and H. Winde, *Z. Chem.*, **7**, 37 (1967); see S. Vinogradov and R. N. Linnell, "Hydrogen Bonding," Van Nostrand-Reinhold, New York, N. Y., 1971, for a summary of current thermodynamic data on hydrogen bonding.
(4) (a) J. E. Del Bene, *J. Chem. Phys.*, **55**, 4633 (1971); (b) *ibid.*, **56**, 4923 (1972); (c) K. Morakuma, *ibid.*, **55**, 1236 (1971); (d) P. A. Kollman and L. C. Allen, *J. Amer. Chem. Soc.*, **93**, 4991 (1971).
(5) A. Johansson, P. A. Kollman, and S. Rothenberg, *Theor. Chim. Acta*, **26**, 97 (1972).
(6) W. F. Giauque and R. A. Ruehrwein, *J. Amer. Chem. Soc.*, **61**, 2626 (1939). The measurements led explicitly to a $\Delta H_D = -3.3$ kcal/mol of which -0.65 kcal/mol may be associated with the (PV) work due to the change in the number of moles during dimerization. This value of -0.65 kcal is based on $R[d(\ln T)/d(1/T)]$ in the present temperature range and is thus the difference between ΔH_D and ΔE_D. See footnote 9.
(7) G. E. Hyde and D. F. Hornig, *J. Chem. Phys.*, **20**, 647 (1952).
(8) ν_1 in HCN was not even observed in the infrared for many years. See, for example, G. Herzberg, "Molecular Spectra and Molecular Structure. II. Infrared and Raman Spectra of Polyatomic Molecules," Van Nostrand, Princeton, N. J., 1945, p 279.
(9) Since $K_p = K_c(RT)^{\Delta n}$ and $\Delta H = \Delta E + \Delta nRT$, the differential form of the usual van't Hoff equation may be modified.

$$\frac{d \ln K_p}{dT} = \frac{\Delta H}{RT^2} = \frac{\Delta E}{RT^2} + \frac{\Delta n}{T} \qquad (a)$$

Now

$$\frac{d \ln K_p}{dT} = \frac{d \ln K_c}{dT} + \Delta n \frac{d \ln T}{dT} \qquad (b)$$

and since

$$d \ln T/dT = 1/T \qquad (c)$$

eq d follows by substituting (c) into (b) and identifying the common terms with those of (a).

$$d \ln K_c/dT = \Delta E/RT^2 \qquad (d)$$

Equation d is integrated to give (1). To avoid ambiguity in assigning an "average" temperature, the difference between ΔH and ΔE may be calculated from (e) since $d \ln T/d(1/T) = -T$.

$$\Delta H = \Delta E - \Delta nR(d \ln T/d(1/T)) \qquad (e)$$

(10) K. Ziegler, "Organic Synthesis, Collect. Vol. I., 2nd ed, H. Gilman and A. H. Blatt, Ed., Wiley, New York, N. Y., 1941, p 314.
(11) IUPAC, "Tables of Wavenumbers for the Calibration of Infra-red Spectrometers," Butterworths, London, 1961. Band assignments are those of Hyde and Hornig, based upon the identity of spectral appearance, and as confirmed by the observed pressure and temperature effects. The assignments given by Herzberg (ref 8) should probably be modified accordingly. Thus the 2089 listing (ν_1) may be assigned to the P branch of ν_1 in the dimer. The 2102.1 listing ($4\nu_2 \leftarrow \nu_1$) does not appear to be a "hot band" and may be assigned to the R branch of ν_1 in the dimer. The 2116.7 listing ($3\nu_2$) then is probably the R branch of ν_1 in the monomer. Frequencies recorded in this work are given in the caption of Figure 1.
(12) The cell dimensions (length = 10 cm, window diameter = 5 cm) and the maximum temperature difference between the wall and window temperatures (50°) may be used to calculate a Grashof number of 121 which leads to a boundary layer thickness of 8.5 cm, nearly as thick as the cell length. A convection layer this wide would be expected to be rather poorly developed within the enclosed cell. *Cf.* J. P. Holman, "Heat Transfer," McGraw-Hill, New York, N. Y., 1963.

A Semiempirical Study of Hydrogen Bonding in the Bifluoride Ion

George J. Jiang and George R. Anderson*

Department of Chemistry, Bowdoin College, Brunswick, Maine 04011 *(Received February 15, 1973)*

Publication costs assisted by The National Science Foundation

A study of hydrogen bonding in the bifluoride ion is reported. A semiempirical potential energy function for the $[FHF]^-$ ion is defined and evaluated by a least-squares procedure using *ab initio* MO data recently reported by Almlöf and also by Kollman and Allen. The new potential function fits the data on the bifluoride ion better than the functions proposed earlier. Using the new potential function, vibrational eigenfunctions and eigenvalues are calculated for hydrogen and deuterium isotopes following the procedures of Anderson and Lippincott. Vibrational frequencies are computed and found to be in good agreement with spectroscopic results.

Introduction

We would like to report a study of hydrogen (H) bonding in the bifluoride ion, HF_2^-. The purpose of this study is to construct a more adequate semiempirical model of H bonding in a chemical system for which theoretical and experimental data are known and from which one might be able to apply what is learned to other H bonded systems. Thus, the bifluoride ion can be an important testing grounds for semiempirical models that may have wide applicability and that may also allow for clearer insight into the properties of HF_2^-.

The potential function reported by Lippincott and Schroeder[1] has been used with notable success since 1955 as a general model for linear H bonds. More recently, an addition to this model was published by Anderson and Lippincott[2] that accounts for zero-point energy effects in H bonding by taking the vibrational *plus* electronic (vibronic) energy into account. Aside from general effects and its ability to reproduce known spectroscopic and structural trends, the Anderson–Lippincott model lacked applicability to specifically known H bonded species.

We have made attempts to remedy this situation within the formulation of the Lippincott–Schroeder (LS) potential, and serious efforts were made to fit symmetrically H bonded systems such as $H_5O_2^+$, $(H_2O)_6$, HF_2^-, and HCl_2^-. Using literature values of bond distances, energies, etc. systematic numerical methods were used to try to reproduce these parameters using the LS potential. Our efforts failed, however, and we have since been looking at new ways of improving upon the semiempirical potential function.

Specifically for the bifluoride ion, the energy of formation for the H bond, $HF + F^- = HF_2^-$, was found experimentally by Waddington[3] to be -58 ± 5 kcal mol^{-1} and theoretically by Dixon, *et al.*,[4] to be -60.23 kcal mol^{-1}. The theoretical results of Neckel, Kuzmany, and Vinek[5] and van Gool, Bruinink, and Bottleberghs[6] agree with the work of Dixon, *et al.* In a recent study using an *ab initio* MO approach, Almlöf[7] calculated the H bond energy to be -51 kcal mol^{-1}. Almlöf's results also gave good agreement with spectroscopic parameters determined experimentally so that we have used his *ab initio* results (27 data points) to help in producing a best fit for the potential function proposed below. Kollman and Allen[8] have also reported *ab initio* calculations on HF_2^-, and their results appear to agree reasonably well with Almlöf's results.

The light-atom vibrational stationary states of HF_2^- and DF_2^- are calculated also following the approach used by Anderson and Lippincott.[2] The results are presented and discussed in relation to known spectroscopic and structural properties of sodium and potassium bifluoride.

Potential Function

Lippincott and Schroeder[1] introduced a general potential function for an X–H···Y linear H bonded system, where X and Y are the participant molecules H bonded through electronegative atoms, such as O, F, Cl, or N. If Y is chemically equivalent to the X and the H atom is equally likely to be found bound on either side of the bond as in HF_2^-, the two internal stretching coordinates generate a symmetric potential surface. The coordinates are defined in Figure 1, ref 2, where s and t measure the linear displacement of the H atom from the two respective fluorine atoms such that the total F···F distance $R = s + t$. The classical equilibrium configuration is given by the e subscript (R_e, V_e, t_e, etc.). When one F atom is removed to infinity, no hydrogen bond is formed. The equilibrium bond length of F–H ($s_{e\infty} = t_{e\infty}$) is 0.914 Å. The potential energy of the HF and F^- fragments at infinity is chosen to be zero ($V_{e\infty} = 0$). The LS potential function thus formulated for linear symmetric hydrogen bonds is given by

$$V_{LS} = D[1 - f(s) - f(t)] + A[e^{-bR} - \tfrac{1}{2}(R_e/R)^m e^{-bR_e}] \quad (1)$$

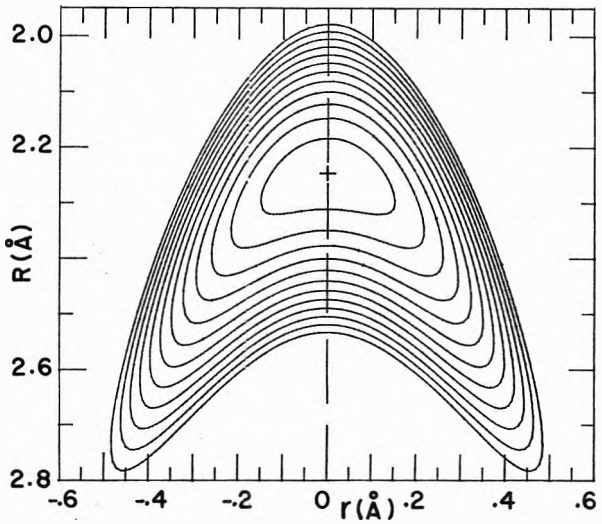

Figure 1. Potential energy contour plot for HF_2^- ion using eq 3. The contour lines are drawn at 500-cm^{-1} intervals starting at $-17{,}500$ to $-12{,}000$ cm^{-1}. The cross marks the potential minimum at $R_e = 2.246$ Å.

The function $f(s)$ and $f(t)$ are symmetric upon exchange of coordinates and are of the form

$$f(s) = e^{-n(s - s_{e\infty})^2/2s}$$

where $n = k_e s_{e\infty}/D$. D is the classical dissociation energy of HF bond (51,300 cm^{-1}). The values of k_e and R_e are 9.655 mdyn/Å and 2.246 Å, respectively. The A, b, and m terms are the constants to be determined. The problem we found with the LS formulation of the potential function was in the need for greater flexibility when trying to fit empirical data and the *ab initio* MO results of Almlöf simultaneously. At infinity ($R = \infty$) the LS model fits very well while near the potential minimum (R_e) it does not.

Initial modification of the LS potential function only removed one restraint on the way in which numerical constants were chosen.

$$V_{LS} = D[1 - f(s) - f(t) + C_1 e^{-bR} - C_2(R_e/R)^m] \quad (2)$$

Here C_1 and C_2 are dimensionless constants replacing the single (A) constant in eq 1. They are evaluated separately by specific empirical restraints imposed upon the model system. The C_1 term is assumed to contribute to a repulsive potential between terminal fluorine atoms while the C_2 term is assumed to contribute attractively. The constants b and m are looked upon as parameters used to make the fit with empirical and theoretical results. Still, this modification (eq 2) was unsatisfactory. This failure led us to consider a three-center repulsive interaction term in the potential function which seems to remove an inherent objection to the LS potential which is the following. Equation 2 unites two diatomic potential functions in a way that allows both chemical bonds to be created simultaneously about the central H atom. These strongly attractive forces are then mediated by the R-dependent (C_1 and C_2) terms operating between the terminal F atoms. Together the model allows for too much chemical bonding, $[F–H–F]^-$, and attempts to compensate for it by adding in too much F···F repulsion (C_1). In retrospect, it seems chemically unreasonable to involve more than the 1s hydrogen orbital in H bonding, so that we modified the potential function as follows.

$$V/D = 1 - f(s) - f(t) + gf(s)f(t) + C_1e^{-bR} - C_2(R_e/R)^m \quad (3)$$

The three-center repulsive interaction term, $gf(s)f(t)$, is inserted to remedy the divalent H-atom problem. For example, when the parameter $g = 1.0$, the first four (chemical bonding) terms contribute *nothing* to the stability of the H bond. Only when the constant is reduced to $g < 1$ does the first group of terms become important to stabilizing the H bond. In this study, a best fit was found for $g = 0.64$ (see below), which seems to be intuitively correct.

Evaluation of the Constants C_1, C_2, and Δs_e. Restraint 1. The potential energy minimum, V_e, is the energy of the H bond exclusive of the vibrational zero-point energy.

$$V_e = D[1 - f(s_e) - f(t_e) + gf(s_e)f(t_e) + C_1e^{-bR_e} - C_2] \quad (4)$$

The value of V_e is known for many H bonded systems and can be used in this procedure to help describe the more complete potential energy surface. The relationship between dependent coordinates at the minimum of the potential energy surface is, of course, $s_e + t_e = R_e$.

Restraint 2. The slope at the bottom of the potential energy surface is defined as zero, and this condition adds two additional restraints on the parameters of the potential energy function evaluated at the equilibrium position.

$$\left(\frac{\partial V}{\partial s}\right)_t\Big|_e = 0 \quad (5a)$$

$$\left(\frac{\partial V}{\partial t}\right)_s\Big|_e = 0 \quad (5b)$$

From these three equations (4, 5a, and 5b) we can derive the constants C_1 and C_2 and evaluate the relationship for Δs_e.

$$C_1 = [mC_2/bR_e - f'(s_e)/b + gf'(s_e)f(t_e)/b]e^{bR_e} \quad (6)$$

$$C_2 = [V_e/D - 1 + f(s_e) + f(t_e) + f'(s_e)/b - gf'(s_e)f(t_e)/b - gf(s_e)f(t_e)]/(m/bR_e - 1) \quad (7)$$

where $f'(s_e) = [n(s_e - s_{e\infty})^2/2s_e - (s_e - s_{e\infty})/s_e]f(s_e)$. The shift in the equilibrium H bond coordinate, Δs_e, is

$$\Delta s_e = s_e - s_{e\infty} = \frac{(t_e - s_{e\infty})(t_e + s_{e\infty})s_e^2f(t_e)[1 - gf(s_e)]}{(s_e + s_{e\infty})t_e^2f(s_e)[1 - gf(t_e)]} \quad (8)$$

If t_e or R_e is specified (and since $s_{e\infty} = 0.917$ Å, a constant), eq 8 implicity defines a value for s_e. It was shown earlier[1] that a similar relationship produces reasonable shifts in equilibrium bond distances close to what is found empirically.

Evaluation of the Constants m, b, and g. The potential energy function has now five empirical-type constants, D, $s_{e\infty}$, k_e R_e, and V_e, and three unspecified parameters, m, b, and g. If the first five are known (approximated) from spectroscopic, crystallographic, or theoretical studies, the latter three may be evaluated in a least-squares fit to the remaining data not dependent upon the first five constants.

Following a data-fitting procedure for HF_2^-, we were able to find a least-squares fit only for $m = 1$ and 6 and not for any others up to $m = 9$. The m value of 6 was used by Anderson and Lippincott[2] in their discussion of the vibronic effects of the hydrogen bond. Lippincott and Schroeder[1] originally pointed out that $m = 1$ and $m = 6$ both gave acceptable potential energy surfaces. In our present fitting procedure, we seem to have verified these earlier findings.

In our best least-squares fit using Almlöf's *ab initio* results, we find $m = 6$ gives the better agreement in reproducing the potential energy data and observed infrared frequency. The parameters g and b are 0.640 and 3.2009 Å^{-1}, respectively. The resulting potential energy surface for HF_2^- ion is shown in Figure 1. Contour lines are drawn at 500-cm^{-1} intervals starting at $-17{,}500$ cm^{-1} to $-12{,}000$ cm^{-1}. The minimum of energy is $-17{,}840$ cm^{-1} (-51 kcal) at $R_e = 2.246$ Å and $r_e = 0$ Å, a relatively flat-bottom single potential well. Although the measured H bond energy (V_e) of HF_2^- is perhaps closer to -58 kcal/mol[3] rather than the Almlöf value of -51 kcal/mol which we are using, the effect of a 14% change in V_e on the spectroscopic predictions (below) is almost negligible (less than 1% change). We therefore feel justified in using the Almlöf and Kollman and Allen data base as reasonable for calculating the low-lying vibrational stationary states of HF_2^-.

Vibrational Calculations. Results and Discussion

The eigenvalues and eigenfunctions of a H atom within a $[F\cdots F]^-$ potential well are calculated assuming "clamped" heavy (F) atom coordinates. The terminal atoms are large in mass compared with hydrogen atom and, therefore, the R coordinate may be kinematically separated from the r coordinate to a reasonable approximation. The potential becomes a one-dimensional function of r, and the F–F separation, R, becomes a parameter to be specified along with the remaining empirical parameters. We will use the notation and procedures developed earlier and reported in ref 2.

The eigenvalue results of the four lowest vibrational states are shown in Figure 2. The ground vibrational state, E_0^+ for hydrogen, has a minimum at an F---F separation of 2.270 ± 0.001 Å in good agreement with Almlöf's results (2.28 Å). The experimental values found for the bifluoride salts are in the region 2.26–2.28 Å.[6] If deuterium is in substituted for hydrogen in the calculations the F- - -F separation at minimum total energy is 2.264 ± 0.001 Å. The isotope shift is small and negative $\Delta R_0 = -0.006$ Å, in excellent agreement with the value -0.0058 Å found by Almlöf calculation.[7] The experimental isotope shift for KHF_2 is $\Delta R_0 = -0.0024$ Å and for $NaHF_2$ is $\Delta R_0 = -0.0046$ Å.[9] The calculations seem to overestimate ΔR_0. This may be in part due to other vibronic effects of the hydrogen bond and by crystal field effects not included in this calculation.

The predictions of infrared and Raman spectra are based upon the assumption of "vertical" transitions from the ground state. The dipole selection rules require even–odd or odd–even transitions while the Raman effect gives rise only to transition among the even–even or odd–odd states.

The infrared fundamentals and overtones for hydrogen and deuterium vibrations are shown in Table I. One of the characteristic features of the strong hydrogen bond is the high anharmonicity of the stretching vibration of the H atom in this bond (ν_H). This can be seen from the fundamental (1490 cm^{-1}) and ν_H overtone (5650 cm^{-1}), a ratio of 3.8. Also, the ratio of $\nu_H/\nu_D = 1.52$ deviates significantly from the harmonic value, $\nu_H/\nu_D = 1.38$. The predicted

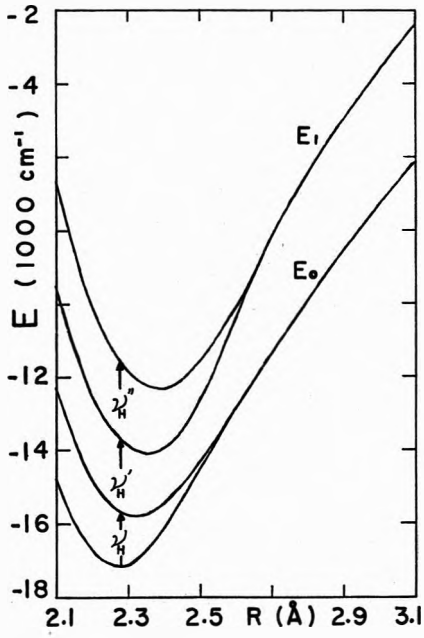

Figure 2. Total energy plot for the H atom is the four lowest vibrational states as a function of F–F distances, R. ν_H is the fundamental transition, ν_H' and ν_H'' are the first and second overtones, respectively.

TABLE I: Calculated Eigenvalues and Infrared and Raman Transitions

H			D			
Energy, cm^{-1}	State	ν_H, cm^{-1}	Energy, cm^{-1}	State	ν_D, cm^{-1}	Ratio[a] ν_H/ν_D
−17,190	0^+		−17,394	0^+		
−15,700	0^-	1490 (fundamental)	−16,404	0^-	990	1.505
−13,720	1^+	3470 (Raman)	−15,119	1^+	2275	1.525
−11,540	1^-	5650 (overtone)	−13,764	1^-	3720	1.519

[a] The harmonic value $\nu_H/\nu_D = 1.38$.

Raman ($E_0^+ \rightarrow E_1^+$) transitions is given but has not been reported.[10] A comparison of our results with those reported by Almlöf and other experimental results are listed in Table II. The asymmetric hydrogen stretching vibration, ν_H, is about 40 cm^{-1} higher than the experimental value, but the deuterium ν_D is lowered by 60 cm^{-1}. General agreement, however, is good.

The symmetric F···F stretching frequency is calculated from the curvature of the ground-state energy diagram (Figure 2) using the harmonic oscillator approximation. It is found to be ν_{F-F} = 694 cm^{-1} whereas the observed frequency, ν_{FF}(obsd) = 600 cm^{-1}, a deviation ~100 cm^{-1}. This discrepancy may be in part due to the approximate method of calculation or in part due to lattice potential energy contribution not included in the *ab initio* MO data. We have assumed that the bifluoride ion is isolated, and no environment effects on FHF^- ion are considered in our calculation. In Table II, the calculated frequencies are also listed for the ν_{H-F} fundamental and the first overtone of the isolated (nonbonded) HF molecule. The agreement of calculated value with experimental value is excellent. From this close agreement, one can see that the same potential energy function that fits the H bonded complex also behaves very well at larger F–F distances far from the potential minimum (see Figure 2, also).

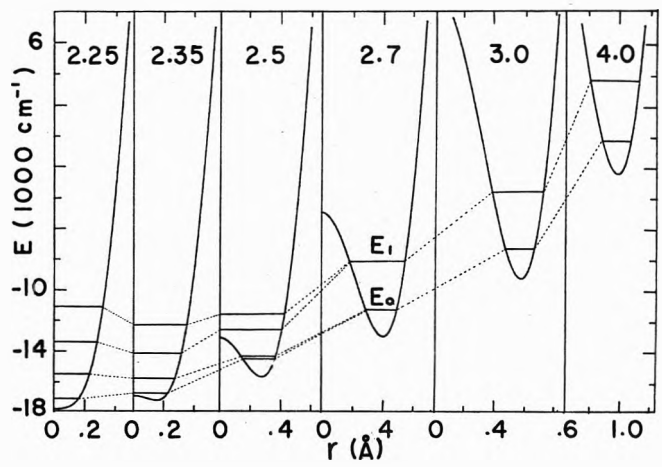

Figure 3. A correlation of vibrational energy levels for different F–F separations, R. Half of the symmetric potential function is shown at each respective R value as a function of r (H atom displacement from the center of the bond).

TABLE II: Comparison of Calculated Infrared Frequency with Almlöf and Experimental Results

	This work	Almlöf	Exptl (KHF_2)
R_0, Å	2.27	2.28	2.277[a]
Isotope shift (ΔR_0), Å	−0.006	−0.0058	−0.0024[b,c]
H asymmetric stretch ν_H, cm^{-1}	1490	1497	1450[b]
D asymmetric stretch ν_D, cm^{-1}	990	1038	1023[b]
Symmetric stretch $\nu_{F\cdots F}$, cm^{-1}	694	666	600[b]
Isolated H–F stretch ν_{H-F}, cm^{-1}	3962.8		3958.38[d]
Isolated H–F stretch ν_{H-F} overtone, cm^{-1}	7783.1		

[a] Reference 9. [b] J. A. Ibers, *J. Chem. Phys.*, **41**, 25 (1964); **48**, 4539 (1968). [c] 0.0046 Å for $NaHF_2$. [d] G. Herzberg, "Molecular Spectra and Molecular Structure I: Spectra of Diatomic Molecules," Van Nostrand, New York, N. Y., 1950.

The vibrational energy levels of bifluoride ion in different F–F separations are shown in Figure 3. At R_e = 2.246 Å, the potential surface has a single minimum and the first four vibrational states (E_0^+, E_0^-, E_1^+, E_1^-) are shown. At the larger F–F separation, R = 2.35 Å, the double minimum of the potential energy curve appears and the vibrational energy levels become closer (see Figure 2, also). At R = 2.50 Å, the first two states E_0^+ and E_0^- are almost degenerate, the splitting (~120 cm^{-1}) is due to the tunnelling effect. The E_1^+ and E_1^- states are also closer to each other while the average separation between the E_0 and E_1 states increase. At R = 2.7 Å, the potential barrier is very high and no appreciable tunnelling occurs. The vibrational states are doubly degenerate. The correlation between states of the various F–F distance are indicated by dashed lines. The central potential barrier increases with increasing R with a limiting value of D (= 51,300 cm^{-1}).

The minimum in energy in F···F separation shown in Figure 2 is dependent upon the quantum vibrational state of the H atom. For the ground vibrational state, R_0^+ = 2.270 Å while the first excited state R_0^- = 2.313 Å. The increase in F···F distance is 0.043 Å. Higher vibrationally excited states have progressively larger F···F mini-

mum energy separations. These properties of the model system would lead one to predict an expansion of the F···F bond distance (or a lattice parameter of the Na or K salt) during the course of vibrational excitation. Following absorption of a photon, ν_H = 1450 cm^{-1}, the H bonded lattice would momentarily expand for the period typical of the lifetime of the excited vibrational state, $\sim 10^{-11}$ sec.

For H bonded species other than the strong bifluoride-type ion, however, the reverse effect may be expected (R contracts, not expands as it does here). This prediction is based upon earlier studies but needs to be more precisely documented by further studies of model H bond cases.

Conclusion

In this study of the bifluoride ion, we have combined experimental and theoretical data so as to fit a newly proposed model for the linear symmetric H bond. The model calculations proceed in two separate steps. First, a two-dimensional potential energy surface is formed on the basis of the two displacement coordinates of the $[FHF]^-$ ion. The approximation then is made for the separation of motion of the heavy (F) and light atoms (H and D) so that, secondly, eigenfunctions and eigenvalues may be calculated for a series of F···F distances (R). These vibrational states of the H bond take zero-point energy effects into account and allow one to predict spectroscopic and structural properties of the system near equilibrium (FHF^-) and in the limit of dissociation ($FH + F^-$). Calculated and measured properties of the HF_2^- ion are in good agreement so that we feel the model system is realistic and may be useful in studying other H bonded systems.

Acknowledgments. We are pleased to acknowledge the National Science Foundation (Grant No. GP-31 725) for the financial support of this study. We would like to thank Professor E. R. Lippincott (University of Maryland) for his valuable comments during the preparation of this manuscript and Mr. R. Patrick Johnson (Bowdoin College, class of 1974) for his work on computer graphics and his programming assistance.

References and Notes

(1) E. R. Lippincott and R. Schroeder, *J. Chem. Phys.*, **23**, 1099 (1955).
(2) G. R. Anderson and E. R. Lippincott, *J. Chem. Phys.*, **55**, 4077 (1971).
(3) T. C. Waddington, *Trans. Faraday Soc.*, **54**, 25 (1958).
(4) H. P. Dixon, H. D. B. Jenkins, and T. C. Waddington, *J. Chem. Phys.*, **57**, 4388 (1972).
(5) A. Neckel, P. Kuzmany, and G. Vinek, *Z. Naturforsch. A*, **26**, 569 (1971).
(6) W. van Gool, J. Bruinink, and P. H. Bottleberghs, *J. Inorg. Nucl. Chem.*, **34**, 3631 (1972).
(7) J. Almlöf, *Chem. Phys. Lett.*, **17**, 49 (1972); also presented at the International Conference on Hydrogen Bonding, Aug 21, 1972, Ottawa, Canada.
(8) P. A. Kollman and L. C. Allen, *J. Amer. Chem. Soc.*, **92**, 6101 (1970).
(9) J. A. Ibers, *J. Chem. Phys.*, **40**, 402 (1964).
(10) The $E_0^+ \rightarrow E_1^+$ Raman transition might be expected to be very weak in intensity because it is equivalent to an overtone of the infrared $E_0^+ \rightarrow E_0^-$ transition. In the harmonic oscillator approximation, its intensity should be zero. See Figure 3.

Effect of Pressure on the Overall and Internal Rotation in Liquid Benzyl Cyanide

J. DeZwaan and J. Jonas*[1]

Department of Chemistry, School of Chemical Sciences, University of Illinois, Urbana, Illinois 61801 *(Received February 22, 1973)*

Publication costs assisted by the U.S. Air Force Office of Scientific Research

The pressure dependence of the deuteron spin–lattice relaxation times of benzyl-4-d_1 cyanide and α,α-dideuteriobenzyl cyanide has been measured up to 3 kbars at 30 and 150°. Detailed temperature dependence of these relaxation times has also been determined at 1 atm. Assuming the validity of the rotational diffusion equation, the deuteron T_1's were analyzed in terms of the rotational diffusion constants for the overall molecular, D_M, and internal, D_I, rotation. In order to calculate the theoretical rotational correlation times, the pressure dependence of viscosity up to 3 kbars at 30 and 150° has also been determined.

Introduction

Nuclear magnetic resonance relaxation rates have been successfully used to study the anisotropic reorientation of molecules in the liquid state.[2-6] It has also been shown that applying pressure to a liquid can have a large effect on the rate of overall molecular reorientation.[7,8] As part of our broader investigations of the dynamic structure of molecular liquids we became interested in the problem of pressure effects on the internal motions[9] of groups within a molecule in the liquid state.

The nuclear magnetic resonance spin–lattice relaxation time, T_1, of a nucleus possessing an electric quadrupole moment ($I > \frac{1}{2}$) yields important information on the reorientational motions of molecules, since the rate of relaxation ($1/T_1$) is simply related to a reorientational correlation time. For a nucleus of spin 1 this relation,[10] valid for isotropic reorientation, is

$$1/T_1 = \tfrac{3}{8}(e^2qQ/\hbar)^2[1 - (\eta^2/3)]\tau \quad (1)$$

where $(e^2qQ/\hbar)$ is 2π times the quadrupole coupling constant in Hz, η is the asymmetry parameter, and τ is the reorientational correlation time. In general this reorientational motion may result from both the overall motion of the molecule and internal motions within the molecule. Recent studies[11,12] have reported the effect of internal rotation on the angular correlation function where both the overall motion and the internal motion are diffusional, and these results are applied here to obtain estimates of the overall molecular and internal rotational diffusion constants. The pressure dependence of the reorientation rates is valuable in determining the reorientational mechanism since the environment of the molecule and the forces on the molecule can be significantly altered without changing the kinetic energy of the molecules.

In this paper the deuterium spin–lattice relaxation times of the two selectively deuterated benzyl cyanides, benzyl-4-d_1 cyanide (I) and α,α-dideuteriobenzyl cyanide (II), are measured as a function of pressure. The relaxation time of I gives a measure of the overall reorientation of the molecule, while the relaxation time of II reflects both the overall molecular reorientation and the internal rotation of the CD_2CN group. The choice of benzyl cyanide is based on a study by Wallach[13] in which it has been shown that the internal motion of CH_2CN in methylbenzyl cyanide proceeds at a rate comparable to the overall molecular motion and, thus, may be described by a rotational diffusion model. Using reported deuteron quadrupole coupling constants, the experimental spin–lattice relaxation times, T_1, are analyzed in terms of the rotational diffusion constants for overall molecular, D_M, and internal, D_I, rotation. The activation volumes for D_M and D_I are calculated.

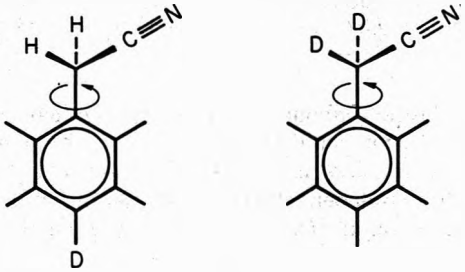

I II

Experimental Section

T_1 Measurements. The pulsed nmr spectrometer and the high-pressure rf probes were described in detail elsewhere.[14] A Varian V-3800-1 high-resolution magnet system equipped with superstabilizer and shim coils was used. The rf probe was made from the titanium alloy IMI-680 (Imperial Metal Industries, England), and the pressures were generated with an Enerpac hand pump and intensifier and measured directly by means of a Bourdon-Heise gauge. A 50:50 mixture of kerosene and 10W motor oil was used as a pressure transmitting fluid. The temperature was controlled to ±0.2° at 30° and ±1.5° at 150° by means of a heating jacket surrounding the probe, and measured with a copper–constantan thermocouple inside the probe. The samples were degassed in a freeze–pump–thaw cycle and were transferred to the high-pressure sample container in an oxygen-free argon atmosphere in a glovebox.[15]

The relaxation times were measured at 9.2 MHz using a 180°–τ–90° pulse sequence with the magnetization being plotted as a function of τ to obtain T_1. Since the signal-to-noise ratio varied from 6:1 to about 3:1, a Fabri-Tek Model 1074 signal-averaging computer was used, with the sample being allowed to equilibrate 10 times T_1 between pulse sequences. The error in T_1 measurements is estimated to be from 4 to 6%.

Viscosity. The pressure dependence of the viscosity was determined with a high-pressure rolling-ball viscometer which has been described elsewhere.[8] The roll times were consistent to within ±1%; but since the density of the liquid had to be estimated, a small error (less than 3%) was introduced. This error is minor because the viscosity depends on the difference of the density of the steel ball and the density of the liquid; but since the density of the ball is much greater than the liquid, the density difference changes by only 4% over the 3-kbar range (based on known densities of other liquids). Thus, even estimating the density of the liquid will reduce this error considerably.

Materials. Benzyl-4-d_1 cyanide was prepared from *p*-bromotoluene by forming the Grignard reagent and hydrolyzing with deuterium oxide. The resulting toluene-4-d_1 was purified by distillation and brominated at the α carbon as given in ref 16. The bromine was then replaced by cyanide as described in ref 17. α,α-Dideuteriobenzyl cyanide was prepared by refluxing benzyl cyanide in a mixture of 60% methanol-d_1 and D_2O in the presence of a small amount of KOH.

A chemical purity of >99% for both compounds was established by gas chromatography. Mass spectra showed the deuteration to be 90% complete for benzyl-4-d_1 cyanide, and high-resolution proton nmr showed 70% complete deuteration for α,α-dideuteriobenzyl cyanide.

Results and Discussion

The relaxation times of benzyl-4-d_1 cyanide (I) are shown in Table I. To calculate the reorientational correlation times for the overall molecular motion ($\tau = \tau_M$; see eq 1) a quadrupole coupling constant is needed. Recent studies[18,19] of the ring deuterons in monosubstituted benzene derivatives indicate that the coupling constants are relatively insensitive to substitution on the ring having a value of 180 ± 5 kHz for a number of substituted benzenes. The asymmetry parameters were also measured[19] and found to be small (0.04–0.06). On this basis a quadrupole coupling constant of 180 kHz was used in the calculations and the asymmetry parameter was neglected.

The experimental results for the overall molecular motion are given in Table I in terms of an overall molecular rotational diffusion constant, D_M, where $D_M = 1/6\tau_M$. These values indicate the large variation that occurs in the rate of reorientation in going from 30° and 3 kbar to 150° and 1 atm. Also shown in Table I are the theoretical diffusion constants, $(D_M)_{theor}$, predicted by the hydrodynamic model[20]

$$(D_M)_{theor} = kT/6V_M\eta f_R \quad (2)$$

where V_M is the molecular volume, η is the viscosity in poise, and f_R is the microviscosity factor as given by Gierer and Wirtz.[21] The molecular volume (1.37×10^{-22} cc/molecule) was obtained from the density (1.05 g/cc) of benzyl cyanide at its melting point and assuming hexagonal close packing. These theoretical rotational diffusion constants are in reasonably good agreement with the experimental values. This supports the validity of our as-

TABLE I: Experimental Deuteron Spin–Lattice Relaxation Times and the Calculated Rotation Diffusion Constants

P, bars	T_1 (ring), sec	η, cP	$D_M \times 10^{-10}$, radian^2/sec		T_1 (CD_2CN), sec	τ_M/τ_{eff}	D_I (eq 3)	$D_I \times 10^{-10}$, radian^2/sec	
			Expt	Theor				Eq 4	Theor
					$T = 30°$				
1	0.184	1.78	1.47	1.75	0.422	1.93	4.15	5.62	8.45
500	0.139	2.51	1.11	1.24	0.320	1.93	3.13	4.24	6.01
1000	0.106	3.46	0.846	0.902	0.242	1.92	2.39	3.23	4.35
1500	0.080	4.64	0.641	0.672	0.183	1.92	1.81	2.45	3.25
2000	0.060	6.42	0.480	0.486	0.138	1.93	1.35	1.83	2.34
2500	0.0455	8.68	0.364	0.359	0.105	1.94	1.03	1.39	1.73
3000	0.0343	12.1	0.274	0.258	0.079	1.94	0.77	1.05	1.25
					$T = 150°$				
1	0.878	0.460	7.03	9.48	1.70	1.63	12.37	19.3	45.8
500	0.749	0.611	6.00	7.14	1.51	1.69	11.79	17.7	34.5
1000	0.638	0.771	5.11	6.13	1.34	1.76	11.24	16.4	27.7
1500	0.547	0.946	4.37	4.61	1.19	1.83	10.71	15.1	22.3
2000	0.465	1.14	3.72	3.82	1.06	1.92	10.38	14.1	18.5
2500	0.398	1.35	3.19	3.23	0.940	1.98	9.62	12.8	15.7
3000	0.339	1.60	2.71	2.73	0.837	2.07	9.13	11.9	13.2

sumption that the overall molecular reorientation of benzyl cyanide can be regarded as a small-step diffusion process.

In our previous study[8] we have introduced the difference between the activation volumes for rotation and η/T as a qualitative measure of the degree of coupling between the rotational and translational motions. The value of ΔV^* for D_M is quite close to ΔV^* for η/T and this reflects a strong coupling between the rotational and translational motion of the benzyl cyanide molecule. This finding also suggests that the overall molecular reorientation is well described by simple rotational diffusion over the entire temperature and pressure range.

The relaxation times of α,α-dideuteriobenzyl cyanide (II) are also given in Table I. To determine the effective correlation time (τ_{eff}) for this motion (*i.e.*, overall plus internal rotation), a coupling constant of 165 kHz as determined for toluene[22] was used. From the ratio of τ_M to τ_{eff} it is seen that the correlation time of the α deuterons is only about one-half as long as τ_M at both 30 and 150°. It is interesting, however, that this ratio remains constant as a function of pressure at 30° while at 150° it varies with pressure beyond experimental error.

Since there are only two correlation times available to interpret the molecular motions, some assumptions regarding the reorientational motion are required. If it is assumed that the molecule as a whole reorients isotropically, its rotation can be described by a single diffusion constant D_M ($D_M = 1/6\tau_M$). Then if the internal reorientation can be represented by an independent diffusion constant, D_I, describing the reorientation of the CD_2CN group relative to the ring, the following expression[13] is obtained

$$\frac{\tau_M}{\tau_{eff}} = \left[\frac{\frac{3}{4}\sin^4\theta}{1 + \frac{2}{3}\rho} + \frac{3\cos^2\theta\sin^2\theta}{1 + \frac{1}{6}\rho} + \frac{1}{4}(3\cos^2\theta - 1)^2\right]^{-1} \quad (3)$$

where θ is the angle between the axis of internal rotation and the carbon–deuterium bond (taken to be 109.5°) and ρ is D_I/D_M.

One could also approximate benzyl cyanide as a symmetric top with a symmetry axis through the 1 and 4 ring carbons. Motion about the axes perpendicular to this "symmetry" axis could then be described by a single diffusion constant, D_M. If it is also assumed that the motion of CD_2CN is independent of the reorientation of the ring about the symmetry axis, the following expression[23] is obtained

$$\frac{\tau_M}{\tau_{eff}} = \left[\frac{\frac{3}{4}\sin^4\theta}{\frac{2}{3}\rho + \frac{1}{3}} + \frac{3\cos^2\theta\sin^2\theta}{\frac{1}{6}\rho + \frac{5}{6}} + \frac{1}{4}(3\cos^2\theta - 1)^2\right]^{-1} \quad (4)$$

where ρ is D_I'/D_M. The usual convention is to denote by $D_\perp$ the rotational diffusion constant for the rotation about axes perpendicular to the main symmetry axis. In our case we take $D_{||} = D_M$. The rotational diffusion constant $D_{||}$ for the rotation about the main symmetry axis is taken equal to D_I'. The sole reason of using the given form of eq 3 and 4 in terms of the ratio τ_M/τ_{eff} was to obtain a convenient measure of how the rate of the internal rotation compares with the rate of the overall molecular rotation.

The quantities D_I and D_I' obtained from these two treatments differ slightly in their interpretation. The diffusion constant, D_I, obtained from eq 3 describes the motion of the CD_2CN group relative to the isotropic motion of the molecule while eq 4 gives the diffusion constant, D_I', describing the rate of reorientation of the group about the symmetry axis. When the value of τ_M/τ_{eff} becomes large (about 3.5) both models give essentially the same value of ρ as would be expected. For example, in toluene the D_I and D_I' are the same since the motion of the methyl group is very fast when compared to the overall molecular rotation. For a value of $\tau_M/\tau_{eff} = 1.93$, eq 4 gives a value of D_I' that is 1.35 times as large as that obtained from eq 3. Due to the approximations involved in both models, however, the internal rotational diffusion constants calculated can only be regarded as estimates of the exact value, but they should at least give a good indication of the true behavior.

Both models predict that if τ_M/τ_{eff} is constant, ρ is constant and therefore D_M and D_I have identical pressure dependences. Thus, at 30° D_I appears to be strongly coupled to viscosity (Figure 1), while at 150° this is no longer

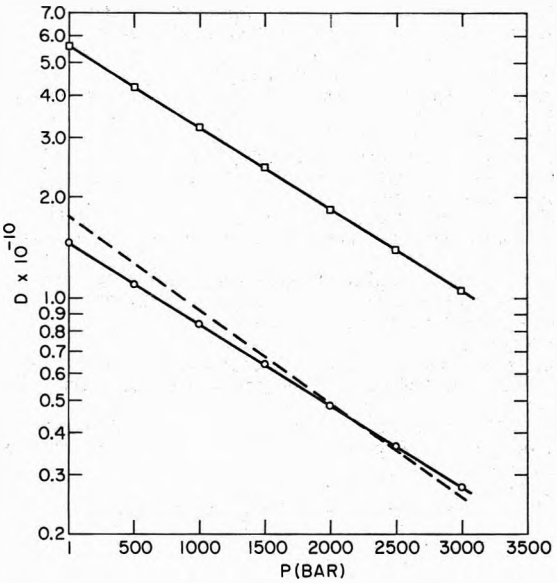

Figure 1. Pressure dependence of the rotational diffusion constants D_M (O), D_I' (□), and $(D_M)_{theor}$ (- - -) in liquid benzyl cyanide at 30°.

TABLE II: Activation Parameters

Quantity	ΔE^* kcal/mol	ΔV^* (30°), cc/mol	ΔV^* (150°), cc/mol
D_M	3.31	14.4	11.2
D_I'	2.5	14.4	5.5
η/T	3.61	16.2	...

true (Figure 2). The values of D_I and D_I' as obtained from eq 3 and 4 are listed in Table I along with the theoretical values predicted by the hydrodynamic model for a sphere having the volume of the CH_2CN group (24.9 cc/mol).[24] We are aware of the oversimplification in this calculation, but it can be regarded as a zero-order approximation. The value of the microviscosity factor f_R (see eq 2) was taken to be 0.113. This is different than the value f_R for a neat liquid (0.163) and arises by considering the radius of the CH_2CN as representing a solute and the radius of the benzyl cyanide molecule as representing a solvent. The agreement between the two values at 30° is quite reasonable considering the nature of the calculation, but at 150° they deviate substantially. This seems to indicate that the internal rotation is no longer of a small-step diffusional nature. Table II shows that the activation volumes ΔV^* for D_M and D_I are identical at 30° but at 150° the activation volume for the overall molecular diffusion is much larger than that for D_I'. This is analogous to our earlier finding[9] in toluene-d_8 where at 100° the $\Delta V^*(D_M)$ was three times as large as $\Delta V^*(D_I)$. Again, these results reflect the difference in functional torques connected with the overall and internal rotation and also indicate the presence of inertial effects influencing the internal rotation at higher temperatures.

As a measure of the applicability of the small angle rotational diffusion model, a quantity χ has been introduced by several authors.[2a,6,25] This quantity is the ratio of the time required for reorientation in the liquid to the theoretical reorientation time of the free rotor, that is

$$\chi = (5/18D_i)(kT/I_i)^{1/2} \quad (5)$$

where D_i and I_i are the diffusion constant and the moment of inertia about the ith axis, respectively. In their

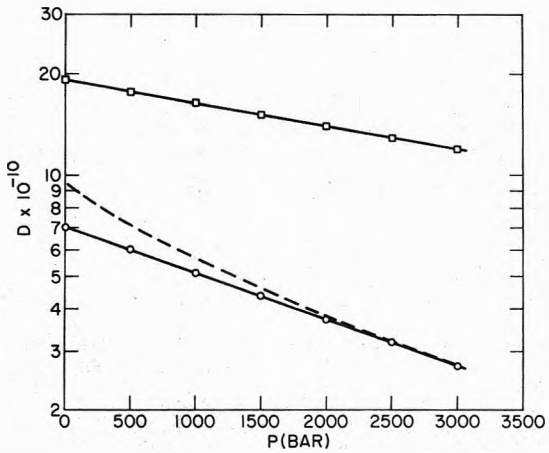

Figure 2. Pressure dependence of the rotational diffusion constants D_M (O), D_I' (□), and $(D_M)_{theor}$ (- - -) in liquid benzyl cyanide at 150°.

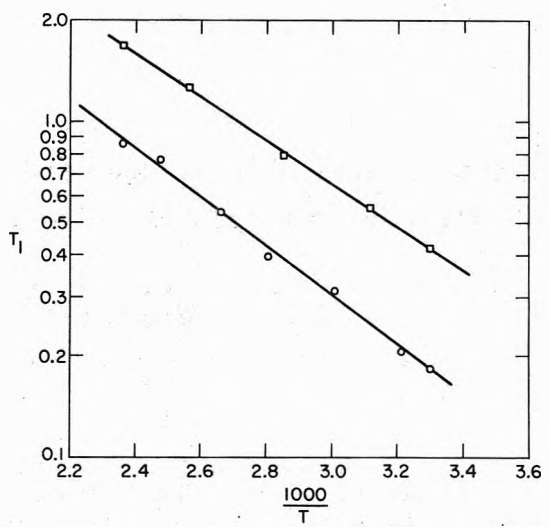

Figure 3. Temperature dependence of the deuteron T_1 in compounds I (O) and II (□).

study,[6] Gillen and Noggle have tentatively proposed the following limits on χ indicative of the various reorientation mechanisms

$\chi < 3$	inertial region
$3 < \chi < 5$	intermediate region
$5 < \chi$	diffusion region

Using the value of 1.88×10^{-38} g cm² which is the moment of inertia of the CD_2CN group about the symmetry axis, χ at 30° ranges from 7.2 to 39 at 1 atm and 3 kbars, respectively; hence, diffusional reorientation is predicted. At 150°, χ ranges from 2.5 to 4.1 over the same pressure range and therefore inertial effects can be expected to influence the reorientational motion of the CD_2CN group, particularly within the lower pressure region.

For comparison purposes with the values obtained by Wallach for methylbenzyl cyanides, the temperature dependences of the relaxation times at 1 atm were also determined and are shown in Figure 3. The activation energy of 2.93 kcal/mol obtained for α,α-dideuteriobenzyl cyanide (II) agrees well with the value of 2.88 kcal/mol that we calculate from Wallach's data on the nitrogen-14 relaxation times in neat benzyl cyanide. Both eq 3 and 4 show Arrhenius-type behavior for ln D_I as a function of $1/T$

with activation energies of 2.3 and 2.5 kcal/mol, respectively.

Acknowledgments. This work was partially supported by the National Science Foundation under Grant No. GP 28268X and by the U. S. Air Force Office of Scientific Research under Contract No. AF 72-2286.

References and Notes

(1) J. S. Guggenheim Fellow, 1973.
(2) (a) T. T. Bopp, *J. Chem Phys.*, **47**, 3621 (1967); (b) D. E. Woessner, B. S. Snowden, Jr., and E. T. Strom, *Mol. Phys.*, **14**, 265 (1968).
(3) J. Jonas and T. M. Di Gennaro, *J. Chem Phys.*, **50**, 2392 (1969).
(4) D. Wallach and W. T. Huntress, Jr., *J. Chem. Phys.*, **50**, 1219 (1969).
(5) A. Allerhand, *J. Chem. Phys.*, **52**, 3596 (1970).
(6) K. T. Gillen and J. H. Noggle, *J. Chem. Phys.*, **53**, 801 (1970).
(7) H. J. Parkhurst, Jr., Y. Lee, and J. Jonas, *J. Chem. Phys.*, **55**, 1368 (1971).
(8) R. A. Assink, J. DeZwaan, and J. Jonas, *J. Chem Phys.*, **56**, 4975 (1972).
(9) D. J. Wilbur and J. Jonas, *J. Chem. Phys.*, **55**, 5840 (1971).
(10) A. Abragam, "The Principles of Nuclear Magnetism," The Clarendon Press, Oxford, 1961, p 314.
(11) D. Wallach, *J. Chem. Phys.*, **47**, 5258 (1967).
(12) D. E. Woessner, B. S. Snowden, Jr., and G. H. Meyer, *J. Chem. Phys.*, **50**, 719 (1969).
(13) D. Wallach, *J. Phys. Chem.*, **73**, 307 (1969).
(14) J. Jonas, *Rev. Sci. Instrum.*, **43**, 643 (1972).
(15) T. L. Brown, D. W. Dickerhoff, D. A. Bafus, and G. L. Morgan, *Rev. Sci. Instrum.*, **33**, 491 (1962).
(16) H. Schmid and P. Karrer, *Helv. Chim. Acta*, **29**, 573 (1946).
(17) M. Gordon, M. L. DePamphilis, and C. E. Griffin, *J. Org. Chem.*, **28**, 698 (1963).
(18) R. A. Assink and J. Jonas, *J. Magn. Resonance*, **4**, 347 (1971).
(19) R. G. Barnes and J. W. Bloom, *J. Chem. Phys.*, **57**, 3082 (1972).
(20) N. Bloembergen, E. M. Purcell, and R. V. Pound, *Phys. Rev.*, **73**, 679 (1948).
(21) A. Gierer and K. Wirtz, *Z. Naturforsch, A*, **8**, 532 (1953).
(22) J. Powell, W. Phillips, L. Melby, and M. Panar, *J. Chem. Phys.*, **43**, 3442 (1965).
(23) D. E. Woessner and B. S. Snowden, Jr., "8th Colloquium on NMR Spectroscopy," Aachen, Germany, April 1971, Springer-Verlag, Berlin, 1971.
(24) A. Bondi, *J. Phys. Chem.*, **68**, 441 (1964).
(25) W. T. Huntress, *Advan. Magn. Resonance*, **4**, 1 (1970).

Interaction between Crystal Violet and Poly(methacrylic acid) in Aqueous Solutions. I. Results from Spectroscopic Measurements and Dialysis

W. H. J. Stork, P. L. de Hasseth, W. B. Schippers, C. M. Körmeling, and M. Mandel*

Gorlaeus Laboratoria der Rijksuniversiteit, Afdeling Fysische Chemie III, Leiden, The Netherlands *(Received January 29, 1973)*

It is shown with the help of spectroscopic and dialysis experiments that Crystal Violet can be bound to poly(methacrylic acid) at all degrees of neutralization (α') and also to the completely undissociated polyelectrolyte. Binding is complete for solutions in which $\alpha' C_p/C_d$ has a value between 1.0 and 1.5 (where C_d is the concentration of the dye in molarity and C_p the concentration of the polyelectrolyte in equivalents per liter) and no unbinding is observed for larger values of this ratio. The shape of the absorption spectrum of the bound dye, the position of the maximum, and the absorption coefficient at this maximum all depend on C_p/C_d and α'. The fluorescence quantum yield of the dye is found to be very large for Crystal Violet bound to the completely undissociated polyelectrolyte but to decrease with increasing α' reaching values of the order of magnitude comparable to the very small quantum yield of free violet for $\alpha' > 0.40$.

1. Introduction

During the last decade much attention has been paid to the interaction between dyes and biological macromolecules.[1] It has become clear, however, that this binding is a complicated physicochemical process. Thus even for the extensively investigated nucleic acid–Acridine Orange system many points remain to be solved. In view of this situation the study of the interaction between dyes and synthetic polyelectrolytes becomes interesting. So far only a few of such studies have been carried out and these often yield conflicting conclusions.

In the present investigation a description of the binding between the cationic dye Crystal Violet (CV) and poly(methacrylic acid) (PMA) has been attempted. The latter is a weak polyacid and was chosen because of its conformational transition, from a compact to an extended mean conformation, upon ionization.[2-4] Thus the influence of ionic strength, polymer charge, and conformation on the binding of the dye could be studied as well as the influence of bound dye on the conformation of PMA. On the other hand, CV is a dye that exhibits in the presence of a polyelectrolyte an enhanced fluorescence analogous to the previously investigated Auramine-O.[5]

Several techniques were applied to study the binding of CV to PMA. Absorption and fluorescence spectroscopy and equilibrium and sedimentation dialysis were used to determine the extent of binding. Results obtained by these methods will be presented in this part of the paper. The influence of bound dye on the conformational transition of the polymer was assessed by potentiometric and viscosimetric titrations. This will be presented in part II,[6] together with a general discussion of all the results obtained.

A few papers on the interaction between PMA and dyes have been published.[5-7] In these papers the binding is always investigated spectroscopically. Conflicting conclusions were drawn however. Some authors claim to have proven that dyes bind only to the compact conformation[5] whereas others state that binding can occur at all values of the degree of ionization, *i.e.*, to both conformations.[7] Our results clearly demonstrate that CV binding to PMA occurs over the whole range of degree of ionization but that this binding has a stabilizing effect on the compact conformation of PMA. Furthermore some interesting changes in the spectroscopic properties of CV upon binding to PMA were observed.

2. Experimental Section

a. Materials. Atactic PMA was prepared and fractionated as described previously.[2] In all experiments a fraction was used which had a molecular weight of 1.3×10^6 by viscosimetric determination according to Wiederhorn and Brown.[8] Nmr measurements on its methyl ester indicate the presence of 10% isotactic, 40% heterotactic, and 50% syndiotactic triads, using methods described in the literature.[9] Solutions of PMA were prepared with conductance water ($\rho > 10^6$ Ω m) and different concentrations obtained by dilution from a concentrated solution. Concentrations were determined potentiometrically. Different degrees of neutralization were obtained by adding known amounts of 0.1 *M* NaOH.

Crystal Violets {[4-[bis[*p*-(dimethylamino)phenyl]methylene]-2,5-cyclohexadien-1-ylidene]dimethylammonium chloride} of commercial origin (U.C.B.) was purified as described elsewhere.[10] It decomposes slowly and was therefore stored at low temperature and in the dark. Checks on the purity were performed regularly. In dilute aqueous solutions and at pH ~7 CV is completely dissociated in the monovalent dye cation (D^+) and Cl^-; these solutions are moderately stable. At low pH, D^+ can bind one or two protons. Lautsch, *et al.*,[11] have found from spectroscopic studies that the dissociation constant of D^+H^+ is 1.09×10^{-2} *M* and of $D^+H_2^2$ into D^+H^+ is 1.56×10^{-1} *M*. This implies that at pH 3.5 the dye is almost completely present as D^+ as was confirmed by Soda and Yoshioka.[12] In alkaline solutions CV reacts with OH^-; according to Goldacre and Phillips[13] an equilibrium, characterized by a pK = 9.36, is reached only slowly. In accordance with these results it has been found in the present investigation that the absorption and fluorescence spectra of CV solutions are independent of pH at 3.5 < pH < 8.0. Measurements on PMA–CV systems have, in general, been confined to this pH range.

At concentrations (C_d) higher than 10^{-5} *M* the CV cation aggregates to form dimers and for $C_d > 10^{-3}$ *M* even larger aggregates, with a change in its absorption spectrum, are formed. The dimerization constant was found[10] to be 6×10^2 M^{-2} in water at 20°. This implies that at $C_d = 10^{-4}$ *M* less than 10% of the dye is aggregated.

Other Materials. NaOH solutions (0.1 *M*) were prepared from Fixanal and Merck ampoules with the usual precautions to avoid contamination by carbonate. Concentration was checked by titration with oxalic acid. NaCl was p.a. quality (British Drug House). For buffers only chemically pure materials were used.

b. Techniques. Absorption spectra were determined with a Zeiss PMQ II spectrophotometer using calibrated glass or quartz cuvets (Dordchem), thermostatted at 20°. Adsorption of the dye, especially to ground surface and luted interfaces, was found to cause important experimental error. Pretreatment of the glassware and rinsing of the cuvets with the solutions to be investigated was not sufficient to completely reduce this induced adsorption error. The nonreproducibility and inaccuracy of the results was therefore found to be slightly larger than to be expected on the basis of the performance of the equipment.

Fluorescence measurements were performed at 20° with the Zeiss PMQ II spectrophotometer with fluorescence attachment ZFM 4 and a Hanau St. 75 mercury lamp. As CV solutions (excited at 18,300 cm^{-1}) exhibit a fluorescence maximum near 13.000 cm^{-1} a Philips 150 CVP photomultiplier tube (with S-1 response) was used; power was collected from a John Fluke 412 B high-voltage power supply (1700 V). This photomultiplier was fixed in a specially constructed cryostat.[14] Cooling by Dry Ice–acetone mixture gave a tenfold improvement of the signal/noise ratio. Background emission, such as Raman scattering or fluorescence from solvent and cuvet, proved to be negligible for all solutions investigated. In order to obtain fluorescence data from the photomultiplier output current a number of corrections must be made.[15-17] Fluctuations in the mercury lamp intensity and in the photomultiplier sensitivity were eliminated by performing measurements relative to a standard supplied by Zeiss. Primary absorption effects were eliminated by measuring fluorescence through the front surface. Corrections for the spectral sensitivity of the instrument were calibrated with standards of known absolute fluorescence spectra.[18-20] From corrected spectra the quantum yield ϕ was obtained by comparison with the spectrum of a 10^{-3} *M* quinine sulfate solution in 0.05 *M* H_2SO_4, assuming for the latter[21,22] ϕ = 0.55.

Sedimentation dialysis experiments were performed in two different ways. Some results were obtained with a Beckman Spinco E analytical ultracentrifuge with photoelectric scanner at 20° and 42,040 rpm. Here the sedimentation process could be closely followed and from the dependence of the absorption on the distance from the rotation center the amount of bound dye could be calculated using the concentration of the dye in the polymer-free phase (neglecting activity coefficient corrections). A dye absorption calibration isotherm was obtained with polymer-free CV solutions under the same experimental conditions and was used for the correction of the sedimentation results for absorption effects. These were relatively important and the accuracy in the determinations at small free dye concentrations was low.

Most experiments were performed using a Beckman L II preparative ultracentrifuge (40-in. rotor) during runs of 45 hr at 20° at 36,000 rpm. Under these conditions all macromolecular components had settled to the bottom of polyallomer centrifuge tubes and the free dye concentration could be measured spectrophotometrically on an aliquot of the supernatant liquid, assumed to be in equilibrium with the polymer phase. Here also a calibration isotherm for the adsorption of dye to the tubes was determined; the adsorption effects were large and moreover poorly reproducible. No systematic difference between the results by both methods were detected.

Equilibrium dialysis experiments were also performed in limited number because CV adsorbed very strongly on the dialysis bags and tubes. The best results were obtained with Sigma 250-11 dialysis sacks prewashed to re-

move inhibitors. After washing in water and removal of the water the sacks were filled with 25 ml of a polyelectrolyte–dye solution and closed by means of a knot. Each bag was placed into a glass tube containing 25 ml of the polyelectrolyte-free dye solution. The tubes were gently shaken in the dark at 20° for 24 hr, a period which was found to be sufficient for the attainment of equilibrium in the most extreme cases. Polymer leakage did not occur. The concentration of the dye outside the sacks was determined spectroscopically. Corrections for the adsorption of the dye were applied as above and the influence of activity coefficients was neglected.

3. Results

a. Absorption Spectroscopy. The spectroscopic results in the visible region where the free dye absorbs ($15{,}000 < \sigma < 22{,}000$ cm^{-1}) ascertain that strong binding between CV and PMA occurs. A characteristic set of absorption spectra for a series of PMA–CV solutions (in the presence of NaCl) at constant degree of neutralization (α') is shown in Figure 1. At constant C_d and salt concentration (C_s) but increasing PMA concentrations (C_p, in moles of monomer per liter) definite changes in the spectrum of the dye are observed. For $\alpha' C_p \leq C_d$ the absorption at the maximum of the free dye (16,900 cm^{-1}) decreases at the expense of a new maximum at larger wave numbers. For $\alpha' C_p > C_d$ a spectral shift to lower wave numbers of this new maximum occurs, the spectra remaining different from the free dye spectrum. This general behavior has been found at all values of α' investigated ($0.1 \leq \alpha' \leq 1$) both in the presence of 2×10^{-3} M NaCl and in the absence of salt. It may be ascribed to binding of CV to PMA, the bound dye absorbing at higher wave numbers than the free dye.

The spectra in each series at constant C_d and α' converge with increasing C_p/C_d ratio to the same limiting curve in the region $15{,}000 < \sigma < 17{,}200$ cm^{-1} around the maximum of the free dye, at least up to $\alpha' C_p/C_d < 3$. This limiting curve is generally reached for values $\alpha' C_p/C_d \sim 1.5$, as seen in Figures 2 and 3. These plots suggest that the binding is complete for $\alpha' C_p/C_d > 1.5$ and that the dye does not return to the unbound state when for $\alpha' C_p/C_d > 1$ the spectral shifts are observed at larger σ. It may rather be assumed that the latter are due to changes in the absorption spectrum of the bound dye. The slight increase in the apparent absorption coefficient $\bar{\epsilon} = E/C_d l$ (where E is the optical density and l the pathlength) in the region $15{,}000 < \sigma < 17{,}200$ cm^{-1} which is observed at certain α' values for $\alpha' C_p/C_d > 3$, is probably also due to this effect rather than to a release of dye, as can be seen from the shape of the spectra.

From the convergence of the spectra in the region $15{,}000 < \sigma < 17{,}200$ cm^{-1} it may be concluded that the limiting curve represents the spectrum of the bound dye with absorption coefficient ϵ_b. For every value of C_p the fraction f of dye bound to PMA can be calculated using the linear relation

$$\bar{\epsilon} = \epsilon_0 + (\epsilon_b - \epsilon_0)f \qquad (1)$$

Here ϵ_0 is the absorption coefficient of free CV obtained from the absorption spectrum of polymer-free dye solutions.[10] A plot of $(\bar{\epsilon} - \epsilon_0)$ against $(\epsilon_b - \epsilon_0)$ yields straight lines indeed (Figure 4), the slope of which represents f. The standard deviation in the slope of these lines is equal to or smaller than 0.02. The absolute error of f may, however, be somewhat larger due to the uncertainty of ϵ_b and the error on ϵ_0 and $\bar{\epsilon}$. Values of f for solutions at different C_p and α' are plotted against $\alpha' C_p/C_d$ in Figure 5. For $C_d \sim 10^{-4}$ M the influence of 2×10^{-3} M NaCl on the values of f is negligible as can be seen in Figure 5. It follows from these f values that binding can become complete ($f = 1$) for all values of α' and that the value of $\alpha' C_p/C_d$ where f reaches unity is lower the smaller α'.

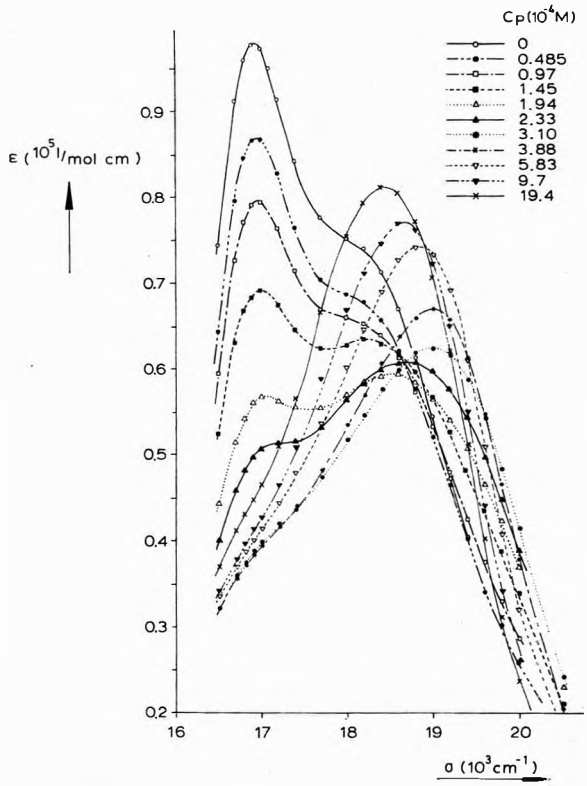

Figure 1. Absorption spectra of CV–PMA solutions: $C_d = 9.7 \times 10^{-5}$ M, $C_{NaCl} = 2 \times 10^{-3}$ M, different concentrations C_p, $\alpha' = 0.40$.

The maximum of the spectrum of the dye in the region $17{,}000 < \sigma < 20{,}000$ cm^{-1} for solutions in which $\alpha' C_p/C_d < 1.5$ (where $f = 1$) shifts to higher wave numbers and lower maximum ϵ with increasing α' (Figure 6). An analogous effect is observed for PMA–CV solutions of constant C_p and C_d but increasing α' (Figure 7). These effects show that the state of the bound dye, as revealed by its absorption spectrum, depends on C_p/C_d and the number of dissociated groups along the chain and will be discussed in more details in part II.

A systematic investigation has been carried out to establish whether the absorption of the PMA–CV systems show any time dependence, particularly in view of some results of poly(acrylic acid)–CV solutions reported by Soda and Yoshioka,[23] and some of the effects found in the potentiometric titration of PMA–CV solutions in the present work (see part II[8]). Within experimental error *no significant time effects* were observed.

b. Dialysis Experiments. The binding of CV to PMA was also investigated by sedimentation dialysis. Here it was assumed that the concentration of free dye in the solution above the macromolecular boundary (analytical centrifuge) or in the supernatant liquid (preparative ultracentrifuge) as determined spectrocopically at $\sigma = 16{,}900$ cm^{-1} corresponds to the concentration of the free dye in equilibrium with the dye bound to the polyelectro-

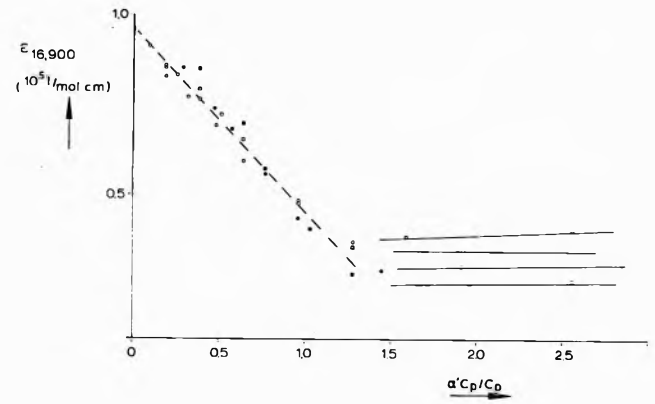

Figure 2. Apparent absorption coefficient $\bar{\epsilon}$ of CV at 16,900 cm^{-1} *vs.* $\alpha' C_p/C_d$ for various values of α' (O, 0.25; □, 0.50; ●, 0.75; ■, 1.00): $C_d = 1.15 \times 10^{-4}$ *M*.

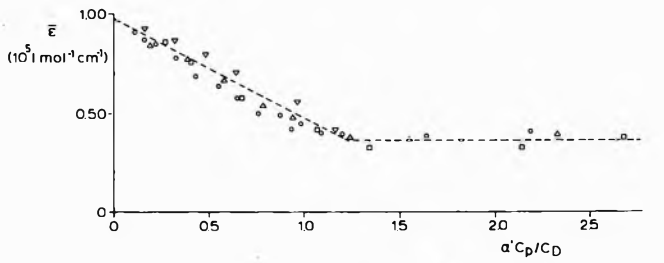

Figure 3. Apparent absorption coefficient $\bar{\epsilon}$ of CV at 16,900 cm^{-1} *vs.* $\alpha' C_p/C_d$ in the presence of NaCl, $C_s = 2 \times 10^{-3}$ *M*, for different values of α' (O, 0.25; △, 0.40; □, 0.65; ▽, 0.74); $C_d = 10^{-4}$ *M*.

lyte. The concentration of bound dye fC_d could thus be calculated from the original total dye concentration, correction for the adsorption to the ultracentrifuge cell being taken into account using the adsorption calibration isotherm. Experiments were carried out at different values of α' and constant NaCl concentration ($C_s = 2 \times 10^{-3}$ *M*) to reduce Donnan effects. In Figure 8 some values of f are shown obtained for PMA–CV systems of constant C_d and variable C_p at two different α' values. For sake of comparison f values from absorption spectroscopy are also represented in the same figure together with the results from equilibrium dialysis. The latter were obtained with buffered solutions of ionic strength 2×10^{-3} *M* at pH 6.8, corresponding to $\alpha' = 0.4$ (phosphate buffer: 0.71×10^{-3} *M* KH_2PO_4 + 0.54×10^{-3} *M* Na_2HPO_4). Here also corrections for adsorption effects were applied. Although there is considerable scattering of the experimental points in Figure 8, presumably due to errors induced by the strong adsorption of CV, the agreement between the results obtained by the three methods is satisfactory.

Experiments with solutions of $C_p = 1.94 \times 10^{-4}$ equiv $l.^{-1}$ and $C_d = 0.97 \times 10^{-4}$ *M* at $\alpha' = 0.65$ but three different concentrations of NaCl yielded $f = 0.87$ ($C_s = 2 \times 10^{-3}$ *M*), 0.82 ($C_s = 5 \times 10^{-3}$ *M*), and 0.78 ($C_s = 2 \times 10^{-2}$ *M*), demonstrating that the sodium ion or the ionic strength has only a slight effect on the binding of CV to PMA (particularly in view of the large uncertainty of the f values obtained with this method). This is in accordance with the spectroscopic results.

For $\alpha' = 0.10$ all solutions investigated ($C_d = 10^{-4}$ *M*, $C_s = 2 \times 10^{-3}$ *M*, $C_p < 6 \times 10^{-4}$ equiv $l.^{-1}$, sedimentation experiments) yielded $f = 1$, *i.e.*, complete binding of the dye. This could indicate binding of CV in slight excess to the negative charge of the polyelectrolyte. Therefore

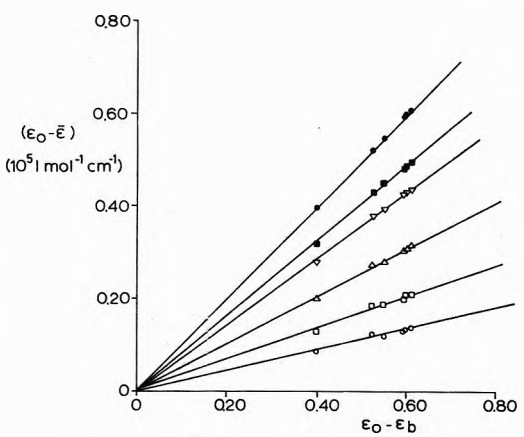

Figure 4. Plots of $(\epsilon_3 - \bar{\epsilon})$ *vs.* $(\epsilon_0 - \epsilon_b)$ of CV–PMA solutions: $C_d = 10^{-4}$ *M*, $C_{NaCl} = 2 \times 10^{-3}$ *M*; different concentrations of C_p ($C_p \times 10^{-4}$: ●, 3.10 *M*; ■, 2.33; ▽, 1.94; △, 1.45; □, 0.97; O, 0.49); $\alpha' = 0.40$.

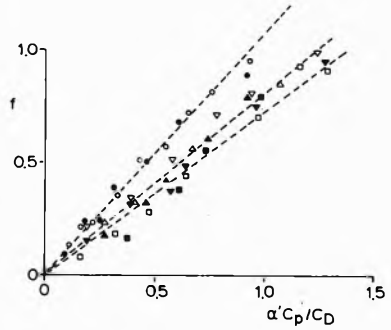

Figure 5. Fraction f of bound dye *vs.* $\alpha' C_p/C_d$ from spectroscopic results for different values of α' in the absence of additional salt (●, 0.25; ▼, 0.50; ▲, 0.75; ■, 1.00) or in the presence of NaCl, $C_s = 2 \times 10^{-3}$ *M* (O, 0.25; ▽, 0.40; △, 0.65; □, 0.75).

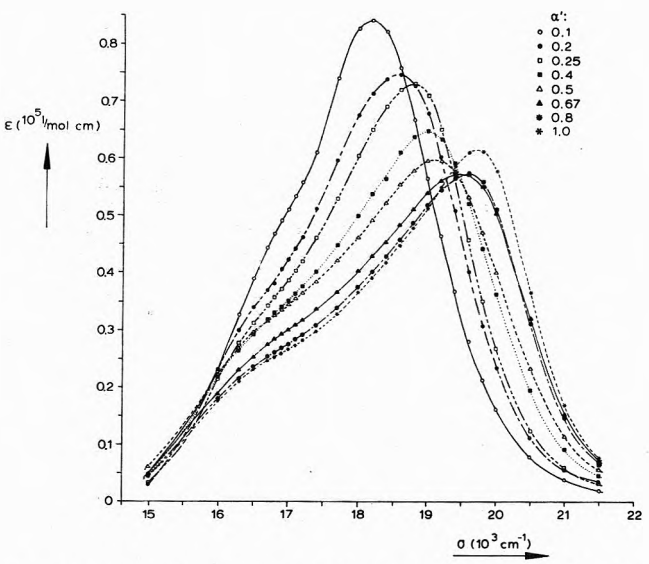

Figure 6. Absorption spectra of CV–PMA solutions of $\alpha' C_p/C_d = 1.5$ for different values of α'; $C_d = 10^{-4}$ *M*.

some sedimentation experiments were performed in PMA solutions acidified with HCl to ensure absence of dissociation for the carboxylic groups. The results, shown in Figure 9, clearly demonstrate that binding of CV occurs to *nondissociated* PMA.

c. Fluorescence Spectroscopy. In aqueous solution Crystal Violet is almost nonfluorescent. The fluorescence of a

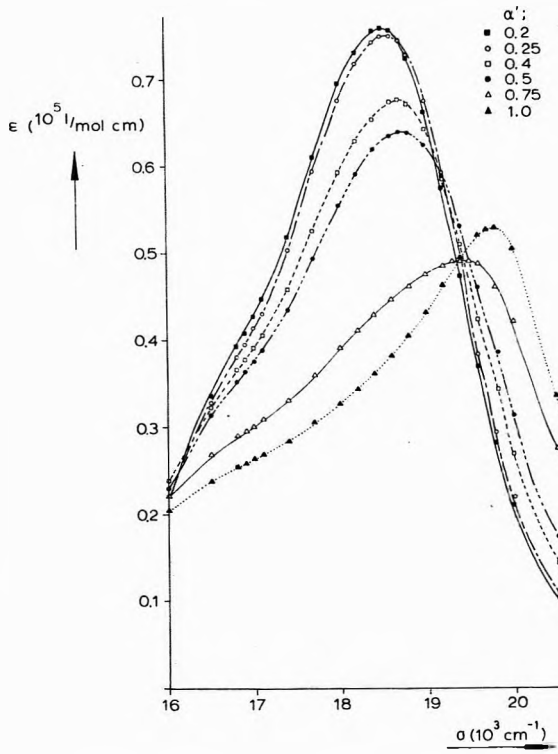

Figure 7. Absorption spectra of CV–PMA solutions of constant C_d/C_d for different values of α'; $C_p = 1.18 \times 10^{-3}$ M, $C_d = 1.15 \times 10^{-4}$ M.

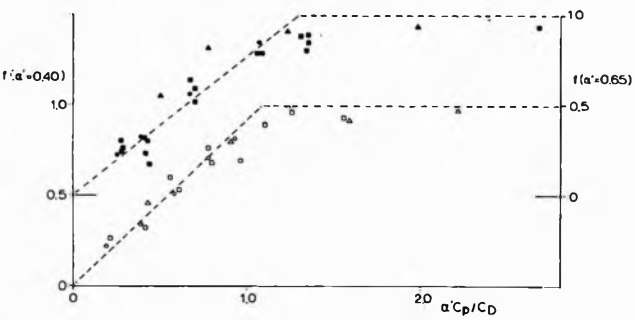

Figure 8. Fraction f of bound dye *vs.* $\alpha' C_p/C_d$ obtained from different measurements at $\alpha' = 0.40$ (O, spectroscopy; □, sedimentation; △, equilibrium dialysis) and $\alpha' = 0.65$ (●, spectroscopy; ■, sedimentation; ▲, equilibrium dialysis).

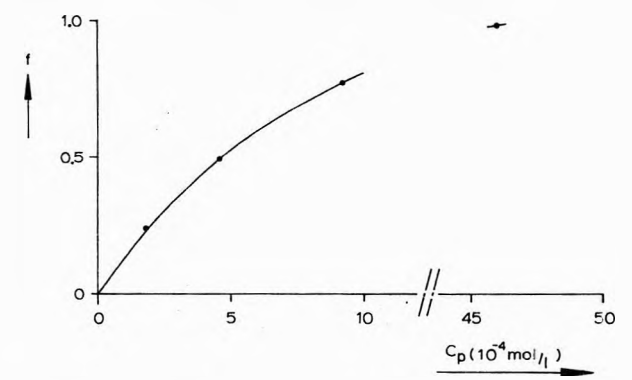

Figure 9. Fraction f of bound dye *vs.* C_p for acidified solutions ($C_{HCl}/C_p = 2.2$) by sedimentation experiments; $C_d = 9 \times 10^{-5}$ M, $C_{NaCl} = 2 \times 10^{-3}$ M.

solution 1.20×10^{-4} M is barely measurable with the equipment used in this investigation; the quantum yield was estimated to be $\phi = 8 \times 10^{-5}$ by the method described in section 2b. The addition of PMA to a CV solution may result in a large increase in the quantum yield. The fluorescence spectra of solutions $C_d = 1.2 \times 10^{-4}$ M and variable C_p, measured at different α' values or in the presence of an excess HCl, were measured. The spectra exhibit a maximum at 13,000 cm^{-1}. Variation of α' or C_p generally affects only the magnitude of ϕ but does not alter the shape of the spectrum. Quantum yields calculated from the maximum of the fluorescence spectrum, at constant C_d and C_p, are shown in Figure 10 as function of the amount of NaOH or HCl added. Here again binding of CV to undissociated PMA may be assumed in view of the large values of ϕ observed in the presence of HCl. It was checked rather extensively whether these fluorescence properties exhibit any time dependence. No systematic effects were observed.

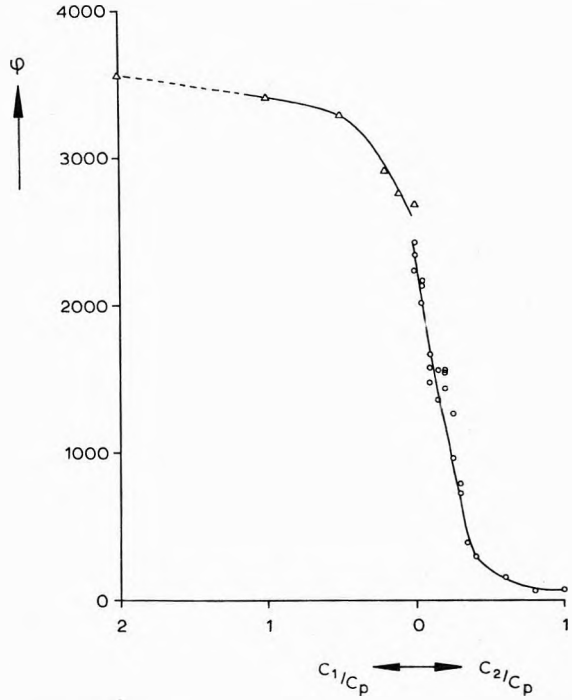

Figure 10. Quantum yield ϕ (arbitrary units) of CV–PMA solutions: $C_d = 1.2 \times 10^{-4}$ M, $C_1 = C_{HCl}$; $C_2/C_p = \alpha'$ (△, $C_p = 4.73 \times 10^{-3}$ M; O, $C_p = 4.65 \times 10^{-3}$ M).

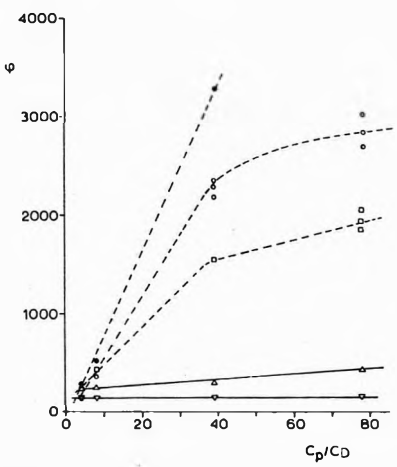

Figure 11. Quantum yield (arbitrary units) of CV–PMA solutions *vs.* C_p/C_d at different charge densities; $C_d = 1.2 \times 10^{-4}$ M (●, C_{HCl}/C_p, 0.5; O, $\alpha' = 0$; □, $\alpha' = 0.2$; △, $\alpha' = 0.4$; ▽, $\alpha' = 0.6$).

The sharp decrease of ϕ with increasing α' to values of the same order of magnitude as for a polymer-free CV solution was also reported by Anufrieva, *et al.*,[5b] for PMA–Auramine-O solutions. As this decrease occurs more or less in the α' range where the conformational transition of PMA in a dye-free solution is observed,[2] these authors concluded that dye is bound only to the compact conformation of PMA (low α') and, when bound, exhibits an enhanced fluorescence intensity because of the high local viscosity in the polymeric region. In view of the results of section 3a and 3b it can be concluded, however, that in the region where ϕ tends to low values most of the dye molecules are still bound to the polyelectrolyte in our experiments as $\alpha' C_p/C_d < 1.5$. Hence the change in fluorescence should be due to other effects. In Figure 11 the change of the quantum yield with increasing C_p/C_d for different states of ionization of the polyelectrolyte has been presented (for some systems with high ϕ the results of repeated experiments have been given to indicate the scattering due to experimental error). At low C_p/C_d, where f is small, all curves converge to the value of ϕ for a PMA-free CV solution. The increase of ϕ with increasing C_p/C_d strongly depends on the degree of neutralization.

4. Conclusions

The results from absorption spectroscopy and dialysis reveal that (a) Crystal Violet can be bound to PMA at all values of α' and even at the completely undissociated macromolecule; (b) the fraction f of dye bound to PMA increases with increasing $\alpha' C_p/C_d$ ratio; (c) the value of $f = 1$ is reached for $1.0 < \alpha' C_p/C_d < 1.5$ and no dye returns to the solution as unbound molecules for larger values of this ratio.

The binding of CV to PMA is accompanied by an important modification in the absorption spectrum, the maximum of the bound dye spectrum being always at a larger wave number than observed with the free dye spectrum. The shape of the spectrum of the bound dye, the position of the maximum, and the value of ϵ at this maximum all depend on C_p/C_d and α'.

The quantum yield of the fluorescence of PMA–CV solutions measured under conditions where $f \sim 1$ may be assumed was very large in the presence of strong acid and decreased with increasing α' reaching for $\alpha' > 0.4$ values of the order of magnitude comparable to the very small quantum yield of polymer-free CV solutions.

A discussion of these results will be presented in part II[6] of this paper.

References and Notes

(1) (a) J. M. Klotz in "The Proteins," H. Neuroth and K. Bailey, Ed., Academic Press, New York, N. Y., 1953, p 727. (b) A. Blake and A. R. Peacocke, *Biopolymers*, **6**, 1225 (1968).
(2) J. C. Leyte and M. Mandel *J. Polym. Sci., Part A-2*, 1879 (1964).
(3) M. Mandel and M. G. Stadhouder, *Makromol. Chem.*, **80**, 141 (1964).
(4) M. Mandel, J. C. Leyte, and M. G. Stadhouder, *J. Phys. Chem.*, **71**, 603 (1963).
(5) (a) T. M. Birshtein, E. V. Anufrieva, T. N. Nekrasova, O. B. Ptitsyn, and T. V. Sheveleva, *Pcl. Sci. USSR*, **7**, 412 (1965); (b) E. V. Anufrieva, T. M. Birshtein, T. N. Nekrasova, O. B. Ptitsyn, and T. V. Sheveleva. *J. Polym. Sci., Part C-16*, 3514 (1968).
(6) W. H. J. Stork, P. L. de Hasseth, G. J. M. Lippits, and M. Mandel, *J. Phys. Chem.*, **77**, 1778 (1973).
(7) V. Crescenzi, F. Quandrifoglio, and V. Vitagliano, *J. Macromol. Sci., Chem.*, **1**, 917 (1967).
(8) N. M. Wiederhorn and A. R. Brown, *J. Polym. Sci.*, **8**, 651 (1952).
(9) D. Braun, M. Herver, U. Johnsen, and W. Kern, *Macromol. Chem.*, **51**, 15 (1961).
(10) W. H. J. Stork, G. J. M. Lippits, and M. Mandel, *J. Phys. Chem.*, **76**, 1772 (1972).
(11) W. Lautsch, W. Broser, W. Biederman, and H. Gnichtel, *J. Polym. Sci.*, 479 (1955).
(12) T. Soda and K. Yoshioka, *J. Chem. Soc. Jap.*, **86**, 1019 (1965).
(13) R. J. Goldacre and J. N. Phillips, *J. Chem. Soc.*, 1724 (1949).
(14) W. H. J. Stork, Thesis, Leiden, 1970.
(15) C. S. Parker and W. T. Rees, *Analyst*, **85**, 587 (1960).
(16) J. H. Chapman, Th. Förster, G. Kortüm, E. Lippert, W. H. Melhuish, G. Nebbia, and C. A. Parker, *Appl. Spectrosc.*, **17**, 171 (1963).
(17) W. E. Ohnesorge, *Anal. Chim. Acta*, **31**, 484 (1964).
(18) E. Lippert, W. Nägele, I. Seibold-Blankenstein, U. Staiger, and W. Voss, *Z. Anal. Chem.*, **170**, 1 (1959).
(19) (a) W. H. Melhuish, *J. Phys. Chem.*, **64**, 762 (1960); (b) *ibid.*, *J. Opt. Soc. Amer.*, **52**, 1256 (1962).
(20) R. J. Argauer and C. E. White, *Anal. Chem.*, **36**, 368 (1964).
(21) (a) W. H. Melhuish, *J. Phys. Chem.*, **65**, 229 (1961); (b) *ibid.*, *J. Opt. Soc. Amer.*, **54**, 183 (1964).
(22) J. W. Eastman, *Photochem. Photobiol.*, **6**, 55 (1967).
(23) T. Soda and K. Yoshioka *J. Chem. Jap.*, **87**, 324 (1966).

Interaction between Crystal Violet and Poly(methacrylic acid) in Aqueous Solutions. II. Potentiometric and Viscosimetric Results. General Discussion

W. H. J. Stork, P. L. de Hasseth, G. J. M. Lippits, and M. Mandel*

Gorlaeus Laboratoria der Rijksuniversiteit, Afdeling Fysische Chemie III, Leiden, The Netherlands *(Received January 29, 1973)*

The binding of Crystal Violet to poly(methacrylic acid) (PMA) strongly affects the macromolecular properties of the polyelectrolyte. The apparent dissociation constant for a given concentration of the polyelectrolyte (C_p) and net degree of charge ($\alpha - r$) decreases with increasing dye concentration for ($\alpha - r$) < 0.5. The region in which the conformation transition of PMA occurs is broadened and is less sharply defined as compared to dye-free solutions. The viscosimetric titration curves of PMA in the presence of Crystal Violet are shifted to higher values of the degree of dissociation α and the limiting specific viscosity at high α is considerably lowered with increasing dye concentration. The discussion of all experimental results on the binding of Crystal Violet to PMA reveals that the binding of the cationic dye probably does not occur at the carboxylate group but is strongly affected by the charge of the polyelectrolyte. This binding is very strong and under most experimental conditions explored the average number r of dye molecule bound per monomeric unit, which is found to be close to α, is maximal. No evidence is found for the formation of localized dimers of bound dye molecules. Although Crystal Violet strongly binds to both conformational states of PMA and modifies their macromolecular characteristics binding to the compact, low α, state seems to be more stable.

1. Introduction

In part I of this paper[1] it has been shown, with the help of spectroscopic and dialysis experiments, that crystal violet (CV) can be bound to poly(methacrylic acid) (PMA) at all different degrees of neutralization α' and also to the completely undissociated polyelectrolyte. The properties investigated were essentially those of the dye molecule. In this part two macromolecular properties of the acid dissociation equilibrium and the viscosity of polyelectrolyte–dye systems will be examined as function of α' and CV concentration (C_d). A general discussion of all experimental results will conclude this paper.

2. Experimental Section

Some potentiometric titrations were performed with a Radiometer automatic titration apparatus (TTT Titrator in conjunction with a SBR 2 Titrigraph and a SBU 1 Syringe buret). Radiometer G 202 C glass electrodes and K 401 calomel electrodes were used. Titrations were performed in a nitrogen atmosphere at 20°. In view of occurring time effects (see below) most titrations were performed by preparation of separate solutions of different degree of neutralization, the pH of which was measured after a fixed equilibration time by the equipment described above.

Viscosimetric measurements were performed automatically with the aid of a Viscosimeter Reader, equipped with a Printing Counter VR-P2 (both manufactured by Rehovot Instruments, Israel). Two Ubbelohde viscosimeters with flow times for water of 49.3 and 94.4 sec at 20.00 ± 0.02° were used. All solutions were prepared separately.

3. Results

a. Potentiometric Titrations. The potentiometric titration of PMA in the presence of dye molecules exhibited several unusual features. First, titrations of PMA–CV solutions with NaOH in the presence of a slight excess of neutral salt (NaCl) were found to have a marked time dependence, contrary to PMA without dye under the same experimental conditions. The pH of PMA–CV solutions neutralized to the required value of α' after mixing dye and polymer (dye-before-neutralization procedure, DbN) decreases for a period of several hours after preparation of the solution (especially near $\alpha' = 0.5$). The pH of solutions prepared by adding CV to previously (partially) neutralized PMA solutions (neutralization-before-dye procedure, NbD) does *not* change with time however. Furthermore the titration curves, obtained with a set of equal solutions but prepared according to both procedures, were different after equilibration for more than 20 hr in the dark. Exhaustive equilibration was performed and found not to alter this conclusion.

At identical α' the solutions prepared according to the DbN procedure always had a *larger* pH, the difference (ΔpH) being dependent on the C_d/C_p ratio (C_p representing the concentration of PMA in equiv per 1 liter), and largest in the α' region where the polyacid in the absence of the dye exhibits a conformational transition.[2] In general $0.1 < \Delta pH < 0.3$. It was found that preparation of the solutions in a third way, completely neutralizing the PMA–CV system with NaOH and subsequently acidifying with HCl to the required α', yield pH values corresponding to those of the NbD procedure.

Some titration curves of PMA at constant C_d obtained by the DbN and the NbD procedure are presented in Figure 1 to show that the qualitative features are the same in both cases (solutions with high C_d/C_p ratio could not always be investigated at low α' due to precipitation phenomena). Both sets of titration curves demonstrate that the presence of the positively charged CV *increases* the pH of partially neutralized PMA solutions with respect to a CV-free PMA solution over a large range of α' values. This is contrary to the effect generally observed with small metallic cations, which also occurs with CV at low α', where according to the results obtained in part I only a fraction of the dye is bound ($f < 1$).

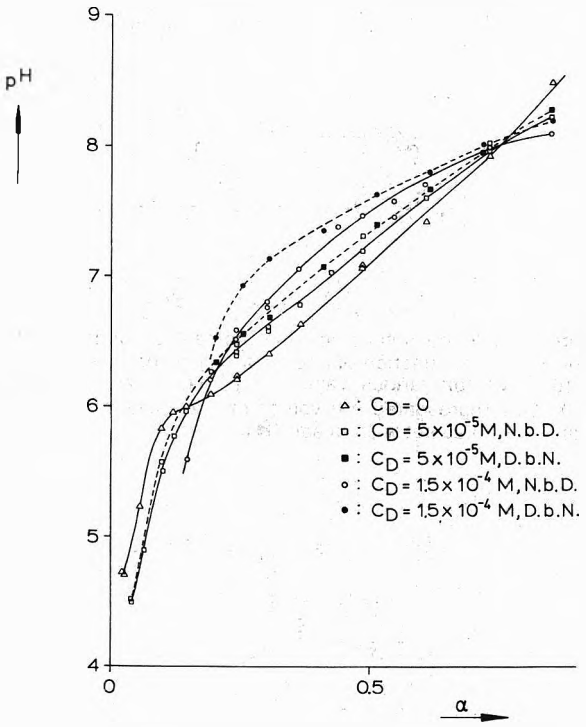

Figure 1. Potentiometric titration curves of PMA–CV solutions: $C_p = 7.84 \times 10^{-4}$ *M*, $C_{NaCl} = 2 \times 10^{-3}$ *M*.

According to the polyelectrolyte theory[3-5] the titration curve of a weak polyacid in a salt solution, where no specific binding interferes with the dissociation of the acidic group and interactions along the chain are negligible, can be represented by the following equation

$$\mathrm{pH} = \mathrm{p}K_0 + \log \frac{\alpha}{1-\alpha} + \frac{0.434}{kT}\left(\frac{\partial F_e}{\partial Z}\right) \qquad (1)$$

Here K_0 is an intrinsic dissociation constant of the acidic group on the macromolecular chain, α is the degree of dissociation of the group proportional to the number (Z) of charged groups on the polyelectrolyte, and F_e represents the electric free energy of the system which can be related to the mean electrostatic potential around a polyion as found by an extended Debye–Hückel treatment for polyelectrolytes.[6] In general the polyelectrolyte correction factor ($\partial F_e/\partial Z$) will depend strongly on the charge of the polyion and the ionic strength (I) of the solution. If the polyelectrolyte undergoes, in the course of the titration, a conformational transition from a characteristic mean conformation to a coil-like state then eq 1 equally applies to each part of the titration curve where the polyacid is completely in either of both states, each characterized however by different value of K_0 and a different expression for F_e. Expression 1 must be modified if specific binding of cation occurs to the negatively charged carboxylate groups as was discussed extensively by Harris and Rice.[7] If binding affects a conformational transition in the course of the titration the theoretical treatment of such cases becomes much more complicated.

For the titration of PMA in the presence of CV it may be assumed that the binding of the dye to the macromolecule does not occur at the carboxylate groups as it has been shown that this binding is also possible to completely undissociated PMA (see part I). This is confirmed by the finding that the pH increases upon binding. Therefore the dissociation of the carboxylic groups on the polyelectrolyte should, in a first approximation, be influenced by dye binding only through the change of the net charge density of the polyion and its influence on ($\partial F_e/\partial Z$). Thus eq 1 may still be used as far as interactions between dye molecules and dye molecules carboxylate groups along the chain may be assumed negligible. In each point of the titration, curve $\mathrm{p}K \equiv \mathrm{pH} + \log(1-\alpha)/\alpha$ (where K is the *apparent dissociation constant*) can be calculated with the help of the degree of dissociation α (obtained from α' with a correction for the autodissociation of the polyacid). Also the net degree of charge ($\alpha - r$) may be known if the average number of dye molecules bound per monomeric unit, $r = fC_d/C_p$, is estimated from the spectroscopic results of part I. In Figure 2 values of pK for three different PMA–CV systems (prepared according to the NbD procedure) are compared to the pK of PMA without dye at equal net degree of charge. Only values corresponding to $(\alpha - r) > 0$ have been used and points for PMA–CV solutions with pH >8 have been omitted in view of the possibility for dye hydrolysis. Note that in practically all systems $\alpha' C_p/C_d > 1.5$ so that $f = 1$.

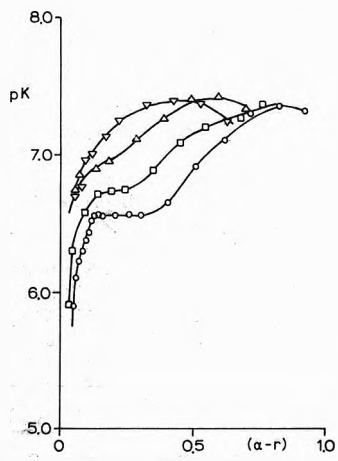

Figure 2. Change of the apparent dissociation constant K with the net degree of charge ($\alpha - r$), $C_p = 7.84 \times 10^{-4}$ *M*, $C_{NaCl} = 2 \times 10^{-3}$ *M*, NbD procedure: C_d = O, 0; □, 5×10^{-5} *M*; △, 10^{-4} *M*; ▽, 1.5×10^{-4} *M*.

Inspection of Figure 2 reveals that for $(\alpha - r) < 0.5$ the pK at a given net degree of charge increases with C_d/C_p and that the region of conformational transition, in the dye-free PMA system characterized by a plateau in the pK values, is smeared out over a much larger region of degree of charge and less sharply defined. It must, therefore, be assumed that the mean conformation of both states of PMA and the transition are strongly affected by binding of CV, a result that is confirmed by the viscosimetric measurements presented below.

b. Viscosimetric Titrations. These are represented in Figure 3 for solutions of the same composition as used in the potentiometric experiments. It was established that the way in which the solutions were prepared *did not* affect the results. The existence of time dependence was checked and found to be small except in cases where degradation of the dye occurs, at high pH.

The curves of Figure 3 demonstrate that the overall shape of η_{sp} *vs.* α', characteristic for the PMA system exhibiting a conformational transition, is conserved but that the influence of CV on the change of the specific viscosity with α' differs greatly from the effect of NaCl of equal ionic strength, thus indicating a strong interaction. Furthermore with increasing C_d not only the viscosimetric ti-

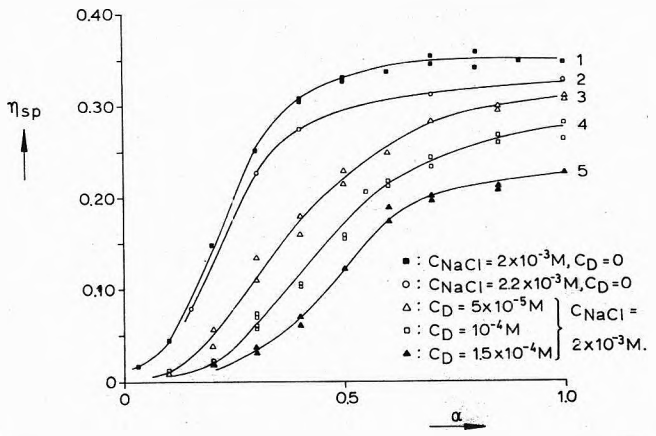

Figure 3. η_{sp} *vs.* α' for PMA–CV solutions, $C_p = 7.84 \times 10^{-4}$ *M*.

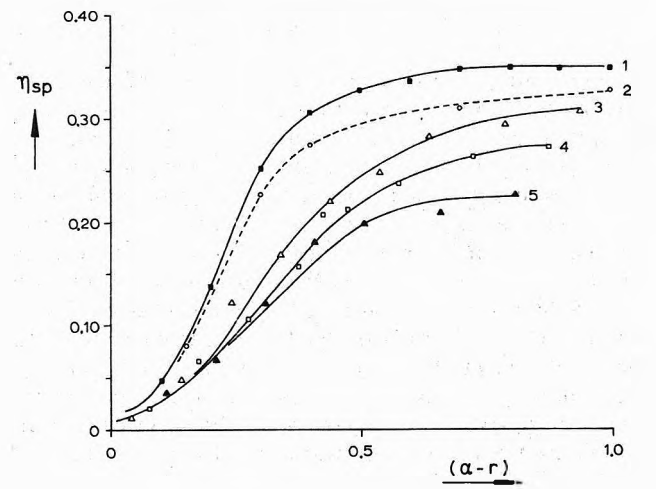

Figure 4. η_{sp} *vs.* $(\alpha - r)$ for PMA–CV solutions (same composition as in Figure 3).

trations curves seem to be shifted to higher α' values but the limiting η_{sp} at high α' is considerably lowered. This last effect is not observed when strong interaction of a cation with PMA is known to take place at the negatively charged carboxylate group, as is, *e.g.*, the case for Cu^{2+} ions.[8] These results thus support the assumption that CV is not directly bound to the carboxylate groups and furthermore prove that no unbinding of the dye occurs at high α', as already found from the experiments in part I. If η_{sp} is plotted against $(\alpha - r)$ analogously to the treatment of the potentiometric results, the curves shown in Figure 4 again demonstrate that electrostatic effects only cannot be responsible for the change in viscosity with increasing C_d. Also, as for the potentiometric results, the influence of bound dye on the mean conformation of both states and the conformational transition is clearly visible through the lowering of η_{sp} and the change in the shape of the curves with increasing C_d/C_p.

4. Discussion

We shall present here a general discussion of all the experimental facts both from this paper and from part I. In the latter it was concluded that strong binding occurs between CV and PMA at all degrees of neutralization (and even for the completely uncharged polyelectrolyte). The potentiometric and viscosimetric results support this conclusion and indicate an influence of the dye binding on

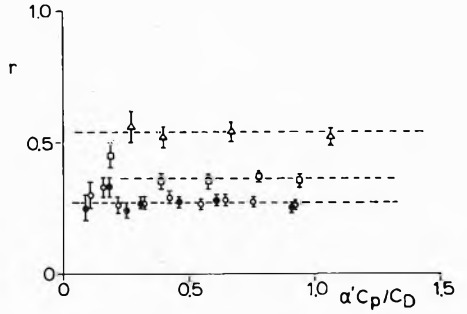

Figure 5. Average number of dye molecules bound per monomeric unit, *r*, as function of $\alpha' C_p/C_d$ ($C_d = 10^{-4}$ *M*; $C_{NaCl} = 2 \times 10^{-3}$ *M*) for various values of α' (○, 0.25; □, 0.40; △, 0.65). Also represented are values of *r* for solutions with same C_d and $\alpha' = 0.25$ but without salt (●).

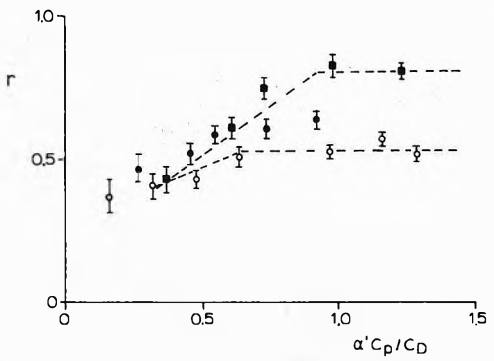

Figure 6. Average number of dye molecules bound per monomeric unit, *r*, as function of $\alpha' C_p/C_d$ ($C_d = 10^{-4}$ *M*) for various values of α' (●, 0.75; ■, 1.00; ○, 0.74 in the presence of NaCl, $C_{NaCl} = 2 \times 10^{-3}$ *M*).

the conformations of the polyion. All experimental evidence points to the fact that domain binding, which can occur with small monovalent cations, cannot be responsible for the effects observed. Neither is specific binding of the dye to the carboxylate groups to be expected. Under these conditions representation of the binding data with the help of binding isotherms would be advisable. From our experimental results no such curves can be derived however. If the number of dye molecules (*r*) bound on the average per monomeric unit, which may be evaluated with the help of the fraction *f* of bound dye obtained from the analysis of the spectroscopic data, is plotted against $\alpha' C_p/C_d$ for solutions of constant C_d and α' for which $f < 1$ (Figures 5 and 6) the curves show that for all solution where $\alpha' < 0.65$, *r* remains practically constant with increasing C_p. This would indicate that for these experimental conditions binding is so strong that *r* is probably equal to its maximum value r_{max}, which is of the same order of magnitude as α'. For higher degrees of neutralization *r* increases with increasing C_p and a limiting value seems to be reached for $\alpha' C_p/C_d > 1.0$ only. However, in view of the fact that for high α' the pH may become larger than the lower limit above which hydrolysis of the dye may occur (pH 8), the latter results should be considered with proper precaution. More experiments, to be performed under much more difficult conditions, are needed to gain information about the shape of the binding curves which may be assumed to deviate considerably from a simple Langmuir isotherm. Such an isotherm applies only to the case of localized binding of independent particles. Deviations will therefore occur if (a) the binding constant changes with the charge of the polyion; (b) interactions

between bound dye molecules are not negligible; (c) binding of the dye influences the conformational statistics of the macromolecule; (d) multilayer adsorption is not to be excluded; and (e) different kinds of binding mechanisms are possible. For the PMA–CV system at least the first three of these effects cannot be excluded, as will be shown below, and no prediction can be made about the shape of the binding isotherm.

The influence of the charge of the polyion on the binding curve may be ascertained from the fact that the fraction of bound dye at constant C_p/C_d strongly depends on α' (see Figure 5 of part I) and from the dependence of r_{max} on α' at constant C_d. This is not in contradiction with the conclusion reached previously that CV does not bind to the charged carboxylate groups and that probably nonelectrostatic interaction forces between PMA and CV should principally be responsible for the dye binding. The interaction between the dye particles and PMA could be split into two parts; on one hand, the dye cations are attracted electrostatically to the negatively charged polyion, increasingly with increasing α'; on the other hand, nonelectrostatic interactions stabilize the binding. It is not to be excluded that a marked difference in the strength of the latter exists between the two PMA conformational states. In case the dye ions would be bound in excess to the electric charge of the polyion the electrostatic attraction between polymer and dye changes into a repulsion. Depending on the strength of the nonelectrostatic attraction and its range compared to the electrostatic repulsion this will result eventually in a situation where further binding of dye molecules is not favored, thus yielding $r_{max} \sim \alpha'$. Electric repulsion probably also limits the amount of dye that can be bound to the completely uncharged PMA. The existence of strong nonelectrostatic interactions is supported by results of Barone, *et al.*,[9] who found from solubility measurements that alkanes and polycyclic aromatic hydrocarbons bind to PMA but only at low α'. This binding was found to be stronger for aromatic hydrocarbons than for alkanes and to increase with increasing molecular weight. However, no binding of these compounds was found in the case of poly(acrylic acid) (PAA) in contrast to what is observed with CV.[10]

As it is known that CV associates in aqueous solutions[10] at concentrations as low as 10^{-4} *M*, it may be assumed that strong interactions along the chain between the bound dye can occur. This is confirmed by the spectroscopic results of part I which show that the spectrum of the completely bound dye may change with increasing $\alpha'C_p/C_d$ or, at constant $\alpha'C_p/C_d$, with α'. From the fact that $1 > r_{max} \sim \alpha'$ it follows that, at equilibrium, the bound dye molecules will probably be distributed over all the monomeric units and that it is likely that binding to monomeric units bearing a charged carboxylate group will be favored due to the lowering of the electrostatic potential energy which results from the localization of the cationic dye in the neighborhood of the anionic charge. The mean distance between two neighboring bound dye molecules along the chain is thus expected to be proportional to $1/r\alpha'$. Inspection of the spectroscopic results for systems where $f = 1$ shows that, at constant C_d and α', the maximum of the spectrum of the bound dye is shifted to lower wave numbers with increasing C_p in accordance with the fact that the free monomeric dye in aqueous solutions has its absorption maximum at a lower wave number than the dimer.[10] Analogously it is found that, at constant C_p and C_d, the maximum shifts to higher wave numbers with increasing α' as is also the case if $\alpha'C_p/C_d$ is kept constant at a value $f \geq 1.5$ (and the mean distance between bound dye molecules will be proportional to $1/\alpha'^2$). If, as is done in Figure 7, the wave number of the absorption maximum σ_{max} is plotted against $1/r\alpha' = C_p/\alpha'C_d$ for a large number of different systems satisfying the condition $f = 1$, a single curve is obtained which extrapolates to $\sigma = 20{,}000$ cm^{-1} for $C_p/\alpha'C_d \rightarrow 0$, a value which is larger than the absorption maximum of the free dimer of CV in aqueous solution.[10] The existence of such a simple curve without discontinuities favors the assumption of interaction between bound dye molecules along the chain with respect to the hypothesis of the formation of localized dimers of adsorbed dye molecules as proposed by Bradley and Wolf[11] or of the multilayer absorption. The former is also evident from the absence of a single isosbestic point in the spectra of bound dye (Figures 1, 6, and 7, part I).

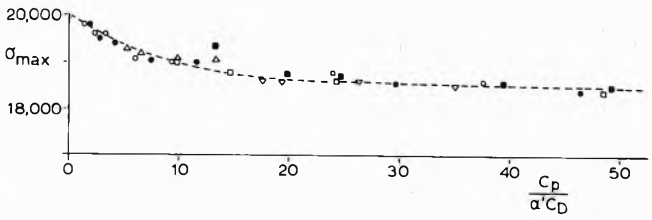

Figure 7. Wave number of the absorption maximum (σ_{max}) of bound dye *vs.* the mean distance between two neighboring bound dyes, proportional to $C_p/\alpha'C_d$, for PMA–CV solutions of various compositions (○, $\alpha'C_p/C_d = 1.5$, different values of α'; ●, $\alpha'C_p/C_d = 1.85$, different values of α'; △, $C_d = 10^{-4}$ *M*, different C_p, $\alpha' = 0.74$; □, $C_d = 10^{-4}$ *M*, different C_p, $\alpha' = 0.40$; ▽, $C_d = 10^{-4}$ *M*, different C_p, $\alpha' = 0.25$; ■, $C_d = 1.1 \times 10^{-4}$ *M*, $C_p = 1.2 \times 10^{-3}$ *M*, different values of α').

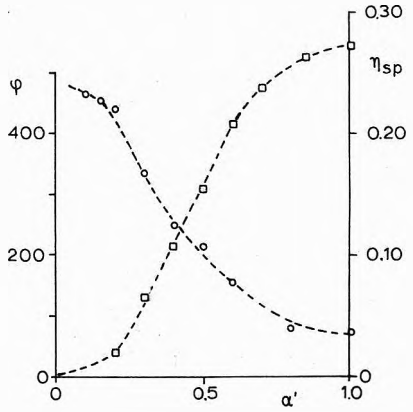

Figure 8. Change of fluorescence quantum yield ϕ and η_{sp} with α' for PMA–CV solutions (○, ϕ for $C_p = 9.3 \times 10^{-4}$ *M*, $C_d = 1.2 \times 10^{-4}$ *M*; □, η_{sp} for $C_p = 7.8 \times 10^{-4}$ *M*, $C_d = 10^{-4}$ *M*).

As discussed already above, the viscosimetric results reveal that the presence of bound dye on the PMA chain results in the following effects (besides reducing the net electric charge): (a) the conformational transition occurs over a greater range of $(\alpha - r)$ and, on the average, at higher values of this parameter, relative to the polyelectrolyte without bound dye; (b) the conformations at high values of $(\alpha - r)$ is characterized by a lower value of η_{sp} than corresponds to the polymer without dye. These results indicate that the binding of CV leads to a stabilization of the compact conformational state of PMA and that the conformational state of PMA at high $(\alpha - r)$ values is also considerably changed by dye binding. Although these conclusions are qualitatively confirmed by the potentio-

metric results the latter do not lend themselves to a quantitative analysis of the influence of the binding of CV on the difference in free energy of both conformational states of PMA in view of the disappearance of a clearly defined region of conformational transition in the pK *vs.* $(\alpha - r)$ curves and the difficulty to take into account dye binding in the theoretical expression for the titration curve. Thus, as is the case in the binding curves, no thermodynamic quantities can be derived from our results.

The experimental data on the fluorescence of the PMA–CV systems show an important decrease in the quantum yield ϕ with increasing α'. As has already been pointed out in part I this decrease cannot be due to unbinding of the dye as was proposed by some authors. It should rather be ascribed to a change in the behavior of the bound dye. Obviously a CV molecule bound to the uncharged polyelectrolyte or to the polyion at low α', when optically excited, is in a less favorable condition to lose its excess energy through a radiationless mechanism (quenching) than when bound to the polyion at high α'. The two most probable effects underlying this interesting phenomenon could be (a) either a change in the conformation of the CV molecule itself with increasing α' (*e.g.*, from a coplanar conformation to a less rigid one) due to direct dye–dye interaction along the chain or (b) the change of the mean conformation of the polyion with increasing α' enhancing the possibility of different quenching mechanisms to become effective. We feel that the latter explanation is the more probable as it is found (Figure 8) that the decrease in ϕ progresses parallelly to the conformational transition accompanied by an increase in η_{sp}. The unfolding of the PMA molecule with increasing α' makes new degrees of freedom available to the bound CV molecule and increases the possibility of quenching the excited dye through interactions with the solvent.

So far we have not discussed the experimental finding that the pH of a PMA–CV solution depends on the way it has been prepared. Most probably this effect is connected with the conformational transition of PMA and the influence of the dye binding on this equilibrium. This is supported by results showing that no such effect is found for PAA–CV solutions and that in the presence of ordinary ions no apparent irreversible behavior is observed for atactic PMA. On the other hand, only hydrogenion activity seems to be affected as the properties of the polyelectrolyte (viscosity) and of the dye (spectra) do not exhibit any marked time effect or dependence on the preparation procedure. The observation that time effects are apparent only for the case in which neutralization follows the addition of dye and that the pH in that case always converge toward the values obtained by the two other procedures, without reaching them completely, however, at the lower range of α' values, favors the interpretation that in the latter the true equilibrium situation is obtained. Apparently in the former case domain binding of the H^+ is enhanced with respect to the real equilibrium conditions but in this stage of the experimental investigation no explanation can be advanced. Further experiments, including the influence of temperature, are necessary in that respect.

Summarizing we may conclude that CV strongly binds to both conformational states of PMA but, apparently, binding to the compact (low α) state is more stable. This binding not only influences the properties of the dye molecules but affects concomitantly the macromolecular characteristics of the PMA. A detailed picture of the binding is still lacking as no statements can be made on the exact sites to which the dyes bind or of the nonelectrostatic interactions stabilizing the binding; both van der Waals forces and hydrophobic bonding may contribute. The attainment of a more detailed description is also severely hampered by our ignorance on the structure and stabilization of the PMA conformations itself.

In a subsequent paper the interaction between Auromine-O and PMA will be discussed.

References and Notes

(1) W. H. J. Stork, P. L. de Hasseth, C. M. Körmeling, W. B. Schippers, and M. Mandel, *J. Phys. Chem.*, **77**, 1772 (1973).
(2) J. C. Leyte and M. Mandel, *J. Polym. Sci., Part A-2*, 1879 (1964).
(3) (a) J. Th. G. Overbeek, *Bull. Soc. Chim. Belg.*, **57**, 252 (1948); (b) A. Arnold and J. Th. G. Overbeek, *Recl. Trav. Chim. Pays-Bas*, **69**, 192 (1950).
(4) A. Katchalsky, *Recl. Trav. Chim. Pays-Bas*, **68**, 879 (1949).
(5) M. Mandel and J. C. Leyte, *J. Electroanal. Chem.*, **37**, 297 (1972).
(6) A. Katchalsky, N. Shavit, and H. Eisenberg, *J. Polym. Sci.*, **13**, 69 (1954).
(7) F. E. Harris and S. A. Rice, *J. Phys. Chem.*, **58**, 725 (1954).
(8) M. Mandel and J. C. Leyte, *J. Polym. Sci., Part A-2*, 2883, 3771 (1964).
(9) (a) G. Barone, V. Crescenzi, B. Pispisa, and F. Quadrifoglio, *J. Macromol. Chem.*, **1**, 761 (1969); (b) G. Barone, V. Crescenzi, A. M. Liquori, and F. Quadrifoglio, *J. Phys. Chem.*, **71**, 2341 (1967).
(10) Manuscript in preparation.
(11) W. H. J. Stork, G. M. Lippits, and M. Mandel, *J. Phys. Chem.*, **76**, 1772 (1972).

Alcohol Association Studies. II. Vapor Pressure, 220-MHz Proton Magnetic Resonance, and Infrared Investigations of *tert*-Butyl Alcohol Association in Hexadecane[1]

Edwin E. Tucker* and Edwin D. Becker

National Institutes of Health, Bethesda, Maryland 20014 *(Received February 2, 1973)*

Publication costs assisted by the National Institutes of Health

The association of *tert*-butyl alcohol in n-$C_{16}H_{34}$ (or in n-$C_{16}D_{34}$) has been studied in the temperature range 20–50° by vapor pressure, 220-MHz proton nmr, and infrared techniques. The data definitely indicate the presence of at least two associated species in the concentration range <0.2 *M*. The commonly assumed predominance of a dimeric alcohol species at low concentrations is not supported by these data. The first important associated species appears to be a chain trimer of exceptional stability. This result is ascribed to the cooperative effect in hydrogen bonding. The least complex association model which best quantitatively and qualitatively explains the three types of data in this study is a two-constant infinite series model with an equilibrium constant for chain trimer formation and a constant for formation of cyclic higher polymers. Polymer end group absorption at the monomer infrared band is shown to occur. Analysis of this effect results in a suggested rationalization of some previous anomalous aspects of infrared data for alcohol solutions.

Introduction

Much of the literature on hydrogen bonding is concerned with the self-association of alcohols. Studies have been carried out with classical physicochemical methods, such as vapor pressure,[2a] *PVT*,[2b] and calorimetric measurements,[3] and with spectroscopic techniques, principally infrared (ir) and proton magnetic resonance (pmr).[4] Data have been interpreted with a variety of models including some postulating only one associated species [*e.g.*, monomer–trimer (1–3),[5] monomer–tetramer (1–4)[6]], some proposing several specific species [*e.g.*, 1–3–8,[7] monomer–dimer–"polymer"[8]], and some based on a large number of species related by regularly varying equilibrium constants (*e.g.*, 1–2–3–4–. . . , or "1–2–∞ model").[9]

Virtually all studies of alcohol hydrogen bonding have used only a single technique, and the failure of these studies to arrive at a consistent model can be ascribed largely to the lack of attempts to correlate more than one type of data for the same alcohol–solvent system over a common range of concentration and temperature. For example, pmr data for methanol and *tert*-butyl alcohol in CCl_4 can be fit reasonably well by simple 1–4 and 1–3 models, respectively,[10] but ir data for alcohol solutions in CCl_4 in the 3700–3300-cm^{-1} region show conclusively that at least two associated species of different order are present.[11]

The present investigation of the association of *tert*-butyl alcohol in *n*-hexadecane was undertaken in order to determine whether an association model can be predicated to correlate the results of three types of measurements: vapor pressure, proton magnetic resonance, and infrared spectral data. Of particular interest also was an answer to whether the previously proposed 1–3–8 model for alcohol solutions[7] would fit the data for *tert*-butyl alcohol solutions or whether a more generalized model must be used to encompass both methanol and *tert*-butyl alcohol association in *n*-hexadecane.

Experimental Section

The *tert*-butyl alcohol used was reagent grade purchased from J. T. Baker Chemical Co., mp 25.5° and bp 82.4°. The alcohol was twice fractionally distilled from CaH_2 to remove traces of water. *n*-Hexadecane (Hx) was purchased from J. T. Baker Co. and purified as previously reported.[7] *n*-Hexadecane-D_{34} (Hx-*d*) was purchased from Merck and Co., Lot No. C-169, isotopic purity >99%. All concentrations were expressed in molar units. Densities for Hx and Hx-*d* were determined in this laboratory at 25, 35, and 45°. For Hx these were 0.7700, 0.7628, and 0.7549 g/cm^3 and for Hx-*d* 0.8870, 0.8789, and 0.8701 g/cm^3. Alcohol densities were taken from literature values.[12]

Vapor pressure measurements for solutions of *t*-BuOH in Hx were made as previously described[7] with the exception of the thermostated pipet being at 30.0° and the use of a Mensor Co. Quartz Manometer to measure pressure (minimum resolution of ±0.003 Torr absolute). These measurements give the pressure of *t*-BuOH above an Hx solution with total apparatus volume and moles of alcohol and solvent accurately determined. Corrections for dissolved air in the added *t*-BuOH were made using a measured air solubility of 5.96×10^{-6} mol of air/g of *t*-BuOH at 30.0°. Temperatures in the range 30–50° were maintained to ±0.005°.

The method of sample preparation for both proton magnetic resonance (pmr) and infrared (ir) studies was very similar. A grease-free vacuum line of accurately determined volume was fitted with ampoules of dry *t*-BuOH and tetramethylsilane (pmr reference) connected by Teflon and stainless steel vacuum fittings. These liquids were degassed by pumping off *ca.* 20% of the initial volumes. Tetramethylsilane was dried by twice distilling under vacuum from Dry Ice–acetone temperature to liquid nitrogen temperature. Infrared and pmr samples were prepared by condensing a measured amount of *tert*-butyl alcohol at

low pressure into either ampoules fitted with grease-free vacuum stopcocks or 5-mm pmr sample tubes containing a degassed, weighed quantity of Hx or Hx-*d*. Pressures condensed were typically of the order of a few Torr and were measured to ±0.003 Torr. Small amounts of TMS at low pressures were also condensed into the pmr tubes from the reservoir at *ca.* −80° and the tubes were then sealed under vacuum with the contents at liquid nitrogen temperature. Sufficient precautions were taken with all sample manipulations so that the water content should have been exceedingly small.

Chemical shift measurements of the *tert*-butyl alcohol OH proton as a function of concentration and temperature in Hx or Hx-*d* solutions were made using a Varian HR-220 spectrometer. The shifts were measured relative to internal TMS by interpolating between two audio side bands. The precision of shift measurement was approximately ±0.002 ppm. A striking point here is that the absolute accuracy of the shift measurement is strictly controlled by errors in sample temperature. Solutions in the concentration range 0.1 to 1.0 *M* show a temperature effect on the OH chemical shift of *ca.* 0.06 ppm/deg toward higher field with increasing temperature. This coefficient is larger by a factor of 6 than the temperature coefficient of the standard reference sample of ethylene glycol. Considering the imprecision with which the sample temperatures can be determined from the standard ethylene glycol shift curve and a probable long term temperature stability of the probe of no better than a few tenths of a degree, we estimate that the possible error in the measured chemical shifts due to temperature effects can be as large as ±0.03 ppm in the medium concentration range. Measurements were made on *t*-BuOH–Hx-*d* solutions in the concentration range 0.003–0.25 *M* and on *t*-BuOH–Hx solutions from 0.1 to 5.0 *M* as well as pure alcohol.

Infrared measurements on solutions of *t*-BuOH in Hx-*d* were made with a Perkin-Elmer 521 spectrometer through the range 3800–3200 cm^{-1}. % T accuracy had been recently determined to be within specifications for this instrument. Calcium fluoride windows were used on both sample and reference cells. A 0–10 mm variable-path stainless steel water-jacketed cell was used as a sample cell. The variable and fixed-path reference cells containing only Hx-*d* were used at ambient temperature. The temperature differential between reference and sample cells produced virtually no error in intensity measurements in the 3800–3400-cm^{-1} region since there is little solvent absorption in this region. The sample cell temperature was regulated by circulating water from a bath controlled to ±0.03°. Parallelism of cell windows was checked repeatedly and adjusted if necessary. The cell zero and short pathlengths were measured by the interference fringe method. The spectral slit width was normally 2 cm^{-1} (approximately 4 cm^{-1} upon ordinate expansion with concurrent slit opening). Several samples of 0.09 *M* and lower concentrations were run at ordinate expansions of 5× or 10× to better determine the concentration dependence of the band near 3500 cm^{-1}.

A decrease in monomer *t*-BuOH absorptivity with increasing temperature was detected. The suggestion that alcohol loss to head space is the primary factor causing monomer absorptivity to decrease with increasing temperature[13] has been rejected by Hoover, *et al.*[14] To verify that no significant amount of alcohol was lost by evaporation to head space at the higher temperatures, we repeated the measurement at 25° after temperature cycling and found a spectrum identical with the initial 25° spectrum.

Data Treatment and Results

Vapor Pressure Data. Table I (deposited)[15] presents the observed pressures over and corresponding concentrations of *t*-BuOH in Hx in the temperature range 30–50°. Several hundred data points are reported. The basic premise of this vapor pressure method is that a distribution of monomeric alcohol between vapor and solution phases exists and is characterized by a distribution coefficient

$$K_D = C_A^S/C_A^V \quad (1)$$

where C_A^S and C_A^V are the concentrations of the monomer in solution and vapor, respectively. Using the customary equilibrium constant expression the analytical or formal alcohol concentration (f_A) in solution may be represented as a sum of terms involving the distribution coefficient, equilibrium constants, and vapor phase monomer concentration (equivalent to monomer alcohol pressure divided by the product of the gas constant R and the temperature in degrees K).[16] Standard least-squares treatments may be used to give a direct noniterative solution of eq 2 since C_A^V is an observable quantity.

$$f_A = K_D C_A^V + 2K_2(K_D C_A^V)^2 + 3K_3(K_D C_A^V)^3 + \ldots . \quad (2)$$

The rather tedious process of solving eq 2 or a related expression numerous times while varying the number of parameters (species) is usually a necessary evil in the treatment of association data. However, before embarking on this process it may be instructive to seek to extract the *minimum* number of associated species necessary to explain the vapor pressure data. If the presence of only one polymer of order n is assumed, then eq 2 reduces to

$$f_A = C_A + nK_nC_A^n \quad (3)$$

and

$$\ln (f_A - C_A) = \ln nK_n + n \ln C_A \quad (4)$$

We may evaluate C_A by determining K_D from the limiting behavior of *t*-BuOH pressure *vs.* concentration data in Hx (independent of associative model). A plot of ln ($f_A - C_A$) *vs.* ln (C_A) should give a straight line with a slope of n. Figure 1 presents such a plot for vapor pressure data at 30° with a maximum concentration of 0.6 *M* *t*-BuOH. The plot is distinctly nonlinear, with a slope at infinite dilution near 3 and at high concentrations near 5. This is direct evidence that *at least* two associated species are present. At low concentrations a trimeric species appears dominant and at the high end a polymer size larger than pentamer is indicated, since an average is being plotted and the high order term is weighted with at least a third-order term. On this basis the least complex model to fit the data within experimental error must contain two polymeric species, such as trimer and hexamer.

Clearly a more complex model with a larger number of species might also be compatible with the data but would in general entail the use of a larger number of equilibrium constants. There is an alternative explanation of the data in terms of only two equilibrium constants for polymer formation—a model with a unique equilibrium constant for the formation of the first important associated species and a constant for the formation of all higher polymers in stepwise fashion such as that proposed by Coggeshall and

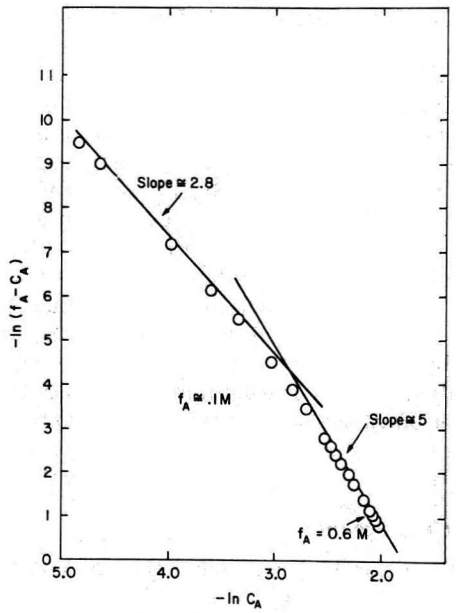

Figure 1. In–In plot for order of polymerization of some *t*-BuOH–$C_{16}H_{34}$ vapor pressure data at 30°.

Saier.[9] Consideration of this type of equilibrium leads to the equation

$$f_A = C_A + 2K_2C_A^2 + 3K_2K_\infty C_A^3 + \ldots + nK_2K_\infty^{n-2} C_A^n \quad (5)$$

where

$$K_2 = \frac{C_{A_2}}{C_A^2};\ K_\infty = \frac{C_{A_n}}{(C_A)(C_{A_{n-1}})} \qquad (\text{all } n>2)$$

With some manipulation we may transform eq 5 to a closed form particularly suited for least-squares analysis.

$$f_A = C_A + \frac{K_2C_A^2(2 - K_\infty C_A)}{(1 - K_\infty C_A)^2} \quad (6)$$

Note that eq 6 is developed with the assumption that a dimer is the first detectable polymer. If, as the vapor pressure data seem to indicate, the limiting low concentration dependence is third order, an analogous procedure can be followed to obtain eq 7 for the case involving only trimer and higher polymers.

$$f_A = C_A + \frac{K_3C_A^3(3 - 2K_\infty C_A)}{(1 - K_\infty C_A)^2} \quad (7)$$

Equation 6 has been previously used in the treatment of amide self-association data[17-20] and perhaps has been used in other circumstances of which we are not aware. For all sets of association data to which equation 6 has been applied the assumption has been made that all polymers in the system are linear or chain polymers and not cyclic. Ginell and Shurgan[21] have asserted that the final form of the equations describing such a process involving two constants is independent of the method of *formation* or degradation of a polymer by adding or subtracting a monomer. This implies that eq 6 and 7 should be valid for situations involving either cyclic or chain polymers of alcohols.

The assumption perhaps most open to question in developing these infinite series models is that the stepwise free energy for formation of all polymers other than the first is invariant. There are good reasons for thinking this assumption to be in error. Implicit in the intuitive picture of the hydrogen bond is a charge movement process converting an alcohol complex joined by a single hydrogen bond to a species with both proton donating and accepting abilities enhanced relative to the free molecules. This concept is presently known as the cooperative effect and was suggested by Frank and Wen[22] in their representation of the structure of water. Recent theoretical calculations tend to support the existence of this effect.[23] If we accept the more realistic viewpoint that the stepwise free energy —for formation of the $(n + 1)$th polymer by addition of a monomer unit to the nth polymer—varies slightly after formation of the first polymer in which cooperative effects may be important—a trimer—an equation may be developed in an attempt to reflect the changing stepwise equilibrium constant.

We have no good foundation for estimating the incremental enthalpy for successive addition of an alcohol monomer to a polymer. It is not unreasonable to believe that an increasingly negative stepwise enthalpy would be offset to a certain extent by an increasingly negative stepwise entropy so that the stepwise free energy would not rapidly become more negative but slowly approach an approximately constant value. This is suggested because of the tendency for both $-\Delta S$ and $-\Delta H$ to increase as hydrogen-bonded complexes become stronger.[24] We make the assumption that the equilibrium constant for the reaction

$$A_n + A = A_{n+1} \quad (n \geq 3)$$

is related to the limiting equilibrium constant by

$$K_{n,n+1} = \frac{n}{n+1}K_\infty \quad (n \geq 3)$$

and then using the relationship

$$K_n = K_{n-1} \times K_{n-1,n} \qquad (n > 3)$$

where

$$K_n = \frac{A_n}{A^n};\ K_{n-1,n} = \frac{A_n}{(A_{n-1})(A)}$$

we obtain the formal concentration of alcohol as

$$f_A = C_A + 3K_3C_A^3(1 + K_\infty C_A + K_\infty^2 C_A^2 + \ldots)$$

which reduces to

$$f_A = C_A + \frac{3K_3C_A^3}{(1 - K_\infty C_A)} \quad (8)$$

Equation 8 is identical to that which would be obtained for considering a series of cyclic complexes formed by addition of successive monomer units starting with trimer as the first polymer. In that case the factors n and $n + 1$ enter specifically as symmetry numbers.[25] For the moment, eq 6, 7, and 8 are most properly viewed as simple empirical relationships. The best that can be hoped for is that at least one of these expressions will give a reasonable fit of the experimental data and have some approximate correspondence to the actual unknown distribution of polymeric alcohol species.

Table II presents the root mean square deviations (RMSD) for a number of least squares fits of a set of *t*-BuOH–Hx vapor pressure data. As we would expect from consideration of Figure 1 no combination of dimer, trimer, and tetramer gives a satisfactory fit of these data. The 1–3–8 model previously proposed for alcohol solutions has a significantly higher RMSD than the 1–3–6 or the 1–3–∞ models. Of particular interest is the fact that the 1–2–∞ model is not comparable in RMSD with either the 1–3–6 or 1–3–∞ models. It may be instructive to take a closer

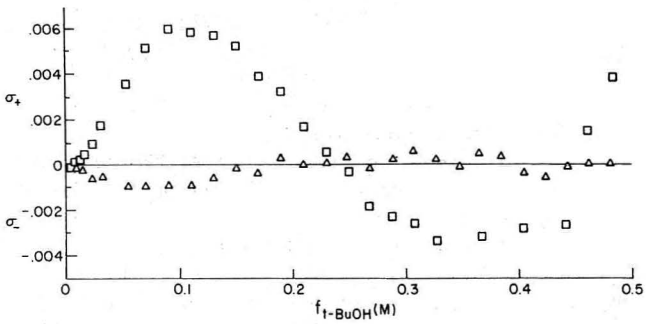

Figure 2. Comparison of deviations between observed and calculated *t*-BuOH concentrations from eq 6 (□) and 7 (△) for vapor pressure data at 40°.

TABLE II: RMSD's for Several Fits of *t*-BuOH Vapor Pressure Data at 45° [a]

Fit	RMSD, $M \times 10^4$	Remarks
1–3	148.3	
1–4	34.3	
1–2–3	71.4	Negative K_2
1–2–4	28.5	Negative K_2
1–3–4	23.9	Negative K_3
1–2–3–4	11.9	Negative K_3
1–2–3–6	2.6	Negative K_2
1–3–8	22.8	
1–3–6	4.3	
1–3–∞ (eq 7)	6.0	
1–3–∞ (eq 8)	5.3	
1–2–∞ (eq 6)	43.6	

[a] Least-squares fits for sets of data taken at other temperatures were essentially identical with respect to RMSD distribution and negative parameters.

TABLE III: Distribution and Equilibrium Constants for *t*-BuOH–Hx Vapor Pressure Data[a]

	T, °C				
	30	35	40	45	50
K_D	77.1	66.7	58.2	51.0	44.5
K_3 (1–3–6), M^{-2}	34.1	23.4	17.0	12.6	8.42
K_3 (eq 7)	24.6	17.3	12.4	9.00	6.52
K_3 (eq 8)	25.5	17.8	12.8	9.26	6.63
K_6 (1–3–6), M^{-5}	6593	3025	1320	593	262
K_∞ (eq 7), M^{-1}	3.72	3.19	2.72	2.32	1.87
K_∞ (eq 8), M^{-1}	4.55	3.90	3.33	2.83	2.35

[a] The following error limits are placed on these least-squares parameters: K_D ± 0.5%, primarily due to adsorption effects; all K_3's are ±2%; K_6 ± 3%; K_∞ ± 1.5%. Parameters determined from individual fits of replicate sets of vapor pressure data should fall within these limits.

look at what the discrepancy in RMSD between these two models entails.

Figure 2 gives a point by point comparison of the actual deviations between observed and calculated *t*-BuOH concentrations from the 1–2–∞ and 1–3–∞ models for a typical set of vapor pressure data. It is readily seen that the experimental data are far better reproduced by assuming a dimer constant of zero and using a unique trimer constant as the first important term in the series.

As a result of the least-squares fits of the vapor pressure data we have three possible models, which do not largely differ on the basis of RMSD, to represent *t*-BuOH association in Hx. Table III presents the least-squares values of the distribution constants and the equilibrium constants for the 1–3–6 and 1–3–∞ models. We are limiting consideration here to those models which both fit the data to an RMSD approaching the expected experimental error and involve no more than two equilibrium constants for polymeric species. We are only interested at this point in the least complex model which fits the experimental data. Models involving additional parameters may be used to fit the data but only at the expense of a more complicated interpretation and a concomitant large increase in the standard errors of the parameters. We look to the pmr and ir data for either the possible corroboration of one of these models or the forced inclusion of a dimeric term.

Pmr Data Treatment and Results

Table IV (deposited)[15] presents the observed chemical shifts and corresponding concentrations of a series of *t*-BuOH–Hx (and Hx-*d*) solutions in the temperature range 20–50°.

Previous pmr data on *t*-BuOH–CCl_4 solutions have been interpreted as more closely fitting a 1–3 rather than a 1–4 equilibrium when only 1–*n* models are considered.[5,10] As we have mentioned, the assumption of a 1–*n* equilibrium ignores the infrared evidence for two or more associated species. Davis, Pitzer, and Rao[26] assumed a monomer–dimer–polymer equilibrium in their pmr study of *t*-BuOH–CCl_4 solutions and calculated enthalpies for dimer formation using equilibrium constants obtained from the apparent limiting slope (at concentrations >0.05 *M*) of chemical shift *vs.* concentration plots.

We seek a reliable method of testing the pmr data for *t*-BuOH–Hx solutions for both the limiting behavior in terms of a dimeric or trimeric equilibrium and the minimum number of associated species present. These objectives may be attained by use of the equation developed by Lippert.[27] Considering the usual Gutowsky–Saika[28] representation of hydrogen-bonded chemical shifts, and for the present limiting consideration to only one polymeric species, we have

$$\nu_{obsd} = \frac{\nu_1 C_A + n\nu_n K_n C_A^{\,n}}{C_A + nK_n C_A^{\,n}} \qquad (9)$$

where ν_1 and ν_n are the pmr chemical shifts of the OH protons in the monomer and *n*-mer. If the *n* OH protons in the polymer are not equivalent (*e.g.*, one proton not hydrogen bonded in a chain polymer), ν_n represents the weighted average of the *n* chemical shifts. From eq 9, together with eq 3, Lippert derived the expression

$$\left(\frac{\Delta\nu}{f_A^{\,n-1}}\right)^{1/n} = [(\nu_n - \nu_1)nK_n]^{1/n} - [(\nu_n - \nu_1)^{1-n}nKn]^{1/n}\cdot\Delta\nu \qquad (10)$$

which has the form

$$\left(\frac{\Delta\nu}{f_A^{\,n-1}}\right)^{1/n} = a - b(\Delta\nu) \qquad (11)$$

where $\Delta\nu$ is the difference between monomer chemical shift and observed chemical shift for a particular f_A value. A plot of the left-hand side of eq 10 *vs.* $\Delta\nu$ for a chosen value of *n* should give a straight line if only the polymer of

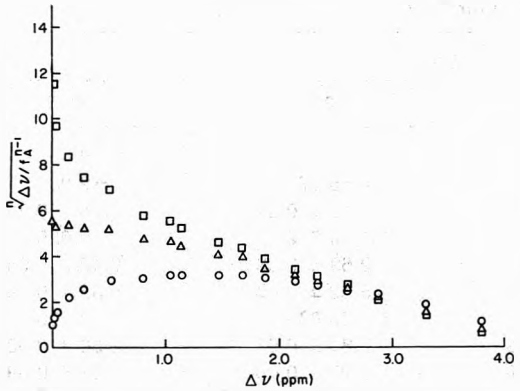

Figure 3. Lippert equation plot for *t*-BuOH–hexadecane pmr data taken at 30°: O, $n = 2$; Δ, $n = 3$; □, $n = 4$.

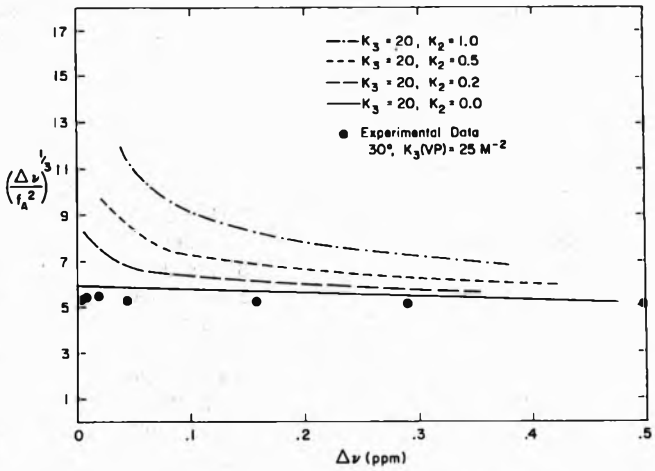

Figure 4. Comparison of third-order plots of theoretical 1–2–3 equilibria with low concentration *t*-BuOH pmr data at 30°.

order n is present. In Figure 3 experimental OH proton chemical shift data at 220 MHz for *t*-BuOH–Hx (and Hx-*d*) solutions at 30.5° are plotted using values of $n = 2$, 3, and 4 in eq 10. All three of the lines show some degree of curvature indicating the presence of more than one polymer. The only line which does not approach the ordinate exponentially is that for $n = 3$ indicating that the low concentration behavior is more nearly third order rather than second or fourth. It might appear that the linearity of the fourth-order plot at higher concentrations suggests that species higher than tetramer are not present. This is an erroneous conclusion. By using chemical shifts of reasonable magnitude we constructed a set of synthetic pmr data for a 1–3–6 equilibrium. A plot of these synthetic data with $n = 4$ is exactly analogous to the fourth-order plot of experimental data in Figure 3. We conclude that pmr data plotted in this fashion will not provide a satisfactory determination of the highest-order polymer in the system. The insensitivity of analyses of pmr data for alcohol solutions to species higher than tetramer has been previously commented upon.[29]

In the low concentration region (down to 0.003 M) the Lippert equation suggests trimer as the predominant bonded species. In order to test the sensitivity of this plot to the presence of dimer in the presence of trimer we constructed a similar plot for $n = 3$ from synthetic data over the range 0.0025–0.07 M alcohol. Several 1–2–3 equilibria were computed using the same chemical shift value for dimer and trimer. Figure 4 shows the calculated curves compared with experimental data. It is readily apparent that this method of plotting pmr data is quite sensitive to a small concentration of dimer in an assumed trimeric equilibrium, and that the experimental data are incompatible with even a modest amount of dimer.

The problem of extracting the true least-squares values of both equilibrium constants and chemical shifts from only pmr data on self-associating systems where more than one complex is formed may be solved only with extreme difficulty. For a description of the equilibria involving two complexes five parameters are required—monomer chemical shift, two complex shifts, and two equilibrium constants. This number of parameters can possibly be reduced to two by extremely careful work on dilute solutions, *i.e.*, determining the monomer shift by extrapolation to zero concentration and finding the slope and intercept of the Lippert plot. However, this procedure places a great deal of weight on the low concentration data. We find the monomer shift by extrapolation but make use of the equilibrium constants obtained from the vapor pressure data to remove these two parameters in fitting the pmr data.

In fitting the *t*-BuOH–Hx pmr data with K_3 and K_6 from the vapor pressure data the following chemical shift expression is used.

$$\nu_{obsd} = (\nu_1 C_A + 3K_3\nu_3 C_A^3 + 6K_6\nu_6 C_A^6)/f_A \quad (12)$$

Formal alcohol concentration is represented by the following equation.

$$f_A = C_A + 3K_3 C_A^3 + 6K_6 C_A^6 \quad (13)$$

To fit the pmr data with the 1–3–∞ models requires that allowance be made for the formation of either linear or cyclic complexes. In previous use of the 1–2–∞ model to fit pmr data for amide solutions the assumption was made that all complexes are chain polymers with an end N–H whose proton has essentially the chemical shift of the monomer.[18] If we use this assumption to treat the present pmr data with eq 7 the following chemical shift expression is obtained

$$\nu_{obsd} = \left[\nu_1 C_A + \frac{K_3 C_A^3}{(1 - K_\infty C_A)}\cdot\nu_1' + \left(\frac{K_3 C_A^3(3 - 2K_\infty C_A)}{(1 - K_\infty C_A)^2} - \frac{K_3 C_A^3}{(1 - K_\infty C_A)}\right)\cdot\nu_\infty\right]\Big/ f_A \quad (14)$$

The term $K_3C_A^3/(1 - K_\infty C_A)$ represents the total end group concentration. ν_1' can be assumed equal to the value of ν_1 found by extrapolation, or ν_1' can be treated as a parameter to be determined in the least-squares fitting routine. A different chemical shift expression using eq 7 is obtained if the trimer is possibly structurally different from the higher polymers, (*e.g.*, the higher polymers are cyclic and the trimer is linear)

$$\nu_{obsd} = \left[\nu_1 C_A + 3K_3\nu_3 C_A^3 + \left(\frac{K_3 C_A^3(3 - 2K_\infty C_A)}{(1 - K_\infty C_A)^2} - 3K_3 C_A^3\right)\cdot\nu_\infty\right]\Big/ f_A \quad (15)$$

In this representation the trimer has a unique chemical shift and the chemical shift of all higher polymers is constant. Another chemical shift relation may be obtained using eq 8 and again considering that the chemical shift of higher polymers is constant and the trimer has a unique shift

TABLE V: RMSD's and Chemical Shifts for Various Fits of *t*-BuOH–Hexadecane Pmr Data[a]

	T, °C			
	21.0	30.6	39.0	49.5
RMSD (ppm) (eq 14)	0.08	0.06	0.04	0.03
ν_1' (14)	−2.86	−5.40	−6.97	−9.08
ν_∞ (14)	7.18 ± 0.32[b]	7.77 ± 0.32	8.12 ± 0.31	8.74 ± 0.33
RMSD (eq 15)	0.060	0.043	0.032	0.025
ν_3 (15)	3.37 ± 0.11	2.95 ± 0.09	2.69 ± 0.08	2.42 ± 0.08
ν_∞ (15)	5.48 ± 0.08	5.41 ± 0.08	5.32 ± 0.07	5.32 ± 0.09
RMSD (eq 16)	0.063	0.045	0.033	0.026
ν_3 (16)	3.60 ± 0.11	3.10 ± 0.09	2.81 ± 0.07	2.50 ± 0.08
ν_∞ (16)	5.47 ± 0.09	5.40 ± 0.08	5.27 ± 0.08	5.22 ± 0.09
RMSD (1–3–6)	0.070	0.058	0.044	0.039
ν_3 (1–3–6)	4.03 ± 0.07	3.57 ± 0.06	3.30 ± 0.05	3.10 ± 0.06
ν_6 (1–3–6)	5.51 ± 0.11	5.47 ± 0.11	5.37 ± 0.10	5.31 ± 0.13

[a] Monomer chemical shift of *t*-BuOH in Hx-*d* is 0.622 ± 0.003 ppm. [b] Calculated chemical shifts are in ppm from TMS as internal reference.

$$\nu_{obsd} = \left[\nu_1 C_A + 3K_3\nu_3 C_A^3 + \left(\frac{3K_3C_A^3}{(1-K_\infty C_A)} - 3K_3C_A^3\right)\cdot\nu_\infty\right]\Big/ f_A \quad (16)$$

The results of fitting the *t*-BuOH pmr data to these equations—using equilibrium constants from the vapor pressure data—are shown in Table V. Equation 14 is seen to be a poor representation of the data since ν_1', the chemical shift for end groups, is found to have totally unreasonable values, far from ν_1. With either eq 15 or 16 good results are obtained, with the RMSD's for the higher temperature data approaching the expected error in chemical shift. RMSD's for the 1-3-6 model are significantly higher than for either of the 1-3-∞ models. It should be noted that the values in Table V are not the "true" least-squares values since those would only be obtained by minimizing the RMSD with respect to both equilibrium constants and chemical shifts. The values in Table V for eq 15 and 16 should not be greatly different from the true values because of the small RMSD's.

There is an iterative mechanism—which we will not describe in detail—for obtaining a very close approximation of the true least-squares fit of pmr data with the 1-3-6 model. The resulting values from this process show an RMSD for data at each temperature of about 0.02 ppm but the equilibrium constants are significantly different from those K_3 and K_6 values from vapor pressure data. In particular, the K_6(pmr) is larger than K_6(vp) and the K_3(pmr) is smaller than K_3(vp) and approaches the K_3(vp) for the 1-3-∞ models. Our conclusion is that the 1-3-6 model will not fit both vp and pmr data for *t*-BuOH–Hx solutions within experimental error while using the same values of equilibrium constants. It appears that either of the 1-3-∞ models provides better correlation of both vp and pmr data.

Infrared Data Treatment and Results

Figure 5 shows the infrared spectrum of Hx-*d* in the 3700–3200-cm^{-1} region and a representative spectrum of a solvent compensated *t*-BuOH solution. In marked contrast to the work of Fletcher, *et al.*, on the infrared spectra of alcohol–hydrocarbon solutions in the first overtone region,[6,30] we find that in the fundamental OH stretching region the spectra of *t*-BuOH–Hx-*d* solutions are quite analogous to spectra of alcohol–CCl_4 solutions.[11] Three bands appear at the approximate frequencies 3624, 3510, and 3350 cm^{-1} with possibly a fourth band near 3400 cm^{-1}. The bands at 3510 and 3350 cm^{-1} shift to higher frequency with increasing temperature. Additionally the monomer absorptivity of *t*-BuOH decreases by about 10% when the temperature is raised from 25 to 45°.

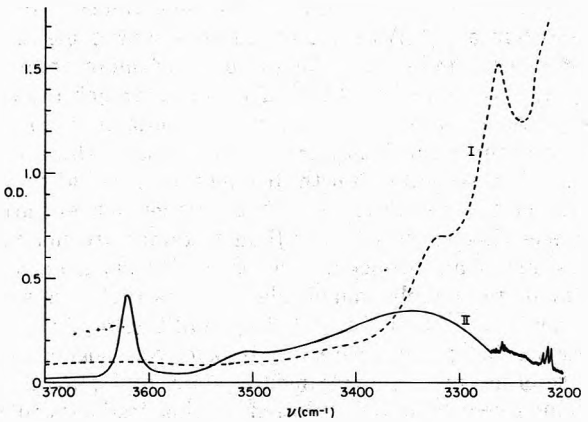

Figure 5. Infrared survey spectra at 25° on Digilab FTS-14 spectrometer: trace I, 1.25-mm path, *n*-$C_{16}D_{34}$ *vs.* air, 300 averaged scans; trace II, 1.25-mm path, ~0.09 *M* *t*-BuOH in *n*-$C_{16}D_{34}$, solvent compensated, 300 averaged scans.

Table VI (deposited)[15] presents absorbances measured for solutions of *t*-BuOH in *n*-$C_{16}D_{34}$ at 25, 35, and 45° to a maximum concentration of *ca.* 0.85 *M*. Recorded absorbances are primarily confined to those at the monomer stretching frequency of 3624 cm^{-1}, but a few values of absorbance at 3510 cm^{-1} are also reported. Absorbances at 3350 cm^{-1} are not reported due to probable large errors since path lengths at which the 3624-cm^{-1} band can be optimally measured give rise to extremely low transmission at 3350 cm^{-1} for concentrations above 0.2 *M* alcohol.

Because several different bands from various species are observed, ir spectra are qualitatively more informative than pmr spectra or vapor pressure data. The quantitative interpretation of the ir data depends, of course, on the correct assignment of the observed bands to the alcohol species present. In particular, we direct our attention to two spectral features: (1) the band at 3624 cm^{-1}, which is certainly due in part, at least, to monomer, but may also contain contributions from nonbonded OH groups of chain

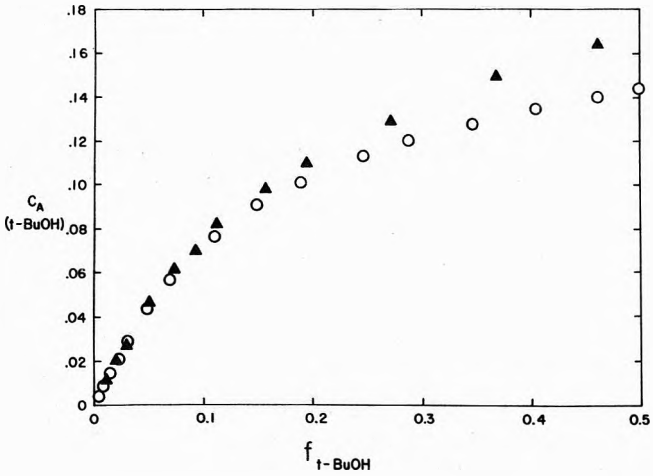

Figure 6. Comparison of apparent monomer concentrations of *t*-BuOH in hexadecane at 35° from infrared data (▲) and vapor pressure data (O) as functions of total *t*-BuOH concentration.

(open) polymers; and (2) the band at 3510 cm^{-1}, which has usually been ascribed to dimer.

Of paramount importance in accurate use of ir data to seek a mathematical description of alcohol polymer formation is the possible presence of contributions to the 3624-cm^{-1} band due to end OH groups of chain polymers at the monomer band. One previous quantitative consideration of end OH group contributions to the monomer band is that of Mecke,[31] who concluded from a comparison of monomer fractions of methanol in CCl_4 calculated from ir measurements and literature vapor pressure data that no extra absorption was present at the monomer band. However, the cancellation studies of Bellamy and Pace showed that at 0.2 *M* methanol in CCl_4 one or more chain polymers were present.[32] A more easily interpretable answer to the problem should result from the comparison of ir data with vapor pressure data on an alcohol–solvent system in which the solvent vapor pressure is negligible. We consider that one of the most important results of the present work is the direct comparison of apparent monomer alcohol concentrations from two independent techniques.

Figure 6 presents a plot of the monomer concentration of *t*-BuOH in *n*-$C_{16}H_{34}$ determined from vapor pressure measurements and the "monomer" concentration of *t*-BuOH in *n*-$C_{16}D_{34}$ determined from ir intensity measurements at 3624 cm^{-1}. The curves show good agreement at low alcohol concentration but diverge rapidly at higher concentrations, with the ir results giving higher apparent monomer concentrations. Note particularly that the monomer concentrations from either measurement are independent of association model. Both values depend only on a distribution coefficient or an absorptivity determined from limiting behavior at infinite dilution. There is no obvious reason for the equilibrium constants for *t*-BuOH association to vary significantly between the deuterated and normal solvents. The observations that the limiting behavior is identical within experimental error (also at 45°) from the vp and ir data and that solutions of comparable concentrations in the two solvents have compatible chemical shifts lend strong support to the view that there is no solvent effect large enough to account for the different curves.

We may examine the effect of most probable errors upon the vapor pressure data to determine whether these could account for an erroneously low *t*-BuOH monomer concentration in solution. One source of error is vapor adsorption on the glass walls of the vapor pressure apparatus. As infinite dilution is approached, adsorption will increase the extrapolated distribution coefficient. The presence of unaccounted for vapor phase polymers at higher alcohol pressures will make the apparent vapor phase monomer higher than its true value and consequently increase the calculated solution monomer. Thus, both of these errors would make the value of the monomer in solution, as calculated from vapor pressure data, higher than the true value. Adsorption on flask walls at higher alcohol pressures would tend to slightly compensate for vapor phase polymer formation. Moreover, it is highly unlikely that the sum of these effects could contribute more than 1% error to the determined vapor phase monomer. We therefore conclude that the significant difference in apparent monomer concentration measured by the vp and ir methods can hardly be rationalized except on the basis of an added contribution to the 3624-cm^{-1} band by the end hydroxyl group of a polymer or polymers.

We do not have sufficient proof to extend this result to infrared studies of other alcohol–solvent systems but we think that the possibility that previous infrared studies have overestimated monomer concentrations must be considered seriously. In particular, this would give a reasonable explanation of the results of Dunken and Fritzsche,[33] who found that the model which best fit infrared data for various alcohol–CCl_4 systems varied as a function of temperature.

Any least-squares analysis based on monomer absorbance must cope, then, with two additional problems: the absorptivity of the end group OH and the specific polymer or polymers contributing to the monomer band.

The 3510-cm^{-1} absorption of alcohol–CCl_4 systems has customarily been assigned primarily to a dimeric species —either cyclic or linear, or a mixture of both. There have been few quantitative justifications of this assignment. If good agreement of our ir data for *t*-BuOH–Hx-*d* solutions with vp and pmr data is to be obtained, then this band must be either primarily due to a trimer or due to a dimer with an amazingly high absorptivity. The results of previous fits of infrared data for certain alcohol–CCl_4 solutions suggest that the 3510-cm^{-1} band could possibly be due to a linear trimer.[7]

The absorbance of the *t*-BuOH band at 3510 cm^{-1} can only be measured over a very limited concentration range before overlap from the band at 3350 cm^{-1} makes possible serious error. For our data, the upper limit is at a *t*-BuOH concentration of *ca.* 0.09 *M* at 35°. Further, the band is very weak throughout the range 0.01–0.09 *M* *t*-BuOH compared with the 3624-cm^{-1} band. The low intensity of the 3510-cm^{-1} band makes the largest relative measurement errors in the concentration range below 0.03 *M* alcohol not due to low intensity alone but due to the neglect of overlap from the monomer band at 3624 cm^{-1}. Assuming that the monomer band is symmetric and reflecting the high-frequency wing about the center of the 3624-cm^{-1} band, we find that very large errors may be made by determining the % T at 3510 cm^{-1} from the base line–peak height distance and neglecting the background due to overlap from the monomer band.

Measurements of absorbances at 3624 cm^{-1} and at 3510 cm^{-1} of *t*-BuOH–Hx-*d* solutions to a maximum concentration of 0.09 *M* alcohol were made at 35°. After making

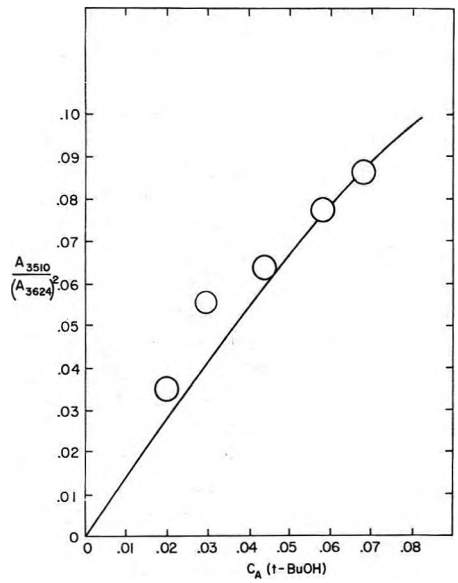

Figure 7. Measured values of *t*-BuOH "dimer" absorbance quotient (O) compared with expected theoretical dependence for trimer only absorbing at 3510 cm^{-1} (—).

the necessary background corrections the absorbance ratio $A_{3510}/(A_{3624})^2$ corresponding to a dimeric equilibrium was plotted as a function of monomer concentration, as shown in Figure 7. Rather than remaining constant, the ratio increases with monomer concentration, thus indicating that the band at 3510 cm^{-1} is due to a species higher than dimer. From one value of absorbance at 3510 cm^{-1} an assumed trimer absorptivity was calculated using K_3 at 35° from the vapor pressure data. The theoretical dependence of $A_{3510}/(A_{3624})^2$ was calculated, using this trimer absorptivity, the vapor pressure K_3, and monomer absorbance data from other independent solutions at 35°. The result, plotted as the solid line in Figure 7, is a good representation of the experimental data. We conclude that the dependence of the 3510-cm^{-1} band upon the monomer band at 3624 cm^{-1} is predominantly third order.

We wish now to utilize this information in making a least-squares fit of the absorbance data for the band at 3624 cm^{-1}, which represents both monomer and nonbonded ("end group") OH. We know of no theoretical or experimental information which gives a clear estimate of the absorptivity of an end OH group, where the oxygen serves as a proton acceptor, relative to the absorptivity of the free monomer. It is reasonable to think that the absorptivity ratio (end OH/free OH) ought to be not far removed from unity and that the ratio should increase upon transfer from a hydrocarbon solvent to a more polar solvent such as CCl_4 since the end OH is increased in "acidity" relative to the free OH. Also, since the work by Bellamy and Pace[32] indicated a lower frequency for the end group relative to the free we expect that the value of the absorptivity ratio at 3624 cm^{-1} will be lower than the actual ratio of absorptivities at the respective maxima.

The difference (P_A) between the true monomer concentration from vapor pressure data and the apparent value from ir (Figure 6) should be directly proportional to the concentration of a chain polymer or polymers with the proportionality constant being the ratio of end group absorptivity to monomer absorptivity. We used the concentration of trimer and polymer from the 1-3-∞ fit of the vapor pressure data to check possible constant ratios. The ratio of P_A to vp trimer concentration is *ca.* 0.6; the ratio of P_A to total polymer concentration (trimer plus all higher polymers) is *ca.* 0.3; and the ratio of P_A to polymer concentration *excluding trimer* was not constant. The ratio value of 0.3 resembled values calculated by Whetsel and Lady[34] in their ir study of phenol self-association, where the assumption was made that all phenol complexes might have end groups contributing to the monomer band.

TABLE VII: RMSD's and Equilibrium Constants for 1-3-∞ Fits of *t*-BuOH-$C_{16}D_{34}$ Infrared Data[a]

T, °C		RMSD, *M*	K_3, M^{-2}	K_∞, M^{-1}
25	Eq 7	0.0020	44.2 ± 1.2	4.78 ± 0.03
	Eq 8	0.0023	46.4 ± 1.5	5.94 ± 0.04
35	Eq 7	0.0017	20.6 ± 0.5	3.23 ± 0.03
	Eq 8	0.0018	21.3 ± 0.5	4.07 ± 0.04
45	Eq 7	0.0018	10.8 ± 0.4	2.29 ± 0.04
	Eq 8	0.0018	11.0 ± 0.5	2.89 ± 0.05

[a] The absorptivity ratio (end OH/free OH) is set at 0.6 for each fit.

As a result of the varying ratio excluding trimer we conclude that the trimer of *t*-BuOH must be a chain polymer and not a cyclic species. It is also apparent that the maximum value we can obtain for the absorptivity ratio arises from a situation where all polymers higher than trimer are cyclic. In the absence of any evidence as to the true magnitude of the absorptivity ratio we will assume that the rato which is closest to unity is the most probable value.

With this assumption, the absorbance per unit length at 3624 cm^{-1} is represented as

$$A_{3624} = \varepsilon^\circ(C_A + bK_3C_A^3) \qquad (17)$$

where b is the absorptivity ratio. The formal concentration of *t*-BuOH in Hx-*d* is given by either eq 7 or 8. With these expressions we used a two-parameter optimum seeking program[7] to search for the best values of K_3 and K_∞ for a particular assumed value of b with input data of monomer absorptivity, absorbance at 3624 cm^{-1}, and formal concentration.

The least-squares values of K_3 and K_∞ for infrared data at 25, 35, and 45° are given in Table VII. These values are, within about 10% error, comparable to the K values from vapor pressure data. We think this to be very respectable agreement considering the additional problem of infrared overlap and the lower precision of infrared data. The b value of 0.6 should be considered only as an approximation. The RMSD values for fits of the infrared data are not extremely sensitive to changes in b between 0.5 and 0.7 but the equilibrium constants change significantly over this range.

Discussion

We begin discussion of this work with mention of salient facts which may be deduced from the three sets of experimental data on *t*-BuOH-Hx solutions without recourse to either extensive assumptions or detailed mathematical treatment of the data.

The vapor pressure data may be analyzed qualitatively by constructing log-log plots of polymer *vs.* monomer concentration, using an extrapolated distribution coefficient. As in Figure 1, the initial slope of such plots is closely third order and increases rapidly at *t*-BuOH concentrations above 0.08 *M*, reaching a value of about 5 at the

highest alcohol concentrations used in this study. Even at concentrations below 0.2 *M* these data cannot be explained by the assumption of a single monomer–*n*-mer equilibrium.

Pmr data for *t*-BuOH–Hx solutions may be analyzed by use of the Lippert equation.[27] The fact that only the third-order plot has a nearly linear intercept is strong evidence for trimer predominance in the very low concentration region (Figure 3). The reversal of slope for the second-order plot is mathematically incompatible with the form of the Lippert equation. Additionally, although we have made no attempts to calculate a dimer constant by the limiting slope method, it is evident from a plot of chemical shift *vs.* concentration for pmr data near room temperature that a limiting slope cannot be defined until concentrations less than 0.01 *M* *t*-BuOH are reached. We can find no evidence from these pmr data for dimer dependence at low concentration levels.

A comparison of infrared and vapor pressure data using only extrapolated monomer absorptivity and distribution coefficients clearly shows that the apparent monomer fraction from ir data is erroneously large, indicating absorption at the monomer OH band by end OH groups in a chain polymer. Careful examination of the dependence of the 3510-cm^{-1} band upon monomer absorbance at 3624 cm^{-1} shows that the absorbance ratio corresponding to dimer dependence increases rapidly with alcohol concentration indicating that the 3510-cm^{-1} band is due to a species larger than dimer.

Significant Dimer Concentration? The present experimental data give no evidence for significant amounts of a *t*-BuOH dimer. This is a decided departure from prior work apparently giving strong evidence for the presence of dimers at low alcohol concentrations in CCl_4 solution. It should be mentioned here that except in rare instances the presence of alcohol dimers has been assumed rather than experimentally proven.

Three types of measurements have given evidence for dimer formation in solution. Infrared measurements[11] which show a nonzero limiting slope of a plot of apparent monomer absorptivity *vs.* concentration have been interpreted as evidence for dimer formation, as has a nonzero limiting slope for OH proton chemical shift *vs.* concentration.[26,35] Also, the apparent second-order dependence of absorbance near 3500 cm^{-1} upon monomer alcohol absorbance has suggested dimer formation in alcohol–CCl_4 solutions.[36] We will restrict discussion to the case of *t*-BuOH.

Recent infrared measurements in this laboratory on *t*-BuOH–CCl_4 solutions have shown that the presence of trace amounts of water can adversely affect the measured absorptivity near 3618 cm^{-1} for dilute *t*-BuOH–CCl_4 solutions. The symmetric stretch of H_2O occurs at about 3618 cm^{-1} in CCl_4 solution. Using an absorptivity estimated from the work of Magnusson[37] we calculate that at a *t*-BuOH concentration of 0.005 *M* the amount of water necessary to cause a 1% error in ϵ_M (in a positive direction) is less than 0.00015 *M*. In successive dilutions usually employed using normal volumetric apparatus significantly larger amounts of water than this may be readily picked up from the atmosphere even if the original CCl_4 is quite dry. Even a 1% error in the extrapolated monomer absorptivity ($\epsilon_M°$) translates into a dimer equilibrium constant of 2.0 M^{-1} at an alcohol concentration of 0.005 *M*. It is not inconceivable that the previous ir measurements reported by Liddel and Becker[11] for *t*-BuOH–CCl_4 solutions were subject to this error.

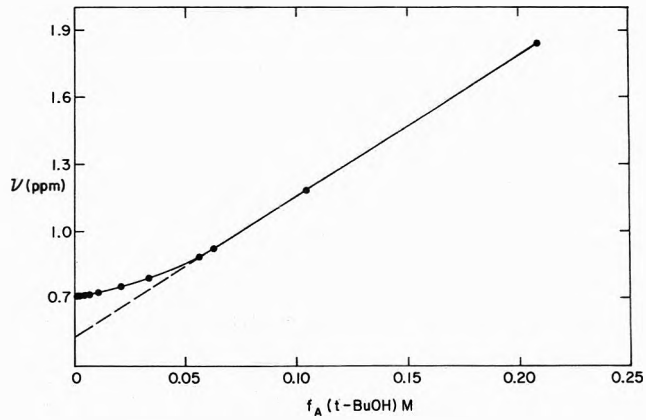

Figure 8. Chemical shift *vs.* concentration for *t*-BuOH–CCl_4 solutions at 21°. Shifts measured at 220 MHz relative to TMS using Varian proton Fourier transform accessory; - - -, limiting slope which would be obtained by use of alcohol concentrations >0.05 *M*.

The analysis of *t*-BuOH–CCl_4 pmr data by the limiting slope method has been reported by Davis, *et al.*[26] The concentration range covered by these authors extended to a lower limit of *ca.* 0.05 *M* alcohol. The limiting slope was established using concentrations between 0.05 and 0.20 *M*. We have obtained 220-MHz proton nmr data for *t*-BuOH–CCl_4 solutions at 21° down to concentrations of 0.001 *M* alcohol. These data are plotted in Figure 8. It is readily apparent that the limiting slope as defined by Davis, *et al.*, is much larger than the true limiting slope. The Lippert plot for these data shows the same behavior as the *t*-BuOH–Hx pmr data plotted in Figure 3, an approximately linear intercept for the third-order plot and a physically meaningless slope for the second-order plot.

Infrared measurements for three alcohols in CCl_4 solution have been interpreted by Hammaker, *et al.*,[36] as giving dimer dependence of the band near 3500 cm^{-1} upon the overtone monomer OH band near 7100 cm^{-1}. We think that there is one major experimental oversight in this work. Hammaker, *et al.*, suggest that background from the tail of the monomer near 3600 cm^{-1} is negligible at 3500 cm^{-1}. From our work it is evident that *ca.* 40% of the absorbance at 3500 cm^{-1} for low alcohol concentrations (*ca.* 0.02 *M* *t*-BuOH) is due to background from the monomer near 3600 cm^{-1}. We may combine the measurements of Hammaker, *et al.*, with the maximum dimer constant we obtain from pmr data on *t*-BuOH–CCl_4 solutions[38] to calculate a dimer absorptivity. Using their value of 28.2 for the ratio dimer absorbance/(monomer absorbance)^2 at 25°, a monomer absorptivity of 2.1 (overtone) and our value of 0.25 for K_2 we calculate a dimer absorptivity of about 500.0 M^{-1} cm^{-1}. This absorptivity is unrealistically large but is most probably a lower limit since the limiting slope dimer constant from the pmr data is overestimated.

There are two effects which can combine to give apparent dimer dependence of the 3500 cm^{-1} band if actually due to a chain trimer. Background absorbance at 3500 cm^{-1} from the wing of the monomer band increases the measured absorbance near 3500 cm^{-1} by substantial amounts at low alcohol concentrations. At concentrations above about 0.05 *M*, contribution to the monomer band

TABLE VIII: Thermodynamic Parameters for *tert*-Butyl Alcohol Association in *n*-Hexadecane ($\Delta E_D^\circ = -5.25 \pm 0.02$ kcal;[a] $\Delta S_D^\circ = -10.7 \pm 0.1$ eu)

Model	$-\Delta H_3^\circ$, kcal/mol	$-\Delta S_3^\circ$, eu	$-\Delta H_\infty^\circ$, kcal/mol	$-\Delta S_\infty^\circ$, eu
1–3–6 (VP)	13.4 ± 0.1	37.4 ± 0.4	31.8 ± 0.3(ΔH_6°)	87.2 ± 1.0(ΔS_6°)
Eq 7 (VP)	13.0 ± 0.1	36.6 ± 0.3	6.64 ± 0.08	19.3 ± 0.3
Eq 8 (VP)	13.2 ± 0.1	37.1 ± 0.3	6.45 ± 0.06	18.2 ± 0.2
Eq 7 (IR)	13.4 ± 0.1	37.5 ± 0.3	6.99 ± 0.04	20.3 ± 0.1
Eq 8 (IR)	13.8 ± 0.1	38.5 ± 0.4	6.85 ± 0.04	19.4 ± 0.1

[a] Represents energy of solution for 1 mol of *tert*-butyl alcohol from the ideal gas state to ideal unit molarity in *n*-hexadecane solution.

by the end OH group of a chain trimer (with an absorptivity approximating that of the *t*-BuOH monomer) effectively reduces the dependence of the absorbance at 3500 cm^{-1} upon the monomer band.

Infrared Frequency Shifts. One of the more perplexing questions arising from studies of the infrared spectra of alcohol solutions has been the distribution of frequency shifts for associated species. Explanations for the small frequency shift (from the monomer) for the 3500-cm^{-1} solution band as opposed to the *ca.* 300-cm^{-1} shift of the "polymer" band at 3350-cm^{-1} have included both structural and energy differences between the low- and high-order species. The concept of energy differences—in the sense of a linear enthalpy–frequency shift relationship—probably cannot be used as an explanation for the differences in frequency shift since no studies of the equilibrium thermodynamics of alcohol association will support a per-bond enthalpy difference between lower and higher species of more than about 20%. Structural differences which involve rather subtle changes in electron distribution about the OH bond are probably the most reasonable explanation for the observed effects.

Infrared matrix studies of alcohol association[39,40] show a progressive appearance of bands at lower frequency from the monomer as alcohol concentration in the matrix is increased. The successive bands for associated species have been attributed to the sequence of dimer, trimer, tetramer, and higher polymers. In solution at room temperature, alcohols show no such distribution of bands; the prominent features, other than the monomer, are broad bands near 3500 and 3350 cm^{-1}. The point to be made here is that the band attributed to dimer in the matrix spectra may not correspond exactly with the 3500-cm^{-1} solution band customarily assumed to be due to dimer also. The frequency difference between bands assigned to dimer and trimer in the matrix spectra is only about 40 cm^{-1}. On comparing the frequency differences between monomer and polymer in both matrix and solution spectra one can readily see that the polymer band in solution appears significantly ($\sim$100 cm^{-1}) toward higher frequency relative to the monomer compared with the corresponding matrix bands. Because of the apparent frequency shift "compression" on going from matrix to solution and the nonequilibrium situation in the matrix one cannot *a priori* identify the 3500 cm^{-1} solution band of alcohols with the dimer band in the matrix spectra. The 3500-cm^{-1} band of alcohol solutions could be due to a dimer or a trimer or a mixture of both.

This suggestion is in accord with the early work of Smith and Creitz,[41] who assigned the band near 3500 cm^{-1} to a chain dimer in the case of the highly hindered alcohol 2,4-dimethyl-3-ethyl-3-pentanol. These authors also suggested that a chain polymer of an alcohol would have a comparable band near 3500 cm^{-1}. Pmr data from this laboratory for the above hindered alcohol in CCl_4 solution also show dimer dependence over approximately the same concentration range as ir data reported by Smith and Creitz.

In the present work on *t*-BuOH the 3500-cm^{-1} band appears to have third-order dependence upon monomer absorbance. One very interesting aspect of the *t*-BuOH–Hx-*d* ir spectra is that there appears to be a band intermediate in frequency between 3510 and 3350 cm^{-1} which accompanies the 3510-cm^{-1} band from its inception at very low alcohol concentrations. This intermediate band is not as intense as the 3510-cm^{-1} band but is significantly broader. If our assignment of the 3500-cm^{-1} band for *t*-BuOH as trimer is correct then it may be possible that the two bonded OH groups in a linear trimer have distinct absorption bands.

Specific Association Model. As a result of correlation of vapor pressure, pmr, and infrared data on *t*-BuOH association we conclude that that association model—involving only two equilibrium constants—which best represents the data is composed of monomer, linear or chain trimer, and successive polymers which are more probably cyclic than chain-like. Due to convergence limitations on the 1–3–∞ equations the applicability of this model is limited to solutions of lower concentration than 1.0 *M* (where the product $(K_\infty C_A)^2 < 1$). Even if this were not the case there is no unambiguous procedure with which to account for probable changes in activity coefficients at higher alcohol concentrations. The model is most properly viewed as a dilute solution model with no stringent applications to solutions approaching pure alcohol.

Table VIII presents the least-squares values of enthalpies and entropies for *t*-BuOH association in *n*-hexadecane. Of particular interest is the fact that all ΔH_3° values are in good agreement regardless of model or type of data. Values of ΔH_∞° from either vp or ir data also agree well.

Previous vapor pressure data for methanol association in Hx were interpreted as fitting a 1–3–8 model.[7] We may briefly examine the reasons why that suggested model is not a good representation for *t*-BuOH association. Figure 9 gives a ln–ln plot of 25° MeOH–Hx vapor pressure data.[7] The limiting behavior at low concentration is approximately third order and the order of polymerization at the high concentration end is approximately seven. These data have been dismissed by Fletcher[30] because of the low concentration range covered and the implausibility of the octamer. In the process of setting up the vapor pressure apparatus for the present study of *t*-BuOH–Hx solutions some measurements for the MeOH–Hx system were made. These data were identical within experimental error with those reported previously.[7] There is little question then

TABLE IX: Thermodynamic Parameters for Infinite Series Fits of Methanol Association in *n*-Hexadecane

Model	$-\Delta H_3°$, kcal/mol	$-\Delta S_3°$, eu	$-\Delta H_\infty°$, kcal/mol	$-\Delta S_\infty°$, eu
1-3-8[7]	11.3 ± 0.1	29.0 ± 0.3	...	...
Eq 7	11.6 ± 0.1	31.2 ± 0.3	5.97 ± 0.03	14.9 ± 0.1
Eq 8	12.1 ± 0.1	32.8 ± 0.2	5.64 ± 0.03	13.5 ± 0.1

that the the MeOH–Hx vapor pressure data previously reported[7] are reproducible and, even though limited to solutions of lower concentration than 0.2 *M*, show significantly higher than the fourth-order dependence upon monomer concentration advanced by Fletcher[30] as a general model for alcohol association. We may add that the pmr data reported by Dixon[42] for MeOH in cyclohexane cannot be used in support of a 1–4 model for methanol association[30] since the 1–4 fit for the pmr data gives no more information than is reported in part I, Table II, *i.e.*, that of the simple models 1–2, 1–3, and 1–4, the monomer–tetramer model is a better fit.[7] What is not reported in ref 7 is that because of the very high order of methanol association a 1–8 fit of the methanol vapor pressure data has a substantially lower RMSD than a 1–4 fit.[43]

The validity of the previously proposed octamer may only be questioned on the basis of the alternate explanation that the high order dependence of methanol polymer concentration upon monomer concentration may equally well be explained by a series of terms higher than trimer. Indeed, if a common association model is possible for methyl and *tert*-butyl alcohol the model of minimum complexity is that of monomer–trimer plus a series of higher polymers.

Table IX presents the enthalpies and entropies calculated from fitting the MeOH–Hx vapor pressure data[7] with use of the infinite series models of eq 7 and 8. As for the *t*-BuOH–Hx data, the RMSD for a 1–2–∞ fit of the methanol data is much larger than for the 1–3–∞ fits. The RMSD's for the 1–3–∞ fits are generally somewhat larger than for the 1–3–8 fit. The temperature dependence of K_3 and K_∞ from the series fits is not as good as that for the 1–3–8 fit.

Trimer Stability. The predominance of a trimer at low alcohol concentration in *t*-BuOH and MeOH–Hx solutions is very possibly one of the more direct experimental observations which could confirm the cooperative effect in hydrogen bonding suggested by Frank and Wen.[22] A chain trimer is the first hydrogen bonded alcohol species whose formation should show cooperative effects if these are significant. A direct comparison of dimer and trimer enthalpies is naturally impossible without an experimental dimer enthalpy. However, by considering several types of measurements, we may be able to set an upper limit on the enthalpy for formation of a chain alcohol dimer.

Infrared measurements of 1:1 complex formation of alcohols with various proton acceptors in CCl_4 solution give enthalpies which are generally less exothermic than −4.0 kcal/mol,[44] with oxygen containing bases forming weaker complexes with alcohols than alcohol–nitrogen base complexes. Vapor pressure measurements for the 1:1 complex MeOH–diethylamine in Hx have given an enthalpy of −4.5 kcal/mol.[45] One may reasonably expect that the enthalpy for formation of a chain alcohol dimer would be less exothermic than the enthalpy for formation of the corresponding alcohol–nitrogen base 1:1 complex. We

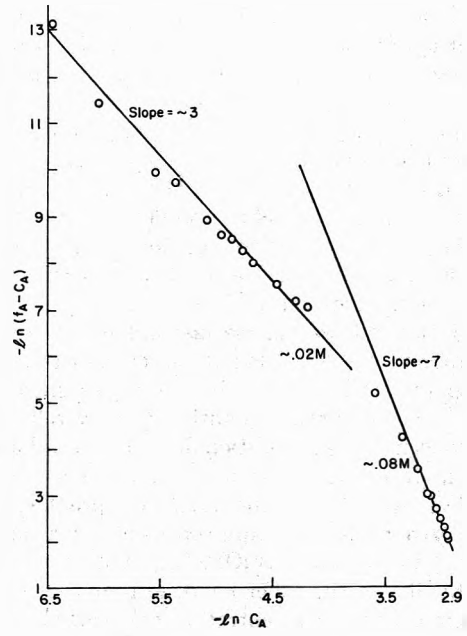

Figure 9. ln–ln plot for order of polymerization of MeOH–Hx vapor pressure data[7] at 25°.

suggest that the enthalpy for formation of a chain alcohol dimer in a hydrocarbon solvent would be less exothermic than −5.0 kcal/mol. The enthalpy values for *t*-BuOH and MeOH trimer formation in Hx are both significantly larger than twice this value. There is additional information from studies of alcohol–amine complexes to support the exceptional stability of an alcohol trimer as compared with a dimer. The experimental enthalpy for a 2:1 methanol–diethylamine complex is −13.8 kcal/mol.[45] This value is about three times as large as the −4.5 kcal/mol enthalpy for formation of the 1:1 methanol–amine complex and consequently was interpreted as evidence for a cooperative effect. Also, vapor pressure studies of methanol–fluorinated alcohol complexes in Hx have shown a vanishingly small quantity of hetero dimer compared with hetero trimer.[46]

Advantages and Disadvantages of the Experimental Techniques. In conclusion, we may assess the relative merits of the three experimental techniques we have used and the unified alcohol association model which results from these data.

The vapor pressure method, although giving no apparent structural information, is an important technique not least due to the high precision obtainable but primarily because a measurable quantity is directly related to monomer concentration. With use of a suitable solvent one can make a direct comparison with monomer alcohol concentration measured by the infrared method.

Least-squares fits of the *t*-BuOH and methanol–Hx vapor pressure data closely reproduce the observed data with either monomer–trimer–large polymer (6 or 8) or monomer–trimer–sequential polymer models. The absence of a measurable concentration of dimer is ascribed to the minimal thermodynamic stability of the dimer compared with the trimer. One may suggest that the fact that the initial slopes in Figures 2 and 9 are slightly less than 3 implies a certain amount of dimer in the low concentration region. There are two reasons why this may not be strictly true. First, there is no clear region where the de-

pendence of polymer concentration upon vapor pressure monomer approaches second order, even down to 0.002 *M* alcohol. Secondly, due to the presence of adsorption effects, the dependence of polymer concentration upon monomer is always going to be slightly less than the true dependence because the measured distribution coefficient will be very slightly larger than the true value. However, we do not claim the total absence of dimeric alcohol species but only say that the concentration of dimer is so small that it lies within the realm of experimental errors in our vp, pmr, and ir data.

Proton magnetic resonance measurements are at a distinct disadvantage for calculations of associative equilibria compared with vp and ir techniques since the pmr data give no measurable quantity directly related to monomer concentration. Additionally, one may have to determine almost twice as many parameters in order to define a given system. The computational problems involved and the extreme temperature sensitivity of a highly associated system, such as *t*-BuOH–Hx, make model comparisons difficult. On the other hand, examination of the limiting chemical shift–concentration behavior at low alcohol concentration can identify the first dominant associated species. In the *t*-BuOH–Hx system this species is a trimer; model equilibria computed for dimer–trimer mixtures support the view that the *t*-BuOH dimer concentration is vanishingly small—within the accuracy of the pmr data. Unequivocal identification of higher order species is not possible; however, the failure to obtain a fit of the pmr data assuming a series of *chain* alcohol polymers suggests that there is some structural difference between the trimer and higher alcohol polymers.

Infrared studies of alcohol association are probably more numerous than the combined total of work using other techniques to study this phenomenon. Inherent limitations on the quantitative interpretation of infrared data have often not been given sufficient weight. The presence of even a small degree of overlap at the monomer band from end groups of chain species can invalidate any apparently constant exponential relationship between the absorbances of monomer and polymer bands. The assumption that the infrared monomer band is an accurate measure of monomer alcohol concentration should not be made unless either specific measurements of monomer activity by another technique show correspondence or cancellation measurements, such as those made by Bellamy and Pace,[32] show no extra component at the monomer band at moderate concentrations. The present data indicate that the upper limit of direct use of monomer absorbance is at *ca.* 0.1 *M* *t*-BuOH. The use of monomer absorbance data, allowing for end group overlap, is limited in our case to solutions of lower concentration than 0.5 *M* *t*-BuOH. Near this concentration and above there is overlap at 3624 cm^{-1} from bands in the 3500–3300-cm^{-1} region. In order to make any use of absorbance at 3624 cm^{-1} after the point of significant polymer overlap is reached the various absorption bands in the 3650–3300-cm^{-1} range would have to be quantitatively and unambiguously resolved.

Coincident absorption at the monomer alcohol band by end groups of chain polymers is undeniably a serious barrier to the interpretation of the infrared spectra of alcohol solutions, but of greater consequence is the fact that this effect offers a possible means of determining the structures of alcohol polymers. If our assumption is correct that the most probable value of the absorptivity ratio of end OH to free OH is near unity, then our ir data require that essentially all *t*-BuOH polymers higher than trimer be cyclic species.

Another specific problem is the coincident absorption of the symmetric stretch of H_2O at the monomer band of *t*-BuOH near 3618 cm^{-1} in CCl_4 solutions. Precise evaluation of the monomer absorptivity of *t*-BuOH in CCl_4 solution is not possible except in extremely dry solutions. This problem is less acute for other alcohols which have monomer bands at shorter wavelengths in CCl_4 solution.

The result of combined use of three techniques to study *t*-BuOH association in *n*-hexadecane is an association model which probably could not have been projected from the isolated use of either of the spectroscopic methods involved. Although we do not suggest that the infinite series models give an exact distribution of the polymeric alcohol species involved, we think that these models are the least complex expressions which can correlate both qualitatively and quantitatively the present experimental data. All other one- and two-constant models tested fail to describe accurately at least one type of data—vapor pressure, proton magnetic resonance, or infrared.

Acknowledgment. E. E. T. acknowledges fellowship support from the Air Force Office of Scientific Research and the National Institute of General Medical Sciences of the National Institutes of Health.

References and Notes

(1) Presented in part at the International Conference on Hydrogen Bonding in Ottawa, Canada, Aug 21–25, 1972.
(2) (a) H. Wolff and H. E. Hoppel, *Ber. Bunsenges. Phys. Chem.*, **72**, 710 (1968); (b) C. B. Kretschmer and R. Wiebe, *J. Amer. Chem. Soc.*, **76**, 2579 (1954).
(3) E. M. Woolley, J. G. Travers, B. P. Erno, and L. G. Hepler, *J. Phys. Chem.*, **75**, 3591 (1971).
(4) For a review of pertinent literature, see A. S. N. Murthy and C. N. R. Rao, *Appl. Spectrosc. Rev.*, **2**, 69 (1968).
(5) W. Storek and H. Kriegsmann, *Ber. Bunsenges. Phys. Chem.*, **72**, 706 (1968).
(6) A. N. Fletcher and C. A. Heller, *J. Phys. Chem.*, **71**, 3742 (1967).
(7) E. E. Tucker, S. B. Farnham, and S. D. Christian, *J. Phys. Chem.*, **73**, 3820 (1969); referred to as part I.
(8) H. C. van Ness, J. vanWinkle, H. H. Richtol, and H. B. Hollinger, *J. Phys. Chem.*, **71**, 1483 (1967).
(9) N. D. Coggeshall and E. L. Saier, *J. Amer. Chem. Soc.*, **73**, 5414 (1951).
(10) M. Saunders and J. B. Hyne, *J. Chem. Phys.*, **29**, 1319 (1958).
(11) U. Liddel and E. D. Becker, *Spectrochim. Acta*, **10**, 70 (1957).
(12) J. Timmermans, "Physico-Chemical Constants of Pure Organic Compounds," Vol. 2, Elsevier, Amsterdam, 1965.
(13) C. A. Swenson, *J. Phys. Chem.*, **71**, 3108 (1967).
(14) G. P. Hoover, E. A. Robinson, R. S. McQuate, H. D. Schreiber, and J. N. Spencer, *J. Phys. Chem.*, **73**, 4027 (1969).
(15) Listings of vapor pressure, proton magnetic resonance, and infrared data for *t*-BuOH solutions in hexadecane will appear immediately following this article in the microfilm edition of this volume of the journal. Single copies may be obtained from the Business Operations Office, Books and Journals Division, American Chemical Society, 1155 Sixteenth St., N.W., Washington, D. C. 20036. Remit check or money order for $4.00 for photocopy or $2.00 for microfiche, referring to code number JPC-73-1783.
(16) As in ref 7, it is noted that the use of total *t*-BuOH pressure in place of monomer pressure involves an error no larger than 1% in vapor pressure monomer at the maximum pressures used in the present study. We have made a slight correction for vapor association using extrapolated values from the work of E. T. Beynon and J. J. McKetta, *J. Phys. Chem.*, 67, 2761 (1963). We emphasize the point that using either corrected pressures or total *t*-BuOH pressures—although changing slightly the absolute values of equilibrium constants—makes no difference in the hierarchy of standard deviations for various fits of the vapor pressure data.
(17) M. Davies and D. K. Thomas, *J. Phys. Chem.*, **60**, 673 (1956).
(18) L. A. LaPlanche, H. B. Thompson, and M. T. Rogers, *J. Phys. Chem.*, **69**, 1482 (1965).
(19) R. D. Grigsby, Ph.D. Dissertation, Oklahoma University, 1966.
(20) L. L. Graham and C. Y. Chang, *J. Phys. Chem.*, **75**, 776 (1971).

(21) R. Ginell and J. Shurgan, *J. Chem. Phys.*, **23**, 964 (1955).
(22) H. S. Frank and W. Y. Wen, *Discuss. Faraday Soc.*, **24**, 133 (1957).
(23) P. A. Kollman and L. C. Allen, *Chem. Pev.*, **72**, 283 (1972).
(24) G. C. Pimentel and A. L. McClellan, *Annu. Rev. Phys. Chem.*, **22**, 347 (1971).
(25) S. D. Christian and E. E. Tucker, unpublished work.
(26) J. C. Davis, Jr., K. S. Pitzer, and C. N. R. Rao, *J. Phys. Chem.*, **64**, 1744 (1960).
(27) E. Lippert, *Ber. Bunsenges. Phys. Chem.*, **67**, 267 (1963).
(28) H. S. Gutowsky and A. Saika, *J. Chem. Phys.*, **21**, 1688 (1953).
(29) J. C. Davis, Jr., and K. K. Deb, *Advan. Magn. Resonance*, **4**, 201 (1970).
(30) A. N. Fletcher, *J. Phys. Chem.*, **76**, 2562 (1972).
(31) R. Mecke, *Discuss. Faraday Soc.*, **9**, 161 (1950).
(32) L. D. Bellamy and R. J. Pace, *Spectrochim. Acta*, **22**, 525 (1966).
(33) H. Dunken and H. Fritzsche, *Spectrochim. Acta*, **20**, 785 (1964).
(34) K. B. Whetsel and J. H. Lady in "Spectrometry of Fuels," Plenum Press, New York, N. Y., 1970, p 259.
(35) E. D. Becker, U. Liddel, and J. Shoolery, *J. Mol. Spectrosc.*, **2**, 1 (1958).
(36) R. M. Hammaker, R. M. Clegg, L. K. Patterson, P. E. Rider, and S. L. Rock, *J. Phys. Chem.*, **72**, 1837 (1968).
(37) L. B. Magnusson, *J. Phys. Chem.*, **74**, 4221 (1970).
(38) Ignoring the fact that the concentration dependence of the OH chemical shift below 0.01 *M* indicates only trimer formation for *t*-BuOH in CCl_4 solution, we may calculate—by the limiting slope method—an apparent dimer constant. Using a chemical shift value calculated from pmr data on a hindered alcohol (E. D. Becker, unpublished work) we arrive at an apparent dimer constant of 0.25 M^{-1}.
(39) M. Van Thiel, E. D. Becker, and G. C. Pimentel, *J. Chem. Phys.*, **27**, 95 (1957).
(40) A. J. Barnes and H. E. Hallam, *Trans. Faraday Soc.*, **66**, 1920 (1970).
(41) F. A. Smith and E. C. Creitz, *J. Res. Nat. Bur. Stand.*, **46**, 145 (1951).
(42) W. B. Dixon, *J. Phys. Chem.*, **74**, 1396 (1970).
(43) E. E. Tucker, unpublished work.
(44) E. D. Becker, *Spectrochim. Acta*, **17**, 436 (1961).
(45) E. E. Tucker, Ph.D. Dissertation, Oklahoma University, 1969.
(46) S. B. Farnham, Ph.D. Dissertation, Oklahoma University, 1970.

Heteroconjugation of Inorganic Anions in Nonaqueous Solvents. I. Perchlorate and Halide Complexes of 1,2-Dihydroxybenzene

Lajos Barcza[1] and Michael T. Pope*

Department of Chemistry, Georgetown University, Washington, D. C. 20007 *(Received February 8, 1973)*

Heteroconjugates of 1,2-dihydroxybenzene (pyrocatechol) with halide and perchlorate anions in nitromethane solution have been investigated by nmr spectroscopy. The computed formation constants (at 37°) of the 1:1 complexes are Cl^-, 418; Br^-, 187; I^-, 27.8; and ClO_4^-, 11.2 M^{-1}. It is proposed that the relatively high stabilities are due to chelate type, twin hydrogen bonds between the pyrocatechol and the anions. Although a stability constant could be calculated for the "inert" perchlorate ion, no interaction could be detected between pyrocatechol and the heteropoly 12-molybdophosphate and 12-molybdosilicate anions.

Introduction

Heteroconjugation in inert solvents of hydrogen bond donors (HB) to anions (A^-)

$$A^- + nHB \rightleftharpoons A(HB)_n^- \quad (1)$$

has been extensively investigated in recent years.[2] Formation constants

$$K = [A(HB)_n^-]/[A^-][HB]^n \quad (2)$$

where $n = 1$ or, rarely, 2, are available for few systems involving inorganic anions other than the halides, however. A number of heteropoly molybdate and tungstate anions, as salts or free acids, are soluble in nonaqueous solvents, and we became interested in the possibility of forming relatively stable heteroconjugates in connection with an investigation of the reactions of these anions with organic substrates. Since the structures[3] of isopoly and heteropoly anions resemble fragments of metal oxide lattices,[4] heteroconjugation presents a way of studying, in homogeneous solution, the interactions of neutral molecules with metal oxide surfaces. Such studies can lead to an understanding of the catalytic activities of both oxides and polyanions.

We report here the formation constants of some inorganic anions with 1,2-dihydroxybenzene (pyrocatechol) in nitromethane as determined by nmr spectroscopy. Pyrocatechol was chosen as the hydrogen bond donor in the hope that it would form chelate type heteroconjugates. Such complexes would be expected to have greater stabilities than singly bonded species, and their formation might be detected even in the polar solvents needed for the polyanion salts.

Experimental Section

Pyrocatechol and the tetra-*n*-butylammonium salts (chloride, iodide, and perchlorate) were obtained from J. T. Baker Chemical Co. These compounds and tetraethylammonium bromide (Aldrich) were dried in a vacuum desiccator over silica gel before use.

Tetrabutylammonium hexamolybdate, $(Bu_4N)_2Mo_6O_{19}$, was prepared according to the method of Fuchs and Jahr.[5] Tetrabutylammonium salts of 12-molybdophosphate and 12-molybdosilicate anions, $(Bu_4N)_3PMo_{12}O_{40}$ and $(Bu_4N)_4SiMo_{12}O_{40}$, were precipitated from aqueous solutions of the sodium salts or free acids by addition of tetrabutylammonium chloride solution. The precipitated salts were recrystallized twice from acetonitrile. The three polyanion salts gave satisfactory C, H, and N analyses, and their infrared spectra showed that they were essentially unsolvated.

Nitromethane (Baker) was dried successively over Drierite and Molecular Sieve Type 5A, and then distilled. The fraction boiling at 101 ± 0.5° was used.

Solutions for nmr were prepared freshly by direct weighing, and contained TMS as an internal standard. The probe temperature of the Varian A-60 spectrometer used was 37 ± 1°.

Calculations of K and $\Delta_{AH_2B^-}$ (defined below) were made on a Hewlett-Packard 9100B Desk Computer.

Results

The chemical shift of the α-methylene protons of the tetrabutylammonium ion was found to be unaffected by the presence of various concentrations of the isopoly or heteropoly molybdate anions, and indicates no significant ion pairing of these species in nitromethane.

The extent of heteroconjugation of the pyrocatechol was determined from the variation of the chemical shift of the phenolic protons (δ_{H_2B}, 6.37). In preliminary experiments it was established that δ_{H_2B} was independent of concentration in the range used, 25–140 mM. Measurements of the relative chemical shifts, $\Delta_M = \delta_M - \delta_{H_2B}$, where δ_M is the observed shift in the presence of anion, were made on solutions containing added quantities of tetrabutylammonium salt. The molar ratio [anion]/[pyrocatechol] was varied from 0.13 to 3.6 and Δ_M ranged from 0.02 to 2.93 ppm for the perchlorate and halide ions. There was no detectable shift of the phenolic proton resonance in the presence of the heteropoly molybdate ions. (Because of the poorer molar solubility of these anions, their highest concentrations and so the ranges of the [anion]/[pyrocatechol] ratios were less than those of the other anions.) In the case of $(Bu_4N)_2Mo_6O_{19}$, a redox reaction occurred which is being investigated further.

The heteroconjugation constants were computed from the following equations[6]

$$C_{H_2B} = [H_2B] + K[H_2B][A^-] \quad (3)$$

$$C_{A^-} = [A^-] + K[H_2B][A^-] \quad (4)$$

$$\Delta_M C_{H_2B} = \Delta_{AH_2B^-} K[H_2B][A^-] \quad (5)$$

where C_{H_2B} and C_{A^-} are the analytical concentrations of pyrocatechol and anion, respectively, and $\Delta_{AH_2B^-}$ is the relative chemical shift of the fully complexed pyrocatechol. K is defined in eq 2. Equations 3–5 were solved for K (and $\Delta_{AH_2B^-}$) by an iterative procedure and the final results are presented in Table I.

TABLE I: Formation Constants of Heteroconjugates of Pyrocatechol with Inorganic Anions in Nitromethane at 37°

Anion	K, M^{-1}	Anion	K, M^{-1}
Cl^-	418 ± 19	I^-	27.8 ± 2.5
Br^-	187 ± 10	ClO_4^-	11.2 ± 0.8

Discussion

The stabilities of the halide complexes follow the trend observed by Lund[7] and by Green, *et al.*[8] The latter workers reported the following formation constants for complexes with 1-phenylethanol in carbon tetrachloride: Cl^-, 130 ± 100; Br^-, 39 ± 14; I^-, 12 ± 3. Data for phenol heteroconjugates are rare, but in the same paper[8] the formation constant for the Br^-–4-methylphenol complex is given as 32 ± 8 M^{-1}. Since we observe a much higher stability for the corresponding pyrocatechol complex, and since this was also measured in a less inert solvent than carbon tetrachloride, we conclude that the pyrocatechol has indeed formed two (chelate type) hydrogen bonds to the anion. In the only other reported study of heteroconjugation by a diphenol, Kolthoff and Chantooni[9] demonstrated the formation of a 2:1 complex, $A_2(H_2B)^{2-}$, of resorcinol (1,3-dihydroxybenzene) with 3,5-dinitrobenzoate; in this system chelation is prevented by steric factors.

The relatively high stabilities of the pyrocatechol complexes allow us to measure the formation constant of a perchlorate heteroconjugate. To our knowledge, this is the first quantitative evidence for hydrogen bonding to the perchlorate ion, although Lund[6] has previously noted a slight interaction between *p*-cresol and perchlorate. There seems to be no reason why perchlorate heteroconjugation should not be more widespread and we are examining other systems.

It is commonly asserted that heteropoly anions, particularly those with the almost spherical Keggin structure, are unsolvated in aqueous solution and do not participate in hydrogen bonding in the crystalline state. Various lines of experimental evidence, including viscosity[10] and diffusion studies,[11] and crystal structure determinations,[3] tend to support that assertion. The results of the present research demonstrate unambiguously that 12-molybdosilicate and 12-molybdophosphate anions are less susceptible to hydrogen bonding than is perchlorate ion. Since there is no apparent steric hindrance to heteroconjugation, these results confirm the very low surface charge density of such polyanions.

Acknowledgments. The support of this research by AFOSR, through Grant No. AF 70-1833, is gratefully acknowledged.

References and Notes

(1) Present address, Institute of Inorganic and Analytical Chemistry, L. Eötvös University, Budapest, Hungary.
(2) M. M. Davis, *Nat. Bur. Stand. (U. S.), Monogr.* **No. 105** (1968).
(3) H. T. Evans, Jr., *Perspect. Struct. Chem.*, **4**, 1 (1971).
(4) L. C. W. Baker, "Advances in the Chemistry of Coordination Compounds," S. Kirschner, Ed., Macmillan, New York, N. Y., 1961, p 604.
(5) J. Fuchs and K. Jahr, *Z. Naturforsch. B*, **23**, 1380 (1968).
(6) These equations do not take into account the effects of cation–anion association. In the solutions that were used such association is negligible: R. L. Buckson and S. G. Smith, *J. Phys. Chem.*, **68**, 1875 (1964); T. Kenjo and R. M. Diamond, *ibid.* **76**, 2454 (1972).
(7) H. Lund, *Acta Chem. Scand.*, **12**, 298 (1958).
(8) R. D. Green, J. S. Martin, W. B. McG. Cassie, and J. B. Hyne, *Can. J. Chem.*, **47**, 1639 (1959).
(9) I. M. Kolthoff and M. K. Chantooni, Jr., *J. Amer. Chem. Soc.*, **85**, 426 (1963).
(10) T. Kurucsev, A. M. Sargeson, and B. O. West, *J. Phys. Chem.*, **61**, 1569 (1957).
(11) L. C. W. Baker and M. T. Pope, *J. Amer. Chem. Soc.*, **82**, 4176 (1960).

Single Ion Enthalpies of Transfer from Water to Aqueous Dimethyl Sulfoxide Solutions[1]

Richard Fuchs* and C. Patrick Hagan

Department of Chemistry, University of Houston, Houston, Texas 77004 *(Received February 26, 1973)*

Enthalpies of solution of tetraphenylphosphonium bromide, sodium tetraphenylborate, sodium bromide, sodium iodide, sodium hydroxide, and tetra-*n*-butylammonium chloride, bromide, and iodide have been measured at 25° in water, DMSO, and seven aqueous DMSO mixtures. From the extrathermodynamic assumption $\Delta\Delta H_s(Ph_4P^+) = \Delta\Delta H_s(^-BPh_4)$, single ion enthalpies of transfer from water to aqueous DMSO mixtures have been calculated for Ph_4P^+, $^-BPh_4$, Bu_4N^+, Na^+, OH^-, Cl^-, Br^-, and I^- ions. $\Delta\Delta H_s$ is positive for Bu_4N^+ ion and negative for Na^+ ion. For chloride, bromide, and hydroxide ions $\Delta\Delta H_s$ is slightly negative for highly aqueous solutions, but becomes positive as DMSO concentration increases.

In recent years there has been a great deal of interest in the changes in solvation that ions undergo upon transfer from a protonic solvent such as water or an alcohol to a dipolar aprotic solvent such as dimethyl sulfoxide. Much of this interest has been generated by the observation that the rates of many organic reactions involving anions are greatly enhanced when the reaction medium is a dipolar aprotic solvent rather than a protonic solvent.[2] The observed rate changes upon solvent transfer have often been attributed to changes in solvation of the reactant anion. In cases where the electrolyte that serves as the anion source is only slightly soluble in dipolar aprotic solvents, it is advantageous to use a protic–dipolar aprotic solvent mixture as the reaction medium. Mixtures of DMSO with water or alcohols have been frequently used.[2]

The nature of aqueous DMSO solutions have received considerable attention. Lindberg and Kenttamaa,[3] and Cowie and Toporowski[4] have attributed the deviations from ideality of viscosities, densities, refractive indicies, and enthalpies of mixing for aqueous DMSO solutions to association interactions between water and DMSO. These interactions are at a maximum when the water–DMSO molar ratio is 2:1. Pulsed nmr studies of aqueous DMSO solutions[5] indicate a minimum of molecular mobility (both rotational and translational) at approximately 0.65 mol fraction of water. Aqueous DMSO solutions are highly structured, and evidence has been presented[6,7] that water hydrogen bonds more strongly to DMSO than to itself. The results of neutron inelastic scattering and X-ray experiments[7] have been interpreted to indicate that addition of small amounts of DMSO to water promotes water structure. Water–water hydrogen bonds are "rigidified" rather than being broken. At higher concentrations of DMSO the water structure is broken down due to water–DMSO interactions. A recent study of the partial molar enthalpies of solution of water and DMSO in mixtures of the two[8] supports the hypothesis that large amounts of water destroy DMSO structure while small amounts of DMSO promote water structure.

Although the solvation of ions in water and in DMSO has been quite extensively studied, little information has appeared in the literature concerning the solvation of ions in the mixtures. The fact that aqueous DMSO solutions containing an anion form extremely powerful kinetic base systems[9] has been interpreted to indicate that anions are only weakly solvated in aqueous DMSO. Fuchs and Plumlee[10] have studied enthalpies of transfer of ions in the H_2O–DMSO system, but their work covered only a limited range of DMSO-rich mixtures.

Results

The enthalpies of solution (ΔH_s) of tetraphenylphosphonium bromide ($Ph_4P^+Br^-$), sodium tetraphenylborate ($Na^+BPh_4^-$), sodium bromide, sodium iodide, sodium hydroxide, and tetra-*n*-butylammonium chloride ($Bu_4N^+Cl^-$), bromide, and iodide have been measured at 25° in water, DMSO, and seven aqueous DMSO mixtures. ΔH_s values are presented in Table I. The concentration range of the salts in the solvent was 1×10^{-4}–5×10^{-4} *M* except for NaOH and NaBr which were 5×10^{-4}–1×10^{-3} *M*. No dependence of the molar enthalpy of solution on concentration was observed within these concentration ranges, with the exception of Bu_4NI in several of the highly aqueous solvents.

From the enthalpies of solution the single ion enthalpies of transfer ($\Delta\Delta H_s$) from water to aqueous DMSO mixtures have been calculated using the extrathermodynamic assumption $\Delta\Delta H_s(Ph_4P^+) = \Delta\Delta H_s(^-BPh_4)$. The single ion transfer values were determined from the following relationships:

$$\Delta\Delta H_s(Ph_4P^+) = \Delta\Delta H_s(^-BPh_4) = \tfrac{1}{2}[\Delta\Delta H_s(Ph_4PBr) + \Delta\Delta H_s(NaBPh_4) - \Delta\Delta H_s(NaBr)]$$

$$\Delta\Delta H_s(Br^-) = \Delta\Delta H_s(Ph_4PBr) - \Delta\Delta H_s(Ph_4P^+)$$

$$\Delta\Delta H_s(Na^+) = \Delta\Delta H_s(NaBPh_4) - \Delta\Delta H_s(^-BPh_4)$$

$$\Delta\Delta H_s(n\text{-}Bu_4N^+) = \Delta\Delta H_s(n\text{-}Bu_4NBr) - \Delta\Delta H_s(Br^-)$$

$$\Delta\Delta H_s(Cl^-) = \Delta\Delta H_s(n\text{-}Bu_4NCl) - \Delta\Delta H_s(n\text{-}Bu_4N^+)$$

$$\Delta\Delta H_s(^-OH) = \Delta\Delta H_s(NaOH) - \Delta\Delta H_s(Na^+)$$

$$\Delta\Delta H_s(I^-) = \Delta\Delta H_s(NaI) - \Delta\Delta H_s(Na^+)$$

Discussion

The Tetraphenylphosphonium Tetraphenylborate Assumption. Parker[11] has recently commented on the essential equivalence of four types of extrathermodynamic as-

TABLE I: Enthalpies of Solution at 25°[a]

% DMSO[b]	Ph_4PBr[c]	$NaBPh_4$[c]	NaBr	Bu_4NCl[d]	Bu_4NBr[d]	Bu_4NI[d]	NaOH	NaI
H_2O	1.9 ± 0.1[e]	−4.5 ± 0.1[f]	−0.12 ± 0.01[g]	−7.4 ± 0.1[h]	−2.0 ± 0.1[i]	4.0 ± 0.1[j,k]	−10.5 ± 0.2	−1.8 ± 0.1[l]
15	4.0 ± 0.1	−1.3 ± 0.1	−0.51 ± 0.03	−5.3 ± 0.1	−0.27 ± 0.05	5.3 ± 0.3[k]	−10.5 ± 0.1	−2.3 ± 0.1
30	4.6 ± 0.1	−0.46 ± 0.03	−0.74 ± 0.01	−2.8 ± 0.1	2.0 ± 0.1	8.5 ± 0.2[k]	−10.4 ± 0.1	−2.8 ± 0.1
50	5.2 ± 0.1	−1.3 ± 0.1	−1.1 ± 0.1	1.4 ± 0.1	5.0 ± 0.1	11.0 ± 0.1[k]	−7.3 ± 0.1	−3.9 ± 0.1
60	4.7 ± 0.1	−4.2 ± 0.1	−1.6 ± 0.1	3.0 ± 0.1	6.8 ± 0.1	11.6 ± 0.1[k]	−6.4 ± 0.1	−4.9 ± 0.1
65	3.7 ± 0.1	−6.0 ± 0.1	−1.9 ± 0.1	3.1 ± 0.1	7.0 ± 0.1	11.9 ± 0.1[h]	−5.7 ± 0.1	−5.4 ± 0.1
70	3.8 ± 0.1	−7.5 ± 0.1	−2.6 ± 0.1	3.6 ± 0.1	7.3 ± 0.3	11.9 ± 0.1[k]	−4.1 ± 0.1	−6.1 ± 0.1
80	2.5 ± 0.1	−10.8 ± 0.2	−3.7 ± 0.1	4.3 ± 0.2	6.7 ± 0.1	11.2 ± 0.3	−3.4 ± 0.1	−7.8 ± 0.1
DMSO	0.34 ± 0.07	−14.3 ± 0.1[m]	−6.2 ± 0.1	2.6 ± 0.1[n]	4.3 ± 0.1[o]	7.2 ± 0.1[p]	0.0	−11.5 ± 0.3[q]

[a] Values of ΔH_s in kcal mol^{-1} are averages of 3 to 12 determinations. [b] Per cent by volume; mole per cent DMSO in mixtures 0, 3, 7, 20, 27.5, 32, 37, 50, 100. [c] Ph = C_6H_5. [d] Bu = *n*-C_4H_9. [e] Average deviation. [f] −4.77 (ref 15). [g] −0.14 [G. Choux and R. L. Benoit, *J. Amer. Chem. Soc.*, **91**, 6221 (1969)]. [h] −7.14 (ref 16); −7.3 (ref 12). [i] −2.02 (ref 16); −2.2 (ref 12). [j] 3.8 (ref 12). [k] Concentration dependent. Not extrapolated to c = 0, so actual error may exceed average deviation (<1.0 kcal mol^{-1}). [l] −1.9 (ref 12); −1.80 (Benoit, footnote *g*). [m] −14.23 (ref 15); −14.2 (ref 12). [n] 3.22 (ref 12); 3.7 (ref 16); 5.1 (ref 12). [o] 4.95 (ref 16); 7.27 (ref 16); 7.2 (ref 12). [p] 11.5 (ref 12); −11.53 (ref 15).

sumptions used in the determination of free energies and enthalpies of transfer of ions from solvent to solvent. Among the $R_4M^+R_4B^-$ assumptions we had previously noted close correlation between the tetrabutylammonium tetrabutylborate and tetrapentylammonium tetrapentylborate results, and the poor agreement of the tetraphenylarsonium tetraphenylborate results with these.[12] We believe that each of these assumptions is about equally valid in principle.[13] However, Ph_4AsCl and $NaBPh_4$ have concentration-dependent values of ΔH_s, particularly in methanol, and large experimental uncertainties result.[12] Friedman[14] has remeasured a number of ΔH_s values in MeOH an DMF, and has derived a set of internally consistent single ion enthalpies of transfer. Unfortunately the single ion values are not consistent with the published enthalpies of transfer of LiBr and LiI,[12] nor with the single ion values derived[12] from the Bu_4NBBu_4 and $(C_5H_{11})_4NB(C_5H_{11})_4$ assumptions for Li^+, Bu_4N^+, and Cl^-, among others. Some of the differences are as large as 4 kcal mol^{-1}. Similar inconsistencies occur for the transfer of ions from MeOH to DMSO. Internal consistency within a set of single ion data is an assurance that all of the ΔH_s measurements are correct *except* those made on the two salts on which the single ion assumption is based, such as $NaBPh_4$ and Ph_4AsCl. If the latter ΔH_s values are incorrect, this results in incorrect values for $\Delta\Delta H_s(Ph_4As^+)$ and $\Delta\Delta H_s(Ph_4B^-)$, from which an incorrect value of $\Delta\Delta H_s(Na^+)$ is derived. If the Na^+ value were, for example, 2 kcal mol^{-1} too endothermic, a Br^- value 2 kcal mol^{-1} too exothermic would result. In turn, other cation and anion $\Delta\Delta H_s$ values would be calculated, each having the same error as Na^+ and Br^-, respectively. When these $\Delta\Delta H_s(M^+)$ and $\Delta\Delta H_s(X^-)$ are added, the values are nevertheless found to agree with the (correct) values of $\Delta\Delta H_s(MX)$. However, it is ΔH_s of the salts Ph_4AsCl and $NaBPh_4$ for which a wide variety of values have been reported in MeOH and DMF. It is, of course, possible that the data[12] for Bu_4NBBu_4, $(C_5H_{11})_4NB(C_5H_{11})_4$, and the lithium halides in MeOH and DMF are incorrect, but until the inconsistencies are explained, Friedman's single ion $\Delta\Delta H_s$ in these solvents must be accepted with reservations.

Arnett has observed a concentration dependent value of ΔH_s for Ph_4AsI in water.[15]

Because Bu_4NBBu_4 is insoluble in highly aqueous solutions (and $NaBBu_4$ is unstable) it was necessary in the present study to use an assumption involving phenyl-substituted salts. We have chosen the assumption $\Delta\Delta(Ph_4P^+) = \Delta\Delta H_s(Ph_4B^-)$ because the salt tetraphenylphosphonium bromide is readily available, and the ΔH_s value in water is concentration independent. (Preliminary results suggest that this is also true in methanol.) Single ion $\Delta\Delta H_s$ values for the transfer from DMSO to 80% DMSO, based on this assumption, are in reasonably good agreement with values from the Bu_4NBBu_4 assumption.[10] Friedman has reported that $\Delta\Delta H_s$ ($H_2O \rightarrow$ DMSO)[16] and $\Delta\Delta H_s$(MeOH → DMF)[14] values for Ph_4As^+ and PhP^+ are rather similar. This is confirmed by the close correspondence between Arnett's[15] single ion $\Delta\Delta H_s(H_2O \rightarrow$ DMSO) based on $\Delta\Delta H_s(Ph_4As^+) = \Delta\Delta H_s(Ph_4B^-)$, and those in Table II derived from $\Delta\Delta H_s(Ph_4P^+) = \Delta\Delta H_s(Ph_4B^-)$.

The use of any $Ph_4M^+Ph_4B^-$ assumption is based on the relationship $\Delta\Delta H_s(Ph_4M^+) = \Delta\Delta H_s(Ph_4B^-) = \frac{1}{2}[\Delta\Delta H_s(Ph_4MX) + \Delta\Delta H_s(NaBPh_4) - \Delta\Delta H_s(NaX)]$. Another distinct advantage in the use of a bromide or iodide salt, such as Ph_4PBr, rather than Ph_4AsCl, is the sol-

TABLE II. Single Ion Enthalpies of Transfer[a] from Water to Aqueous DMSO at 25°

% DMSO[b]	Ph_4P^+ [c]	Bu_4N^+ [d]	Na^+	^-OH	Cl^-	Br^-	I^-
15	2.8	2.4	0.4	−0.4	−0.3	−0.7	−1.0
30	4.1	5.4	0.9	−0.8	−0.8	−1.4	−1.9
50	3.7	8.4	−0.5	3.7	0.4	−0.5	−1.6
60	2.3	8.3	−2.0	6.1	2.1	0.5	−1.1
65	1.0	8.2	−2.5	7.3	2.3	0.8	−1.1
70	0.7	8.1	−3.7	10.1	2.9	1.2	−0.6
80	−1.0	7.1	−5.3	12.4	4.6	1.6	−0.7
100	−2.6[e]	5.3[f]	−7.2[g]	17.7	4.7[h]	1.0[i]	−2.5[j]

[a] The estimated error in single ion $\Delta\Delta H_s$ values is 0.2–0.3 kcal mol^{-1}. These standard deviations were calculated as the square root of the sum of the squares of the average deviations of all values in Table I involved in the determination of the single ion value. [b] Per cent by volume. [c] Or Ph_4B^-. [d] Bu = n-C_4H_9. [e] −2.3 (ref 16); reported values for Ph_4As^+ −2.84 (ref 16), −2.32 (ref 15). [f] 6.05 (ref 16). [g] −6.62 (ref 16), −7.15 (ref 15). [h] 4.49 (ref 16), 4.89 (ref 15). [i] 0.83 (ref 16), 1.34 (ref 15). [j] −3.05 (ref 16), −2.52 (ref 15).

ubility of NaBr (but not NaCl) in most polar solvents. This makes $\Delta\Delta H_s$(NaX) easily obtainable by direct measurement of two ΔH_s values. The use of tetraphenylphosphonium bromide rather than arsonium salts clearly provides a number of experimental advantages, and it is recommended.

Solvation of Ions in Aqueous DMSO. Changes in ion solvation resulting from solvent changes are reflected in the free energy of transfer. When the transfer involves organic solvents, $\Delta\Delta G_s$ is primarily determined by $\Delta\Delta H_s$.[17] However, when water is one of the solvents the entropy term ($T\Delta S$) may be at least equally important.[17] In the following discussion enthalpy rather than free-energy changes will be considered, and the term "solvation" refers only to that portion of solvation (change) which results from the enthalpy of transfer.

The addition of DMSO to water causes desolvation of the large tetrabutylammonium ion over the entire solvent composition range. A maximum desolvation of about 8 kcal mol^{-1} occurs when the DMSO concentration is about 50–60% by volume. This solvent composition is very close to the DMSO·$2H_2O$ solvent composition (65% by volume DMSO) at which aqueous DMSO solutions show maximum solvent structure.[3,4] Further addition of DMSO results in a slight increase in Bu_4N^+ solvation, but even in pure DMSO the ion is about 5.3 kcal mol^{-1} less solvated than in water. Apparently the large, symmetrical ion does not interact strongly with either water or DMSO,[18] and the extent to which the ion is solvated in aqueous DMSO mixtures is quite sensitive to the amount of structure of the solvent. Since aqueous DMSO mixtures are more highly structured than either water or DMSO[3,4,6,7] the ion is desolvated, relative to its solvation in water, in all aqueous DMSO mixtures. All ions, especially large ones, tend to lose "apparent" solvation as solvent–solvent interactions increase. The ion–solvent attractions may remain unchanged, but more energy is needed to make "holes" in the solvent to accommodate the ions. The energy required increases with the size of the hole needed.

The large Ph_4P^+ and $^-BPh_4$ ions might be expected to show solvation behavior similar to that of Bu_4N^+ ion. Ph_4P^+ reaches its maximum desolvation at about 30% by volume DMSO, well below the DMSO·$2H_2O$ solvent composition. DMSO in excess of 30% by volume results in enhanced solvation of the ion, which in pure DMSO is almost 3 kcal mol^{-1} more solvated than in water. Unlike the Bu_4N^+ ion, Ph_4P^+ probably interacts with the DMSO molecule through large dipole-induced dipole forces[13] resulting in increased solvation of the ion as the DMSO content of the aqueous mixture increases.

A similar situation occurs in the case of the sodium ion. Maximum desolvation occurs at about 30% DMSO, and the ion becomes more strongly solvated upon the further addition of DMSO. The sodium ion can interact strongly with the DMSO molecule through ion–dipole interactions. In pure DMSO the ion is about 7 kcal mol^{-1} more solvated than in water, as would be expected from the greater basicity of DMSO.

Addition of 30–40% DMSO to water causes an increase of about 1–2 kcal mol^{-1} in the solvation of the anions. Perhaps this increase in solvation is due to the structure-promoting effect on water of small amounts of added DMSO. The increase in water structure can occur through increased water–water hydrogen bonding. Because hydrogen bonding is the principal interaction responsible for the solvation of small anions in water, the enhanced ability of water to donate hydrogen bonds when small amounts of DMSO are present results in increased solvation of the anions. The mechanism by which small amounts of DMSO are able to promote water structure is not understood.

When the concentration of added DMSO exceeds 30–40% the hydroxide ion is increasingly desolvated, and in pure DMSO the ion is almost 18 kcal mol^{-1} less solvated than in water. The halide ions are also desolvated with increasing DMSO concentration, but reach a maximum desolvation at about 80% by volume DMSO. In solvent mixtures containing greater than 80% DMSO chloride ion undergoes little change in solvation, bromide ion gains about 1 kcal mol^{-1}, and iodide ion gains about 2 kcal mol^{-1}. These mixtures contain a molar excess of DMSO. The DMSO·$2H_2O$ concentration is 65% by volume DMSO. The solvation behavior of the anions in solvent mixtures containing greater than 80% DMSO reflects the relatively strong interactions of DMSO with large polarizable anions. For example, upon transfer from 80% DMSO to pure DMSO hydroxide ion is desolvated by 6 kcal mol^{-1} while the larger, more polarizable iodide ion is *more* solvated by about 2 kcal mol^{-1}.

Experimental Section

Reagents. The dimethyl sulfoxide was Baker Analyzed reagent grade stated to contain 0.04% water. The DMSO was further dried by storing over 4A molecular sieve. Aqueous DMSO mixtures were prepared volumetrically with distilled water. Tetraphenylphosphonium bromide was dissolved in a 9:1 (v/v) acetone–2-propanol mixture,

reprecipitated by the addition of an equal volume of benzene, and vacuum dried (<0.1 Torr) at 100° (mp 297–298.5°). Sodium tetraphenylborate, sodium bromide, and sodium iodide were vacuum dried at 100° for 24 hr. Sodium hydroxide (assay 99%) was handled in a drybox under dry nitrogen. A small amount was pulverized and dried under vacuum at 100° for 24 hr. Tetra-*n*-butylammonium chloride was dried in a dichloromethane solution with 3A molecular sieve. After decantation and evaporation of the solvent the salt was vacuum dried for 24 hr. Tetra-*n*-butylammonium iodide was recrystallized from a benzene–heptane mixture and dried under vacuum at 50° for 24 hr.

Calorimetry. Except as noted below, the calorimetric procedure was that described previously.[19] Most solid samples were weighed into a sample holder consisting of a short piece of glass tubing to which a polyethylene cap had been fitted. The cap was attached to the glass tubing with a polypropylene thread. The sample holder was attached to an extension tube using a short section of rubber tubing (which is not immersed in solvent) and a closely fitting polypropylene rod was inserted through the extension tube into the sample holder. The sample was introduced near the bottom of the calorimeter by depressing the polypropylene rod to dislodge the polyethylene cap. Because the sample holder was not absolutely vapor tight, all sodium hydroxide samples were weighed into glass bulbs. All other compounds gave the same results with the new sample holder or glass bulbs.

The thermistor inside the calorimeter served as one arm of a Wheatstone bridge. The bridge imbalance signal was led to a digital multimeter (Keithley Model 160) which served as the null meter, and the amplified output voltage was recorded. The calorimeter was immersed in a water bath maintained at 25.00° with regulation to ±0.001°. Samples were weighed to 0.01 mg on a microbalance inside a nitrogen-filled drybox.

The value of 0.0 kcal mol^{-1} reported here for the ΔH_s of sodium hydroxide in DMSO is not believed to be due to failure of sodium hydroxide to dissolve because (a) when the calorimeter was opened no solid sodium hydroxide was observed. We have determined that this amount of sodium hydroxide in DMSO can be seen if it is not dissolved. (b) We have determined the value of ΔH_s for sodium hydroxide in 99% by volume DMSO to be -0.4 ± 0.1 kcal mol^{-1}. (c) A plot of ΔH_s *vs.* per cent DMSO in the solvent for sodium hydroxide extrapolates to a value of $\Delta H_s = 0$ in 100% DMSO.

References and Notes

(1) Support of this research by the Robert A. Welch Foundation (Grant No. E-136) is gratefully acknowledged. Presented at the 3rd International Conference on Non-Aqueous Solvents, East Lansing, Mich., July 5–7, 1972.
(2) For an extensive review and references see A. J. Parker, *Chem. Rev.*, **69**, 1 (1969).
(3) J. J. Lindberg and J. Kenttamaa, *Suomen Kemi.*, **33B**, 104 (1960).
(4) J. M. G. Cowie and P. M. Toporowski, *Can. J. Chem.*, **39**, 2240 (1961).
(5) K. J. Picker and D. J. Tomlinson, *Trans. Faraday Soc.*, **67**, 1302 (1971).
(6) R. Fuchs, J. J. McCrary, and J. J. Bloomfield, *J. Amer. Chem. Soc.*, **83**, 4281 (1961).
(7) G. J. Safford, P. C. Schaffer, P. S. Leung, G. F. Doebbler, G. W. Brady, and E. F. X. Lyden, *J. Chem. Phys.*, **50**, 2140 (1969).
(8) F. Rallo, R. Rodante, and P. Silverstroni, *Thermochim. Acta*, **1**, 311 (1970).
(9) For extensive reviews and references see (a) I. M. Kolthoff and T. B. Reddy, *Inorg. Chem.*, **1**, 189 (1962); (b) R. Stewart and J. P. O'Donnell, *Can. J. Chem.*, **42**, 1681 (1964); (c) K. Bowden, *Chem. Rev.*, **66**, 119 (1966).
(10) R. Fuchs and D. Plumlee, *Thermochim. Acta*, **2**, 515 (1971).
(11) R. Alexander, A. J. Parker, J. H. Sharp, and W. E. Waghorne, *J. Amer. Chem. Soc.*, **94**, 1148 (1972); B. G. Cox and A. J. Parker, *ibid.*, **95**, 402 (1973).
(12) R. Fuchs, J. L. Bear, and R. F. Rodewald, *J. Amer. Chem. Soc.*, **91**, 5797 (1969).
(13) However, see J. F. Coetzee and W. R. Sharpe, *J. Phys. Chem.*, **75**, 3141 (1971).
(14) C. V. Krishnan and H. L. Friedman, *J. Phys. Chem.*, **75**, 3606 (1971).
(15) E. M. Arnett and D. R. McKelvey, *J. Amer. Chem. Soc.*, **88**, 2598 (1966). By careful extrapolation of ΔH_s measurements to c = 0 these authors have obtained single ion values which we believe are quite reliable, and in no case differ by more than 0.3 kcal mol^{-1} from those reported in Table II.
(16) C. V. Krishnan and H. L. Friedman, *J. Phys. Chem.*, **73**, 3934 (1969).
(17) B. G. Cox and A. J. Parker, *J. Amer. Chem. Soc.*, **95**, 402 (1973).
(18) N. P. Yao and D. N. Bennion, *J. Electrochem. Soc.*, **118**, 1097 (1971); *J. Phys. Chem.*, **75**, 1727 (1971).
(19) R. F. Rodewald, K. Mahendran, J. L. Bear, and R. Fuchs, *J. Amer. Chem. Soc.*, **90**, 6698 (1968).

Isotope Effect and the Molecular Mechanism of the Second Viscosity Coefficient of Water

E. McLaughlin

Department of Chemical Engineering, Louisiana State University, Baton Rouge, Louisiana 70803 *(Received March 30, 1972)*

The sound absorption data in water and heavy water are analyzed to yield the second viscosity coefficient which is discussed in terms of the basic molecular mechanistic processes involved compared with those operative in shear viscosity.

Introduction

In the formulation of statistical theories of transport processes in liquids information is required on the molecular mechanisms of transport. One method of obtaining such information is the study of the transport properties of isotopic molecules where the masses and moments of inertia can be altered without significant changes occurring in the parameters of the intermolecular potential. This technique has already been used[1,2] in connection with shear viscosity and thermal conductivity. In the present paper it is used to examine the basic molecular mechanisms in the viscous processes determining the second viscosity coefficients of water.

Viscosity Coefficients

In the absence of external forces the one-dimensional Navier–Stokes equation for an isotropic fluid can be written

$$\frac{Du}{Dt} = -\frac{\partial p}{\partial x} + \eta\nabla^2 u + \frac{\partial}{\partial x}\operatorname{div} v(\eta' + \eta) \qquad (1)$$

where D/Dt is the substantial time derivative, u the x component of the hydrodynamic or center of mass velocity v, p the thermodynamic pressure, and η and η' the first and second viscosity coefficients. The first coefficient of viscosity is more commonly known as the coefficient of shear viscosity. The two coefficients arise naturally in the equation of motion from the assumption of the linear Cauchy–Poisson or generalized Newton's law between stress and rate of strain.[3]

To date the most important experimental source of information on η' and $K = (\eta' + \frac{2}{3}\eta)$ comes from a study of the absorption of sound waves.[4] For the case of plane sound waves where motion is in the x direction alone and the waves are assumed infinitesimal then eq 1 reduces to

$$\rho_0\frac{\partial u}{\partial t} = -\frac{\partial p}{\partial x} + (\eta' + 2\eta)\frac{\partial^2 u}{\partial x^2} \qquad (2)$$

where ρ_0 is the density of the medium before passage of the sound wave. This equation combined with the linearized equations of continuity, energy balance, and equation of state forms a wave equation the solution of which is[5] represented by a damped harmonic wave with an absorption coefficient α_a given by

$$\frac{\alpha_a}{\nu^2} = \frac{2\pi^2}{\rho_0 v_{os}^3}\left[(\eta' + 2\eta) + \frac{(\gamma - 1)\lambda}{c_p}\right] \qquad (3)$$

$$= \frac{2\pi^2}{\rho_0 v_{os}^3}\left[\tfrac{4}{3}\eta + K + \frac{(\gamma - 1)\lambda}{c_p}\right] \qquad (4)$$

ν is the sonic frequency, v_{os} the Laplacian speed of sound, λ the coefficient of thermal conductivity, and γ the specific heat ratio.

Equation 4 shows that the absorption of sound arises from the various dissipative processes associated with the transport phenomena in the fluid. In practice the absorption contribution arising from thermal conduction is negligible compared with that arising from viscous processes and can be discarded. The resulting expression then provides a method of evaluating K or η' from experimental absorption measurements as

$$K = \tfrac{4}{3}[(\alpha_a/\alpha_c) - 1]\eta$$

where α_c is the classical absorption calculated assuming $K = 0$.

Figure 1 gives the experimental sound absorption data of water[6] and heavy water[7] (D_2O) for temperatures in the range between 5 and 50° in the form of the ratio α_a/α_c with the spread on the water results given by Pinkerton included. For the case of heavy water the 15 and 50° points included are based on interpolated and extrapolated values, respectively, of α_c. Examination of this figure shows that although there is considerable scatter the results apparently decrease with increasing temperature, and in what follows values of α_a/α_c from the smooth curves are used in the calculations in order to detect trends as a function of temperature. Table I lists the various viscosity coefficients of water and heavy water. The shear coefficients are from Hardy and Cottingham[8] and the smoothed α_a/α_c values from which K and η' were obtained are also given. Before discussing these results based on continuum mechanics in terms of the molecular processes included, it is necessary to consider the isotope effect which has already been used as a diagnostic criterion in this context.[1,2,9]

Isotope Effect

To obtain some experimental information on the molecular mechanistic processes determining the viscosity coefficients the study of these properties for pairs of isotopic molecules can be used.

If a pair of molecules interact with a potential characterized by two parameters ϵ and σ which are respectively a characteristic energy of interaction and a characteristic molecular diameter then the three viscosity coefficients may be written[9] in the dimensionless form

$$\eta^* = \eta\sigma^2/\sqrt{m\epsilon}$$

$$\eta'^* = \eta'\sigma^2/\sqrt{m\epsilon}$$

TABLE I: Absorption and Viscosity Data for Water and Heavy Water

	Water				Heavy water						
T, °C	η, 10^{-3} kg m^{-1} sec^{-1}	K, 10^{-3} kg m^{-1} sec^{-1}	η', 10^{-3} kg m^{-1} sec^{-1}	α_a/α_c	η_i, 10^{-3} kg m^{-1} sec^{-1}	K_i, 10^{-3} kg m^{-1} sec^{-1}	η_i', 10^{-3} kg m^{-1} sec^{-1}	α_a/α_c	K_i/K	η_i'/η'	η_i/η
5	1.519	4.638	3.625	3.290	1.983	5.102	3.781	2.930	1.100	1.043	1.305
10	1.307	3.813	2.942	3.188	1.675	4.234	3.117	2.896	1.110	1.059	1.282
15	1.139	3.231	2.472	3.128	1.437	3.587	2.629	2.872	1.110	1.063	1.262
20	1.002	2.793	2.125	3.090	1.247	3.079	2.248	2.852	1.102	1.058	1.245
30	0.798	2.169	1.637	3.040	0.973	2.277	1.728	2.832	1.096	1.056	1.219
40	0.653	1.750	1.315	3.010	0.785	1.902	1.379	2.817	1.087	1.049	1.202
50	0.547	1.458	1.093	3.000	0.650	1.567	1.134	2.808	1.075	1.055	1.188

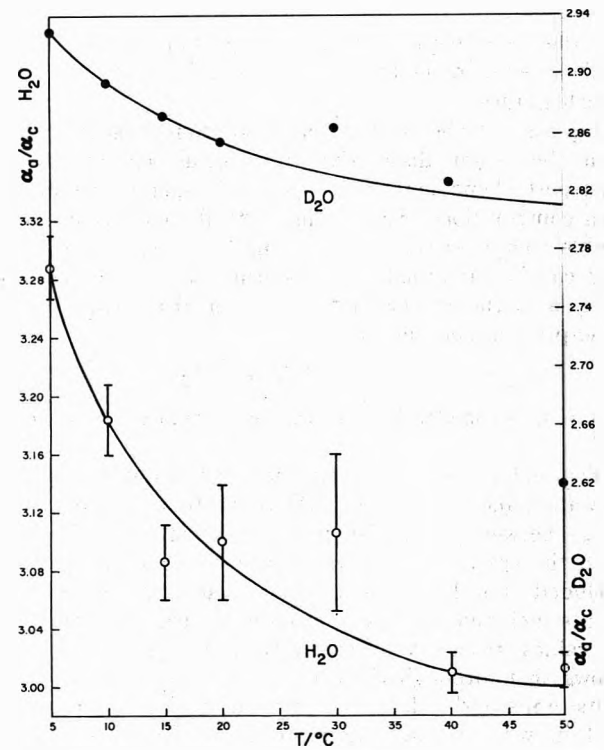

Figure 1. Ratios (α_a/α_c) measured to classical absorption coefficients of water (O) and heavy water (●) as functions of temperature.

$$K^* = K\sigma^2/\sqrt{m\epsilon}$$

where η^*, η'^*, and K^* are universal functions of kT/ϵ and $V/N\sigma^3$ only. For a pair of isotopic molecules where ϵ and σ are virtually identical it follows that

$$\eta_i/\eta = \eta_i'/\eta' = K_i/K = (m_i/m)^{1/2} \qquad (5)$$

where the subscript i refers to the isotopically substituted species.

Equation 5 shows that all three viscosity ratios should be given by the square root of the mass ratio provided[9] the intermolecular potential is spherically symmetric and hence the equation of motion is of the form

$$F = m(\mathrm{d}v/\mathrm{d}t)$$

For nonspherical molecules Pople has pointed out that eq 5 would not be expected to hold as conservation of angular momentum would also have to be considered.

Discussion

Examination of Table I shows for the shear viscosity, as has already been pointed out by Pople, that as the temperature is increased the ratio decreases from its value at the lowest temperature where it is close in magnitude to the square roots of the three principal moments of inertia $(I_{Ai}/I_A)^{1/2} = 1.340$; $(I_{Bi}/I_B)^{1/2} = 1.414$; $(I_{ci}/I_c)^{1/2} = 1.390$. This indicates that rotational motion is an important mechanism for momentum transport in water but that this contribution decreases in importance as the temperature increases. For the second viscosity, however, as in the case of thermal conductivity[1] the ratio η_i'/η_i is, within the experimental accuracy, constant at 1.055 ± 0.004 which corresponds closely to the square root of the mass ratio $(m_i/m)^{1/2} = 1.054$. This suggests that rotational motion is not an important contribution to the mechanism of momentum transfer involved in the second viscosity coefficient. In the case of thermal conductivity it has been suggested[10] that the result there is consistent with the picture that to transfer heat the molecules need only oscillate about their mean equilibrium positions in the temperature gradient which contrasts with the case of shear viscosity where imposition of the velocity gradient $\partial u/\partial y$ will necessarily require that intermolecular forces between adjacent layers are continually disrupted and this is unlikely to occur with the absence of rotational motion.

The acceptance of these conclusions then leads us back to the physical process of the motion involved in div v. As agreement with the square root of the mass law for the second viscosity coefficient implies no rotational motion of the molecules as occurs in shear flow then it is suggested that η' is the proportionality constant in the case where the dilation of the fluid is a change of volume at constant shape where $\sigma_{11} = \sigma_{22} = \sigma_{33} = -\bar{p}$ and the fluid is contracting uniformly with $\partial u/\partial x = \partial v/\partial y = \partial w/\partial z$ such as a uniformly contracting sphere where the molecules do not rotate. When such an element contracts nonuniformly as, for example, in the more general case of a sphere dilating to an ellipse of smaller volume, the normal stresses are then not all equal and η' and η both enter the proportionality between $(\bar{p} - p)$ and $\partial v_i/\partial x_i$ in the form of the bulk viscosity.

References and Notes

(1) E. McLaughlin, *Physica*, **26**, 650 (1960).
(2) J. K. Horrocks, E. McLaughlin, and A. R. Ubbelohde, *Trans. Faraday Soc.*, **59**, 1110 (1963).
(3) J. Serrin, "Handbuch der Physik," Vol. VIII/I, J. Springer, Berlin, 1959, p 178.
(4) L. Rosenhead, *Proc. Roy. Soc., Ser. A*, **266**, 1 (1954).
(5) P. Biquard, *Rev. d'Acoustique*, **1**, 93 (1932).
(6) J. Pinkerton, *Nature (London)*, **160**, 128 (1947).
(7) R. Pancholy, *J. Acoust. Soc. Amer.*, **25**, 1003 (1953).
(8) R. C. Hardy and R. L. Cottingham, *J. Res. Nat. Bur. Stand. U.S.*, **42**, 572 (1949).
(9) J. A. Pople, *Physica*, **19**, 668 (1953).
(10) E. McLaughlin, *Quart. Rev. Chem. Soc.*, **14**, 236 (1960).

Electronic Spectra of Trapped Electrons in Organic Glasses at 4°K. V. Aliphatic Amines

Toshiyasu Ito, Kenji Fueki,*

Department of Synthetic Chemistry, Faculty of Engineering, Nagoya University, Chikusa-ku, Nagoya, Japan

Akira Namiki, and Hirotomo Hase

Research Reactor Institute, Kyoto University, Kumatori-cho, Sennan-gun, Osaka, Japan *(Received December 29, 1972)*

Publication costs assisted by Nagoya University

Optical absorption measurements have been carried out on trapped electrons in aliphatic amine glasses at 4 and 77°K. A slight red shift or no shift of the absorption spectrum at 4°K relative to that at 77°K has been observed for trapped electrons in several amines. The wavelength at the absorption maximum in the optical spectra at 77°K is generally correlated to matrix polarity. A comparison is also made between the efficiency of electron trapping at 4°K and that at 77°K for some of the amines.

Introduction

In the few years we have been studying optical absorption of trapped electrons in organic glasses at 4°K, which include water–ethylene glycol mixtures,[1] methanol and ethanol[2] and their mixtures,[3] methyltetrahydrofuran,[2] and hydrocarbons,[4] and have obtained significant information about the trapped electrons. In this work we extend such optical study to trapped electrons in aliphatic amine glasses. The amines are interesting substances particularly for the following reasons: first, the magnitudes of their permanent dipole moment are significantly smaller than those of alcohols and, in view of matrix polarity, amines bridge the gap between alcohols and hydrocarbons; second, amines have a variety of molecular structure including the primary, secondary, and tertiary amines. In a previous paper[5] we reported the electron spin resonance and preliminary optical absorption measurements on trapped electrons in aliphatic amine glasses at 77°K. Recently we have made a photobleaching study of trapped electrons in the amine glasses at 77°K.[6] In this work we have measured the optical absorption spectra of trapped electrons in several amine glasses at 4°K and those at 77°K which have not been reported. We also include in this paper the optical absorption parameters obtained in this work which are more accurate than those reported in a previous paper.[5] Based on these results we discuss the optical absorption characteristics, the relaxation of electron traps, and the relative efficiency of electron trapping at 4 and 77°K.

Experimental Section

Aliphatic amines (2-methyl-*n*-amylamine, *sec*-butylamine, isopropylamine, isobutylamine, isoamylamine, 1,2-propanediamine, diisopropylamine, *N*-methyl-*n*-butylamine, 3-methylpiperidine, triethylamine, and tripropylamine) were purified by refluxing over potassium hydroxide pellets followed by repeated middle-cut distillation in a nitrogen atmosphere. A middle portion from distillation was treated with sodium blocks and distilled under vacuum on a freshly prepared sodium mirror. Water (5 vol %) was added to some of the samples (isopropylamine, isobutylamine, and isoamylamine) which made the glasses stable.

The purified amines were transferred to quartz optical absorption cells (optical path length, 1.5 or 4 mm), and the samples were irradiated by ^{60}Co γ-rays at 4 and 77°K in the dark. The total dose delivered to the samples was 2.5×10^5 rads at 4°K and 1.7×10^5 or 3.4×10^5 rads at 77°K. Optical absorption spectra were taken on a Shimadzu MPS-50L spectrophotometer at 4 and 77°K.

Results and Discussion

The experimental results are given in Table I and Figures 1–3. Table I summarizes the optical absorption parameters of trapped electrons and the relative efficiency of electron trapping at 4 and 77°K. λ_{max} and $W_{1/2}$ are the wavelength at the absorption maximum and the half-height width of the absorption spectrum, respectively. η is the ratio of the electron trapping efficiency (or trapped electron yield) at 4°K to that at 77°K, and it has been evaluated on the assumption that the trapped electron yield is proportional to the area under the observed absorption curve in the wave number range <25,000 cm^{-1}. Some of the observed absorption spectra are illustrated in Figures 1–3 which represent the primary (2-methyl-*n*-amylamine), secondary (*N*-methyl-*n*-butylamine), and tertiary amine (triethylamine), respectively. Since the experimental data are more comprehensive at 77°K than at 4°K, we will first look at the results obtained at 77°K and then compare these results with those at 4°K.

It can be seen in Table I that the wavelength of maximum absorption, λ_{max}, at 77°K generally depends on the type of amine: ~1000–1200 nm for the primary amines, ~1200–1500 nm for the secondary amines, and ~1700 nm for the tertiary amines. Since the magnitude of the permanent dipole moment is ~1.1 D for the primary amines, ~0.85 D for the secondary amines, and ~0.66 D for the tertiary amines,[7] the trend in λ_{max} mentioned above may be correlated to the magnitudes of the permanent dipole moment of the amines provided that other factors such as the molecular size are similar. In fact, such a correlation has been substantiated in a recent theoretical study on trapped electrons in amine glasses.[8] It is also seen in Table I that λ_{max} depends on the molecular structure of the individual amine. For example, λ_{max} decreases with an increase in the carbon chain length in a series of simi-

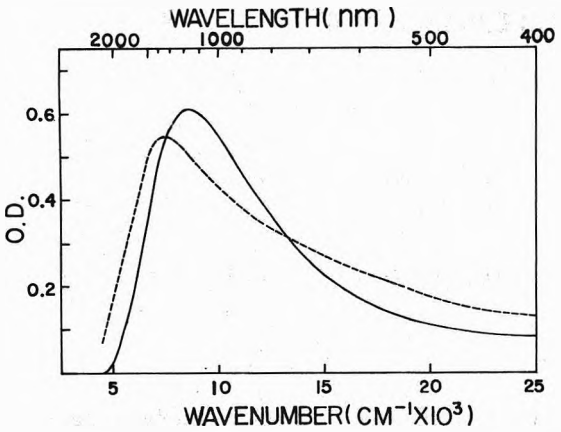

Figure 1. Optical absorption spectra of trapped electrons in 2-methyl-*n*-amylamine. The broken line spectrum was obtained for the sample irradiated at a dose of 2.5 × 10^5 rads at 4°K. The solid line spectrum was obtained for the sample irradiated at a dose of 1.7 × 10^5 rads at 77°K.

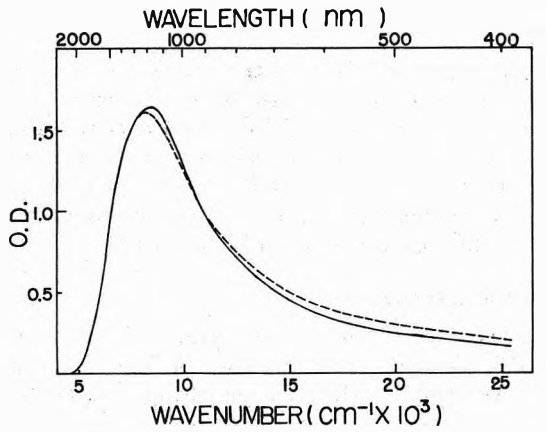

Figure 2. Optical absorption spectra of trapped electrons in *N*-methyl-*n*-butylamine. The broken line spectrum was obtained for the sample irradiated at a dose of 2.5 × 10^5 rads at 4°K. The solid line spectrum was obtained for the sample irradiated at a dose of 3.4 × 10^5 rads at 77°K.

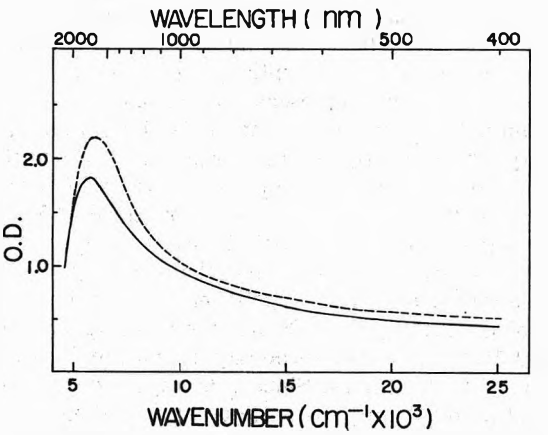

Figure 3. Optical absorption spectra of trapped electrons in triethylamine. The broken line spectrum was obtained for the sample irradiated at a dose of 2.5 × 10^5 rads at 4°K. The solid line spectrum was obtained for the sample irradiated at a dose of 3.4 × 10^5 rads at 77°K.

lar compounds such as isopropylamine, isobutylamine, and isoamylamine. In a recent work,[9] the same trend in λ_{max} was observed for solvated electrons in isopropyl alcohol, isobutyl alcohol, and isoamyl alcohol. The 1,2-propanediamine having two amino groups yields λ_{max} at the shortest wavelength among all the amines examined. It is interesting to note that the absorption spectrum of solvated or trapped electrons in liquid or glassy ethylene glycol which has two hydroxyl groups exhibits λ_{max} at a wavelength shorter than those in the primary alcohols having only one hydroxyl group.[2,9,10] A pronounced effect of the molecular structure on λ_{max} is observed for trapped electrons in diisopropylamine and *N*-methyl-*n*-butylamine, both of which were the secondary amines. The diisopropylamine has two bulky groups adjacent to the nitrogen atom, and such a molecular structure perhaps makes it difficult to reduce the electron cavity volume in this matrix as much as in the matrices having less bulky groups adjacent to the nitrogen atom.

TABLE I: Optical Absorption Parameters of Trapped Electrons in Aliphatic Amines at 4 and 77°K

Compound	4°K λ_{max}, nm	4°K $W_{1/2}$, eV	77°K λ_{max}, nm	77°K $W_{1/2}$, eV	η
2-Methyl-*n*-amylamine	1380	1.12	1180	0.87	0.8
sec-Butylamine	1220	0.63	1130	0.60	1.0
Isopropylamine[a]			1080	0.53	
Isobutylamine[a]			1060	0.89	
Isoamylamine[a]			1000	0.94	
1,2-Propanediamine	980	0.82	980	0.84	1.3
Diisopropylamine	~1600		1480	0.54	
N-Methyl-*n*-butylamine	1210	0.70	1175	0.66	1.3
3-Methylpiperidine			1350	0.77	
Triethylamine	1680	0.62	1680	0.72	1.4
Tripropylamine	1680	0.94	1680	0.89	

[a] These samples contained 5 vol % water.

There is no clear distinction about the half-height width, $W_{1/2}$, of the absorption spectrum between the primary, secondary, and tertiary amines. It can be seen, however, that the larger the molecular size, the broader the bandwidth when $W_{1/2}$ is compared within a group of similar compounds: isopropylamine, isobutylamine, and isoamylamine; triethylamine and tripropylamine.

We now discuss the results obtained at 4°K. It can be seen in Table I and Figures 1–3 that the absorption spectra at 4°K are in general similar to those at 77°K. Slight red shifts in λ_{max} at 4°K relative to that at 77°K are observed for trapped electrons in the primary and secondary amines, the greatest observed shift being 200 nm for trapped electrons in 2-methyl-*n*-amylamine. However, the absorption spectrum of trapped electrons in 1,2-propanediamine at 4°K is identical with that at 77°K. The absorption spectrum of trapped electrons in diisopropylamine at 4°K had a very flat shape and it was difficult to locate its λ_{max} precisely. The wavelength of maximum absorption in the optical spectra of trapped electrons in the tertiary amines at 4°K is the same as that at 77°K.

The half-width of the absorption spectrum at 4°K does not change very much from that at 77°K for trapped electrons in all the amines examined. Considering the accuracy of measurement, we refrain from saying that the difference in $W_{1/2}$ between 4 and 77°K listed in Table I has any significance, except for trapped electrons in 2-methyl-*n*-amylamine whose $W_{1/2}$ at 4°K is definitely greater than that at 77°K.

The observation that there is no or only a small temperature dependence of the optical spectra of trapped elec-

trons in the amines between 4 and 77°K is in remarkable contrast to the well-known optical property of solvated electrons in polar liquids where the optical absorption has a large negative temperature coefficient of the position of the maximum absorbance.[11-13]

Since solvent molecules can move rather freely in liquids, a liquid dielectric medium can respond to the presence of solvated electrons and rearrange configurationally to attain its lowest energy state. In contrast, the motions of matrix molecules are considered to be restricted in glassy solids, the extent of which depends on the molecular structure of the individual compound as well as the temperature. In view of our very limited knowledge of molecular motions in glassy solids at low temperature, it is not possible at present to discuss the rearrangement of a glassy medium due to the presence of trapped electrons as fully as we can for that of a liquid medium. Such a situation exists for most of the amine glasses. An attempt was made previously to investigate the molecular motions in triethylamine glass, in which it was demonstrated that the motions of bulk molecules were frozen in at 77°K.[14]

Now let us consider the case where trapped electrons exist in a glassy matrix. The matrix molecules far from a trapped electron would not suffer a strong influence by the trapped electron because matrix rigidity probably dominates the effect of an electric field due to the trapped electron. However, a strong electric field acts on the molecules in the vicinity of the trapped electron and would induce the rotation of these polar molecules, in some cases almost independently of temperature, forming a locally relaxed electron trap.

Keeping these general considerations in mind, we may derive some information on the relaxation of electron traps in the amine glasses from a comparison of the observed absorption spectra at 4 and 77°K. We infer that the electron traps in the amine glasses are locally relaxed at 77°K. Such an interpretation is consistent with the theoretical results on trapped electrons in the amine glasses at 77°K which are based on the model of locally relaxed traps.[8] We also conclude that the electron traps are relaxed at 4°K to the same extent as those at 77°K for the amines which yield the identical absorption spectra of trapped electrons at 4 and 77°K. It seems reasonable to suggest that the electron traps are incompletely relaxed at 4°K for the amines which give a slight red shift of the absorption spectra of trapped electrons at 4°K relative to those at 77°K, but their maxima lie at shorter wavelengths compared to λ_{max}, 1500 nm, in the absorption spectrum of trapped electrons in ethanol glass at 4°K.[15] There was a dramatic change in the absorption spectrum of trapped electrons in ethanol glass when the temperature was raised from 4 to 77°K, and such an observation led to the interpretation that the electron traps in ethanol glass at 4°K are unrelaxed.[15]

It should be pointed out that both the optical absorption spectra and the electron spin resonance spectra of trapped electrons in the tertiary amines at 77°K[5] are very similar to those of trapped electrons in hydrocarbon glasses at 77°K.[4] Thus, we are tempted to state that trapped electrons in the tertiary amine glasses are surrounded by the methyl groups of the amine molecules in the first solvation shell, resulting in very weak interactions with the nitrogen atoms.

Finally, we comment on the efficiency of electron trapping or the yield of trapped electrons at 4°K relative to that at 77°K. Such a relative efficiency in the amine glasses is given in Table I as η. It can be seen in Table I that the value of η range from 0.8 to 1.4 and the values for the primary amines are somewhat smaller than that for the tertiary amine although the number of data is limited. These values are compared to a value of η, 1, obtained for trapped electrons in ethanol glass.[15]

Acknowledgment. The authors wish to express their thanks to Professor T. Higashimura for his encouragement and valuable discussion and to Mr. M. Noda for his assistance in optical absorption measurements.

References and Notes

(1) T. Higashimura, M. Noda, and T. Warashina, *J. Chem. Phys.*, **53**, 1152 (1970).
(2) H. Hase, M. Noda, and T. Higashimura, *J. Chem. Phys.*, **54**, 2975 (1971).
(3) H. Hase, M. Noda, T. Higashimura, and K. Fueki, *J. Chem. Phys.*, **55**, 5411 (1971).
(4) H. Hase, T. Higashimura, and M. Ogasawara, *Chem. Phys. Lett.*, **16**, 214 (1972).
(5) S. Noda, K. Fueki, and Z. Kuri, *Chem. Phys. Lett.*, **8**, 407 (1971).
(6) S. Noda, K. Fueki, and Z. Kuri, *Can. J. Chem.*, **50**, 2699 (1972).
(7) R. C. Weast, Ed., "Handbook of Chemistry and Physics," 50th ed, Chemical Rubber Publishing Co., Cleveland, Ohio, 1969.
(8) K. Fueki, D.-F. Feng, and L. Kevan, *J. Amer. Chem. Soc.*, **95**, 1398 (1973).
(9) R. R. Hentz and G. Kenney-Wallace, *J. Phys. Chem.*, **76**, 2931 (1972).
(10) B. G. Ershov, I. E. Makarov, and A. K. Pikaev, *High Energy Chem.*, **1**, 414 (1967).
(11) B. D. Michael, E. J. Hart, and K. H. Schmidt, *J. Phys. Chem.*, **75**, 2798 (1971).
(12) K. N. Jha, G. L. Bolton, and G. R. Freeman, *J. Phys. Chem.*, **76**, 3876 (1972).
(13) I. Hurley, T. R. Tuttle, Jr., and S. Golden in "Metal-Ammonia Solutions," M. Sienko and J. J. Lagowski, Ed., Butterworths, London, 1970, p 503.
(14) H. Tsujikawa, K. Fueki, and Z. Kuri, *J. Chem. Phys.*, **47**, 256 (1967).
(15) H. Hase, T. Warashina, M. Noda, A. Namiki, and T. Higashimura, *J. Chem. Phys.*, **57**, 1039 (1972).

Predicted Properties of the Superheavy Elements. II. Element 111, Eka-Gold[1]

O. L. Keller, Jr.,* C. W. Nestor, Jr., Thomas A. Carlson,

Oak Ridge National Laboratory, Oak Ridge, Tennessee 37830

and Burkhard Fricke

Northwestern University, Evanston, Illinois 60201 and Gesellschaft für Schwerionenforschung, Darmstadt, Germany

(Received February 20, 1973)

Publication costs assisted by Oak Ridge National Laboratory

The chemical properties of element 111, eka-gold, are predicted through the use of the periodic table, relativistic Hartee–Fock–Slater calculations, and various qualitative theories which have established their usefulness in understanding and correlating properties of molecules. The results indicate that element 111 will be like Au(III) in its chemistry with little or no tendency to show stability in the I or II states. There is a possibility that the 111^- ion, analogous to the auride ion, will be stable.

Introduction

In paper I of this series[2a] plans were mentioned for the use of heavy ion accelerators in the search for superheavy elements. These plans have subsequently moved forward in the U. S. and abroad. In the U. S., at the Berkeley Super HILAC, a team of chemists from several U. S. and European laboratories is preparing to study possible superheavy elements. Further predictions are needed now as a guide for such experiments. The tools we have for making chemical predictions are the periodic system of the elements, the relativistic Hartree–Fock–Slater program for calculating energies and radii of electrons in atoms, and various approximate theories which have proven useful over the years in correlating properties of molecules.

If we assume that the periodic table continues to build up with its usual symmetry, element 111 will occur in group Ib with Cu, Ag, and Au. The energy eigenvalues presented for Cu, Ag, Au, and 111 have been calculated using a relativistic Hartree–Fock–Slater (HFS(rel)) program developed at Oak Ridge[2b] and the HFS(rel) code of Fricke and Waber[3] (a further development of the program of Liberman, Cromer, and Waber[4]). The $6d^97s^2$ ground-state electronic configuration for 111 obtained from both codes was confirmed by a relativistic Hartree–Fock calculation through the courtesy of Dr. Joseph B. Mann. Although the details in the Fricke and Oak Ridge codes differ somewhat, the individual energies given in the tables are, for our purposes, identical. The Oak Ridge code obtains binding energies from the use of Koopmans' theorem and Slater's approximate exchange potential,[5] whereas Fricke obtains the binding energies from subtraction of total energies and the use of two-thirds times Slater's exchange potential. For well-known reasons neither code can give exact agreement with experiment. Therefore we always compare our calculated values with the available experimental or semiempirical energy values for Cu, Ag, and Au. As detailed below these comparisons allow us to correct the calculated values for 111 because the physical basis for the errors in the region around element 114 should be the same as for the lighter members of the respective series.

Possible physical changes that are not taken into account in the (HFS(rel)) calculations that conceivably could affect the valence electrons in elements 111 through 120 are (1) the interaction of the electrons with the zero-point electromagnetic field (vacuum fluctuation); (2) the interaction of the electrons with the polarized negative energy electron sea (vacuum polarization); (3) the electron–electron magnetic interactions; (4) the retardation terms which arise from the finite velocity (speed of light) of the electromagnetic interaction of the electrons as they themselves approach the speed of light; (5) and the error in the Slater exchange term *vs.* exact exchange as found in a relativistic Hartree–Fock calculation. The energy variations due to these causes in the elements around 114 have been found too small to have chemical significance by Mann[2a,6] and by Fricke and Waber.[7] The following assumptions are more serious: (1) the use of Koopmans' theorem by which eigenvalues are used to determine the binding energies, (2) our inability to include electron correlation, and (3) the use of an average energy for an incompletely filled subshell rather than a specific coupling scheme. As shown in the tables, in some instances ionization potentials were obtained from differences in total energies between initial and final states, and in these instances agreement with results from eigenvalues is quite satisfactory. The uncertainties in the latter three assumptions are present for the lighter elements as well as for the heavier elements. We shall therefore assume that the errors in the atomic calculations for element 111 are of the same character as in Cu, Ag, and Au. The corrections to the energies obtained by comparing the calculated values for Cu, Ag, and Au to literature values are therefore assumed to be extrapolatable to 111. The interpretation of the chemistry of 111 is nonetheless found to be more difficult than for 113 and 114 because the ground electronic state and the electrons of lowest energy are found to be different from those of its congeners. The results we present

TABLE I

Element	Configuration	Electrons	Binding energies, eV: Oak Ridge[a]	Fricke[b]	Semiempirical and experimental energies[c]
Cu	$3d^{10}4s^1$	$3d_{3/2}$	10.1		11
		$3d_{5/2}$	9.8	10.5	10.4
		$4s_{1/2}$	7.1	7.7	7.73
Ag	$4d^{10}5s^1$	$4d_{3/2}$	12.5		
		$4d_{5/2}$	11.8	11.8	12.4
		$5s_{1/2}$	6.9	7.2	7.58
Au	$5d^{10}6s^1$	$5d_{3/2}$	12.2		12.5
		$5d_{5/2}$	10.4	10.4	11.1
		$6s_{1/2}$	8.4	8.7	9.23
111	$6d^97s^2$	$6d_{3/2}$	13.4		(13)[d]
		$6d_{5/2}$	10.1	10.0	(10.7)
		$7s_{1/2}$	11.7	11.9	(12.6)

[a] Based on eigenvalues determined from Oak Ridge code[2a] using full Slater exchange. [b] Based on differences in total energies from solutions of wave functions of Fricke[3] using $\frac{2}{3}$ Slater exchange. [c] Reference 8. [d] Suggested extrapolated values for element 111.

here are therefore of a more general nature than those in paper I.

Energy Levels of Outer Electrons in Group Ib Elements

In Table I we give the results of the (HFS(rel)) calculations for the energy eigenvalues of the $d_{3/2}$, $d_{5/2}$, and $s_{1/2}$ electrons of the group Ib elements along with the literature values. The Oak Ridge and Fricke calculations are seen to agree with the literature values[8] for the binding energies rather well.

As noted previously the ground-state configuration of 111 is $6d^97s^2$. This configuration was found to be more stable than the $6d^{10}7s^1$ by 4.2 (Oak Ridge) and by 2.9 eV (Fricke). The first ionization potential of 111 therefore refers to a d electron rather than to an s electron as in the lighter members of the series. Also, as seen in the table, the splitting of the $d_{3/2}$ and $d_{5/2}$ levels increases through the series to the point that they actually span the $s_{1/2}$ level in 111. Whereas the s electron in silver and copper is able to act in some cases more or less as an individual valence electron, some type of hybridization is always involved in gold compounds. In addition to noting the magnitudes of the energies and the relative spacing of the d and s shells, it is also helpful to inspect the computed electron density maps. As seen in Figure 1, at the arrows marking the Slater atomic radii, in copper and silver the $s_{1/2}$ density is about equal to the $d_{5/2}$, but in Au and 111 it is somewhat less. Also in the tail of the charge distribution at large radii the $s_{1/2}$ density is much larger for Cu and Ag than the $d_{5/2}$ density whereas in Au and 111 both these densities are about equal. The probability is therefore low that the $s_{1/2}$ electrons in 111 will act individually as valence electrons. That is to say, in 111, as in Au, we can expect hybridization to accompany chemical reaction.

Ionization Potentials and Atomic Radius

In Table II we give the ionization potentials as obtained by the two HFS(rel) codes as compared to experiment. Agreement between the two codes is again good. Two different approaches are used to obtain the calculated atomic radii given in Table II for comparison with Slater's empirical values.[9] The radial expectation values $\langle r \rangle$ calculated by the Oak Ridge code are listed in ref 2a. From the calculations of Waber and Cromer[10a] and of Fricke and Waber,[10b] we obtained the radius of maximum charge density in the outermost shell. Since, as compared to experiment, the value of $\langle r \rangle$ is consistently too high, and the value of the radius of the charge density maximum is consistently too low, we have no trouble bracketing the "experimental" value of the atomic radius of 111.

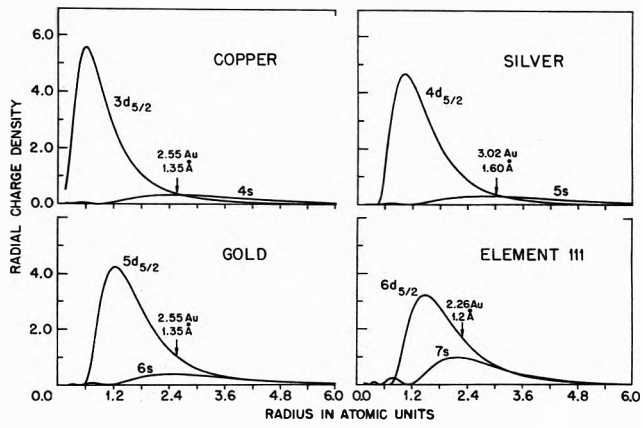

Figure 1. Comparison of $s_{1/2}$ and $d_{5/2}$ electron densities as calculated by Fricke in group Ib elements. The arrows mark the positions of the Slater atomic radii (Au = atomic units).

Excited State Energies

Our subsequent discussions of the chemistry of element 111 will require s–p, s–d, and d–p separation energies in the neutral and +1 ion. The results are given in Table III for comparison with available experimental values. The agreement is excellent; so we assume the values for 111^+ and neutral are reliable. Because of their importance to our subsequent discussions, it should be noted that the calculations for the +1 and neutral species both agree that the d–p separation in gold is essentially equal to the s–p separation in 111.

Relative Stabilities of the Oxidation States of Element 111

In the absence of complexing agents, and at ordinary temperature, the most stable oxidation state of copper is II and of gold is III. In both cases there is much important chemistry in the I state involving complexes, however. In the case of silver, the most stable and important state by far is the I, with the II having a very high oxidation potential. There is, therefore, no trend as one goes to higher Z in group Ib that points toward the most stable oxidation state to be expected for element 111, and the predictions must be made on other criteria.

Gold(III) chemistry is nicely explained on the basis of valence bond theory. In gold(III) compounds, which are always four coordinate, the ligands form a square planar arrangement around the gold atom indicating dsp^2 hybridization for the gold orbitals. The valence state, as shown in Figure 2a, requires the promotion of a 5d electron to a 6p electronic orbital. Au(III) uses all unpaired electrons for bond formation, and also gains an electron pair by forming an anion such as $AuCl_4^-$. As shown in Table III, the d to p promotion requires ~5.9 eV. Therefore, in gold(III) compounds, it is an experimental fact that the bond and

TABLE II

Ion	Configuration	Ionization energy, eV: Oak Ridge[a]	Ionization energy, eV: Fricke[b]	Ionization energy, eV: Exptl[c]	Radial expectation $\langle r \rangle$[d]	Radius max density outer shell[e]	Slater atomic radius[f]
Cu neutral	4s	7.141	7.7	7.724	1.59	1.19	1.35
+1	$3d^{10}$	19.61		20.29	0.50		
+2	$3d^{9}$	37.41		36.83	0.47		
+3	$3d^{8}$	58.24			0.43		
Ag neutral	5s	6.914	7.18	7.574	1.68	1.29	1.60
+1	$4d^{10}$	20.81		21.48	0.69		
+2	$4d^{9}$	35.05		34.82	0.67		
+3	$4d^{8}$	50.73			0.63		
Au neutral	6s	8.358	8.72	9.22	1.50	1.19	1.35
+1	$5d^{10}$	19.56	19.37	20.5	0.81		
+2	$5d^{9}$	32.30	31.79		0.77		
+3	$5d^{8}$	46.20			0.74		
+4	$5d^{7}$	61.08			0.71		
111 neutral	$6d^{9}7s^{2}$	10.14	9.96	(10.7)	1.3	1.14	(1.2)
+1	$6d^{8}7s^{2}$	20.74			1.3	1.12	
+2	$6d^{8}7s$	30.9					
+3	$6d^{8}$	41.6					
+4	$6d^{7}$	54.5					

[a-c] See corresponding footnote to Table I. [d] Calculated from solutions for appropriate ions using code from ref 2a. [e] Calculated from solutions of appropriate ions using code from ref 10. [f] Reference 9.

TABLE III[a]

		Cu^+	Ag^+	Au^+	111^+	Au^0	111^0
d–s separation	d^9s above ground state[b]	2.9	4.6(4.6)	1.6(1.6)	−2.1(−2.0)	(0.8)	(2.9)
	d^9s above ground state[c]	2.7	4.8	1.9			
d–p separation	d^9p above ground state[b]	8.8	9.9(9.8)	7.0(7.7)	$4.6(d^{10}–d^9p)$ $(5.9–d^8s^2–d^7s^2p)$	(5.9)	(3.3)
	d^9p above ground state[c]	8.2	9.9	7.8			
s–p separation	$(d^9s–d^9p)$[b]	5.9	5.3(5.2)	5.4(6.1)	7.1(7.9)	(5.1)	(6.2)
	$(d^9s–d^9p)$[c]	5.5	5.1	5.9			

[a] Values in eV. [b] Present work; Fricke results shown in parentheses; Oak Ridge results (as calculated on differences in total energies) shown without parentheses. [c] J. D. Dunitz and L. E. Orgel, *Advan. Inorg. Radiochem.*, **2**, 1 (1960).

lattice or solvation energies are sufficiently high to furnish this hybridization energy (and also furnish the heat of sublimation of gold) with enough Gibbs' free energy left over to stabilize the complex. Therefore, if the promotion energy to the valence state of 111(III) is ~6eV, and if it appears that the bond energies of compounds of 111(III) will be about the same or higher than analogous compounds of gold(III), and if it also appears that the heat of sublimation will not be substantially higher, we can then expect that 111 will have a chemistry similar to Au(III).

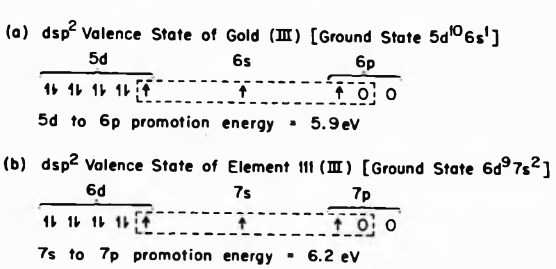

Figure 2. Valence bond pictures for Au(III) and 111(III).

As shown in Figure 2b, the valence state of 111(III) requires the promotion of a 7s to a 7p electron. In Table III, this promotion energy is seen to be ~6.2 eV, or about the same as the promotion energy required for Au(III). The next question concerns the heat of sublimation of 111. The values of the heats of sublimation of Cu, Ag, and Au at 298°K are 3.54, 2.97, and 3.67 eV, respectively.[11] There is no trend, and the values are similar. Will the change from $d^{10}s^1$ to d^9s^2 ground-state configuration change the heat of sublimation of 111 greatly? A look at the heats of sublimation and ground-state configurations of Pt, Au, and Hg[11] in the following table indicates that the formation of the closed shell s^2 configuration will perhaps more than counterbalance the breaking of the d^{10} closed shell.

	Pt	Au	Hg
Electronic configuration	$4f^{14}5d^96s^1$	$4f^{14}5d^{10}6s^1$	$4f^{14}5d^{10}6s^2$
Heat of sublimation (298°K), eV	5.85	3.67	0.634

The bond energies in 111(III) compounds should be at least as strong as those in Au(III) compounds because 111

TABLE IV

Element	Configuration	Electron affinities, eV: Oak Ridge[a]	Fricke[b]	Exptl[c]
Cu	$3d^{10}4s^1$	0.6	1.0	1.226
Ag	$4d^{10}5s^1$	0.7	0.9	1.303
Au	$5d^{10}6s^1$	1.4	2.1	2.3086
111	$6d^97s^2$	1.0	1.3	

[a,b] See corresponding footnotes to Table I. [c] Reference 13.

is expected to be smaller in radius than Au. Good overlap of its wave functions with those of the ligands should therefore occur. The inner electron repulsion will be larger, but there are indications that this is of minor importance since gold easily achieves dsp^2 hybridization whereas Cu and Ag do not.

Since the promotion energy and heat of sublimation of 111 should be similar to gold, and the bonding at least as strong, we expect 111 to form strong complexes in the oxidation state of III and be similar to Au(III) in its chemistry.

There probably will not be a stable oxidation state of II for element 111. Au(II) is exceedingly rare if it exists at all, and Ag(II) is only difficultly attained. The stability of Cu(II) relative to Cu(I) and Cu(III) is not clearly understood, but it probably involves a delicate balance between ionic and covalent bonding, with the balance tipping toward ionic bonding because of crystal field stabilization. This delicate balance cannot be expected to occur in 111 because of the very high ionization potential of 31 eV *vs.* 28.0 for copper(II). Even gold(II) with an ionization energy of 29.7 eV does not exist.

We expect that 111(I) will be very unstable, and that if it exists at all it will be in complexes involving the highly polarizable cyanide ligands which stabilize Au(I). In Table II we note that 111 has a very high ionization energy of 10.7 eV, about 1.5 eV higher than Au. 111(I) can therefore be expected to be noble indeed. Furthermore, Cu(I) and Ag(I) are stabilized by a great change in radius that occurs when a single electron is ionized. As shown in column 7 of Table II, a decrease of about 1 Å occurs in these two cases. The decrease in radius in going to the +1 ion from the neutral species results in much larger lattice energies in crystals and solvation energies in solution than would otherwise be the case. For gold the corresponding decrease is seen to be somewhat less and for 111 no decrease occurs. Gold forms a quasistable I state with covalent properties. For the case of 111, the high ionization potential and small change in radius can be expected to preclude the formation of 111(I) except, perhaps, with cyanide.

Another intriguing possibility for a stable oxidation state of 111 is the −1 ion analogous to the auride[12] ion found in CsAu and RbAu. Cesium auride is a semiconductor whose bonding appears to be highly ionic. The crystals have the CsCl structure. Whether 111 will act in a similar way to Au depends on its electron affinity. The electron affinity of gold[13] is about 2.3 eV. The electron affinities of Cu and Ag, which have not been found to form compounds containing themselves as −1 ions, are about 1.2 and 1.3 eV, respectively.

In order to evaluate whether 111 will act like gold or like copper and silver in this instance, we need to be able to compute the electron affinity. This is a difficult problem, even in the lighter elements, because electron–electron correlation assumes such a major role.[14,15] Even though our codes could not be reasonably expected to give accurate results, we nevertheless carried out the calculations as a matter of interest for purposes of comparison. The results, given in Table IV, are seen to be in the correct order with Cu and Ag about equal and Au somewhat higher. According to these calculations element 111 is seen to lie between Au, which forms a negative ion in chemical compounds, and Cu and Ag which do not. We would therefore suggest strongly that experimentalists be aware of the possible stability of the 111^- ion, and its possible chemical importance.

Acknowledgment. We wish to express our appreciation to Professor Glenn T. Seaborg for pointing out to us the importance of chemical predictions in the superheavy elements region. We also wish to thank him for numerous stimulating discussions during the course of this work.

References and Notes

(1) Research sponsored by the U. S. Atomic Energy Commission under contract with the Union Carbide Corporation.
(2) (a) O. L. Keller, Jr., J. L. Burnett, T. A. Carlson, and C. W. Nestor, Jr., *J. Phys. Chem.*, **74**, 1127 (1970); (b) C. C. Lu, T. A. Carlson, F. B. Malik, T. C. Tucker, and C. W. Nestor, Jr., *Atomic Data*, **3**, (1971).
(3) B. Fricke, W. Greiner, and J. T. Waber, *Theor. Chim. Acta*, **21**, 235 (1971); B. Fricke and W. Greiner, *Phys. Lett. B*, **30**, 317 (1969).
(4) D. Liberman, D. T. Cromer, and J. T. Waber, *Comp. Phys. Commun.*, **2**, 107 (1971).
(5) J. C. Slater, *Phys. Rev.*, **81**, 385 (1951); see also W. Kohn and L. J. Sham, *Phys. Rev.*, **140**, A1113 (1965); R. D. Cowan, A. C. Larson, D. Liberman, J. B. Mann, and J. T. Waber, *Phys. Rev.*, **144**, 5 (1966).
(6) J. B. Mann, *J. Chem. Phys.*, **51**, 841 (1969); J. B. Mann, Robert A. Welch Foundation Conference. The Transuranium Elements, Houston, Tex., Nov 1969.
(7) B. Fricke and J. T. Waber, *J. Chem. Phys.*, **57**, 371 (1972).
(8) W. Lotz, *J. Opt. Soc. Amer.*, **60**, 2061 (1970); M. O. Krause, "Electron Energy Levels in Free Atoms from $Z = 1$ to $Z = 60$," ORNL-TM-2943, April 1970; C. E. Moore, "Atomic Energy Levels," National Bureau of Standards, 1958.
(9) J. C. Slater, "Quantum Theory of Molecules and Solids," McGraw-Hill, Vol. 2, New York, N. Y., 1965, p 103.
(10) (a) J. T. Waber and D. T. Cromer, *J. Chem. Phys.*, **42**, 4116 (1965); (b) B. Fricke and J. T. Waber, *ibid.*, **56**, 3246 (1972).
(11) D. R. Stull and G. C. Sinke, *Advan. Chem. Ser.*, **No. 18**, 1 (1956).
(12) (a) A. Sommer, *Nature (London)*, **152**, 215 (1943); (b) W. E. Spicer, A. H. Sommer, and J. G. White, *Phys. Rev.*, **115**, 57 (1959).
(13) H. Hotop, R. A. Bennett, and W. C. Lineberger, Proceedings of the Twenty-Fifth Annual Gaseous Electronics Conference, 17–20 Oct 1972, The University of Western Ontario, London, Canada.
(14) (a) E. Clementi and A. D. McLean, *Phys. Rev.*, **133**, A419 (1964); (b) E. Clementi, A. D. McLean, D. L. Raimondi, and M. Yoshimine, *Phys. Rev.*, **133**, A1274 (1964).
(15) B. L. Moiseiwitsch, *Advan. At. Mol. Phys.*, **1**, **61** (1965).

Redox Mechanisms in an Ionic Matrix. III. Kinetics of the Reaction $NO_2^- + \frac{1}{2}O_2 = NO_3^-$ in Molten Alkali Nitrates

F. Paniccia and P. G. Zambonin*

Istituti di Chimica Analitica e Generale, Università degli Studi, 70126 Bari, Italy *(Received February 7, 1973)*

The kinetics of the homogeneous-phase oxidation of nitrite by molecular oxygen ($NO_2^- + \frac{1}{2}O_{2(g)} = NO_3^-$) in a molten matrix of (sodium–potassium) nitrate were studied in the temperature range 545–690°K by following the oxygen pressure variations over the reacting system. Within the experimental oxygen pressure and nitrite concentration ranges ($80 < P_{O_2} < 900$ Torr; $0.1 < [NO_2^-] < 0.5$ *m*) the reaction rate can be described by the expression $-d[NO_2^-]/dt = k[NO_2^-][O_2]$ which is consistent with the mechanism: $NO_2^- + O_{2(g)} \xrightarrow{\text{slow}} NO_3^- + O$; $NO_2^- + O \xrightarrow{\text{fast}} NO_3^-$. The results, directly comparable with those relevant to the oxidation of nitrite by peroxide and superoxide ions, permit some considerations about the influence of the bond energy of the species O_2, O_2^-, and O_2^{2-} on the relevant kinetic parameters. By considering the solubility data and the temperature coefficient relevant to the dissolution of oxygen, kinetic and thermodynamic data referred to the heterogeneous process $NO_2^- + \frac{1}{2}O_{2(g)} = NO_3^-$ could be obtained. This permitted a reasonable comparison of the present results with the findings previously obtained by Freeman for the high-temperature direct oxidation of pure sodium and potassium nitrite.

Introduction

In the course of a recent study,[1] the kinetic behavior of the reaction: nitrite + superoxide = nitrate + peroxide has been investigated in the molten (Na,K)NO_3 eutectic at the temperature of about 500°K. The process, characterized[2] by the overall reaction

$$2NO_2^- + 2O_2^- = 2NO_3^- + O_2^{2-} \qquad (1)$$

has been found to proceed according to an autocatalytic mechanism prevailing on the "direct" reaction between NO_2^- and O_2^-. The result, explainable[1] in terms of a higher reactivity (with nitrite) of peroxide instead of superoxide can be, perhaps, related to the lower[1,3] bond energy of O_2^{2-} compared to O_2^-. For a better understanding of the role played by the oxygen–oxygen bond on this kind of reactions, a study on the kinetics between nitrite and molecular oxygen

$$NO_2^- + {}^1/_2O_2 = NO_3^- \qquad (2)$$

was performed under the same experimental conditions at which the work with O_2^{2-} and O_2^- has been carried out.

Another point of interest in studying the kinetics of reaction 2 lies in the fact that it represents the reverse of the main step always hypothesized in the decomposition of nitrate ions. Previously this reaction has been studied only at high temperatures (830–1050°K) where other processes can become[4-7] concomitant. In the course of the present work, reaction 2 has been studied in the temperature interval 550–690°K in the absence of any appreciable side reaction.

Experimental Section

Chemicals. The solvent was an equimolar mixture (≃200 g) of reagent grade sodium and potassium nitrate (Carlo Erba, Milan) containing initial concentrations of sodium nitrite 0.2–0.5 *m*. Cylinder oxygen (S.I.O., Milan) was purified by keeping it in contact with Ascarite (A. H. Thomas Co., Philadelphia, Pa.) to remove CO_2 and with Molecular Sieves 5A (Carlo Erba, Milan) cooled at −80° to remove water.

Apparatus and Procedures. The reaction cell was composed of a cylindrical glass vessel connected with a mercury manometer, a thermostated bulb (necessary for the calibration of the system), a vacuum line, and a gas inlet. Constant temperature conditions were obtained by an aluminum thermostatic block holding a rotating magnet suitable for stirring the melt.

The calibration of the system was made by expanding an inert gas (known volume, pressure, and temperature) contained in the thermostated bulb, in the previously evacuated reaction cell. On the basis of the pressure values before and after the gas expansion, a correlation between pressure and moles of gas contained in the reaction cell at a given melt temperature was readily obtained. This calibration method was preferred to a direct geometrical measurement of the cell volume, since it is independent of temperature gradients always present in high-temperature thermostated systems. For more details see ref 8.

The introduction of oxygen in the reaction cell was done after long vacuum degassing of the melt. When the desired oxygen pressure over the melt was obtained, the apparatus was flame-sealed, leaving in connection with the reaction cell only the manometer used to follow the oxygen disappearance. Under these experimental conditions any gas leak was excluded and very long kinetic experiments (up to several months) could be performed.

The disappearance of a number of moles of oxygen in the gas phase could be easily obtained according to

$$\Delta n_{O_2} = A(T)\Delta P \qquad (3)$$

where $A(T)$ is the temperature-dependent conversion factor obtained by the described calibration.

The oxygen concentration of the melt at various temperatures was calculated by the relation

$$\log K_H = -|3.53| - \frac{926}{T} \quad (4)$$

which can be derived from the solubility data given in ref 8b. K_H indicates the equilibrium solubility coefficient expressed as moles of oxygen dissolved per 1000 grams of melt per atmosphere, and T is the absolute temperature. In effect a continuous equilibrium situation between oxygen in the gas and liquid phases is to be considered valid since the rate of dissolution of the gas under the present experimental conditions has been found to be fast compared to the disappearance of oxygen because of reaction 2. It is indicative in this sense upon comparison of the examples of solubility kinetics given in ref 8b with the results described in the next section. A control of the actual nitrite concentrations at the beginning and at the end of each experiment was done by classical titrimetric methods after dissolution in water of quenched melt samples.

Results and Discussion

Typical examples of oxygen pressure decays (the fastest in the course of the entire work) observed in the presence of a solution of nitrite in molten nitrates are reported in Figure 1. Similar curves were obtained in the temperature interval 550–690°K, under oxygen pressures and nitrite concentrations contained in the ranges $80 < P_{O_2} < 900$ Torr and $0.1 < [NO_2^-] < 0.5$ m, respectively. Titrations performed at the end of each experiment have shown that the total disappearance of nitrite was double the consumption of oxygen. On the basis of relation 3

$$2\Delta n_{O_2} = \Delta n_{NO_2^-} \quad (5)$$

The results are in agreement with the overall stoichiometry expressed by eq 2.

Treatment of Data and Proposed Mechanism. The simplest way to express the mechanism of reaction 2 is

$$NO_2^- + O_{2(s)} \xrightarrow{\text{slow}} NO_3^- + O \quad (6)$$

$$O + NO_2^- \xrightarrow{\text{fast}} NO_3^- \quad (7)$$

$$2NO_2^- + O_{2(s)} = 2NO_3^- \quad (2a)$$

where the role of fast step assigned to reaction 7 is justified by the high rates usually associated with free-radical involving processes and by the high concentration of nitrite (0.1–0.5 m) present in solution. By considering reaction 6 as the rate-determining step, the reaction rate can be expressed by

$$\text{rate} = -\frac{d[NO_2^-]}{dt} = k_6[NO_2^-][O_2] \quad (8)$$

and in first approximation

$$-\frac{\Delta[NO_2^-]}{\Delta t} = k_6[NO_2^-][O_2] \quad (9)$$

where the left-hand term can be practically evaluated from the slope of pressure–time curves such as those of Figure 1.

A relation between the pressure variation ΔP and the variation of the nitrite concentration, $[NO_2^-]$, can be obtained by eq 3 and 5

$$\frac{\Delta n_{NO_2^-}}{W} = \frac{2\Delta n_{O_2}}{W} = \frac{2A(T)\Delta P}{W} \quad (10)$$

i.e.

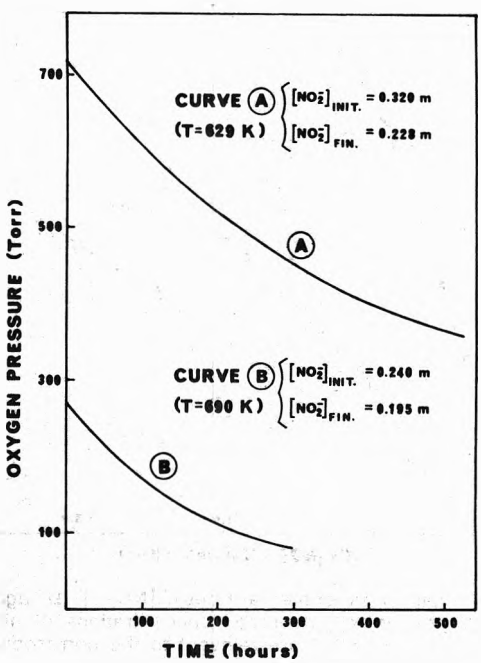

Figure 1. Examples of kinetic decays of oxygen pressures in the presence of sodium nitrite contained in a molten equimolar matrix of (Na,K)NO_3. The initial and final concentrations of nitrite as well as the working temperatures are specified. The curves, reported as continuous, represent the interpolation of a series of a high number of experimental points.

$$\Delta[NO_2^-] = \frac{2A(T)\Delta P}{W} \quad (10')$$

where W is the weight (in kilograms) of the melt.

The actual concentration of nitrite and oxygen in the molten solutions can be obtained, at any time, in the following way

$$[NO_2^-] = [NO_2^-]_0 - 2A(T)\frac{P_0 - P}{W} \quad (11)$$

$$[O_2] = K_H P \quad (12)$$

where $[NO_2^-]_0$ and P_0 are the initial concentration of nitrite and the initial oxygen pressure, respectively, K_H is the Henry's coefficient reported in eq 4, and P is the value of the oxygen pressure at a given time in the course of the kinetic process. This calculation is valid since one can suppose (see Experimental Section) a continuous equilibrium situation between oxygen in the gas phase and in solution, that is to say that the process

$$O_{2(g)} \rightarrow O_{2(s)} \quad (13)$$

represents a fast step prior to the homogeneous-phase mechanism of reaction 2a. Plots of $\Delta[NO_2^-]/\Delta t$ *vs.* the product of the concentrations of oxygen and nitrite relevant to some of the present experiments are reported in Figure 2. The closely linear shape of the curves is in agreement with the second-order model expressed by eq 8 and 9.

The numerical values of k_6 calculated on the basis of the least-square method and referred to the disappearance of nitrite are summarized in column 2 of Table I. From the Arrhenius plot of Figure 3 the activation energy of the process ($\Delta E = 19.0 \pm 0.5$ kcal/mol) has been calculated. By assuming that the heat of activation is approximately equal to the energy of activation ($\Delta H^* \simeq \Delta E$) the activa-

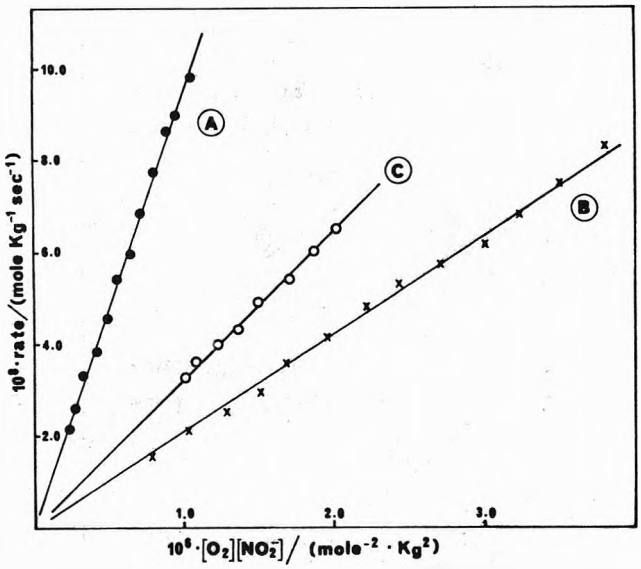

Figure 2. Plots of experimental rates $\Delta[NO_2^-]/\Delta t$, against the product of the actual "average" concentrations of nitrite and oxygen. Curves A and B are relevant to the corresponding experiments described in Figure 1.

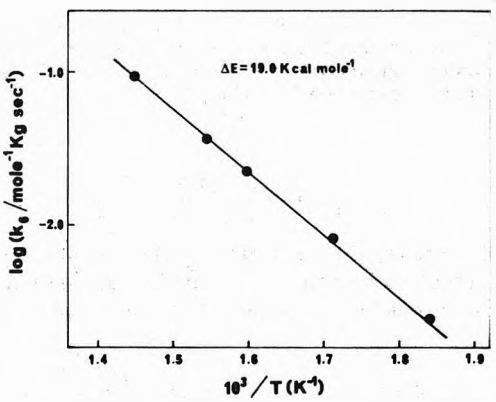

Figure 3. Arrhenius plot of the kinetic data relevant to the homogeneous-phase reaction: $NO_2^- + \frac{1}{2}O_2 = NO_3^-$ in molten (Na,K)NO_3.

TABLE I: Kinetic and Thermodynamic Data Relevant to the Homogeneous-Phase Reaction $NO_2^- + \frac{1}{2}O_2 = NO_3^-$ in an Equimolar Matrix of (Na,K)NO_3

T, °K	k_6, mol^{-1} kg sec^{-1}	ΔF^*, kcal mol^{-1}	ΔS^*, cal °K^{-1}	ΔE, kcal mol^{-1}
545	2.2×10^{-3}	39.3	−37.2	
584	7.7×10^{-3}	40.7	−37.1	19.0 ± 0.5
629	2.2×10^{-2}	42.6	−37.5	
648	3.3×10^{-2}	43.4	−37.6	
690	9.7×10^{-2}	44.9	−37.5	

tion free energies and entropies can be determined

$$\Delta S^* = \frac{\Delta H^*}{T} - R\left(\ln k_6 - \ln \frac{kT}{h}\right) \quad (14)$$

$$\Delta F^* = \Delta H^* - T\Delta S^* \quad (15)$$

where k_6 is the second-order kinetic constant of reaction 6 and the other symbols have their usual significance in thermodynamics.

The relevant values are reported in Table I. The preexponential factor was calculated to be

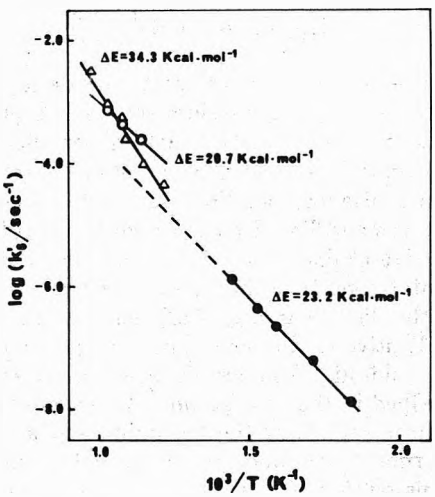

Figure 4. Arrhenius plots relevant to the heterogeneous-phase reaction $NO_2^- + \frac{1}{2}O^2{}_{(g)} = NO_3^-$ in different solvents: molten (Na,K)NO_3, ●; molten Na NO_2, Δ; molten KNO_2, O.

TABLE II: Kinetic and Thermodynamic Data Relevant to the Heterogeneous-Phase Reaction $NO_2^- + \frac{1}{2}O_2 = NO_3^-$ in an Equimolar Matrix of (Na,K)NO_3 Referred to a Constant Oxygen Pressure of 1 Atm

T, °K	k_6', sec^{-1}	ΔF, kcal mol^{-1}	ΔS, cal °K^{-1}	ΔE, kcal mol^{-1}
545	1.3×10^{-8}	52.3	−53.8	
584	5.9×10^{-8}	54.4	−53.8	
629	2.2×10^{-7}	57.0	−54	23.2 ± 0.5
648	3.7×10^{-7}	58.1	−54.2	
690	1.3×10^{-6}	60.3	−54	

$$A = k_6 e^{-(\Delta E/RT)} = 9.1 \times 10^4 \text{ mol}^{-1} \text{ kg sec}^{-1} \quad (16)$$

In the oxygen molecule the O–O bond is equivalent to 118 kcal/mol, a value about 6 times higher than the activation energy involved in the overall process 2a. This seems to suggest that, under our experimental conditions, the prevailing kinetic path for the oxidation of nitrite does not involve the "direct" breakage of the oxygen molecule. If atomic oxygen is formed in the course of the reaction, it must be produced by interaction of O_2 with a second species. This is in agreement with the reaction mechanism formulated for reaction 2a (steps 6 and 7).

By considering the results of the present work and of parallel studies[1,9] it can be concluded that the rate-determining steps for the three processes of oxidation of nitrite by peroxide, superoxide, and oxygen are

$$NO_2^- + O_2^{2-} \rightarrow \text{products} \quad (k_{17} = 1.7 \times 10^{-2}) \quad (17)$$

$$NO_2^- + O_2^- \rightarrow \text{products} \quad (k_{18} = 1.9 \times 10^{-4}) \quad (18)$$

$$NO_2^- + O_2 \rightarrow \text{products} \quad (k_6 = 5.0 \times 10^{-4}) \quad (6)$$

where the given second-order kinetic constants are referred to a temperature of 500°K. The value at 500°K for k_6 is obtained by extrapolation of the curve of Figure 3. As mentioned in the Introduction, hypothesis has been made that the higher reactivity of peroxide could be related to its lower bond energy. From this point of view a lower reactivity of molecular oxygen with respect to the more weakly bonded superoxide was also expected. The fact that, on the contrary, the experimental value of k_6 is

ε little higher than k_{18} indicates that other factors must play an important role in the kinetic process. One is likely the electrostatic repulsion between the reacting species: in particular the absence of this effect in the case of molecular oxygen can practically balance the disadvantage of a higher bond energy with respect to the superoxide ion.

Comparison with Literature Findings. The only literature data which can be compared with the ones described in the present paper are those obtained[4,5] by Freeman, who has studied the kinetics for the oxidation of pure sodium and potassium nitrite by molecular oxygen in the temperature range 830–1050°K. Freeman's data are relevant to the heterogeneous-phase process

$$NO_2^- + {}^1/_2O_{2(g)} = NO_3^- \qquad (2b)$$

and referred to a constant pressure of oxygen (1 atm) over the entire temperature range. For this reason the kinetic constants (k_6') are expressed as first order (sec^{-1}) and the relevant ΔE values summarize the thermal effect of the dissolution of oxygen in the reaction medium (eq 13) and of the homogeneous-phase reaction 2a.

In order to compare our data with those reported in ref 4 and 5, the values (mol^{-1} kg sec^{-1}) given in Table I were converted to the new dimension (sec^{-1}) on multiplying them by the relevant Henry's constant computed on the basis of eq 4. The pseudo-first-order constants obtained and the relevant thermodynamic data are given in Table II.

Arrhenius plots of all the presently available[10] kinetic data, relevant to reaction 2, are reported in Figure 4. The accordance between Freeman's and our data appears fairly good when considering the uncertainties related to this kind of comparison, mainly the fact that Arrhenius plots can be considered linear only in limited temperature intervals.

A final observation can be concerned with the fact that the high-temperature kinetic data given in ref 4 and 5 could be partially influenced by the presence of species having, as recently[6,11] demonstrated, a certain catalytic effect on reaction 2 or similar processes. This is the case for the oxides of Fe, Cr, and Ni certainly present in traces in the systems studied by Freeman which were contained in stainless-steel reaction vessels.

Another possible factor which can lead to a catalytic action[12] on the high-temperature oxidation of nitrite by oxygen is the presence of peroxide and superoxide ions. It has been, in fact, demonstrated[13] that these species are present in nitrite melts at temperatures around 900–1000°K. This probably according to a mechanism such as

$$2NO_2^- \rightleftarrows N_2 + 2O_2^- \qquad (19)$$

$$2O_2^- \rightleftarrows O_2^{2-} + O_2 \qquad (20)$$

$$O_2^{2-} \rightleftarrows O^{2-} + {}^1/_2O_2 \qquad (21)$$

which has been suggested[7] by Bond and Jacobs and which is in agreement with some interesting experimental observations. For example, it has been found[4] that while one-half of the available nitrogen was evolved from a nitrite melt (maintained at 1000°K under an argon atmosphere), after 2 hr only about ⅛ of the available oxygen could leave the liquid phase. In the presence of gaseous oxygen, equilibrium 20 can be shifted to the left so that the formation of peroxide is less probable; however, the complete absence of a catalytic mechanism such as that described in ref 12 cannot be *a priori* excluded.

Acknowledgment. This work was carried out with the financial assistance of the Italian National Research Council (C.N.R.).

References and Notes

(1) P. G. Zambonin and A. Cavaggioni, *J. Amer. Chem. Soc.*, **93**, 2854 (1971).
(2) P. G. Zambonin and J. Jordan, *J. Amer. Chem. Soc.*, **89**, 6365 (1967); **91**, 2225 (1969).
(3) P. G. Zambonin, F. Paniccia, and A. Bufo, *J. Phys. Chem.*, **76**, 422 (1972).
(4) E. S. Freeman, *J. Phys. Chem.*, **60**, 1487 (1956).
(5) E. S. Freeman, *J. Amer. Chem. Soc.*, **79**, 838 (1957).
(6) J. Cases-Casanova, *Bull. Soc. Chim. Fr.*, 429, 435 (1959).
(7) B. D. Bond and P. W. M. Jacobs, *J. Chem. Soc.*, 1265 (1966).
(8) (a) P. G. Zambonin, V. L. Cardetta, and G. Signorile, *J. Electroanal. Chem.*, **28**, 237 (1970); (b) E. Desimoni, F. Paniccia, and P. G. Zambonin, *ibid.*, **38**, 373 (1972); (c) F. Paniccia and P. G. Zambonin, *J. Chem. Soc., Faraday Trans. 1*, **68**, 2083 (1972).
(9) In ref 1 the value of k_{18} has been estimated to be $<5 \times 10^{-4}$ mol^{-1} kg sec^{-1}; more recent studies have indicated $k_{18} = 1.9 \times 10^{-4}$ mol^{-1} kg sec^{-1} (work in preparation).
(10) Attention is called on the fact that while the Freeman's data were obtained in a molten matrix of nitrite containing nitrate, the data reported in Table II are relevant to a nitrate melt containing nitrite.
(11) W. K. Rudloff and E. S. Freeman, *J. Phys. Chem.*, **74**, 3317 (1970).
(12) The catalytic action of O_2^{2-} and O_2^- on reaction 2, demonstrated in the course of a study in progress in this laboratory, can be expressed for instance on the basis of mechanisms such as

$$O_{2(g)} = O_{2(s)}$$
$$O_{2(s)} + O_2^{2-} = 2O_2^-$$
$$2(O_2^{2-} + NO_2^- = NO_3^- + O^{2-})$$
$$2(O^{2-} + O_2^- = O_2^{2-} + O^-)$$
$$O^- + O^- = O_2^{2-}$$
$$O_{2(g)} + 2NO_2^- = 2NO_3^- \qquad (2b)$$

(13) K. Leschewski and W. Dagenhard, *Ber.*, **72B**, 1763 (1939).

Molecular Orbital Calculations of the Electronic Spectra of Aromatic Hydrocarbon Mononegative Ions

Z. H. Khan, Z. H. Zaidi,[1] and B. N. Khanna*

Department of Physics, Aligarh Muslim University, Aligarh, U.P., India *(Received October 16, 1972)*

The Ruedenberg LCAO–MO method with TBM, IRM, TBX, and IRX approximations using very limited CI is used to study the electronic spectra of naphthalene, anthracene, and pyrene mononegative ions, and the results are compared with the FE–MO calculations. The calculated values are in fairly good agreement with experimental results, especially for the pyrene anion where remarkable success is achieved. On the basis of these calculations, an attempt is made to settle the discrepancy in the assignment of the absorption spectrum of the pyrene ion.

Introduction

The optical absorption spectra of aromatic hydrocarbon ions have been studied theoretically[2-6] as well as experimentally.[7-14] Most of the LCAO–MO and SCF methods used in these calculations were originally developed to study the spectra of the neutral hydrocarbons.[15-17] Although the general agreement between theory and experiment is satisfactory, for the pericondensed systems it is not as good as for the catacondensed systems. The free-electron MO (FE–MO) theory[18,19] also does not give encouraging results for the pericondensed hydrocarbons. However, the results for the latter are greatly improved in the calculations of Hummel and Ruedenberg[20] which are based on Ruedenberg's "tight-binding" (TB) and "intra-ring" (IR) approximations[21] in the LCAO–MO theory using an average distance of 1.395 Å (M) for all the bonds as well as exact internuclear distances (X). In the tight-binding approximation, the overlap effect is taken into account between the neighbor atoms only, while in the intra-ring approximation the overlap is considered between all those atoms which lie within a distance of the benzene diameter, *i.e.*, 2.8 Å. The overlap contribution from atoms lying at still larger distances, being very small, is neglected. Besides these refinements, the treatment has an improvement over the FE–MO and the other LCAO–MO methods in the sense that it also takes into account the effect of nonconjugated neighbors, hydrogen and carbon.

Theoretical treatment for the pyrene anion too, like its neutral molecule, presents an obstacle in the understanding of its spectrum. This is obvious from the work of Balk, *et al.*,[2] who have possibly misassigned a weak electronic transition of pyrene anion lying at 13.9 kK as B_{2u} (short-axis polarized). Their assignment is based on the Hückel calculation using configuration interaction. This is in disagreement with the polarization studies of Zandstra,[9] who reassigned this transition as B_{1u} (long-axis polarized). Although the FE–MO calculation favors the assignment of Zandstra, the energies of other transitions calculated by this method are not in close agreement with the experimental results. Therefore, it seems plausible to apply Ruendenberg's TBM, IRM, TBX, and IRX approximations[21] to the pyrene ion as well. The calculations based on these approximations confirm the measurements of Zandstra and also compare favorably with the observed spectrum. For a more comprehensive study we have also included the mononegative ions of naphthalene and anthracene in our calculations which have already been studied by the FE–MO method.[22]

Calculations

As the hydrocarbons under investigation have an even number ($2n$) of π electrons which occupy n bonding orbitals, therefore their mononegative ions will have one more electron, the odd electron being in the first antibonding orbital, *i.e.*, in the $(n + 1)$th MO. Here we make the assumption that the addition of the odd electron to the antibonding orbital does not seriously affect the other orbitals. It is also assumed that the orbital energies and the eigenvectors for the mononegative ions are the same as those for the neutral hydrocarbons given by Scherr,[23] Ham and Ruedenberg,[24] and Hummel and Ruedenberg.[25]

To a first approximation, we consider only the one-electron excitations shown in Figure 1. The transitions are identified by the representation of the direct product of the ground and excited state wave functions in the D_{2h} point group. Moreover, we restrict our configuration-interaction treatment only to those configurations which arise due to the excitations from the three highest fully- or half-filled orbitals to the three lowest completely unfilled orbitals so as to cover the spectral region experimentally known. In the TBM and IRM approximations for anthracene, we also include one more bonding and antibonding orbitals (not shown in Figure 1) due to symmetry conditions.

As is evident from Figure 1, transitions of three types of symmetries are obtained—B_{1u}, B_{2u}, and B_{3g},[26] the first two being allowed and the third one forbidden. All the one-electron transitions, except the transition $k \leftarrow n$, give rise to antisymmetrized wave functions which are doublets, the latter giving two doublets and a quadruplet. Since quadruplet–doublet transition is forbidden, therefore it has not been taken into consideration. Thus we are left only with two doublet wave functions of symmetry B_{1u}, four of B_{2u}, and one of B_{3g}. The configuration interaction leads to secular determinants with a 2×2 and a 4×4 matrix of symmetries B_{1u} and B_{2u}, respectively. The calculation of the matrix elements involves the evaluation of the electron-interaction integrals. These integrals were calculated by using the Ruedenberg method[19] in the FE–MO theory and the Mulliken approximation[27] in the TBM, IRM, TBX, and IRX approximations.

TABLE I: Calculated and Observed Transition Energies (in kK) of the Electronic Spectra of the Anions and Cations of Naphthalene (N), Anthracene (A), and Pyrene (P)

			Calculated					Observed		
				LCAO-MO method				Anion		
Ion	Symmetry of transition	Polarization[a]	FE-MO method[b]	TBM approx	TBX approx	IRM approx	IRX approx	Ref 8	Ref 9	Cation Ref 22, 28[c]
N	B_{3g}	Forbidden	5.7	11.3	8.6	9.8	7.3	7.8		
	B_{2u}	x	12.2	19.0	16.6	14.7	14.5	12.3	11.9	
	B_{1u}	y	20.8	21.9	23.7	21.1	22.3			
	B_{1u}	y	34.9	39.0	38.6	32.3	32.6	27.3	27.5	27.2
	B_{2u}	x	23.4	30.9	27.1	27.3	28.4	30.9	31.0	30.0
	B_{2u}	x	32.7	38.1	37.1	37.0	36.6		33.9	33.9
	B_{2u}	x	40.7	48.1	46.1	46.3	43.4		43.6	
A	B_{3g}	Forbidden	8.8	13.8	13.3	14.6	12.0	11.2	11.0	11.0
	B_{2u}	x	9.9	15.8	11.8	11.5	10.3	14.0	14.0	14.0
	B_{1u}	y	15.2	14.5	16.1	14.7	16.3			
	B_{1u}	y	22.0	33.2	32.1	28.2	27.4	24.9	25.0	24.5
	B_{2u}	x	18.0	19.0	22.5	23.1	23.2	27.1	27.0	26.5
	B_{2u}	x	27.5	34.6	33.1	33.3	32.3	30.7	30.7	29.3
	B_{2u}	x	35.1	45.3	40.0	40.6	39.7		39.0	
P	B_{3g}	Forbidden	8.9	11.5	11.5	9.9	10.0			
	B_{2u}	x	11.1	13.4	12.3	11.2	10.1	9.9	10.0	12.5
	B_{1u}	y	12.9	13.1	12.5	12.9	11.7	13.9	14.3	15.2
	B_{1u}	y	27.0	27.7	25.2	25.2	23.8	20.3	20.4	22.2
	B_{2u}	x	24.3	24.5	25.2	24.3	25.0	26.0	26.3	27.4
	B_{2u}	x	31.6	30.8	31.0	30.5	30.6		31.3	31.3
	B_{2u}	x	41.7	38.9	39.0	38.3	38.3		37.5	36.4

[a] The letters x and y denote the directions of polarization along the long axis of naphthalene and anthracene and short axis of pyrene, and vice versa, respectively. [b] For naphthalene and anthracene anions see ref 22; pyrene anion, present work. [c] See ref 22 for naphthalene and anthracene cations and ref 28 for pyrene cation.

All the calculations needed for the work were done on the IBM 1130 computer at the Computer Centre, Aligarh Muslim University.

Results and Discussion

The calculated transition energies for naphthalene, anthracene, and pyrene anions are presented in Table I and are compared with the observed spectra for the anions[8,9] and cations[22,28] of the corresponding hydrocarbons. The transition energies designated B_{2u} are x-polarized (long symmetry axis of naphthalene and anthracene, and short symmetry axis of pyrene), and those designated B_{1u} are y-polarized (short symmetry axis of naphthalene and anthracene, and long symmetry axis of pyrene).

According to our calculations the lowest-energy transition for naphthalene and pyrene anions should be B_{3g} (symmetry-forbidden). The same is predicted for the anthracene anion also by the TBM approximation and the FE-MO method. However, the calculations based on the TBX, IRM, and IRX approximations show that the lowest-energy transition for anthracene anion should be B_{2u}. Perhaps this discrepancy may be removed if one takes into account more configurations of B_{2u} symmetry. The B_{3g} transition has been observed for the naphthalene and anthracene ions, but not for the pyrene ion. Hoijtink, *et al.*,[3] have assigned the first band on the longer-wavelength side of the spectrum of naphthalene ion as B_{1u} which has been reassigned as B_{3g} by Hinchliffe, *et al.*[4] The latter assignment is confirmed from the present calculations. We assign the next electronic transition in these ions as B_{2u} in agreement with the polarization studies of Zandstra.

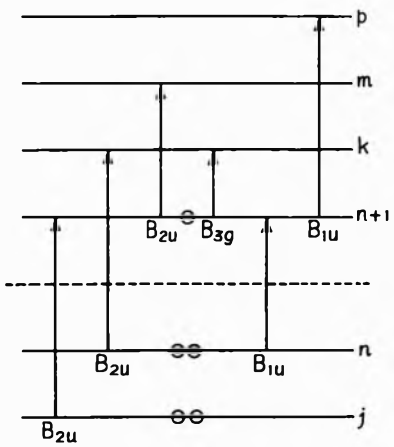

Figure 1. The symmetries of one-electron transitions for the hydrocarbon mononegative ions.

The different methods of calculations predict two B_{1u} transitions. After configuration interaction, the lower-energy band becomes weaker in intensity while the other becomes strong. The first B_{1u} transition, which is weak, has been observed in the spectrum of pyrene ion, while it has not been observed in the naphthalene and anthracene ions and is expected to be hidden in the vibrational progression of the first B_{2u} band. We disagree with Balk, *et al.*,[2] in the assignment of the lower-energy B_{1u} transition of pyrene ion as B_{2u}. Our assignment is supported by the polarization measurements.[9] The second B_{1u} band is very

strong and has been observed for all the ions under investigation.

The ionic spectra show three bands at higher energies which are x-polarized and have been assigned as B_{2u}. For naphthalene and anthracene, the FE-MO method underestimates the energies of these bands, while these are generally overestimated by the TBM approximation. For these transitions of pyrene ion, there is a close resemblence among all the calculations. The calculations of Hinchliffe, *et al.*,[4] show that the lower-energy transitions of naphthalene and anthracene anions are very well predicted by the Pariser-Parr and simplified Pariser-Parr methods, but the results for the higher-energy transitions are not as good as predicted by the present calculations.

In general, the results based on the intra-ring approximations are slightly better than the TBM approximation and the FE-MO method in most of the cases. Moreover, the Ruedenberg approximations, which led to results in close agreement with experiments for pyrene molecule, are markedly successful for its ion also.

Acknowledgment. We wish to thank Professor Rais Ahmed for providing the facilities of the Department. Z. H. K. gratefully acknowledges the receipt of a fellowship from the Council of Scientific and Industrial Research, India.

References and Notes

(1) Department of Physics, Jamia College, Jamia Millia University, New Delhi-25.
(2) P. Balk, S. de Bruijn, and G. J. Hoijtink, *Recl. Trav. Chim.*, **76**, 860, 907 (1957).
(3) G. J. Hoijtink, N. H. Velthorst, and P. J. Zandstra, *Mol. Phys.*, **3**, 533 (1960).
(4) A. Hinchliffe, J. N. Murrell, and N. Trinajstic, *Trans. Faraday Soc.*, **62**, 1362 (1966).
(5) A. Ishitani and S. Nagakura, *Theor. Chim. Acta*, **4**, 236 (1966).
(6) J. Wasilewski, *Acta Phys. Polon.*, **A38**, 349 (1970).
(7) D. E. Paul, D. Lipkin, and S. I. Weissman, *J. Amer. Chem. Soc.*, **78**, 116 (1956).
(8) P. Balk, G. J. Hoijtink, and J. W. H. Schreurs, *Recl. Trav. Chim.*, **76**, 813 (1957).
(9) P. J. Zandstra, Thesis, Free University, Amsterdam, 1959.
(10) G. J. Hoijtink and P. J. Zandstra, *Mol. Phys.*, **3**, 371 (1960).
(11) N. Christodouleas and W. H. Hamill, *J. Amer. Chem. Soc.*, **86**, 5413 (1964).
(12) K. H. J. Buschow and G. J. Hoijtink, *J. Chem. Phys.*, **40**, 2501 (1964).
(13) T. Shida and W. H. Hamill, *J. Chem. Phys.*, **44**, 2375 (1966).
(14) B. Badger and B. Brocklehurst, *Trans. Faraday Soc.*, **65**, 2588 (1969).
(15) R. Pariser and R. G. Parr, *J. Chem. Phys.*, **21**, 466, 767 (1953).
(16) J. A. Pople, *Proc. Phys. Soc. London, Sect. A*, **68**, 81 (1955).
(17) (a) H. C. Longuet-Higgins and L. Salem, *Proc. Roy. Soc., Ser. A*, **257**, 445 (1960); (b) E. Weltin, J. P. Weber, and E. Heilbronner, *Theor. Chim. Acta*, **3**, 114 (1964).
(18) K. Ruedenberg and C. W. Scherr, *J. Chem. Phys.*, **21**, 1565 (1953).
(19) N. S. Ham and K. Ruedenberg, *J. Chem. Phys.*, **25**, 1, 13 (1956).
(20) R. L. Hummel and K. Ruedenberg, *J. Phys. Chem.*, **66**, 2334 (1962).
(21) K. Ruedenberg, *J. Chem. Phys.*, **34**, 1861, 1878, 1884, 1892, 1897, 1907 (1961).
(22) (a) Z. H. Zaidi and B. N. Khanna, *J. Chem. Phys.*, **50**, 3291 (1969); (b) *Indian J. Pure Appl. Phys.*, **7**, 753 (1969); (c) *ibid.*, **9**, 44 (1971).
(23) C. W. Scherr, *J. Chem. Phys.*, **21**, 1582 (1953).
(24) N. S. Ham and K. Ruedenberg, *J. Chem. Phys.*, **29**, 1199 (1958).
(25) R. L. Hummel and K. Ruedenberg, "Pi-Electronic Excitations in Aromatic Molecules," U. S. A.E.C. Report I.S. 450, Ames Laboratory, Ames, Iowa, 1962.
(26) The notations are in agreement with the Recommendations of the Joint Commission for Spectroscopy, *J. Chem. Phys.*, **23**, 1997 (1955).
(27) R. S. Mulliken, *J. Chim. Phys.*, **46**, 500, 521 (1949).
(28) Z. H. Khan and B. N. Khanna, *J. Chem. Phys.*, In press.

COMMUNICATIONS TO THE EDITOR

Optical Properties of Sodium L-1,3,5-Triphenyl-Δ^2-pyrazolinyl Sulfate

Publication costs assisted by the Nishina Memorial Foundation

Sir: Optical rotatory dispersion (ORD), due to the difference in velocity of the left (L) and right (R) circularly polarized light, and circular dichroism (CD), the difference in absorption for the L and R light, are the spectroscopic consequence of molecular dissymmetry. ORD and CD of chiral molecules have been extensively applied to the study of the conformation of chiral molecules in their excited states.[1-3] Fluorescent chiral molecules should similarly exhibit some degree of circular polarization in their fluorescence or phosphorescence.[4] This phenomenon is of interest and of potential importance, because it is expected to provide very valuable information on the molecular conformation of these compounds in their electronically excited states.[4-8] The optical activity of the ordinarily chiral molecule essentially originates in either the conformational or the configurational characteristic of the molecules, while some chiral molecules inherit their optical activity from both these characteristics. In these cases, it is very difficult to separate the configurational contribution owing to the optical activity of these molecules from that due to the conformation. There is some possibility of overcoming this difficulty by use of circularly polarized fluorescence (CPF), if the molecules are fluorescent.

There are very few reports about CPF[9,10] and its application to the study of molecular conformation in the excited state.[5-8] This may be due to lack of instrumentation for the investigation of CPF which has enough sensitivity for detecting small amounts of circularly polarized light present in a large background of unpolarized fluorescence.[11] Realizing these points early, we commenced our study of CPF, and a recent article on the same subject by Gafni and Steinberg[8] prompted us to report our preliminary finding on CPF of sodium L-1,3,5-triphenyl-Δ^2-pyrazolinyl sulfate (I).

1,3,5-Triphenyl-Δ^2-pyrazoline and its derivatives have been investigated extensively for their use as optical brighteners[12,13] and scintillators[14-17] because of their strong fluorescent activity. Since these compounds have an asymmetric carbon at the 5 position of their pyrazoline ring, the L or R form should exhibit optical activity, suggesting the presence of circularly polarized components in the fluorescence light. There are, however, almost no studies on the optical activity of these compounds except that of I by Neunhoeffer and Ulrich.[10] They also reported their finding on elliptically polarized fluorescence of I. However, we find many unclear points in their paper, because the instruments used by them seem inadequate for carrying out precise measurement of that phenomenon. The above explanations are the very reason why we chose I as the object of our study on CPF.

According to the method of Neunhoeffer and Ulrich,[10] the racemic compound I was synthesized from phenylhydrazine-*p*-sulfonic acid and benzalacetophenone, and brucine was used for the racemic resolution. An Hitachi ESP-3 spectrophotometer, an Hitachi MPF-2A fluorescence spectrophotometer, a JASCO J-15 spectropolarimeter, and a JASCO J-10 spectropolarimeter were used for measurements of uv, fluorescence, excitation, ORD, and CD spectra, respectively. Uv, CD, and ORD spectra of I in MeOH are shown in Figure 1. Figure 2 is fluorescence, excitation, and CPF[18] spectra of I in MeOH (excitation, 365 mμ; fluorescence, 450 mμ).

It has been considered that the fluorescence and the strong uv band at 358 mμ of I are attributed to planarity of the molecule and the presence of two substituents, capable of interaction by way of the mesomeric forms IIa and IIb.[13,15,19,20] From the X-ray study on the crystal structure of 1,3-diphenyl-Δ^2-pyrazoline (III),[2] however, it has become evident that the molecule is not completely planar; the dihedral angle between planes of phenyl ring is 11°, and rotations about the C(6)–N(1) and C(3)–C(7) bonds give the molecule a slight propeller shape. The pyrazoline ring appears to be significantly nonplanar; the N(2)–C(3) bond has only 39% double bond character; the N(1)–N(2) bond length is significantly shorter than the single-bond distance and must have appreciable double bond character. Similarly, bonds C(6)–N(1) and C(3)–C(7), between the pyrazoline and phenyl rings, are both shorter than the single-bond distance, suggesting that conjugation between the phenyl rings occurs *via* atom N(1), N(2), and C(3). The presence and the nature of the substituent in the 5 position of III has little influence demonstrat-

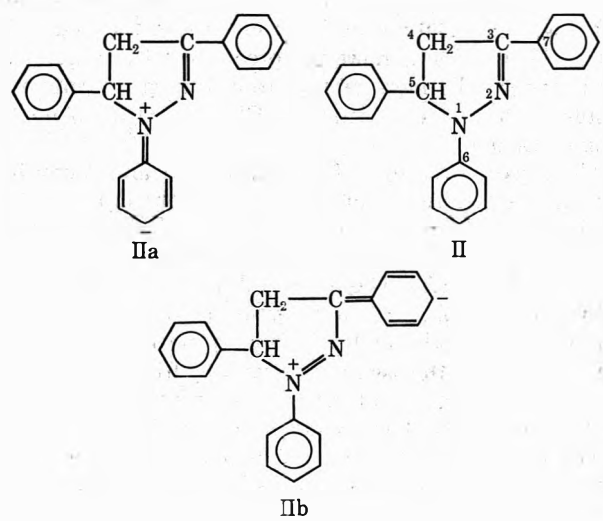

IIa II

IIb

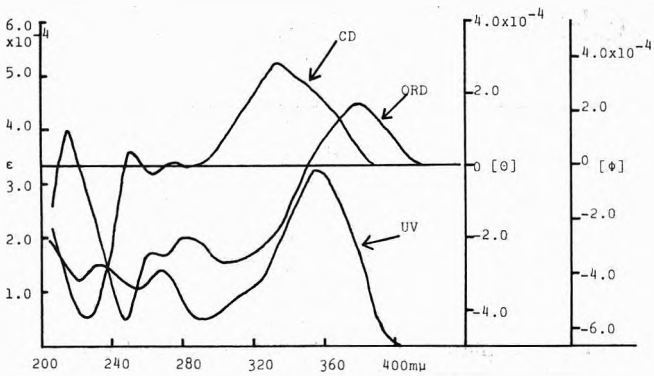

Figure 1. Uv, CD, and ORD spectra of sodium L-1,3,5-triphenyl-Δ^2-pyrazolinyl sulfate in MeOH.

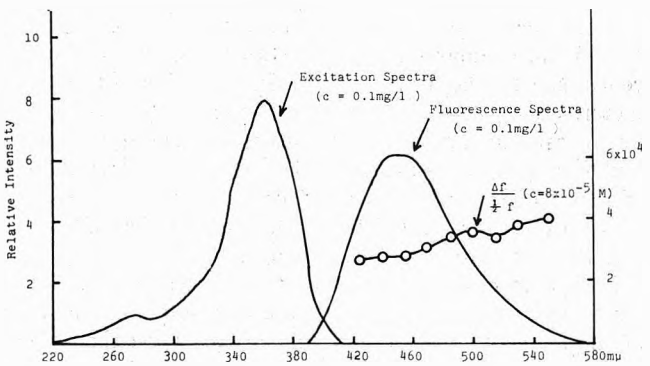

Figure 2. Fluorescence, excitation and circularly polarized fluorescence spectra of sodium L-1,3,5-triphenyl-Δ^2-pyrazolinyl sulfate in MeOH (excitation, 365 mμ; fluorescence, 450 mμ).

ing its isolation from the conjugated system.[19,20] Therefore, it is quite reasonable to apply the results obtained from X-ray study on III to the crystal structure of I. Thus, the nonplanar mesomeric chromophore of IIa and IIb should be responsible for the strong uv and excitation bands at 358 mμ and for a strong 450-mμ fluorescence band.

A strong CD band and Cotton effect around 350 mμ may be assigned not only to the optical activity induced in that mesomeric chromophore by its dissymmetric environment, but also to the inherently asymmetric property of that chromophore which is shown in its slight propeller shape.[21] A weak CD band at 275 mμ shows an interesting coincidence with a weak 275-mμ band of excitation spectra. The uv band at 268 mμ is said to arise from the phenyl ring, while 236-mμ uv band belongs to the pyrazoline ring.[14,22] They are, however, probably all strongly coupled, and result, more or less, from the entire composite system. The same is true for CD and ORD bands at around 250 mμ, also.

The maximum value of the absorption anisotropy factor, $\Delta\epsilon/\epsilon$, estimated from CD data is of the order of 16×10^{-4}; while that of the emission anisotropy factor, $\Delta f/0.5f$, is of the order of 4×10^{-4}, which is smaller than the former by a factor of 4. The marked difference between those values is most probably a reflection of the change in the conformation of the molecule in its electronically excited state.[8] Both in the cases of *trans*-β-hydrindanone[5,7] and 1,1′-bianthracene-2,2′-dicarboxylic acid,[8] the maximum of $\Delta f/0.5f$ is located at the same wavelength as that of fluorescence spectra. However, that is not in the case for our compound, and what is observed is the tendency of a gradual increase in $\Delta f/0.5f$ with longer wavelength. It is not easy to give a satisfactory explanation for this tendency. It may be attributed, however, to vibrational structure of the electronic emission bands.

Since it has become evident that our apparatus for CPF measurement has insufficient sensitivity and accuracy for detecting the small amount of circularly polarized light present in a large background of unpolarized fluorescence, we are making necessary improvements to our apparatus. We are also trying to synthesize sodium L-1,3-diphenyl-5-methyl-Δ^2-pyrazolinyl sulfate and sodium L-1,3-diphenyl-5-*tert*-butyl-Δ^2-pyrazolinyl sulfate, and to carry out spectroscopic measurements of these compounds, such as uv, CD, ORD, fluorescence, excitation, and CPF. In order to gain a better understanding of molecular structure of these compounds, we simultaneously intend to synthesize sodium L-1,5-diphenyl-3-methyl-Δ^2-pyrazolinyl sulfate and sodium L-1,5-diphenyl-3-*tert*-butyl-Δ^2-pyrazolinyl sulfate, and to investigate the optical properties of these compounds.

Acknowledgment. The authors are indebted to Professor Y. Ooshima for his kind instruction in the synthesis of sodium L-1,3,5-triphenyl-Δ^2-pyrazolinyl sulfate, and to Professor T. Matsuo for his interest in this study. We are grateful to Mr. S. Hashiya for his assistance in the electronics involved in this work. We wish to thank Japan Spectroscopic Co. Ltd. for CD and ORD measurements of our sample. We extend our sincere thanks to Professor I. Z. Steinberg for the CPF measurement of our sample as well as his instructive comments on our study of CPF, and further to Professor L. J. Oosterhoff and Dr. H. P. J. M. Dekkers for their kind advice on this work.

References and Notes

(1) C. Djerassi, "Optical Rotatory Dispersion," McGraw-Hill, New York, N. Y., 1960.
(2) L. Velluz, M. Legrand, and M. Grojean, "Optical Circular Dichroism," Academic Press, New York, N. Y., 1965.
(3) P. Crabbe, "Optical Rotatory Dispersion and Circular Dichroism in Organic Chemistry," Holden-Day, San Francisco, Calif., 1965.
(4) P. P. Feofilov, "The Physical Basis of Polarized Emission," Consultants Bureau, New York, N. Y., 1961.
(5) C. A. Emeis and L. J. Oosterhoff, *Chem. Phys. Lett.*, **1**, 129 (1967).
(6) H. P. J. M. Dekkers, C. A. Emeis, and L. J. Oosterhoff, *J. Amer. Chem. Soc.*, **91**, 4589 (1969).
(7) C. A. Emeis and L. J. Oosterhoff, *J. Chem. Phys.*, **54**, 4809 (1971).
(8) A. Gafni and I. Z. Steinberg, *Photochem. Phitobiol.*, **15**, 93 (1972).
(9) L. Grisebach, *Z. Phys.*, **101**, 13 (1936).
(10) O. Neunhoeffer and H. Ulrich, *Z. Electrochem.*, **59**, 122 (1955).
(11) I. Z. Steinberg and A. Gafni, *Rev. Sci. Instrum.*, **43**, 409 (1972).
(12) B. H. Chase and J. M. Evans, *J. Chem. Soc.*, 4825 (1964).
(13) A. Wagner, C. W. Schellhammer, and S. Petersen, *Angew. Chem., Int. Ed. Engl.*, 5, 699 (1966).
(14) R. H. Wiley, C. H. Jarboe, F. N. Hayes, E. Hansbury, J. T. Nielsen, P. X. Callahan, and M. C. Sellars, *J. Org. Chem.*, **23**, 732 (1958).
(15) R. Huisgen, A. Gotthardt, and R. Grashey, *Angew. Chem., Int. Ed. Engl.*, **1**, 49 (1962).
(16) S. R. Stanley, S. Loshaek, and K. C. Tsuo, *J. Phys. Chem.*, **66**, 404 (1962).
(17) S. R. Sandler and K. C. Tsuo, *J. Chem. Phys.*, **39**, 1062 (1963).
(18) The measurement was carried out by Mr. J. Schlessinger and Mr. A. Gafni with Dr. Steinberg's instrument[11] for the CPF measurement at his laboratory in the Weizmann institute of Science. We are very grateful to them for their help in this measurement.
(19) O. Neunhoeffer and D. Rosahl, *Z. Electrochem.*, **57**, 81 (1953).
(20) Z. Raciszewski and J. F. Stephen, *J. Amer. Chem. Soc.*, **91**, 4338 (1969).
(21) B. Duffin, *Acta. Crystallogr., Sect. B*, **24**, 1256 (1968).
(22) G. F. Duffin and J. D. Kendall, *J. Chem. Soc.*, 408 (1954).

Textile Research Institute
School of Engineering
Fukui University
Fukui, Japan 910

Yohji Shindo*
Takashi Miura

Received January 10, 1973

From the borders of organic chemistry . . . To the borders of theoretical physics:

Inorganic Chemistry brings you a broad range of authoritative information presenting both experimental and theoretical studies in all phases of inorganic chemistry.

Each month, this rapidly growing journal brings you the data you need on synthesis and properties of new compounds, quantitative studies regarding structure, and thermodynamics of inorganic reactions.

When you've seen the 50 or more papers offered in each issue, you'll also want to look through the Notes and Correspondence sections for their concise exchange of scientific views and ideas.

To order INORGANIC CHEMISTRY today, just complete and return the form below.

. . *another ACS service*

Inorganic Chemistry

Inorganic Chemistry
American Chemical Society
1155 Sixteenth Street, N.W.
Washington, D.C. 20036

Yes, I would like to receive INORGANIC CHEMISTRY at the one-year rate checked below:

	U.S.	*Canada*	*Latin America*	*Other Nations*
ACS Member Personal-Use One-Year Rate	☐ $18.00	☐ $22.00	☐ $22.00	☐ $23.00
Nonmember	☐ $54.00	☐ $58.00	☐ $58.00	☐ $59.00

Bill me ☐ Bill company ☐ Payment enclosed ☐

Name

Street Home ☐ Business ☐

City State Zip

P-73

Electrodeposition of Coatings

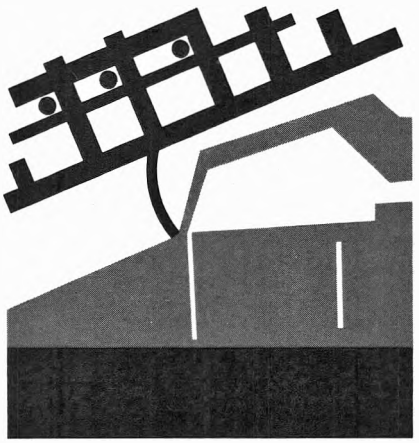

ADVANCES IN CHEMISTRY SERIES No. 119

A symposium sponsored by the Division of Organic Coatings and Plastics Chemistry of the American Chemical Society, with George E. F. Brewer, Chairman.

Seventeen papers report major new developments and research in the area of electrodeposition of organic coatings. This extensive collection discusses all aspects of this complex process including the advantage of better corrosion protection, lower cost, and virtual absence of pollution.

Principal topics covered:

- conversion and coatings; pretreating metals; surface changes; power supplies
- new polymers, copolymers, and pigments; preparation of resins; cathodic electrodeposition
- kinetics; dynamic simulation; throwing power
- bath maintenance; design of merchandise; influence of solvents

Each chapter offers material of permanent reference value for the industrial chemist working with automotive and appliance primers, as well as general-purpose one-coat systems.

243 pages with index Cloth (1973) $13.45.
Postpaid in U.S. and Canada, plus 40 cents elsewhere.

Other recommended books in the ADVANCES IN CHEMISTRY SERIES include:

No. 109 Chemical Reaction Engineering
Fixed and fluid bed reactors, polymerization kinetics and reactor design, optimization of reactor performance catalysis in gas–solid surface reactions, two-phase slurry reactors, industrial process kinetics, and transient operation.
685 pages with index Cloth (1972) $16.50

No. 107 Industrial Color Technology
Summarizes present knowledge of colorant formulation and evaluation and its application to industrial processing. Basic colorimetry, instrumentation, color difference metrics, and color as an aspect of appearance; 32 color plates.
177 pages with index Cloth (1972) $11.50

No. 104 Pesticides Identification at the Residue Level
Is our environment really becoming more toxic, or are pesticides falsely condemned by instruments designed as quantitative rather than qualitative tools? Eleven papers discuss philosophical aspects of ultramicroanalysis, instrumental techniques, microchemical methods, and biological assay.
182 pages with index Cloth (1971) $8.50

No. 103 Origin and Refining of Petroleum
Twelve papers on petroleum origin, deposits, Athabasca tar sands; catalytic reforming, hydrocracking, alkylation, isomerization; ethylene, propylene, vinyl chloride in processing; homogeneous catalysis; future of oil in Canada.
230 pages with index Cloth (1971) $10.00

No. 102 Molecular Sieve Zeolites—II
Thirty-six papers from the Second International Conference on Molecular Sieve Zeolites covering sessions on sorption and catalysis.
459 pages with index Cloth (1971) $16.00

No. 99 Multicomponent Polymer Systems
Thirty-seven papers on systems from olefin, diene, vinyl halide, styrene, acrylic, urethane, and epoxy resins as well as from polyamides, polyesters, polyarylenes, and others. Theory, processing, and applications are included. Nine papers on polyblends, the rest on copolymers.
598 pages with index Cloth (1971) $16.50

No. 97 Refining Petroleum for Chemicals
Up-to-date status report on the advances made in an exciting new industry. Emphasis is on basic processing with specific discussions centering around the chemical reactions used, new developments in these reactions, products and economics, and new processing concept.
293 pages with index Cloth (1970) $11.50

No. 96 Engineering Plastics and Their Commercial Development
A "how-to-do-it" book with discussion and case histories on developing plastics in profitable commercial products. Topics include use research, process development, and patent and legal aspects including clear warnings on contributory infringement. Engineering properties of over 50 plastic products are included.
128 pages with index Cloth (1969) $7.50

No. 92 Epoxy Resins
Sixteen papers on formulation and performance of epoxy resins. Processes and reactions are discussed including condensation reactions, gelation, synthesis, electro-deposition, curing, and reactivity.
230 pages with index Cloth (1970) $10.50

No. 91 Addition and Condensation Polymerization Processes
Twenty-six chapters devoted to process improvements and the polymerization kinetics of common monomers. The last 22 papers deal with new and improved polymers designed for specific uses or properties.
767 pages with index Cloth (1969) $19.50

Order from: **Special Issues Sales**
American Chemical Society, 1155 Sixteenth St., N.W., Washington, D.C. 20036